PERFORMANCE ANALYSIS OF COGNITIVE HYBRID SATELLITE-TERRESTRIAL NETWORKS FOR FUTURISTIC WIRELESS COMMUNICATIONS

Ph.D. Thesis

by

VIBHUM SINGH

DEPARTMENT OF ELECTRICAL ENGINEERING

INDIAN INSTITUTE OF TECHNOLOGY INDORE

JULY 2021

PERFORMANCE ANALYSIS OF COGNITIVE HYBRID SATELLITE-TERRESTRIAL NETWORKS FOR FUTURISTIC WIRELESS COMMUNICATIONS

A THESIS

Submitted in partial fulfillment of the

requirements for the award of the degree

of

DOCTOR OF PHILOSOPHY

by

VIBHUM SINGH

DEPARTMENT OF ELECTRICAL ENGINEERING

INDIAN INSTITUTE OF TECHNOLOGY INDORE

JULY 2021

INDIAN INSTITUTE OF TECHNOLOGY INDORE

CANDIDATE'S DECLARATION

I hereby certify that the work which is being presented in the thesis entitled "**PERFORMANCE ANALYSIS OF COGNITIVE HYBRID SATELLITE-TERRESTRIAL NETWORKS FOR FUTURISTIC WIRELESS COMMUNICATIONS**" in the partial fulfillment of the requirements for the award of the degree of **DOCTOR OF PHILOSOPHY** and submitted in the **DEPARTMENT OF ELECTRICAL ENGINEERING**, **Indian Institute of Technology Indore**, is an authentic record of my own work carried out during the time period from June 2017 to July 2021 under the supervision of Dr. Prabhat Kumar Upadhyay, Associate Professor, Department of Electrical Engineering, Indian Institute of Technology Indore, India.

The matter presented in this thesis has not been submitted by me for the award of any other degree of this or any other institute.

Vibhum Singh
22-07-2021

Signature of the student with date
(VIBHUM SINGH)

This is to certify that the above statement made by the candidate is correct to the best of my/our knowledge.

22-07-2021

Signature of Thesis Supervisor with date
(Dr. PRABHAT KUMAR UPADHYAY)

VIBHUM SINGH has successfully given his Ph.D. Oral Examination held on 25th **October 2021**.

25-10-2021

Signature of Thesis Supervisor with date
(Dr. PRABHAT KUMAR UPADHYAY)

ACKNOWLEDGEMENTS

I take this opportunity to acknowledge my heartfelt gratitude to all those who have directly or indirectly helped me throughout my PhD. First and foremost, I thank God Almighty for giving me the strength, knowledge, and enlightenment to undertake this research work. Then, I would like to express my deep sense of respect and gratitude to my supervisor and mentor, Dr Prabhat Kumar Upadhyay, for his invaluable guidance, sustained inspiration, and kind support towards my thesis work. He has given me all the freedom to pursue my research, and provided helpful career advice and suggestions, extending beyond academic boundaries, whenever needed. He has always been my source of inspiration during my stay at IIT Indore and will be, all my life.

Next, I would like to sincerely thank my comprehensive evaluation of research progress committee members Prof Abhinav Kranti and Dr Abhishek Srivastava for their interesting discussions and suggestions towards my research. I am thankful to all the faculty members and the staff at IIT Indore for their cooperation throughout my thesis work.

My appreciation also goes to all the members of the Wireless Communications (WiCom) Research Group for creating a friendly and conducive environment. It was my privilege to share the lab with Chandan Kumar Singh and Alok Kumar Shukla. I am immensely grateful to my seniors Dr Devendra Singh Gurjar, Dr Sourabh Solanki, and Dr Vinay Bankey for providing their help and valuable suggestions both technically and non-technically during my work. I am extremely thankful to Dr Shishir Maheshwari, Dr Vinay Kumar Tiwari, and Ajinkya Sonawane for making a wonderful company and sharing all the casual and valued moments which helped me during the hardship of this work. Special thanks go to my friend Abhinav Sharma for all the cheerful talks and encouragement, and also for his caring nature. I am also thankful to my colleagues Puneet Singh Thakur and Shaik Parvez for being great friends and sharing the magic moments of my life at IIT Indore.

I would like to thank the Ministry of Human Resource Development (MHRD), Government of India and IIT Indore for providing financial assistance. I will also thank the finance, administration, academic, and R&D sections for all the necessary support.

Above all, the most valued gratitude is expressed for my mother, Vijay Lakshmi Rathaur, my brother, Shivam Singh, and my bhabhi, Sudha Singh, for their unbounded love, endless support, and faith in me, without which I would have not been able to achieve the greatest milestone of my life.

Lastly, I want to thank everyone who were part of this journey and has, in one way or another, helped me to successfully complete this research work.

Vibhum Singh

Dedicated to
my family

ABSTRACT

The explosion of mobile applications and their integration in various aspects of everyday life necessitates the deployment of modern wireless systems that can handle such exponentially rising data traffic. High-speed broadband access, high capacity, low signal latency, long battery lifetime, wide coverage, etc., are the most important requirements to be considered for deploying the next-generation communication networks. In this regard, hybrid satellite-terrestrial networks (HSTNs) have emanated as a promising and prevalent infrastructure for future wireless networks owing to their capability of providing high throughput with ubiquitous coverage. In HSTNs, satellite communication and terrestrial networks are incorporated to enable their potential applications in the field of navigation, disaster relief, and broadcasting. The performance of HSTNs can be further enhanced while exploiting the cooperative communication techniques using amplify-and-forward (AF) and decode-and-forward (DF) based relaying protocols, which may extend the satellite coverage especially in the unpopulated and suburban areas. However, the static allocation of the frequency spectrum in traditional ways in HSTNs does not meet the requirements of future wireless networks. As such, in HSTNs, the spectral resources allocated to satellites get underutilized, whereas terrestrial spectral resources are becoming overutilized day by day due to the escalating growth in mobile data traffic. This eventually necessitates the efficient utilization of limited spectral resources. In this context, integrating the cognitive radio approach using underlay and overlay paradigms in HSTNs has become an efficient way of improving the spectrum utilization efficiency. This evokes a propitious architecture referred to as cognitive HSTN (CHSTN), which allows the simultaneous data transmissions of both primary satellite network and secondary terrestrial network over the same frequency band, subject to satisfying the quality-of-service (QoS) constraint at the primary user (PU). With such QoS restrictions from the PUs, it becomes challenging to improve the performance of secondary network. To address the design objectives of the future wireless networks, this thesis comprehensively investigates the performance of CHSTNs under the appropriately modelled shadowed-Rician fading for the satellite links and Nakagami-m fading for the terrestrial links, by exploring the various spectral-efficient schemes.

Firstly, we consider an overlay multiuser hybrid satellite-terrestrial spectrum sharing (OMHSTSS) system. Herein, we exploit both direct and relay links from

a primary satellite source to multiple terrestrial users with the coexistence of a secondary transmitter-receiver pair on the ground. Based on an overlay approach, the secondary transmitter (ST) provides an AF-based relay cooperation to the primary satellite network that employs opportunistic scheduling of multiple users. The underlying user scheduling strategy is based on satisfying the criterion of minimal outage probability (OP) for the primary network, and eventually, exploring more opportunities of the spectrum sharing for the secondary terrestrial network. To assess the performance of this analytical framework, we proficiently derive the exact and asymptotic closed-form expressions of the OP for primary and secondary networks, and further highlight the corresponding achievable diversity orders. Consequently, it can be inferred that the achievable diversity order of the primary network directly depends on the number of PUs. We also discuss the power allocation policy to explore more opportunities for the secondary spectrum access.

Then, we analyze the performance of an overlay CHSTN (OCHSTN) consisting of a primary satellite source-receiver pair and a secondary transmitter-receiver pair on the ground while taking into account the practical hardware impairments (HIs) at the user devices. Herein, we manifest analytically that, for the higher data rates, the HIs invoke ceiling effects which reprehensibly cap the fundamental capacity of the system. To mitigate the effect of HIs, we propose an adaptive relaying (AR) protocol for both AF and DF operations and compare its performance with the competitive fixed relaying (FR) schemes. The proposed AR protocol efficiently utilizes the available spectrum resources to enhance the system performance. Hereby, we comprehensively analyze AR-based AF (AAF) and AR-based DF (ADF) operations by deriving the OP expressions for primary and secondary networks in the presence of HIs. We showcase that the ADF relaying is more robust and resilient to HIs when compared with AAF relaying. Further, based on the derived OP expressions for the primary network, we identify two important ceiling effects, namely, relay cooperation ceiling (RCC) and direct link ceiling (DLC), and highlight their impacts on the system performance. We also provide the tolerable limit of HIs level for the given rate requirements.

Next, we investigate the performance of an overlay multiuser cognitive satellite-terrestrial network (OMCSTN) comprising a primary satellite source with its multiple terrestrial receivers and a secondary transmitter-receiver pair on the ground.

Herein, the primary satellite source employs a non-orthogonal multiple access (NOMA) scheme to simultaneously serve its all users, while the ST assists the primary communication through cooperative relaying technique in exchange for spectrum access. For this overall set-up, we obtain the closed-form expressions of the OP for primary satellite network and secondary terrestrial network by adopting pertinent heterogeneous fading models. Also, we examine the asymptotic outage behaviour at a high signal-to-noise ratio (SNR) for the primary and secondary networks, and thereby calculate the achievable diversity orders. A comparison with benchmark orthogonal multiple access (OMA) scheme reveals that the proposed NOMA-assisted OMCSTN provides remarkable performance improvement while utilizing the spectrum resource efficiently.

Further, different from the overlay approach employed in the aforementioned works, we consider an underlay paradigm in the subsequent research works. Hereby, we investigate the performance of an underlay CHSTN (UCHSTN) comprising a primary satellite source with its multiple terrestrial primary receivers (PRs) and a ST with its pre-paired users that are deployed on the ground based on a cooperative-NOMA (C-NOMA) scheme. Herein, the nearby NOMA user works in full-duplex (FD) mode while employing a DF relaying strategy for improving the performance of the far-away NOMA user. Importantly, we consider the realistic assumptions of FD-based loop self-interference and NOMA-based imperfect successive interference cancellation (SIC). By exploiting the mutual interference between primary and secondary networks, we analyze the performance of the secondary network in terms of OP, ergodic sum rate, and throughput. Further, to perform a more comprehensive analysis, both perfect SIC (pSIC) and imperfect SIC (ipSIC) situations are taken into account for the FD mode and the benchmark half-duplex (HD) mode for comparison purposes. Also, we examine the asymptotic OP behaviour at a high SNR to assess the achievable diversity orders. Our results manifest that FD C-NOMA outperforms HD C-NOMA for the case of ipSIC, whereas for the case of pSIC, HD C-NOMA can outperform FD C-NOMA in the high SNR regime.

Lastly, we explore the performance of an underlay CHSTN constituting a primary satellite source with its multiple terrestrial PRs and two NOMA secondary terrestrial users exchanging their information with the help of a HD DF-based secondary relay. We demonstrate there exists an inevitable inter-user interference (IUI) due to the NOMA scheme, which poses a detrimental impact on the performance of the secondary network. Hence, to achieve the improved performance and subsequently the low latency requirements, the wireless content caching is employed, whereby the relay can store the most popular contents of both the NOMA users. Hereby, exploiting the mutual interference between primary and secondary networks, and the realistic assumption of NOMA-based ipSIC, we analyze the performance of CHSTN for the schemes viz., cache-free (CF) two-way relaying (TWR) NOMA and cache-aided (CA) TWR-NOMA, in terms of OP, throughput, and average transmission time. Also, we examine the asymptotic OP behaviour at a high SNR to assess the achievable diversity orders. We manifest that zero diversity order results for both the schemes due to unavoidable IUI. However, one can visualize the remarkable performance improvements for CA TWR-NOMA scheme over its CF TWR-NOMA counterpart, owing to the reduced IUI and the efficient utilization of available spectrum resources.

Above all, this thesis addresses various technical aspects for realization of CHSTNs and eventually provides useful insights into the practical system design. All the theoretical developments, proposed schemes, and strategies hereunder are primarily aimed at improving the spectral efficiency and reliability of the CHSTNs for their possible applications in the future wireless networks.

CONTENTS

LIST OF FIGURES

List of Symbols

- Basic arithmetic and calculus notations have standard definitions.

Elementary & Special Functions

Notation	Definition
$\Gamma(\cdot)$	Gamma function
$\Upsilon(\cdot,\cdot)$	lower incomplete Gamma function
$\Gamma(\cdot,\cdot)$	upper incomplete Gamma function
$J_v(\cdot)$	Bessel function of order v
$\mathcal{K}_v(\cdot)$	modified Bessel function of the second kind of order v
$G_{p,q}^{m,n}\left[\cdot\middle\vert \begin{smallmatrix}\cdot\\ \cdot\end{smallmatrix}\right]$	Meijer's G-function
${}_1F_1(\cdot;\cdot;\cdot)$	confluent hypergeometric function of the first kind
$\log_i(\cdot)$	logarithm to base i

Probability & Statistics

Let X be a random variable, and $\mathcal{A}$ be an arbitrary event.

Notation	Definition
$\mathbb{E}(\cdot)$	expectation
$f_X(\cdot)$	probability density function (PDF) of X
$F_X(\cdot)$	cumulative distribution function (CDF) of X
$\Pr[\mathcal{A}]$	probability of $\mathcal{A}$
$X \sim \mathcal{CN}(\mu,\sigma^2)$	X is complex Gaussian distributed with mean μ and variance σ^2

Miscellaneous

Notation	Definition
$\triangleq$	equality by definition
$n!$	factorial of n
$\mathcal{C}_r^n = \binom{n}{r} = \frac{n!}{r!(n-r)!}$	binomial coefficient
$(a)_n = \frac{\Gamma(a+n)}{\Gamma(a)}$	Pochhammer symbol
$\arg\max_i b_i$	index i corresponding to the largest b_i
$\arg\min_i b_i$	index i corresponding to the smallest b_i
$\min(b_1,b_2)$	minimum of scalars b_1 and b_2
$\max(b_1,b_2)$	maximum of scalars b_1 and b_2

List of Abbreviations

2D	Two-Dimensional
3GPP	Third-Generation Partnership Project
5G	Fifth-Generation
AF	Amplify-and-Forward
AR	Adaptive Relaying
AS	Average Shadowing
AWGN	Additive White Gaussian Noise
B5G	Beyond 5G
CA	Cache-Aided
CDF	Cumulative Distribution Function
CF	Cache-Free
CHSTN	Cognitive HSTNs
C-NOMA	Cooperative NOMA
CSI	Channel State Information
DF	Decode-and-Forward
DS	Direct Satellite
DST	DS Transmission
E-E	End-to-end
DVB-SH	Digital Video Broadcast-Satellite Handheld
EVM	Error Vector Magnitude
ESR	Ergodic Sum Rate
FD	Full-Duplex
FR	Fixed Relaying
GEO	Geostationary earth orbit
HD	Half-Duplex
HIs	Hardware Impairments
HS	Heavy Shadowing
HSTNs	Hybrid Satellite-Terrestrial Networks
i.i.d.	Independent and Identically Distributed
IUI	Inter-User Interference
LI	Loop Self-Interference
LoS	Line-of-Sight
MRC	Maximal-Ratio Combining

NOMA	Non-Orthogonal Multiple Access
OMA	Orthogonal Multiple Access
OP	Outage Probability
PDF	Probability Density Function
PR	Primary Receiver
PT	Primary Transmitter
PU	Primary User
QoS	Quality-of-Service
SIC	Successive Interference Cancellation
SINR	Signal-to-Interference-Plus-Noise Ratio
SNR	Signal-to-Noise Ratio
SNDR	Signal-to-Noise-and-Distortion Ratio
SR	Secondary Receiver
ST	Secondary Transmitter
SU	Secondary User
TWR	Two-Way Relaying

CHAPTER 1

INTRODUCTION

The explosion of mobile applications and their integration in various aspects of everyday life necessitates the deployment of modern wireless systems that can handle such exponentially rising data traffic. We have already witnessed the evolution of communication technology from first-generation (1G) to fourth-generation (4G). High-speed broadband access, high capacity, low signal latency, long battery lifetime, wide coverage, etc., are the most important requirements to be considered for deploying the next-generation communication networks. In this regard, satellite communication systems have earned significant consideration due to their advantage of providing wide radio coverage. As such, one satellite may cover an area of thousands of kilometers in radius and efficiently provide signal coverage at a lower cost. Albeit, terrestrial networks can provide high-speed data services at a low cost. Thus, satellite and terrestrial networks can be coalesced to harvest the benefits of both the systems. Such hybrid networks, commonly referred to as hybrid satellite-terrestrial networks (HSTNs) [1], have been identified as an efficient solution to compete with the high data rate and wide coverage requirements. HSTNs have emanated as a promising and prevalent infrastructure for the future wireless networks owing to their capability of providing high throughput with ubiquitous coverage. In HSTNs, satellite communication and terrestrial networks are incorporated to enable their potential applications in the field of navigation, disaster relief, and broadcasting, especially in the unpopulated and suburban areas [2]. However, a masking effect may arise due to the presence of obstacles and shadowing between the satellite and terrestrial user, which devastates the system performance of HSTNs [3]. To combat this masking effect and further enhance the coverage and reliability, numerous research studies have been coordinated towards such networks while exploiting the cooperative communication techniques using amplify-and-forward (AF) and decode-and-forward (DF) based relaying protocols [4]-[6].

A HSTN has been extensively used in Digital Video Broadcast-Satellite Handheld (DVB-SH) [7] standard using a geostationary earth orbit (GEO) satellite at S frequency band. However, the operational frequency band depends on various application scenarios and service requirements (like broadcasting, navigation, personal mobile communication, disaster or emergency scenario, etc.) across different countries. Moreover, there is an increasing interest and involvement in third-generation partnership project (3GPP) working group, from the satellite communication industry, for an integrated satellite and terrestrial network infrastructure in the context of fifth-generation (5G). In essence, the newest 3GPP Releases under 5G development provide a promising opportunity to integrate space components with terrestrial networks. Thereby, the coexistence and cooperation between these networks would greatly benefit the 5G and beyond 5G (B5G) wireless communications.

Nevertheless, the static allocation of the frequency spectrum in traditional ways in HSTNs does not meet the requirements of future wireless networks. As such, in HSTNs, the spectral resources allocated to satellites get underutilized, whereas terrestrial spectral resources are becoming overutilized day by day due to the escalating growth in mobile data traffic. This eventually necessitates the efficient utilization of limited spectral resources. Therefore, for such a hybrid system, it is crucial to find out the efficient ways to share the resources of space-based networks with terrestrial networks. To realize the spectral-efficient design of HSTNs, we focus on four key-enabling technologies which are briefly described as follows:

1.1 Cognitive Radio

Cognitive radio (CR) technology has been proposed for mitigating the spectrum scarcity problems in wireless communication systems. In CR networks, unlicensed secondary users (SUs) are benefited by sharing the spectrum with licensed primary users (PUs) network, provided that such spectrum sharing does not deteriorate the quality-of-service (QoS) of the primary network [8]. There are three main paradigms for spectrum sharing, namely, interweave, underlay, and overlay [9].

Interweave Approach: In interweave approach, the SUs opportunistically access the unoccupied spectrum (also known as white spaces) of PUs without causing any interference to their transmission. The major disadvantage of this approach is that the SUs are required to sense the spectrum hole before transmission, and therefore, is highly sensitive to the primary traffic behavior and spectrum sensing errors. This approach may not be suitable for dense networks due to the lack of availability of spectrum holes.

Underlay Approach: In underlay approach, SUs can share the spectrum with PUs by satisfying the interference power criterion (also called interference temperature limit) toward the PUs. In contrast to the interweave model, the underlay model has the advantage that the SUs can directly occupy licensed spectrum without considering the behavior of the PUs' traffic patterns. However, the SUs need to obtain the channel state information (CSI) of the pertaining links towards PUs for controlling their transmission power. Owing to the constrained power at SUs, in this paradigm, improving the performance of SUs is critical and challenging.

Overlay Approach: In this approach, SUs may be allowed to transmit over the spectrum owned by the PUs in exchange for cooperation to the PUs' signals transmission on a priority basis. Thereby, in contrast to underlay model, the overlay paradigm does not pose stringent transmit power restrictions to the SUs.

To this end, integrating the CR approach in HSTNs has become an efficient way of improving the spectrum utilization efficiency. This evokes a propitious architecture referred to as cognitive HSTNs (CHSTNs) [10], which allows the simultaneous data transmissions of both primary satellite network and secondary terrestrial network over the same frequency band, subject to satisfying the QoS constraint at the PU.

1.2 Cooperative Relaying

Cooperative relaying has been reckoned as an effectual approach to counteract the effect of multipath fading in wireless communications. It can be widely classified into two categories viz., fixed relaying (FR) and adaptive relaying (AR).

1.2.1 Fixed Relaying

In this relaying, the distribution of the channel resources between source and relay is performed in a fixed manner. Although such protocols are easy to implement, they have the disadvantage of low bandwidth efficiency. FR includes commonly adopted AF and DF protocols.

Amplify-and-Forward Relaying: In AF relaying protocol, the relay simply amplifies the signal received from its source and transmits it further to the destination. Here, amplification is done essentially to combat the effect of the fading between the source and relay channel. This protocol has the main drawback of noise amplification by the relay. However, reduced hardware complexity is advantageous over its DF counterpart.

Decode-and-Forward Relaying: DF relaying is also known as regenerative relaying. In DF relaying protocol, relay decodes the signal received from its source, then re-encodes it and transmits to the destination. While doing this, there is a chance of an error propagation owing to the decoding and forwarding the incorrect signal by the relay, making the decoding process meaningless. One possible way to reduce this error is error correction codes, whereas another solution is AR.

1.2.2 Adaptive Relaying

AR includes an incremental relaying protocol which relies upon the limited feedback from the destination. In this, cooperative node adaptively performs the relaying operation based on the decoding of the signal through direct link. Specifically, depending on the success/failure of the signal via direct transmission, the relaying cooperation is invoked. And, once the cooperation is triggered, its operation becomes similar to the FR. Hereby, firstly, the source node transmits its information to the destination as well as to the relay node. Then, if destination node is able to successfully decode the information signal from the source node, it sends an error-free one-bit feedback to the cooperative node indicating that the relaying cooperation is not needed. But if, it is not, then the feedback requests that the relay forwards the received signal from the source. AR is found to be more spectral-efficient compared to FR.

Depending on the data flow direction, relaying operation can be further categorized into one-way relaying (OWR) and two-way relaying (TWR).

1.2.3 One-Way Relaying

In this relaying protocol, the messages are transmitted in only one direction, i.e., from the source to relay or user destination. Consequently, two orthogonal time slots are needed to deliver the one message between the source and destination, owing to the half-duplex (HD) operation of the nodes. Thus, the bi-directional information exchange between source and user destination would need four time phases which makes OWR relatively less spectral-efficient compared with TWR.

1.2.4 Two-Way Relaying

To ameliorate further the spectral efficiency loss in OWR, TWR technique is introduced [11], where two nodes exchange their information with the aid of a relay by employing AF or DF strategy as discussed above in this section. TWR protocol utilizes either two or three time phases for the bi-directional information exchange.

1.3 Non-Orthogonal Multiple Access

Future wireless networks have to effectively satisfy the needs of high spectral efficiency and massive connectivity. In this respect, the non-orthogonal multiple access (NOMA) [12] has been viewed as one of the most promising technologies for future wireless networks. The basic concept of NOMA is to serve the multiple users simultaneously at the transmitter side by superposing and providing different power levels to them in the same time/frequency resources. Then the desired signals are decoded at the receiver while employing the successive interference cancellation (SIC) technique. In the mean time, the cooperative relaying technique has been introduced into the original NOMA scheme to obtain a spatial diversity gain for the far-away NOMA user with worse link quality, referred to as cooperative NOMA (C-NOMA) [13]. Herein, the nearby NOMA user with better link quality detects the information of far-away NOMA user and further acts as a relay to forward that information during the cooperation phase. In such a way, the far-away user receives two copies of its desired signals, i.e., one from the base station (BS) and the other from the signal forwarded by the nearby user. By merging these two copies and grasping the advantages of spatial diversity gains, one can realize the improvement in reliability of the far-away NOMA user.

1.4 Wireless Caching

Recently, wireless caching is being explored for addressing the demands of growing capacity for rich multimedia traffic in the 5G and beyond cellular networks [14].

The main idea of caching is to store the popular contents nearer to the users by storing them into the router, relay, etc., during the off-peak traffic periods which is commonly referred to as the cache placement phase. During the delivery phase, the users can directly access their contents from there rather than fetching via transmissions from the source networks [15]. This results in reduced latency and subsequently the increased spectral efficiency [16].

1.5 Motivation and Objectives

In this section, we present the motivation and objectives behind the research work in this thesis.

1.5.1 Motivation

Spectral efficiency, seamless data connectivity, wide coverage, etc., are the important design objectives for future wireless networks, i.e., 5G and B5G [17]. To improve the spectral efficiency, CR is a promising technology which can eliminate the spectrum under-utilization problem. Thus, the integration of CR approach into HSTNs can make a remarkable improvement in the performance of next-generation wireless networks. Since the majority of existing works on CHSTNs focused on the performance analysis using underlay paradigm [18]-[20], the authors in [21] have considered the overlay scenario by considering multiple secondary relays, however, by assuming single PU. Nevertheless, future satellite communication systems are required to satisfy a large number of PUs by providing high information transfer rate at a reasonable cost and QoS. Moreover, the multi-user architecture has been incorporated in a number of standards like IEEE 802.11s and IEEE 802.16j [22]. Further, the incorporation of a more spectral-efficient scheme viz., AR, has also been overlooked in the literature. Also, they have assumed an ideal hardware transceiver for the spectrum sharing network nodes. Note that, in practice, the radio-frequency (RF) transceivers may experience hardware distortions due to phase noises, in-quadrature phase (IQ) imbalances, and amplifier non-linearities [23]. These distortions may cause a deleterious impact on the performance of CHSTNs owing to the involvement of low-cost user devices. This is prominent in overlay spectrum sharing scheme because the secondary transceiver requires the use of inexpensive hardware components in order to keep the expenditures manageable for operators. Even though the effect of the hardware distortions can be partially mitigated through appropriate calibration or compensation techniques, there remains a residual distortion. Therefore, it is reasonable to analyze the impact of hardware imperfection on overlay CHSTNs with AR protocol.

On another front, future wireless networks have to meet the demands of high data rate and a huge number of users effectively. In this respect, the conventional orthogonal multiple access (OMA) scheme in CHSTNs can not accomplish such requirements owing to its limitation of serving one user at a time, and thus, the available spectrum resource in CHSTNs is still underutilized. Although the NOMA scheme has gained a great interest in conjunction with CHSTNs, but mostly by considering the underlay spectrum sharing approach [24]. Different from this, the authors in [25] have employed the overlay approach in their work. However, they have considered only a single PU with no direct satellite (DS) communication.

Since the overlay approach employs sophisticated signal processing and coding techniques, the underlay approach is favoured and broadly utilized owing to its simplicity in implementation. Nevertheless, in underlay, the coverage and capacity of the secondary network remain limited due to the SU's transmit power constraints. Therefore, the amalgamation of C-NOMA scheme into CHSTNs can remarkably ameliorate the performance against the stipulated transmit power constraints on the SUs. But this improvement in the performance of CHSTNs requires additional bandwidth costs for the system owing to HD relaying, which may offset the performance gain guaranteed by cooperative communication. To further improve the performance of CHSTNs, it is important to consider the C-NOMA scheme with full-duplex (FD) relaying mode. To this end, most of the existing works in CHSTNs are based on the conventional NOMA scheme and are conjectured the subsistence of perfect SIC (pSIC) [24]-[27]. However, in practice, the NOMA technique causes many implementation issues, such as complexity scaling and error propagation [28]. Consequently, these critical factors will lead to an error in decoding, causing residual interference signal (IS), which may pose limitations on the capacity of the CHSTNs. Thus, it becomes essential to investigate the deleterious impacts of imperfect SIC (ipSIC) on CHSTNs with FD C-NOMA scheme.

Further, the TWR technique is deemed more spectral-efficient when compared with its OWR counterpart [11]. Thus, exploiting this TWR technique into NOMA-based CHSTNs can further enlarge the coverage and capacity of the secondary network [29]. However, as such, there exists an inevitable inter-user interference (IUI)[1], which postures a detrimental impact on the performance of the secondary network. Hereby, integrating the caching technique in TWR-NOMA-based CHSTN will not only mitigate this IUI significantly but also reduce the average end-to-end (E-E) transmission times. As such, both the NOMA users can now retrieve their contents from the relay based on the availability of desired contents. In this context, most of the existing works on NOMA-based CHSTNs are relied on the OWR networks and have not considered the potential attributes of wireless caching. Also, they have taken into account the unrealistic assumption of pSIC with no residual interference incurred. Thus, it would be significant to investigate the detrimental impacts of ipSIC on CHSTNs with both cache-free (CF) and cache-aided (CA) TWR-NOMA schemes.

1.5.2 Objectives

The aforementioned research voids have motivated us to achieve the following objectives towards the design of future wireless networks:

- To assess the performance of overlay CHSTNs with multiple PUs.
- To investigate the performance of hardware-impaired overlay CHSTNs with AR protocol.
- To analyze the performance of NOMA-assisted overlay multiuser CHSTNs.
- To explore the performance of underlay CHSTNs with FD/HD C-NOMA schemes under the ipSIC/pSIC situations.
- To characterize the performance of underlay CHSTNs with CF/CA TWR-NOMA schemes under the realistic assumption of ipSIC.

With above-stated objectives, this thesis presents the comprehensive performance analysis of CHSTNs over generalized fading channels. We address the various technical aspects of CHSTNs through exhaustive mathematical analysis and highlight important guidelines towards the design of futuristic wireless networks.

[1]Based on the NOMA protocol, a node experiences interference from the other signals when it first tries to decode the signal with larger power. Such interference is referred to as IUI.

1.6 Thesis Outline and Contributions

Given the importance of efficiently utilizing the available spectrum for HSTNs, we aim to comprehensively analyze the performance of CHSTNs by using various spectral-efficient schemes under the appropriately modelled shadowed-Rician fading[2] for the satellite links and Nakagami-m fading[3] for the terrestrial links. Throughout this thesis, we adopt these hybrid fading channels for performance analysis. The current chapter introduces the reader to the background of the work, outlines the research objectives and their motivation, and discusses various technologies involved in this thesis work. The main contributions from the other chapters are summarized as follows:

- In Chapter 2[4], we investigate the outage performance of an overlay multiuser hybrid satellite-terrestrial spectrum sharing (OMHSTSS) system. Herein, we exploit both direct and relay links from a primary satellite source to multiple terrestrial users with the coexistence of a secondary transmitter-receiver pair on the ground. Based on an overlay approach, the secondary transmitter (ST) provides an AF-based relay cooperation to the primary satellite network that employs opportunistic scheduling of multiple users. The underlying user scheduling strategy is based on satisfying the criterion of minimal outage probability (OP) for the primary network, and eventually, exploring more opportunities of the spectrum sharing for the secondary terrestrial network. To assess the performance of this analytical framework, we proficiently derive the closed-form expressions of the OP for primary and secondary networks. Hereby, we discuss the power allocation policy to explore more opportunities for the secondary spectrum access. We further assess the asymptotic OP behaviour at a high signal-to-noise ratio (SNR) to delve into the diversity performance of primary and secondary networks. Consequently, it can be inferred

[2]In general, the shadowed-Rician fading model observes the statistical characterizations of the satellite channels accurately [30]. Further, for analyzing the system performance of CHSTNs, this model gives rise to a computationally efficient tool as compared with other satellite channel models like Loo's model [31], and hence, widely explored in the literature (see [18]-[21], [24]-[27], and references cited therein).

[3]Nakagami-m fading is a generalized model which captures a variety of fading scenarios of terrestrial wireless channels and incorporates the well-known Rayleigh fading as a unique case [32].

[4]The contributions of this chapter are presented in the following paper:

1. V. Singh, S. Solanki, and P. K. Upadhyay, "Cognitive relaying cooperation in satellite-terrestrial systems with multiuser diversity," *IEEE Access*, vol. 6, pp. 65539-65547, Oct. 2018.

that the achievable diversity order of the primary network directly depends on the number of PUs. Finally, we validate our theoretical developments using Monte Carlo simulations.

- In Chapter 3[5], we analyze the performance of an overlay CHSTN (OCHSTN) consisting of a primary satellite source-receiver pair and a secondary transmitter-receiver pair on the ground while taking into account the practical hardware impairments (HIs) at the user devices. Herein, we manifest analytically that, for the higher data rates, the HIs invoke ceiling effects which reprehensibly cap the fundamental capacity of the system. To mitigate the effect of HIs, we propose an AR protocol for both AF and DF operations and compare its performance with the competitive FR schemes. The proposed AR protocol efficiently utilizes the available spectrum resources to enhance the system performance. Hereby, we comprehensively analyze AR-based AF (AAF) and AR-based DF (ADF) operations by deriving the OP expressions of the primary and secondary networks in the presence of HIs. We showcase that the ADF relaying is more robust and resilient to HIs when compared with AAF relaying. Further, based on the derived OP expressions for the primary network, we identify two important ceiling effects, namely, relay cooperation ceiling (RCC) and direct link ceiling (DLC), and highlight their impacts on the system performance. We also provide the tolerable limit of HIs level for the given rate requirements.

- In Chapter 4[6], we investigate the performance of an overlay multiuser cognitive satellite-terrestrial network (OMCSTN) comprising a primary satellite source with its multiple terrestrial receivers and a secondary transmitter-receiver pair

[5]The contributions of this chapter are presented in the following papers:

1. V. Singh, S. Solanki, P. K. Upadhyay, D. B. da Costa, and J. M. Moualeu, “Impact of hardware impairments on cognitive satellite-terrestrial relaying with a direct link,” in *Proc. IEEE 17th Annual Consumer Communications & Networking Conference (CCNC)*, Las Vegas, USA, Jan. 2020, pp. 1-6.
2. V. Singh, S. Solanki, P. K. Upadhyay, D. B. da Costa, and J. M. Moualeu, “Performance analysis of hardware-impaired overlay cognitive satellite-terrestrial networks with adaptive relaying protocol,” *IEEE Systems Journal*, vol. 1, no. 15, pp. 192-203, Mar. 2021.

[6]The contributions of this chapter are presented in the following paper:

1. V. Singh, P. K. Upadhyay, and M. Lin, “On the performance of NOMA-assisted overlay multiuser cognitive satellite-terrestrial networks,” *IEEE Wireless Communication Letters*, vol. 9, no. 5, pp. 638-642, May 2020.

on the ground. Herein, the primary satellite source employs a NOMA scheme to simultaneously serve its all users, while the ST assists the primary communication through cooperative relaying technique in exchange for spectrum access. For this overall set-up, we obtain the closed-form expressions of the OP for primary satellite network and secondary terrestrial network by adopting pertinent heterogeneous fading models. Also, we examine the asymptotic outage behaviour at a high SNR for primary and secondary networks, and thereby calculate the achievable diversity orders. A comparison with benchmark OMA scheme reveals that proposed NOMA-assisted OMCSTN provides remarkable performance improvement while utilizing the spectrum resource efficiently.

- In Chapter 5[7], we investigate the performance of an underlay CHSTN (UCHSTN) comprising a primary satellite source with its multiple terrestrial primary receivers (PRs) and a ST with its pre-paired users that are deployed on the ground based on a C-NOMA scheme. Herein, the nearby NOMA user works in FD mode while employing a DF relaying strategy for improving the performance of the far-away NOMA user. Importantly, we consider the realistic assumptions of FD-based loop self-interference (LI) and NOMA-based ipSIC. By exploiting the mutual interference between primary and secondary networks, we analyze the performance of the secondary network in terms of OP, ergodic sum rate (ESR), and throughput. Further, to perform a more comprehensive analysis, both pSIC and ipSIC situations are taken into account for the FD mode and the benchmark HD mode for comparison purposes. Also, we examine the asymptotic OP behaviour at a high SNR to assess the achievable diversity orders. Our results manifest that FD C-NOMA outperforms HD C-NOMA for the case of ipSIC, whereas for the case of pSIC, HD C-NOMA can outperform FD C-NOMA in the high SNR regime.

[7]The contributions of this chapter are presented in the following papers:

1. V. Singh, V. Bankey, and P. K. Upadhyay "Underlay cognitive hybrid satellite-terrestrial networks with cooperative-NOMA,"in *Proc. IEEE Wireless Communications and Networking Conference (WCNC)*, Seoul, South Korea, May 2020, pp. 1-6.
2. V. Singh and P. K. Upadhyay, "Exploiting FD/HD cooperative-NOMA in underlay cognitive hybrid satellite-terrestrial networks," *IEEE Transactions on Cognitive Communication and Networking*, Jun. 2021, doi:10.1109/TCCN.2021.3089164.

- In Chapter 6[8], we explore the performance of an underlay CHSTN constituting a primary satellite source with its multiple terrestrial PRs and two NOMA secondary terrestrial users exchanging their information with the help of a HD DF-based secondary relay. We demonstrate there exists an inevitable IUI due to the NOMA scheme, which poses a detrimental impact on the performance of the secondary network. Hence, to achieve the improved performance and subsequently the low latency requirements, the wireless content caching is employed, whereby the relay can store the most popular contents of both the NOMA users. Hereby, exploiting the mutual interference between primary and secondary networks, and the realistic assumption of NOMA-based ipSIC, we analyze the performance of CHSTN for the schemes viz., CF TWR-NOMA and CA TWR-NOMA, in terms of OP, throughput, and average transmission time. Also, we examine the asymptotic OP behaviour at a high SNR to assess the achievable diversity orders. We manifest that zero diversity order results for both the schemes due to unavoidable IUI. However, one can visualize the remarkable performance improvements for CA TWR-NOMA scheme over its CF TWR-NOMA counterpart, owing to the reduced IUI and the efficient utilization of available spectrum resources.

Finally, in Chapter 7, we draw the conclusions from the work in this thesis and provide the possible future directions. Besides, the proofs of useful theorems/lemmas are relegated into the appendices.

[8]The contributions of this chapter are presented in the following paper:

1. V. Singh and P. K. Upadhyay, "Exploiting cache-free/cache-aided TWR-NOMA in cognitive hybrid satellite-terrestrial networks," *IEEE Transactions on Vehicular Technology*, under review.

CHAPTER 2

OVERLAY MULTIUSER COGNITIVE HYBRID SATELLITE-TERRESTRIAL NETWORKS

HSTNs have received significant research interest over the past few years. This is owing to their providing obliquities coverage and uninterrupted data connectivity. On the other hand, CR technology has been appeared as a prominent solution for alleviating the spectrum under-utilization problem in HSTNs [33]. Thus far, the majority of existing works on CHSTNs have focused on the performance analysis using underlay paradigm [18]-[20]. Particularly, in an underlay model [34], the power at the SU is constrained to satisfy the interference power criterion towards the PU. Whereas, in an overlay model, the SU helps in the transmission of the PU's signal on a priority basis through cooperative relaying, and in return, it gets an opportunity for spectrum access [35]. Therefore, overlay model does not impose tight restriction on transmit power of the SU. In this regard, various aspects of cooperative and cognitive HSTNs have been considered in [36]. In [21], authors have considered the overlay scenario by considering multiple secondary relays, however, by assuming single PU. Nevertheless, future satellite communication systems are required to satisfy a large number of PUs by providing high information transfer rate at a reasonable cost and QoS. Although few works have examined the multiuser spectrum sharing schemes [37]-[40], they are intended for terrestrial systems under homogeneous Nakagami-m or Rayleigh fading channels. However, for a hybrid satellite-terrestrial system, performance analysis of such multiuser spectrum sharing schemes over heterogeneous fading channels has not been done so far. It is worth pointing that such analysis postures new mathematical intricacies because of complicated channel modelling and optimal scheduling of multiple PUs with involved correlation due to a common satellite-relay link.

Inspired by the above discussion, in this chapter, we examine an overlay multiuser hybrid satellite-terrestrial spectrum sharing (OMHSTSS) system. Herein, we consider a downlink communication scenario where a primary satellite communicates with one of the best selected terrestrial users with the cooperation of a secondary network comprising a single transmitter-receiver pair on the ground. The ST can act as an AF relay for the primary satellite communications and share the spectrum for its own transmission. Relying on the overlay paradigm, the ST splits its power in such a way that some of its available power is used to relay the signal from the satellite and the rest is used to transmit its own signal. Particularly, our main contributions can be outlined as follows:

- We propose an OMHSTSS system where opportunistic selection criterion for the best satellite user is designed by exploiting both the direct and relay links in an optimal manner. The underlying PU selection strategy is based on satisfying the criterion of minimal OP for the primary network, and eventually, getting an opportunity for secondary spectrum access. For this, we first characterize the E-E SNRs over the hybrid channels.

- By considering the shadowed-Rician fading model for the satellite links and the Nakagami-m fading model for the terrestrial links, we proficiently derive the closed-form expressions of the OP for the primary and secondary networks. Hereby, we discuss the power allocation policy to explore more opportunities for the secondary spectrum access.

- We further derive the asymptotic behaviour of the OP expressions to delve into the diversity performance of the primary and secondary networks. In addition, we consider both heavy shadowing (HS) and average shadowing (AS) scenarios for the satellite links to provide more insight into the system performance.

The rest of this chapter is organized as follows. In Section 2.1, we elaborate the OMHSTSS system by deriving the E-E SNRs over hybrid channels. We characterize the hybrid channels and analyze the outage performance of the primary network in Section 2.2. The performance of the secondary network is investigated in Section 2.3. Section 2.4 illustrates the numerical and simulation results, and finally, summary of the chapter is presented in Section 2.5.

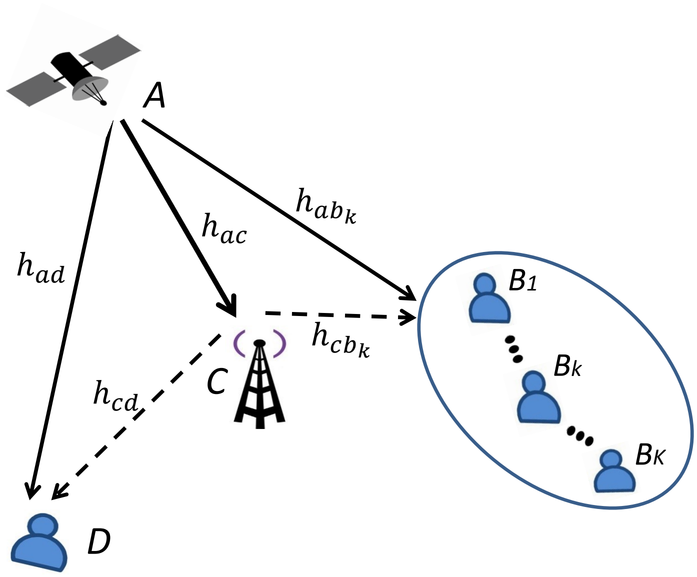

Figure 2.1: OMHSTSS system model. Ist phase (→) & IInd phase (- - →) transmissions.

2.1 System Descriptions

As illustrated in Fig. 2.1, we consider an OMHSTSS system wherein a primary satellite network and a secondary terrestrial network coexist over the same spectrum. Primary satellite A wants to communicate with one out of other K PUs $\{B_k\}_{k=1}^{K}$ and the ST node C is seeking the spectrum access opportunities to establish the communication with its intended secondary receiver (SR) D. Hereby, ST employs AF-based relay cooperation towards assisting the primary transmission, and in exchange, it can share the spectrum with primary satellite source to transmit its own signal to node D. The channel coefficients corresponding to the various links $A \to B_k$, $A \to C$, $A \to D$, $C \to B_k$, and $C \to D$ are represented by h_{ab_k}, h_{ac}, h_{ad}, h_{cb_k}, and h_{cd} respectively. The effect of an additive white Gaussian noise (AWGN) with mean zero and variance σ^2 is considered at all the receiving nodes.

Hereby, with the aid of an AF relay cooperation, the E-E communication occurs in two time phases. For this, a PU is appropriately selected (say B_k) based on some criterion which will be disclosed in the subsequent section. During the first phase of the information transfer, satellite A transmits an information signal x_a (obeying $\mathbb{E}[|x_a|^2] = 1$) to B_k which is simultaneously being received by the secondary nodes

C and D. Accordingly, the signals received at B_k, C, and D can be expressed as

$$y_{ai} = \sqrt{P_a} h_{ai} x_a + n_{ai}, \tag{2.1}$$

where $i \in \{b_k, c, d\}$, P_a denotes the transmission power at node A, and the term n_{ai} represents the AWGN. During the second phase, the node C first uses the AF relaying technique to forward the primary signal y_{ac} to node B_k, and at the same time, it intends to transmit its information signal x_c to node D. For this simultaneous transmission, the node C uses some power allocation policy and splits its transmit power P_c for superimposing the signals x_c and y_{ac} to generate a combined signal which can be given as

$$z_c = \sqrt{\mu P_c} \frac{y_{ac}}{\sqrt{|y_{ac}|^2}} + \sqrt{(1-\mu) P_c} x_c, \tag{2.2}$$

where $\mu \in (0,1)$ represents the power allocation factor. Thus, the signals received at the respective nodes B_k and D, represented by y_{cb_k} and y_{cd} , from C can be written as

$$y_{cj} = h_{cj} z_c + n_{cj}, \tag{2.3}$$

where $j \in \{b_k, d\}$ and n_{cj} is the AWGN. As such, the E-E SNR at B_k via direct link can be given as

$$\Lambda_{ab_k} = \eta_a |h_{ab_k}|^2, \tag{2.4}$$

whereas, via relay link, it can be expressed as

$$\Lambda_{acb_k} = \frac{\mu \Lambda_{ac} \Lambda_{cb_k}}{(1-\mu)\Lambda_{ac}\Lambda_{cb_k} + \Lambda_{ac} + \Lambda_{cb_k} + 1}, \tag{2.5}$$

where $\Lambda_{ac} = \eta_a |h_{ac}|^2$ with $\eta_a = \frac{P_a}{\sigma^2}$ and $\Lambda_{cb_k} = \eta_c |h_{cb_k}|^2$ with $\eta_c = \frac{P_c}{\sigma^2}$. From (2.3), it is apparent that the signal received at node D includes a component x_a from primary signal which creates an interference for the SR. This interference can be further successfully cancelled out by considering an assumption that the primary signal received at node D in the first transmission phase is decoded properly [35].

Thus, the E-E SNR at D can be expressed as

$$\Lambda_{acd} = \frac{(1-\mu)\Lambda_{cd}(\Lambda_{ac}+1)}{\mu\Lambda_{cd}+\Lambda_{ac}+1}, \tag{2.6}$$

where $\Lambda_{cd} = \eta_c|h_{cd}|^2$.

2.2 Outage Performance of Primary Network

When the achievable rates of the users are decided by their QoS, the OP is an essential measure for analyzing the performance. It can be defined as the probability that instantaneous SNR at receiver falls below a certain threshold γ_{th}, i.e.,

$$P_{\text{out}}(\gamma_{\text{th}}) = \Pr\big[\Lambda < \gamma_{\text{th}}\big]. \tag{2.7}$$

In this section, we analyze the performance of the primary network by deriving analytical expressions for OP. We examine the OP with or without spectrum sharing while considering the existence of a potential direct ($A \to B_k$) link. Further, we assess the diversity order by deriving the asymptotic OP expression. Moreover, we evaluate the effective value of power allocation factor μ for spectrum sharing between primary and secondary networks. For subsequent performance analysis, we first characterize the statistics for underlying hybrid channels.

2.2.1 Statistical Characterizations for Channels

Considering the shadowed-Rician fading for the pertinent satellite links, the probability density function (PDF) of the channel gains $|h_{ai}|^2$, for $i \in \{b_k, c, d\}$, can be obtained as [4]

$$f_{|h_{ai}|^2}(x) = \alpha_i\, \mathrm{e}^{-\beta_i x}\, {}_1F_1\left(m_{ai}; 1; \delta_i x\right),\ x \geq 0, \tag{2.8}$$

where $\alpha_i = (2\flat_{ai}m_{ai}/(2\flat_{ai}m_{ai}+\Omega_{ai}))^{m_{ai}}/2\flat_{ai}$, $\beta_i = 1/2\flat_{ai}$, $\delta_i = \Omega_{ai}/(2\flat_{ai})(2\flat_{ai}m_{ai}+\Omega_{ai})$ with $2\flat_{ai}$ and Ω_{ai} be the respective average powers of the multipath components and line-of-sight (LoS), and m_{ai} denotes fading severity parameter. For the arbitrary integer value of the fading severity parameters, we first simplify the term ${}_1F_1\left(m_{ai}; 1; \delta_i x\right)$ in (2.8), and thereby, express the PDF of $\Lambda_{ai} = \eta_a|h_{ai}|^2$ as [5]

$$f_{\Lambda_{ai}}(x) = \alpha_i \sum_{\kappa=0}^{m_{ai}-1} \frac{\zeta(\kappa)}{(\eta_a)^{\kappa+1}} x^{\kappa} \mathrm{e}^{-\left(\frac{\beta_i-\delta_i}{\eta_a}\right)x}. \tag{2.9}$$

Herein, $\zeta(\kappa) = (-1)^{\kappa}(1-m_{ai})_{\kappa}\delta_i^{\kappa}/(\kappa!)^2$. As such, the cumulative distribution function (CDF) $F_{\Lambda_{ai}}(x)$ can be derived by performing the integration of the PDF in (2.9) using [41, eq. 3.351.2] as

$$F_{\Lambda_{ai}}(x) = 1 - \alpha_i \sum_{\kappa=0}^{m_{ai}-1} \frac{\zeta(\kappa)}{(\eta_a)^{\kappa+1}} \sum_{p=0}^{\kappa} \frac{\kappa!}{p!} \left(\frac{\beta_i - \delta_i}{\eta_a}\right)^{-(\kappa+1-p)} x^p \mathrm{e}^{-\left(\frac{\beta_i-\delta_i}{\eta_a}\right)x}. \tag{2.10}$$

Since we consider Nakagami-m fading channels for the terrestrial links of the considered network, the channel gains $|h_{cj}|^2$, for $j \in \{b_k, d\}$, are assumed to follow the Gamma distribution with average power Ω_{cj} and fading severity parameter m_{cj}. Hence, the PDF and CDF of $\Lambda_{cj} = \eta_c|h_{cj}|^2$ can be given, respectively, as

$$f_{\Lambda_{cj}}(x) = \left(\frac{m_{cj}}{\Omega_{cj}\eta_c}\right)^{m_{cj}} \frac{x^{m_{cj}-1}}{\Gamma(m_{cj})} \mathrm{e}^{-\frac{m_{cj}}{\Omega_{cj}\eta_c}x} \tag{2.11}$$

and

$$F_{\Lambda_{cj}}(x) = \frac{1}{\Gamma(m_{cj})} \Upsilon\left(m_{cj}, \frac{m_{cj}}{\Omega_{cj}\eta_c}x\right). \tag{2.12}$$

Hereafter, we use $Y_{ac} = |h_{ac}|^2$ and $Y_{cb_k} = |h_{cb_k}|^2$ for notational simplicity. Also, as in previous works [5], [42], we follow independent and identically distributed (i.i.d.) channels towards the multiple PUs by considering that they are clustered relatively close together. Thus, for convenience, we omit the index k from all the notations of the pertaining channel parameters in the succeeding sections.

2.2.2 Direct Satellite Transmission Only

Let us consider the case of DS transmission (DST) only where a best user is being selected. In this case, the OP of primary network for a threshold rate R_p is given by

$$P_{\text{out}}^{\text{DST}}(R_p) = \Pr\left[\log_2\left(1 + \max_{k\in\{1,\ldots,K\}} \Lambda_{ab_k}\right) < R_p\right], \tag{2.13}$$

where to minimize the OP, we have used the selection criteria based on maximizing Λ_{ab_k}. As such, (2.13) can be further expressed as

$$P_{\text{out}}^{\text{DST}}(R_p) = \prod_{k=1}^{K} F_{\Lambda_{ab_k}}(\gamma_p'), \tag{2.14}$$

where $\gamma_p' = 2^{R_p} - 1$. From here, the OP can be evaluated using (2.10). Further, to obtain the asymptotic OP, (2.14) can be approximated at high SNR as

$$P_{\text{out}}^{\text{DST}}(R_p) \underset{\eta_a \to \infty}{\approx} \left[\frac{\alpha_b}{\eta_a}\gamma_p'\right]^K. \tag{2.15}$$

It can be clearly seen from (2.15) that the achievable diversity order is K irrespective of the fading severity parameter m_{ab}.

2.2.3 Spectrum Sharing with DST

Let us now consider the case when spectrum sharing is allowed and the DST also exists. Hereby, we utilize the maximal-ratio combining (MRC) between (2.4) and (2.5) with best PU selection. The best PU will be selected based on minimizing the OP of the primary network. Consequently, the OP for primary network in OMHSTSS system for a threshold rate R_p can be expressed as

$$\begin{aligned} P_{\text{out}}(R_p) &= \Pr\left[\frac{1}{2}\log_2\left(1 + \max_{k \in \{1,\ldots,K\}} (\Lambda_{ab_k} + \Lambda_{acb_k})\right) < R_p\right] \\ &= \Pr\left[\max_{k \in \{1,\ldots,K\}} \Lambda_{(k)} < \gamma_p\right], \end{aligned} \tag{2.16}$$

where $\Lambda_{(k)} = \Lambda_{ab_k} + \Lambda_{acb_k}$ and $\gamma_p = 2^{2R_p} - 1$. To solve (2.16) further, order statistics can not be applied directly as in the earlier case. Since $\{\Lambda_{(k)}\}_{k=1}^K$ include a common term Y_{ac}, this makes the random variables $\{\Lambda_{(k)}\}_{k=1}^K$ correlated. Hence, to proceed further, we find the K-th order statistic, which is conditioned on $Y_{ac} = u$, to represent

$$P_{\text{out}}(R_p) = \int_0^\infty \left[F_{\Lambda_{(k)}}(\gamma_p|u)\right]^K f_{Y_{ac}}(u)du. \tag{2.17}$$

Hereby, to solve (2.17), we need to evaluate the conditional CDF $F_{\Lambda_{(k)}}(\gamma_p|u)$, which can be expressed as

$$F_{\Lambda_{(k)}}(\gamma_p|u) = \Pr\left[(\Lambda_{ab_k} + \Lambda_{acb_k}) < \gamma_p|u\right] = \int_0^{\gamma_p}\int_0^{\gamma_p - y} f_{\Lambda_{acb_k}}(\varphi|u) f_{\Lambda_{ab_k}}(y) d\varphi dy. \tag{2.18}$$

Now, from (2.18), we first compute the CDF $F_{\Lambda_{acb_k}}(\varphi|u)$, which can be written as

$$F_{\Lambda_{acb_k}}(\varphi|u) = \Pr\left[\Lambda_{acb_k} < \varphi|u\right] = 1 - \Pr\left[\Lambda_{acb_k} > \varphi|u\right]. \tag{2.19}$$

To evaluate (2.19), we can represent the SNR expression for Λ_{acb_k} from (2.5), after some manipulations, as

$$\Lambda_{acb_k} = \frac{1}{\left(\frac{1-\mu}{\mu}\right) + \frac{1}{\mu\Lambda_{ac}\Lambda_{cb_k}}\left(\Lambda_{ac} + \Lambda_{cb_k} + 1\right)}. \tag{2.20}$$

Further, (2.20) can be approximated at high SNR regime as

$$\Lambda_{acb_k} \approx \frac{1}{\xi + \frac{1}{\mu}\left(\frac{1}{\Lambda_{ac}} + \frac{1}{\Lambda_{cb_k}}\right)}, \tag{2.21}$$

where $\xi = \frac{1-\mu}{\mu}$. Now, making use of the harmonic mean approximation for a minimum of two positive numbers [42], (2.21) can be written as

$$\Lambda_{acb_k} \approx \frac{1}{\xi + \frac{1}{\mu}\frac{1}{\min(\Lambda_{ac}, \Lambda_{cb_k})}}. \tag{2.22}$$

Note that although the approximation in (2.22) is based on a high SNR assumption, it leads to quite accurate results in entire range of operating SNR as illustrated in Section 2.4. Hereby, on inserting (2.22) into (2.19), and after performing some manipulations, (2.19) can be modified as

$$F_{\Lambda_{acb_k}}(\varphi|u) \approx 1 - \Pr\left[\mu\left(\frac{1}{\varphi} - \xi\right)\min(\Lambda_{ac}, \Lambda_{cb_k}) > 1|u\right], \tag{2.23}$$

which can be further expressed as

$$F_{\Lambda_{acb_k}}(\varphi|u) \approx \begin{cases} \Pr\left[\varsigma(\varphi)\min(\Lambda_{ac}, \Lambda_{cb_k}) < 1|u\right], \text{for } \xi < \frac{1}{\varphi}, \\ 1, \qquad\qquad\qquad\qquad\qquad\qquad \text{otherwise}, \end{cases} \tag{2.24}$$

where $\varsigma(\varphi) = \mu\left(\frac{1}{\varphi} - \xi\right)$. Consequently, the required CDF can be deduced as

$$F_{\Lambda_{acb_k}}(\varphi|u) \approx \begin{cases} 1, & \text{for } \eta_a\varsigma(\varphi)u < 1, \\ \Pr\left[\eta_c\varsigma(\varphi)Y_{cb_k} < 1\right], & \text{for } \eta_a\varsigma(\varphi)u > 1. \end{cases} \tag{2.25}$$

Even utilizing the above CDF expression in (2.18), it is still troublesome to obtain a closed-form solution. Therefore, with the help of a M-step staircase approximation approach [43] for the involved triangular integral region in (2.18), the conditional

CDF can be expressed as

$$F_{\Lambda_{(k)}}(\gamma_p|u) \approx \sum_{i=0}^{M-1}\left\{F_{\Lambda_{ab_k}}\left(\frac{i+1}{M}\gamma_p\right) - F_{\Lambda_{ab_k}}\left(\frac{i}{M}\gamma_p\right)\right\}F_{\Lambda_{acb_k}}\left(\frac{M-i}{M}\gamma_p|u\right). \tag{2.26}$$

Now, using (2.25) into (2.26) and thereby exploiting the result into (2.17), one can find the OP expression $P_{\text{out}}(R_p)$. It can be observed from (2.26) that $F_{\Lambda_{(k)}}(\gamma_p|u)$ includes a series of $F_{\Lambda_{acb_k}}\left(\frac{M-i}{M}\gamma_p|u\right)$ that captures different values based on i-th index and range of u from (2.25). Hence, for solving the integration in (2.17), we consider the different ranges of u as

$$\begin{aligned} P_{\text{out}}(R_p) \approx & \int_0^{1/\eta_a\varsigma(\gamma_p/M)} \left[F_{\Lambda_{(k)}}(\gamma_p|u)\right]^K f_{Y_{ac}}(u)du \\ & + \sum_{\substack{j=1\\M\geq 2}}^{M-1} \int_{1/\eta_a\varsigma(j\gamma_p/M)}^{1/\eta_a\varsigma((j+1)\gamma_p/M)} \left[F_{\Lambda_{(k)}}(\gamma_p|u)\right]^K f_{Y_{ac}}(u)du \\ & + \int_{1/\eta_a\varsigma(\gamma_p)}^{\infty} \left[F_{\Lambda_{(k)}}(\gamma_p|u)\right]^K f_{Y_{ac}}(u)du. \end{aligned} \tag{2.27}$$

As it can be notified from (2.27) that each integral component is having different region of u for which the integrands will not remain same, it must be evaluated carefully. Hereby, invoking the result from (2.25) and (2.26), $P_{\text{out}}(R_p)$ in (2.27) can be expressed as

$$\begin{aligned} P_{\text{out}}(R_p) \approx & \left[\sum_{i=0}^{M-1}\left\{F_{\Lambda_{ab_k}}\left(\frac{i+1}{M}\gamma_p\right) - F_{\Lambda_{ab_k}}\left(\frac{i}{M}\gamma_p\right)\right\}\right]^K F_{Y_{ac}}\left(\frac{1}{\eta_a\varsigma\left(\frac{1}{M}\gamma_p\right)}\right) \\ & + \sum_{\substack{j=1\\M\geq 2}}^{M-1}\left[\sum_{i=0}^{M-j-1}\left\{F_{\Lambda_{ab_k}}\left(\frac{i+1}{M}\gamma_p\right) - F_{\Lambda_{ab_k}}\left(\frac{i}{M}\gamma_p\right)\right\}\right. \\ & \left. + \sum_{i=M-j}^{M-1}\left\{F_{\Lambda_{ab_k}}\left(\frac{i+1}{M}\gamma_p\right) - F_{\Lambda_{ab_k}}\left(\frac{i}{M}\gamma_p\right)\right\}F_{Y_{cb_k}}\left(\frac{1}{\eta_c\varsigma\left(\frac{M-i}{M}\gamma_p\right)}\right)\right]^K \\ & \times\left(F_{Y_{ac}}\left(\frac{1}{\eta_a\varsigma\left(\frac{j+1}{M}\gamma_p\right)}\right) - F_{Y_{ac}}\left(\frac{1}{\eta_a\varsigma\left(\frac{j}{M}\gamma_p\right)}\right)\right) \\ & + \left[\sum_{i=0}^{M-1}\left\{F_{\Lambda_{ab_k}}\left(\frac{i+1}{M}\gamma_p\right) - F_{\Lambda_{ab_k}}\left(\frac{i}{M}\gamma_p\right)\right\}F_{Y_{cb_k}}\left(\frac{1}{\eta_c\varsigma\left(\frac{M-i}{M}\gamma_p\right)}\right)\right]^K \\ & \times\left(1 - F_{Y_{ac}}\left(\frac{1}{\eta_a\varsigma(\gamma_p)}\right)\right). \end{aligned} \tag{2.28}$$

It is noteworthy that our derived OP expression is presented directly in terms of the CDFs $F_{\Lambda ab_k}(\cdot)$ and $F_{Y_{ij}}(\cdot)$, for $Y_{ij} \in \{Y_{ac}, Y_{cb_k}\}$. Therefore, our analytical model is generalized and can be used for various fading scenarios. For the considered shadowed-Rician fading for satellite links and Nakagami-m fading for terrestrial links, we insert the CDF expressions from (2.10) and (2.12) into (2.28) to obtain the desired OP expression.

Now, one can derive the expression of asymptotic OP for the primary network to provide insight on the achievable diversity order. In the high SNR regime ($\eta_a, \eta_c \to \infty$, with $\frac{\eta_a}{\eta_c}$ be a constant ratio), CDFs used in (2.10) and (2.12) can be approximated [42] as

$$F_{\Lambda_{ai}}(x) \approx \frac{\alpha_i}{\eta_a} x \text{ and } F_{\Lambda_{cj}}(x) \approx \frac{1}{\Gamma(m_{cj}+1)} \left(\frac{m_{cj} x}{\Omega_{cj} \eta_c} \right)^{m_{cj}}. \tag{2.29}$$

On inserting the above approximated CDF expressions into (2.28), an asymptotic OP can be expressed as

$$\begin{aligned} P_{\text{out}}^{\text{asy}}(R_p) \approx & \left[\sum_{i=0}^{M-1} \left\{ \frac{\alpha_b}{\eta_a} \frac{i+1}{M} \gamma_p - \frac{\alpha_b}{\eta_a} \frac{i}{M} \gamma_p \right\} \right]^K \frac{\alpha_c}{\eta_a \varsigma(\gamma_p/M)} \\ & + \sum_{\substack{j=1 \\ M \geq 2}}^{M-1} \left[\sum_{i=0}^{M-j-1} \left\{ \frac{\alpha_b}{\eta_a} \frac{i+1}{M} \gamma_p - \frac{\alpha_b}{\eta_a} \frac{i}{M} \gamma_p \right\} + \sum_{i=M-j}^{M-1} \left\{ \frac{\alpha_b}{\eta_a} \frac{i+1}{M} \gamma_p - \frac{\alpha_b}{\eta_a} \frac{i}{M} \gamma_p \right\} \right. \\ & \qquad \left. \times \frac{1}{\Gamma(m_{cb}+1)} \left(\frac{m_{cb}}{\Omega_{cb} \eta_c \varsigma\left(\frac{M-i}{M}\gamma_p\right)} \right)^{m_{cb}} \right]^K \\ & \quad \times \left(\frac{\alpha_c}{\eta_a \varsigma\left(\frac{j+1}{M}\gamma_p\right)} - \frac{\alpha_c}{\eta_a \varsigma\left(\frac{j}{M}\gamma_p\right)} \right) \\ & + \left[\sum_{i=0}^{M-1} \left\{ \frac{\alpha_b}{\eta_a} \frac{i+1}{M} \gamma_p - \frac{\alpha_b}{\eta_a} \frac{i}{M} \gamma_p \right\} \frac{1}{\Gamma(m_{cb}+1)} \left(\frac{m_{cb}}{\Omega_{cb} \eta_c \varsigma\left(\frac{M-i}{M}\gamma_p\right)} \right)^{m_{cb}} \right]^K \\ & \quad \times \left(1 - \frac{\alpha_c}{\eta_a \varsigma(\gamma_p)} \right). \end{aligned} \tag{2.30}$$

From (2.30), it can be inferred that the diversity order of the primary network is $K + \min(1, m_{cb}K)$ and it does not depend on the fading severity parameters of the satellite links.

2.2.4 Power Allocation factor μ for Spectrum Sharing

Regarding the power allocation strategy for the ST, we need to obtain an appropriate value of μ while satisfying the QoS criterion of the primary network. From

(2.24), the condition $\xi < \frac{1}{\varphi}$ can be re-expressed as $\varphi < \mu'$, where $\mu' = \frac{1}{\xi}$ or $\frac{\mu}{1-\mu}$. Hereby, for a certain threshold γ_p, the allowable range of power allocation factor of the primary network can be calculated as $\frac{\gamma_p}{1+\gamma_p} < \mu < 1$. Relying on the imposed QoS constraint, the ST can decide the effective value of μ so that the OP of primary network in OMHSTSS system lies below or at most equal to that for DST only scheme. Accordingly, the value of μ is obtained numerically depending on the following condition [35]

$$P_{\text{out}}(R_p) \leq P_{\text{out}}^{\text{DST}}(R_p). \tag{2.31}$$

Moreover, a lesser value of μ can provide more spectrum sharing opportunities towards the secondary network.

2.3 Outage Performance of Secondary Network

Considering a threshold rate R_s, the OP of the secondary network can be given by

$$P_{\text{out}}(R_s) = \Pr\left[\frac{1}{2}\log_2(1 + \Lambda_{acd}) < R_s\right], \tag{2.32}$$

which can be expressed using (2.6) and performing some manipulations as

$$P_{\text{out}}(R_s) = \Pr\left[\frac{\mu\Lambda_{cd}(\Lambda_{ac} + 1)}{\mu\Lambda_{cd} + \Lambda_{ac} + 1} < \mu'\gamma_s\right], \tag{2.33}$$

where $\gamma_s = 2^{2R_s} - 1$. Hereby, to evaluate the $P_{\text{out}}(R_s)$, we first make use of the bound $\frac{XY}{X+Y} < \min(X, Y)$ [44] to approximate (2.33) as

$$P_{\text{out}}(R_s) \approx \Pr\big[\min(\mu\Lambda_{cd}, \left(\Lambda_{ac} + 1)\right) < \mu'\gamma_s\big]. \tag{2.34}$$

The evaluation of (2.34) requires the CDF of $\Lambda_{ac}+1$, which can be obtained by applying the transformation of variables as

$$F_{\Lambda_{ac}+1}(x) = \begin{cases} 0, & \text{if } x < 1, \\ F_{\Lambda_{ac}}(x-1), & \text{if } x \geq 1. \end{cases} \tag{2.35}$$

Since the CDF in (2.35) is not continuous for $x \in [0, \infty)$, the OP in (2.34) can be expressed as

$$P_{\text{out}}(R_s) \approx \begin{cases} F_{\mu\Lambda_{cd}}(\mu'\gamma_s), & \text{if } \gamma_s < \frac{1}{\mu'}, \\ F_{\Lambda_{ac}}(\mu'\gamma_s - 1) + F_{\mu\Lambda_{cd}}(\mu'\gamma_s) & \\ -F_{\Lambda_{ac}}(\mu'\gamma_s - 1)F_{\mu\Lambda_{cd}}(\mu'\gamma_s), & \text{if } \gamma_s \geq \frac{1}{\mu'}, \end{cases} \tag{2.36}$$

where the CDF of $\mu\Lambda_{cd}$ can be determined using (2.12) as

$$F_{\mu\Lambda_{cd}}(x) = F_{\mu\Lambda_{cd}}\left(\frac{x}{\mu}\right) = \frac{1}{\Gamma(m_{cd})}\Upsilon\left(m_{cd}, \frac{m_{cd}}{\Omega_{cd}\eta_c\mu}x\right). \tag{2.37}$$

Note that our derived OP expression for secondary network is also generalized as in the earlier case of primary network. To further delve into the system performance, we evaluate the asymptotic OP expression at high SNR regime ($\eta_c \to \infty$), using the approximated CDF expressions given in (2.29), as

$$P_{\text{out}}(R_s) \approx \begin{cases} \frac{1}{\Gamma(m_{cd}+1)}\left(\frac{m_{cd}\mu'\gamma_s}{\Omega_{cd}\mu\eta_c}\right)^{m_{cd}}, & \text{if } \gamma_s < \frac{1}{\mu'}, \\ \frac{\alpha_c}{\eta_c}(\mu'\gamma_s - 1) + \frac{1}{\Gamma(m_{cd}+1)}\left(\frac{m_{cd}\mu'\gamma_s}{\Omega_{cd}\mu\eta_c}\right)^{m_{cd}} & \\ -\Bigg[\frac{\alpha_c}{\eta_c}(\mu'\gamma_s - 1) & \\ \quad \times\frac{1}{\Gamma(m_{cd}+1)}\left(\frac{m_{cd}\mu'\gamma_s}{\Omega_{cd}\mu\eta_c}\right)^{m_{cd}}\Bigg], & \text{if } \gamma_s \geq \frac{1}{\mu'}. \end{cases} \tag{2.38}$$

From (2.38), it can be inferred that the secondary network achieves a diversity order of $\min(1, m_{cd})$ for the high rate requirements while, for the low rate requirements, the diversity order can be decided mainly through parameter m_{cd}.

2.4 Numerical and Simulation Results

In this section, numerical and simulation results are presented to elucidate the effect of important parameters on the performance of OMHSTSS system. For this, we set $R_p = 0.5$ bps/Hz so that $\gamma_p' = 0.414$, $\gamma_p = 1$, $\Omega_{cb} = 1$, $m_{cb} = 1$, and $\eta_a = \eta_c = \eta$ as the SNR. The satellite links are subject to HS and AS with their parameters as presented in TABLE 2.1 [45]. Further, we set $M = 50$ for making the relative approximation error [43] negligible.

Fig. 2.2 demonstrates the OP versus SNR curves for primary network by setting $\mu = 0.70$. Particularly, analytical and asymptotic OP curves are drawn for HS and

Table 2.1: Satellite Link Parameters [with $i \in \{b, c, d\}$].

Shadowing	m_{ai}	$\flat_{ai}$	Ω_{ai}
HS	2	0.063	0.0005
AS	5	0.251	0.279

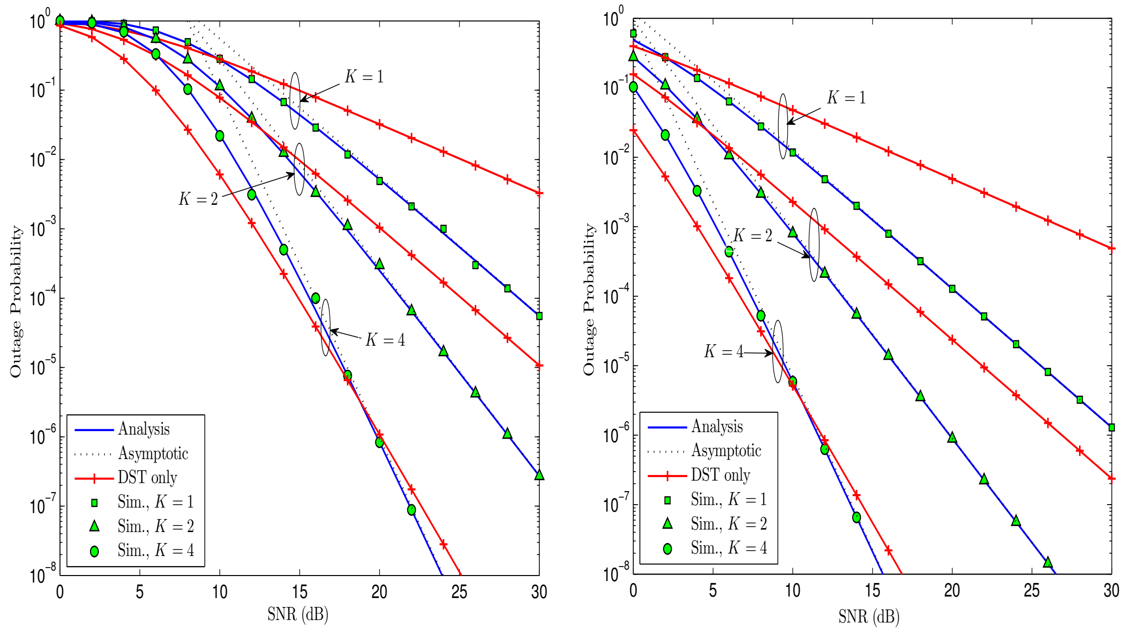

(a) (b)

Figure 2.2: OP versus SNR curves for primary network (a) Under HS; (b) Under AS.

AS scenarios, and by seeing the curves, it can be inferred that both the curves are well matched with the exact simulation results at medium to high SNR regime. For the comparison purpose, the OP curves for the DST scheme are also plotted. Hereby, it can be verified that considered OMHSTSS can outperform the DST only scheme, especially in mid-to-high SNR regimes. Since OMHSTSS requires two times more bandwidth as required in DST scheme, the target SNR threshold (for a fixed value of target rate) relatively increases for the OMHSTSS system, which degrades its performance in the low SNR regime. However, one can manifest the diversity advantage in the mid-to-high SNR regime, and accordingly, OMHSTSS outperforms the DST scheme without spectrum sharing. Further, it can be notified that outage performance is significantly improved due to exploitation of diversity by considering the case of multiuser scheduling. Moreover, the resulting diversity order of $K + \min(1, m_{cb}K)$ can be validated using the pertinent curves.

Fig. 2.3 depicts the desirable values of the spectrum sharing factor μ for the considered network under HS and AS scenarios. Relying on the spectrum sharing

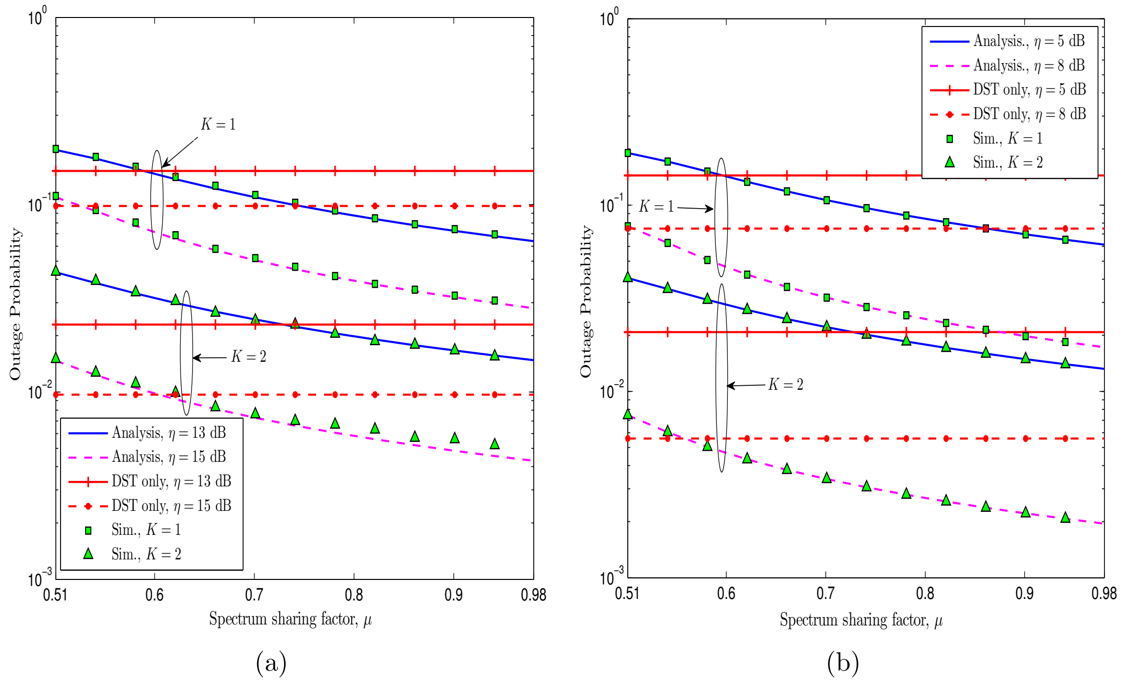

Figure 2.3: OP versus μ curves for primary network (a) Under HS; (b) Under AS.

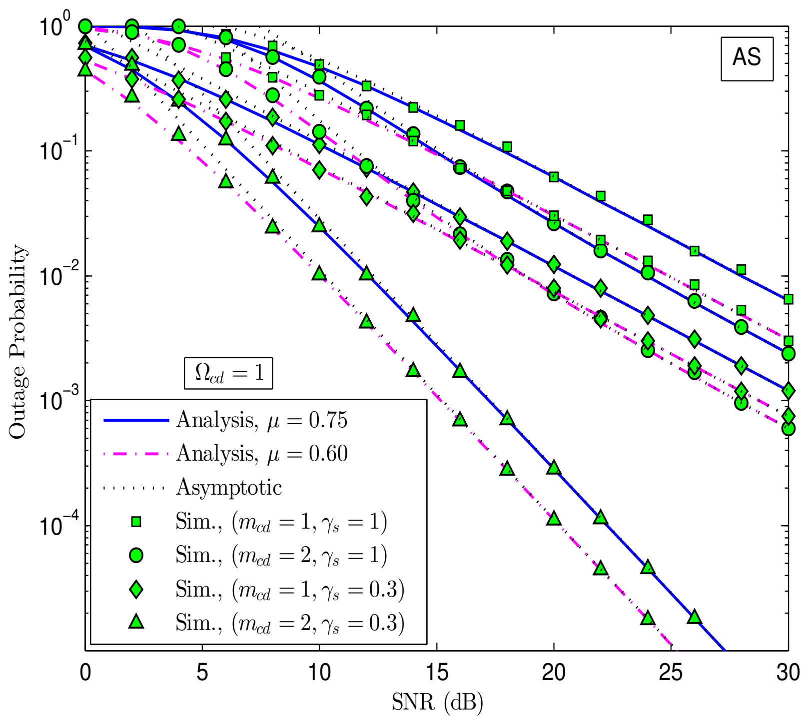

Figure 2.4: OP versus SNR curves for secondary network.

condition given in Section 2.2.4, we obtain the critical value of μ (say μ^*) at the intersecting points between the curves of OMHSTSS and DST only schemes. For $\gamma_p = 1$, the acceptable limit of μ^* is $0.5 < \mu^* < 1$ which is based on the condition $\frac{\gamma_p}{1+\gamma_p} < \mu < 1$. Thus, all the OP curves exhibit unity value for $\mu \leq 0.5$ and this could drive the system into outage. Moreover, for a given SNR, it can be observed that μ^* increases with an increase of K. This is owing to the better performance of DST only scheme as compared to OMHSTSS in a low SNR regime. However, as SNR increases, one can realize the decrease in the values of μ^* which suggests that the spectrum sharing is possible for these cases. On the contrary, it improves the outage performance of the secondary network by providing more power for spectrum access.

Fig. 2.4 illustrates the OP versus SNR curves for the secondary network. Here, we set two values $\mu = 0.75$ and $\mu = 0.60$, while $\Omega_{cd} = 1$, to obtain the analytical and asymptotic curves using the derived OP expressions from Section 2.3. One can clearly observe that the analytical and asymptotic curves are in agreement with the exact simulation results in the medium to high SNR regime. Analyzing the respective curves, one can also verify the diversity order. For instance, at high rate requirement i.e., $\gamma_s = 1$, it can be seen that the diversity order is unity irrespective of the fading parameter m_{cd}. In contrast, at low rate requirement, i.e., $\gamma_s = 0.3$, the diversity order solely depends on the fading severity parameter m_{cd}. Moreover, one can see the improvement in OP performance of secondary network while decreasing the values of μ.

2.5 Summary

In this chapter, we have analyzed the performance of an OMHSTSS system in which a secondary terrestrial network competes for spectrum access with a primary satellite network. Unlike other existing works, we have considered the multiuser downlink scenario where opportunistic selection criterion for the best satellite user is designed by exploiting both the direct and the relay links in an optimal manner. We assessed the overall system's performance by deriving the closed-form expressions of outage probability for both primary and secondary networks and highlighting the corresponding achievable diversity orders. We also provided useful insights on power splitting factor to explore additional spectrum sharing opportunities towards the secondary network.

CHAPTER 3

IMPACT OF HARDWARE IMPERFECTION IN OVERLAY COGNITIVE HYBRID SATELLITE-TERRESTRIAL NETWORKS WITH ADAPTIVE RELAYING PROTOCOL

HSTNs have emerged as an attractive way of achieving high throughput with a broad coverage area. In HSTNs, satellite communications and terrestrial networks are integrated to provide useful services in broadcasting, navigation, and disaster relief. Recently, CR technology has become prominent for HSTNs to improve the spectrum utilization efficiency [10], [46]. Various research works have been conducted for such wireless networks, namely CHSTNs, by using two prevalent spectrum sharing approaches viz., underlay [18], [47], [48] and overlay [21]. Particularly, the authors in [18] analyzed the performance of the secondary terrestrial network under a stringent interference temperature constraint imposed by the primary satellite user. A robust secure beamforming issue of 5G cellular system operating at millimeter-wave frequency, while coexisting with a primary satellite network was studied in [47]. The authors in [48] investigated the secure communication of the CHSTN with software-defined architecture, where a gateway is acting as a control center to provide an advantage of the resource allocation for the wireless systems. As such, in above-mentioned works, the interference management between primary and secondary networks would be a major concern to maintain the QoS of the primary system. On this front, the authors in [21] studied an overlay model in which the terrestrial SUs can get the spectrum access by providing relay cooperation to the primary satellite communication on a priority basis. Such an overlay approach offers a promising solution for CHSTNs, as it can facilitate the network connectivity through inherent cooperative relaying, especially when the primary DS link gets blocked due to the masking effect. So far, the overlay model for CHSTNs has not been explored fully and the existing works are relied upon the traditional FR strategy which compels the secondary transceiver to relay the primary signal even when the primary DS link is strong enough.

Moreover, the aforementioned works on CHSTNs have assumed an ideal hardware transceiver for the spectrum sharing network nodes. Note that, in practice, the RF transceivers may experience hardware distortions due to phase noises, I/Q imbalances, and amplifier non-linearities [23], [49], [50]. These distortions may cause a deleterious impact on the performance of CHSTNs owing to the involvement of low-cost user devices. This is prominent in overlay spectrum sharing scheme because the secondary transceiver requires the use of inexpensive hardware components in order to keep the expenditures manageable for operators. Even though the effect of the hardware distortions can be partially mitigated through appropriate calibration or compensation techniques, there still remains a residual distortion [23]. This has been treated as an aggregate effect from many HIs and modeled by an additive distortion noise in [49]. Although few recent works [51], [52] have studied the impact of such HIs on the performance of CHSTNs, they focussed particularly on the underlay spectrum sharing scheme.

Fueled by the above discussion, in this chapter, we analyze the performance of an overlay CHSTN (OCHSTN) by employing an AR protocol while considering that all the user nodes in the network are inflicted by HIs. Specifically, we consider a downlink communication scenario where a secondary terrestrial network seeks the spectrum access opportunities in exchange for the cooperation towards the primary satellite network. The proposed AR protocol invokes secondary relay cooperation adaptively, relying upon the limited feedback mechanism from the PU. Thereby, it efficiently utilizes the available degrees-of-freedom to improve the OCHSTN performance even in the presence of HIs. Note that the performance analysis of such a system postures new mathematical intricacies because of the involved joint effects of overlay paradigm's sophisticated signal processing and hardware distortions over a heterogeneous fading channel environment. In summary, the major contributions of the chapter are given as follows:

- We propose an AR protocol for the OCHSTN and compare its performance with the traditional FR protocol. We observe that the proposed AR protocol can substantially improve the network performance over the FR protocol and hence can be more useful in practice, especially, to counteract on the effects of HIs.

- We comprehensively analyze AAF and ADF operations by deriving the OP expressions of primary and secondary networks in the presence of HIs. We showcase that the ADF relaying is more robust and resilient to HIs when compared with AAF relaying.

- Further, based on the derived OP expressions for the primary network, we identify two important ceiling effects, namely, RCC and DLC, and highlight their impacts on the system performance. We also provide the tolerable limit of HIs level for the given rate requirements.

- Based on the overlay approach, we provide guidelines to decide the value of power allocation factor for the effective secondary network cooperation.

The rest of the chapter is structured as follows. In Section 3.1, we illustrate the system model and derive the E-E signal-to-noise-and-distortion ratios (SNDRs) over heterogeneous fading channels. In Section 3.2, we analyze the performance of primary network by deriving the expressions of the OP for AAF and ADF strategies. Section 3.3 analyzes the outage performance of the secondary network while discussing the impact of ceiling effects into the system performance. Section 3.4 investigates the robustness of AAF and ADF relaying against the HIs. Numerical and simulations results are depicted in Section 3.5, and finally, summary of the chapter is presented in Section 3.6.

3.1 System Descriptions

In this section, we describe the considered system model while deriving the E-E SNDR expressions for the AF and DF relaying. Moreover, we discuss in detail the proposed AR protocol for the considered system.

3.1.1 System Model

As shown in Fig. 3.1, we consider an OCHSTN where a terrestrial ST node C seeks access to the spectrum of primary satellite system in order to communicate with its own SR node D. However, ST is allowed to access the spectrum based on the condition that it should assist the primary transmission between satellite A and its terrestrial user B[1]. We assume that a DS link exists between nodes A and B. All the network nodes are assumed to be equipped with a single antenna

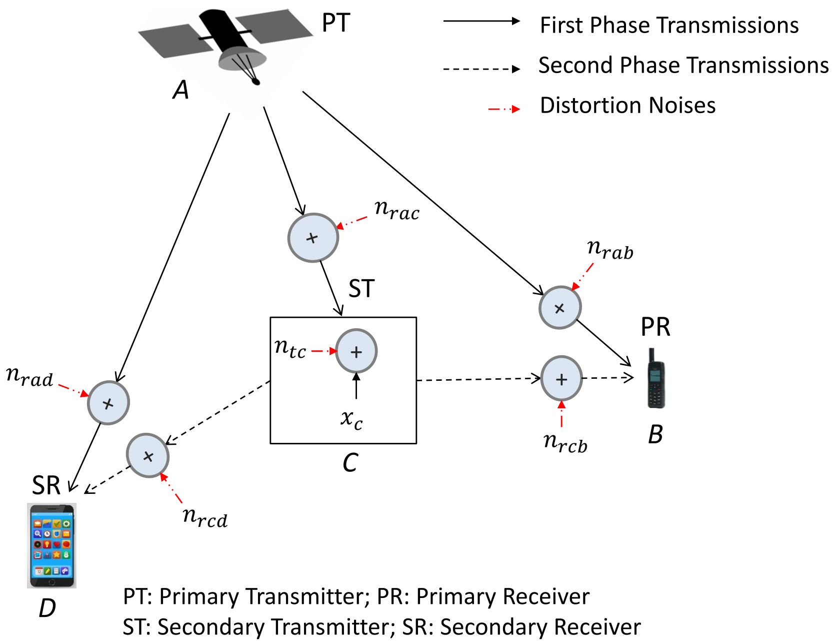

Figure 3.1: OCHSTN System model.

device. Further, all the user devices are assumed to have less-expensive (low-quality) transceiver components, and hence, they are more prone to HIs. Herein, we consider two schemes of secondary cooperation, i.e., AF-based and DF-based relaying at the ST node C to forward the primary's data by employing an AR protocol. The various channel coefficients pertaining to the satellite links $A \rightarrow B$, $A \rightarrow C$, and $A \rightarrow D$ follow shadowed-Rician fading and are represented by h_{ab}, h_{ac}, and h_{ad}, respectively. The channel coefficients for terrestrial links $C \rightarrow B$ and $C \rightarrow D$ are denoted by h_{cb} and h_{cd}, respectively, and are assumed to follow Nakagami-m fading. The AWGN at all the receiving nodes is modeled as $\mathcal{CN}(0, \sigma^2)$.

3.1.2 SNDR Formulation

The overall communication in the considered OCHSTN follows a two-phase transmission process based on the proposed AR protocol. In the first phase, satellite A

[1]In a practical scenario, source A may represent a GEO satellite and node B could be a hand-held device as incorporated in DVB-SH service (in S-band) [7], whereas the secondary nodes C and D can represent femtocell users who generally do not have a dedicated spectrum for their communication [53]. Another prospective scenario may comprise a S/C band satellite system coexisting with secondary network representing a TV transmitter-receiver pair (in UHF/S band) [54]. In a futuristic system model, ST (relay) could be a low-power repeater which is located at the rooftop of a building or on an unmanned aerial vehicle in order to achieve coverage in urban areas where the satellite range is infeasible.

broadcasts an information signal x_a, complying $\mathbb{E}[|x_a|^2] = 1$, to B which is also being overheard by the secondary nodes C and D. Accordingly, the respective received signals at B, C, and D, denoted by y_{ab}, y_{ac}, and y_{ad}, can be written as

$$y_{ai} = \sqrt{P_a} h_{ai} x_a + n_{rai} + v_{ai}, \tag{3.1}$$

where $i \in \{b, c, d\}$, P_a denotes the transmit power at A, $n_{rai} \sim \mathcal{CN}(0, \lambda_{rai}^2 P_a |h_{ai}|^2)$ is the distortion noise induced in receive processing, with λ_{rai} being the level of impairment measured experimentally as error vector magnitude (EVM)[2], and v_{ai} is AWGN term. As such, the resultant SNDRs at B and C via DS links can be given, respectively, as

$$\Lambda_{ab}^{\mathrm{DS}} = \frac{\Lambda_{ab}}{\Lambda_{ab}\lambda_{rab}^2 + 1} \tag{3.2}$$

and

$$\Lambda_{ac}^{\mathrm{DS}} = \frac{\Lambda_{ac}}{\Lambda_{ac}\lambda_{rac}^2 + 1}, \tag{3.3}$$

where $\Lambda_{ab} = \eta_a |h_{ab}|^2$ and $\Lambda_{ac} = \eta_a |h_{ac}|^2$, with $\eta_a = \frac{P_a}{\sigma^2}$.

In what follows, we describe the two relaying operations and thereby obtain the corresponding expressions to SNDR.

AF Relaying

In the second phase of information exchange, node C amplifies the received primary signal y_{ac} with a gain $\mathcal{G}$ and superimposes it with its own information signal x_c to generate a combined signal z_c^{AF}. For this simultaneous transmission, ST node uses an omnidirectional antenna and splits its power P_c such that the fraction μP_c is used to forward the signal y_{ac} while the remaining portion $(1-\mu)P_c$ of the power is used to transmit the signal x_c, where the factor $\mu \in (0,1)$ represents the power allocation parameter. Thus, the signal transmitted by the ST node is given by

$$z_c^{\mathrm{AF}} = \sqrt{\mu P_c} \mathcal{G} y_{ac} + \sqrt{(1-\mu) P_c} x_c + n_{tc}, \tag{3.4}$$

[2] These EVMs can be defined as the ratio of distortion-to-signal magnitude, and can be obtained as given in [55].

where $n_{tc} \sim \mathcal{CN}(0, \lambda_{tc}^2 P_c)$ denotes the distortion noise in relay transmit processing, with λ_{tc} being the level of impairment. For amplification, the variable gain [56] can be expressed as $\mathcal{G} = \sqrt{\frac{1}{P_a|h_{ac}|^2+\lambda_{rac}^2 P_a|h_{ac}|^2+\sigma^2}}$. Thereafter, the respective received signals at nodes B and D can be denoted by y_{cb}^{AF} and y_{cd}^{AF}, being represented as

$$y_{cj}^{\text{AF}} = h_{cj} z_c^{\text{AF}} + n_{rcj} + v_{cj}, \tag{3.5}$$

where $j \in \{b, d\}$, $n_{rcj} \sim \mathcal{CN}(0, \lambda_{rcj}^2 P_c |h_{cj}|^2)$ is the distortion noise in receive processing, with λ_{rcj} being the level of impairment, and v_{cj} is the AWGN term. Hence, the SNDR at node B, via the relay link, can be expressed as

$$\Lambda_{acb} = \frac{\mu \Lambda_{ac} \Lambda_{cb}}{\tau_p \Lambda_{ac} \Lambda_{cb} + \varepsilon \Lambda_{ac} + \omega_p \Lambda_{cb} + 1}, \tag{3.6}$$

where $\Lambda_{cb} = \eta_c |h_{cb}|^2$ with $\eta_c = \frac{P_c}{\sigma^2}$, $\tau_p = (1-\mu) + \mu(\lambda_{rcb}^2 + \lambda_{tc}^2)(1+\lambda_{rac}^2) + \lambda_{rac}^2$, $\varepsilon = 1 + \lambda_{rac}^2$, and $\omega_p = 1 + \mu(\lambda_{tc}^2 + \lambda_{rcb}^2)$. From (3.1), it is clear that D overhears the primary signal in the first phase. As such, it may utilize this overheard signal to cancel the primary's interfering signal in the second phase [35]. Consequently, the E-E SNDR at D is obtained as

$$\Lambda_{acd} = \frac{(1-\mu)\Lambda_{cd}(\varepsilon \Lambda_{ac} + 1)}{\tau_s \Lambda_{ac} \Lambda_{cd} + \varepsilon \Lambda_{ac} + \omega_s \Lambda_{cd} + 1}, \tag{3.7}$$

where $\Lambda_{cd} = \eta_c |h_{cd}|^2$, $\tau_s = \mu \lambda_{rac}^2 + (1-\mu)(1+\lambda_{rac}^2)(\lambda_{tc}^2 + \lambda_{rcd}^2)$, and $\omega_s = \mu + (1-\mu)(\lambda_{tc}^2 + \lambda_{rcd}^2)$.

DF Relaying

Herein, after the signal reception in first transmission phase, node C employs DF-based relaying and attempts to decode the primary signal x_a. If decoding is successful, ST superimposes the decoded signal x_a and x_c to generate a combined signal z_c^{DF}. Thus, the signal transmitted by the ST node is given by

$$z_c^{\text{DF}} = \sqrt{\mu P_c} x_a + \sqrt{(1-\mu) P_c} x_c + n_{tc}. \tag{3.8}$$

Hereafter, the respective received signals at nodes B and D from C can be given by y_{cb}^{DF} and y_{cd}^{DF}, being represented as

$$y_{cj}^{\text{DF}} = h_{cj} z_c^{\text{DF}} + n_{rcj} + v_{cj}. \tag{3.9}$$

Further, the overall SNDR expressions at node B and D, based on (3.8) and (3.9), can be expressed, respectively, as

$$\Lambda_{e_p} = \frac{\mu\Lambda_{cb}}{\rho_p\Lambda_{cb} + 1} \tag{3.10}$$

and

$$\Lambda_{e_s} = \frac{(1-\mu)\Lambda_{cd}}{\rho_s\Lambda_{cd} + 1}, \tag{3.11}$$

where $\rho_p = (1-\mu) + \mu(\lambda_{tc}^2 + \lambda_{rcb}^2)$ and $\rho_s = (1-\mu)\lambda_{\mathrm{eq}}^2$ with $\lambda_{\mathrm{eq}}^2 = \lambda_{tc}^2 + \lambda_{rcd}^2$.

3.1.3 Proposed Adaptive Relaying Protocol

In this protocol, cooperative node C adaptively performs the relaying operation based on the decoding of the primary signal x_a at node B in the first phase of transmission. Specifically, depending on the success/failure of the direct primary's transmission ($A \to B$), the relaying cooperation from C is invoked. For this, the mutual information of the DST can be written as

$$\mathcal{I}_{ab} = \log_2\left(1 + \Lambda_{ab}^{\mathrm{DS}}\right). \tag{3.12}$$

If node B is able to successfully decode the information signal from node A, i.e., if $\mathcal{I}_{ab} \geq R_p$, where R_p is a target threshold rate, it sends an error-free one-bit feedback[3] to the cooperative node C indicating that the relaying cooperation is not needed. For this case, all the available power at ST can be utilized for the information transmission to its intended receiver D. Thereby, the performance of secondary network can be enhanced.

In the case of no cooperation, the signal transmitted by the ST node can be given by

$$z_c^{\mathrm{noc}} = \sqrt{P_c}x_c + n_{tc}. \tag{3.13}$$

[3]Hereby, it is assumed that the feedback/acknowledge time is negligible compared to the information processing time [57], [58]. Note that such feedback is to be sent on a separate low-bandwidth error-free channel and hence incurs negligible delay.

The signal thus received at node D from C can be given as

$$y_{cd}^{\text{noc}} = h_{cd} z_c^{\text{noc}} + n_{rcd} + v_{cd}. \tag{3.14}$$

Hereby, using (3.13) and (3.14), E-E SNDR expression at node D can be expressed as

$$\Lambda_{cd}^{\text{noc}} = \frac{\Lambda_{cd}}{\Lambda_{cd}\lambda_{\text{eq}}^2 + 1}. \tag{3.15}$$

On the other hand, if B is unable to decode the signal from A in the first phase, i.e., if $\mathcal{I}_{ab} < R_p$, it sends a negative feedback to C. Thus, the cooperation from ST is invoked and further information exchange operation follows either AF or DF relaying protocol. Moreover, for DF relaying, if the primary signal x_a could not be decoded at ST after the first transmission phase, ST can utilize all its available power to transmit the information to its own intended receiver. Hence, E-E SNDR expression at node D can be given by (3.15).

For the subsequent analysis, we refer the AR protocol based AF and DF relaying as AAF and ADF relaying, respectively. The proposed AR protocol can also be illustrated with the help of a flowchart as shown in Fig. 3.2. Some important terms used in the flowchart are explained as follows:

(i) DST- It is described for two feasible cases i.e., without spectrum sharing (in Section 3.2.2) and with spectrum sharing (in Section 3.2.3).

(ii) RCC- RCC effect is said to occur in the system when the relay ceases to cooperate with the primary communication due to undesired constraints on the threshold data rate γ_p. Hereby, the performance of the primary network solely depends on the DST only (described in Section 3.2.4).

(iii) DLC- After the occurrence of the RCC phenomenon, as γ_p exceeds some threshold, the overall primary system goes into outage and this phenomenon is referred to as DLC (described in Section 3.2.4).

Remark 3.1: The above proposed AR protocol may cost slightly more system expenses than FR. This can be, primarily, owing to the fact that the proposed AR protocol requires a limited feedback mechanism which, in turn, may induce slightly higher complexity. However, it is worthwhile to note that the benefits offered (as witnessed by the numerical results) by this scheme far outweigh its limitations

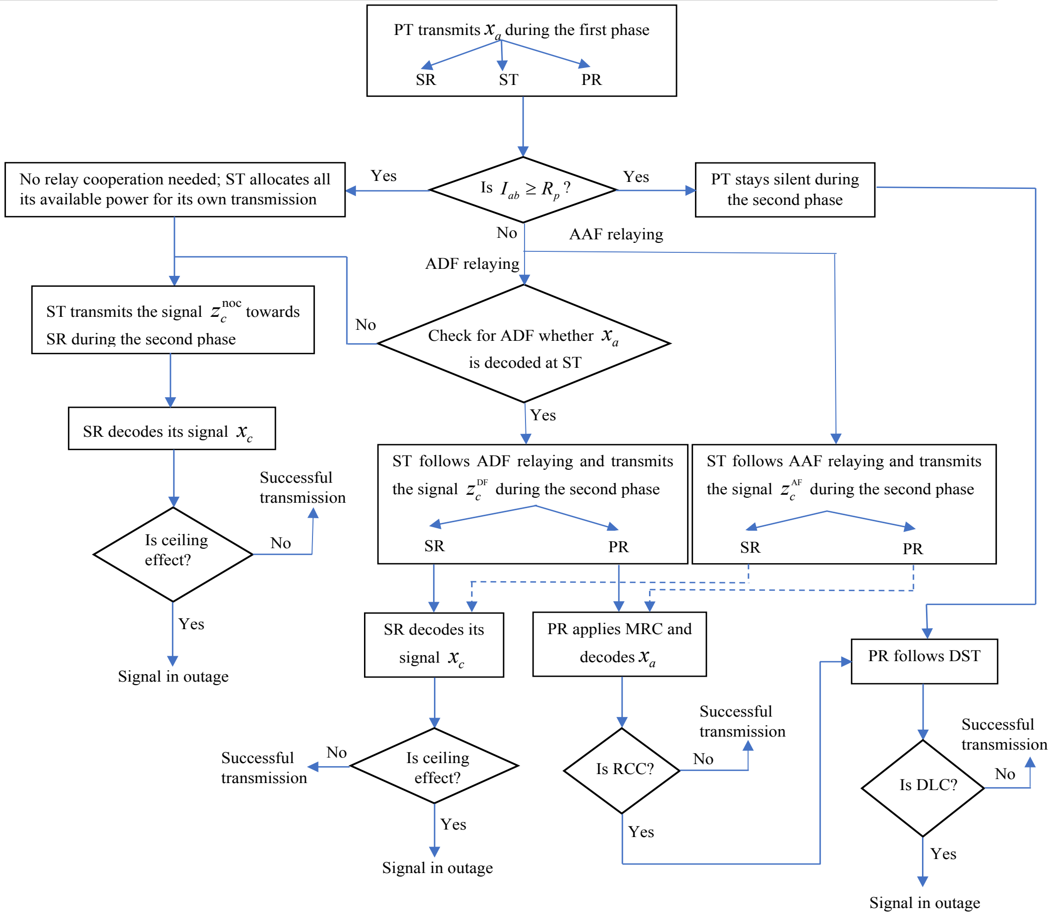

Figure 3.2: Flow chart for the proposed AR protocol.

and, therefore, AR protocol may be useful primarily for the applications where performance of the system is more important than the cost constraints. On the other hand, FR is a simpler scheme and may be preferable for the applications where cost of the system is of paramount importance.

3.2 Outage Performance of Primary Network

In this section, we derive the expressions for the OP of primary network for both AAF and ADF relaying strategies while considering the presence of a DS ($A \rightarrow B$) link. Further, we consider two cases of DST i.e., with or without spectrum sharing. For this, we first present the statistics of the underlying fading channels.

3.2.1 Statistical Characterization for Channels

Considering the satellite links under the shadowed-Rician fading model, the PDF of $|h_{ai}|^2$, $i \in \{b, c, d\}$, is given by [4], [5]

$$f_{|h_{ai}|^2}(x) = \alpha_i \, \mathrm{e}^{-\beta_i x} \, {}_1F_1 \left(m_{ai}; 1; \delta_i x \right), \;\; x \geq 0, \tag{3.16}$$

where $\alpha_i = (2\flat_{ai}m_{ai}/(2\flat_{ai}m_{ai}+\Omega_{ai}))^{m_{ai}}/2\flat_{ai}$, $\beta_i = 1/2\flat_{ai}$, $\delta_i = \Omega_{ai}/(2\flat_{ai})(2\flat_{ai}m_{ai} + \Omega_{ai})$, with Ω_{ai} and $2\flat_{ai}$ being the respective average powers of the LoS and multipath components, and m_{ai} is the fading severity parameter. For analytical tractability, we consider the integer value of the fading severity parameter [45], [52] in the subsequent analysis. As such, the respective PDF and CDF expressions of $\Lambda_{ai} = \eta_a|h_{ai}|^2$ can be expressed as [5]

$$f_{\Lambda_{ai}(x)} = \alpha_i \sum_{\kappa=0}^{m_{ai}-1} \frac{\zeta(\kappa)}{(\eta_a)^{\kappa+1}} x^{\kappa} \mathrm{e}^{-\left(\frac{\beta_i-\delta_i}{\eta_a}\right)x} \tag{3.17}$$

and

$$F_{\Lambda_{ai}}(x) = 1 - \alpha_i \sum_{\kappa=0}^{m_{ai}-1} \frac{\zeta(\kappa)}{(\eta_a)^{\kappa+1}} \sum_{p=0}^{\kappa} \frac{\kappa!}{p!} \left(\frac{\beta_i-\delta_i}{\eta_a}\right)^{-(\kappa+1-p)} x^p \mathrm{e}^{-\left(\frac{\beta_i-\delta_i}{\eta_a}\right)x}, \tag{3.18}$$

where $\zeta(\kappa) = (-1)^{\kappa}(1-m_{ai})_{\kappa}\delta_i^{\kappa}/(\kappa!)^2$.

Under Nakagami-m fading for the terrestrial links, the channel gain $|h_{cj}|^2$ is assumed to follow the Gamma distribution with the respective PDF and CDF expressions of $\Lambda_{cj} = \eta_c|h_{cj}|^2$, $j \in \{b, d\}$, can be given by

$$f_{\Lambda_{cj}}(x) = \left(\frac{m_{cj}}{\Omega_{cj}\eta_c}\right)^{m_{cj}} \frac{x^{m_{cj}-1}}{\Gamma(m_{cj})} \mathrm{e}^{-\frac{m_{cj}}{\Omega_{cj}\eta_c}x} \tag{3.19}$$

and

$$F_{\Lambda_{cj}}(x) = \frac{1}{\Gamma(m_{cj})} \Upsilon\left(m_{cj}, \frac{m_{cj}}{\Omega_{cj}\eta_c}x\right), \tag{3.20}$$

where Ω_{cj} is the average power and m_{cj} be the fading severity parameter.

3.2.2 DST with no Spectrum Sharing

Here, we consider that DST provides communication through the DS link only i.e., without allowing for the spectrum sharing. Basically, we analyze this scheme as a benchmark to compare with the performance of the considered OCHSTN. As such, considering a pre-defined target rate R_p, the OP of primary network using DST only can be given by

$$P_{\text{out}}^{\text{DS}}(R_p) = \Pr\left[\log_2\left(1 + \Lambda_{ab}^{\text{DS}}\right) < R_p\right]. \tag{3.21}$$

Hereby, (3.21) can be re-expressed as

$$P_{\text{out}}^{\text{DS}}(R_p) = \Pr\left[\Lambda_{ab}^{\text{DS}} < \gamma_p'\right] = F_{\Lambda_{ab}^{\text{DS}}}(\gamma_p'), \tag{3.22}$$

where $\gamma_p' = 2^{R_p} - 1$. Now, the CDF in (3.22) can be expressed using (3.2) as

$$F_{\Lambda_{ab}^{\text{DS}}}(\gamma_p') = \Pr\left[\Lambda_{ab} < \frac{\gamma_p'}{1 - \lambda_{rab}^2 \gamma_p'}\right]. \tag{3.23}$$

Further, $F_{\Lambda_{ab}^{\text{DS}}}(\gamma_p')$ in (3.23) can be evaluated, depending upon the condition on the threshold data rate γ_p', as

$$F_{\Lambda_{ab}^{\text{DS}}}(\gamma_p') = \begin{cases} F_{\Lambda_{ab}}\left(\frac{\gamma_p'}{1-\lambda_{rab}^2\gamma_p'}\right), & \text{if } \gamma_p' < \frac{1}{\lambda_{rab}^2}, \\ 1, & \text{if } \gamma_p' \geq \frac{1}{\lambda_{rab}^2}. \end{cases} \tag{3.24}$$

Thus, on invoking (3.18) into (3.24), the required OP can be computed.

3.2.3 DST with Spectrum Sharing

Enabling spectrum sharing in HSTNs has two main benefits. First, it provides network coverage even when the DS link is disrupted due to obstacles and shadowing, and second, it can accommodate additional SUs to improve the spectral efficiency. Herein, we analyze the performance of DST with spectrum sharing for OCHSTN considering AAF and ADF relaying schemes as follows:

AAF relaying

For a target rate R_p, OP of the primary network for AAF relaying can be expressed as

$$P_{\text{out}}^{\text{AF}}(R_p) = \Pr\left[\Lambda_{ab}^{\text{DS}} < \gamma_p',\ \Lambda_{ab}^{\text{DS}} + \Lambda_{acb} < \gamma_p\right], \tag{3.25}$$

where $\gamma_p = 2^{2R_p} - 1$. Further, $P_{\text{out}}^{\text{AF}}(R_p)$ in (3.25) can be expressed as

$$\begin{aligned} P_{\text{out}}^{\text{AF}}(R_p) &= \Pr\left[\Lambda_{ab}^{\text{DS}} < \min(\gamma_p - \Lambda_{acb}, \gamma_p')\right] \\ &= \underbrace{\Pr\left[\Lambda_{ab}^{\text{DS}} < \gamma_p',\ \gamma_p' < \gamma_p - \Lambda_{acb}\right]}_{I_1} \\ &\quad + \underbrace{\Pr\left[\Lambda_{ab}^{\text{DS}} < \gamma_p - \Lambda_{acb}, \gamma_p' \geq \gamma_p - \Lambda_{acb}\right]}_{I_2}. \end{aligned} \tag{3.26}$$

To derive the OP in (3.26), we need to evaluate the two probability terms I_1 and I_2. We first obtain the probability term I_1 as

$$I_1 = \Pr\big[\Lambda_{ab}^{\mathrm{DS}} < \gamma_p',\ \Lambda_{acb} < \gamma_p - \gamma_p')\big] = F_{\Lambda_{ab}^{\mathrm{DS}}}(\gamma_p')\ F_{\Lambda_{acb}}(\gamma_p - \gamma_p'), \tag{3.27}$$

where the last equality results from the statistical independence between the two events. Now, to evaluate (3.27), the required $F_{\Lambda_{acb}}(\cdot)$ is derived as follows in Theorem 1.

Theorem 1. *The CDF $F_{\Lambda_{acb}}(x)$ under hybrid satellite-terrestrial fading channels of OCHSTN can be given by*

$$F_{\Lambda_{acb}}(x) = \begin{cases} \psi_1(x), & \text{if } x < \frac{\mu}{\tau_p}, \\ 1, & \text{if } x \geq \frac{\mu}{\tau_p}, \end{cases} \tag{3.28}$$

where $\psi_1(x)$ is given as

$$\begin{aligned}\psi_1(x) = 1 - 2\alpha_c \sum_{\kappa=0}^{m_{ac}-1} \sum_{l=0}^{\kappa} \sum_{m=0}^{l} \sum_{g=0}^{m+m_{cb}-1} \frac{\zeta(\kappa)}{(\eta_a)^{\kappa+1}} \frac{\kappa!}{l!} M^{-(\kappa+1-l)} N^{m_{cb}} \frac{1}{\Gamma(m_{cb})} \binom{l}{m} \\ \times e^{-\left(\frac{(\omega_p M + N\varepsilon)x}{\theta_x}\right)} \left(\frac{M\varepsilon x^2 + Mx\theta_x}{N}\right)^{\frac{g-l+1}{2}} \frac{x^l \omega_p^m (\varepsilon x)^{m+m_{cb}-1-g}}{\theta_x^{m+m_{cb}}} \\ \times \binom{m+m_{cb}-1}{g} \mathcal{K}_{g-l+1}\left(\frac{2}{\theta_x}\sqrt{(M\varepsilon x^2 + Mx\theta_x)N}\right),\end{aligned} \tag{3.29}$$

with $\theta_x = \mu - \tau_p x$ (for $\theta_x > 0, x < \frac{\mu}{\tau_p}$), $M = \frac{\beta_c - \delta_c}{\eta_a}$, and $N = \frac{m_{cb}}{\Omega_{cb}\eta_c}$.

Proof. See Appendix A. ∎

It should be pointed out that the condition $x < \frac{\mu}{\tau_p}$ in (3.28) makes the ST's cooperation helpful, otherwise the CDF $F_{\Lambda_{acb}}(x)$ takes on unity value. This phenomenon is referred to as RCC, and hereby, the performance of the primary network solely depends on the DST scheme. After substituting (3.24) and (3.28) into (3.27), I_1 can be obtained.

Next, we evaluate the term I_2 according to

$$I_2 = \Pr\big[\Lambda_{acb} < \gamma_p - \Lambda_{ab}^{\mathrm{DS}},\ \Lambda_{acb} \geq \gamma_p - \gamma_p')\big] = \int_{\gamma_p-\gamma_p'}^{\gamma_p - y} \int_0^{\gamma_p} f_{\Lambda_{acb}}(x) f_{\Lambda_{ab}^{\mathrm{DS}}}(y) dx dy, \tag{3.30}$$

which can be further simplified as

$$I_2 = \int_0^{\gamma_p} F_{\Lambda_{acb}}(\gamma_p - y) f_{\Lambda_{ab}^{\mathrm{DS}}}(y) dy - \int_0^{\gamma_p} F_{\Lambda_{acb}}(\gamma_p - \gamma_p') f_{\Lambda_{ab}^{\mathrm{DS}}}(y) dy. \tag{3.31}$$

On using the expression of $F_{\Lambda_{acb}}(x)$ into (3.31), it is extremely hard to get a closed-form solution for I_2. Hence, using an L-step staircase approximation approach [43] for the included triangular integral region in (3.31), I_2 can be expressed as

$$I_2 \approx \sum_{i=0}^{L-1} \left\{ F_{\Lambda_{ab}^{\mathrm{DS}}}\left(\frac{i+1}{L}\gamma_p\right) - F_{\Lambda_{ab}^{\mathrm{DS}}}\left(\frac{i}{L}\gamma_p\right) \right\} F_{\Lambda_{acb}}\left(\frac{L-i}{L}\gamma_p\right) - F_{\Lambda_{acb}}(\gamma_p - \gamma_p') F_{\Lambda_{ab}^{\mathrm{DS}}}(\gamma_p). \tag{3.32}$$

Finally, inserting I_1 and I_2 into (3.26), the analytical expression of $P_{\mathrm{out}}^{\mathrm{AF}}(R_p)$ can be obtained. As such, depending upon the conditions on the threshold γ_p, $P_{\mathrm{out}}^{\mathrm{AF}}(R_p)$ can be expressed, using (3.24) and (3.28), for the following cases:

- When $\gamma_p < \frac{\mu}{\tau_p}$,

$$\begin{aligned} P_{\mathrm{out}}^{\mathrm{AF}}(R_p) &\triangleq P_1(R_p) \\ &= F_{\Lambda_{ab}^{\mathrm{DS}}}(\gamma_p') F_{\Lambda_{acb}}(\gamma_p - \gamma_p') - F_{\Lambda_{acb}}(\gamma_p - \gamma_p') F_{\Lambda_{ab}^{\mathrm{DS}}}(\gamma_p) \\ &+ \sum_{i=0}^{L-1} \left\{ F_{\Lambda_{ab}^{\mathrm{DS}}}\left(\frac{i+1}{L}\gamma_p\right) - F_{\Lambda_{ab}^{\mathrm{DS}}}\left(\frac{i}{L}\gamma_p\right) \right\} F_{\Lambda_{acb}}\left(\frac{L-i}{L}\gamma_p\right). \end{aligned} \tag{3.33}$$

- When $\frac{\mu}{\tau_p} \leq \gamma_p < \frac{\mu}{\tau_p} + \gamma_p'$,

$$\begin{aligned} P_{\mathrm{out}}^{\mathrm{AF}}(R_p) &\triangleq P_2(R_p) \\ &= F_{\Lambda_{ab}^{\mathrm{DS}}}(\gamma_p') F_{\Lambda_{acb}}(\gamma_p - \gamma_p') - F_{\Lambda_{acb}}(\gamma_p - \gamma_p') F_{\Lambda_{ab}^{\mathrm{DS}}}(\gamma_p) \\ &+ \sum_{i=0}^{L-1} \left\{ F_{\Lambda_{ab}^{\mathrm{DS}}}\left(\frac{i+1}{L}\gamma_p\right) - F_{\Lambda_{ab}^{\mathrm{DS}}}\left(\frac{i}{L}\gamma_p\right) \right\}. \end{aligned} \tag{3.34}$$

- When $\frac{\mu}{\tau_p} + \gamma_p' \leq \gamma_p < \frac{1}{\lambda_{rab}^2}$,

$$\begin{aligned} P_{\mathrm{out}}^{\mathrm{AF}}(R_p) &\triangleq P_3(R_p) \\ &= F_{\Lambda_{ab}^{\mathrm{DS}}}(\gamma_p') - F_{\Lambda_{ab}^{\mathrm{DS}}}(\gamma_p) + \sum_{i=0}^{L-1} \left\{ F_{\Lambda_{ab}^{\mathrm{DS}}}\left(\frac{i+1}{L}\gamma_p\right) - F_{\Lambda_{ab}^{\mathrm{DS}}}\left(\frac{i}{L}\gamma_p\right) \right\}. \end{aligned} \tag{3.35}$$

- When $\gamma_p \geq \frac{1}{\lambda_{rab}^2}$,

$$P_{\text{out}}^{\text{AF}}(R_p) = 1. \tag{3.36}$$

Hereby, based on the above cases, the OP of the primary network for AAF relaying can be expressed as

$$P_{\text{out}}^{\text{AF}}(R_p) = \begin{cases} P_1(R_p), & \text{if } \gamma_p < \frac{\mu}{\tau_p}, \\ P_2(R_p), & \text{if } \frac{\mu}{\tau_p} \leq \gamma_p < \frac{\mu}{\tau_p} + \gamma_p', \\ P_3(R_p), & \text{if } \frac{\mu}{\tau_p} + \gamma_p' \leq \gamma_p < \frac{1}{\lambda_{rab}^2}, \\ 1, & \text{otherwise .} \end{cases} \tag{3.37}$$

ADF relaying

For a target rate R_p, the OP of the primary network for ADF relaying can be written as

$$P_{\text{out}}^{\text{DF}}(R_p) = \Pr\big[\Lambda_{ab}^{\text{DS}} < \gamma_p',\ \Lambda_{ac}^{\text{DS}} < \gamma_p\big] + \Pr\big[\Lambda_{ab}^{\text{DS}} < \gamma_p',\ \Lambda_{ac}^{\text{DS}} \geq \gamma_p,\ \Lambda_{ab}^{\text{DS}} + \Lambda_{e_p} < \gamma_p\big], \tag{3.38}$$

which can be further expressed as

$$P_{\text{out}}^{\text{DF}}(R_p) = \underbrace{F_{\Lambda_{ab}^{\text{DS}}}(\gamma_p') F_{\Lambda_{ac}^{\text{DS}}}(\gamma_p)}_{I_3} + \underbrace{\bar{F}_{\Lambda_{ac}^{\text{DS}}}(\gamma_p) \Pr\big[\Lambda_{ab}^{\text{DS}} < \gamma_p', \Lambda_{ab}^{\text{DS}} + \Lambda_{e_p} < \gamma_p\big]}_{I_4}, \tag{3.39}$$

where $\bar{F}_{\Lambda_{ac}^{\text{DS}}}(\cdot) = 1 - F_{\Lambda_{ac}^{\text{DS}}}(\cdot)$ denotes the complementary CDF. Hereby, solution of (3.39) needs evaluation of two probability terms I_3 and I_4. For I_3, it requires the CDFs $F_{\Lambda_{ab}^{\text{DS}}}(\gamma_p')$ and $F_{\Lambda_{ac}^{\text{DS}}}(\gamma_p)$, which can be obtained by following the steps in Section 3.2.2. Further, I_4 can be evaluated in a similar way as (3.26), and is expressed as

$$\begin{aligned} I_4 &\approx \Pr\big[\Lambda_{ab}^{\text{DS}} < \min(\gamma_p - \Lambda_{e_p},\ \gamma_p')\big] \bar{F}_{\Lambda_{ac}^{\text{DS}}}(\gamma_p) \\ &= \Bigg[F_{\Lambda_{ab}^{\text{DS}}}(\gamma_p')\ F_{\Lambda_{e_p}}(\gamma_p - \gamma_p') + \sum_{i=0}^{L-1} \left\{ F_{\Lambda_{ab}^{\text{DS}}}\left(\frac{i+1}{L}\gamma_p\right) - F_{\Lambda_{ab}^{\text{DS}}}\left(\frac{i}{L}\gamma_p\right) \right\} \\ &\qquad \times F_{\Lambda_{e_p}}\left(\frac{L-i}{L}\gamma_p\right)\Bigg] \bar{F}_{\Lambda_{ac}^{\text{DS}}}(\gamma_p). \end{aligned} \tag{3.40}$$

To simplify (3.40), we need to evaluate the CDF $F_{\Lambda_{ep}}(\gamma_p - \gamma_p')$ which can be expressed, using (3.10), as

$$F_{\Lambda_{ep}}(x) = \begin{cases} F_{\Lambda_{cb}}\left(\frac{x}{\mu - \rho_p x}\right), & \text{if } x < \frac{\mu}{\rho_p}, \\ 1, & \text{if } x \geq \frac{\mu}{\rho_p}. \end{cases} \tag{3.41}$$

On inserting the expressions of $F_{\Lambda_{ep}}(\cdot)$, $F_{\Lambda_{ab}^{\mathrm{DS}}}(\cdot)$, and $\bar{F}_{\Lambda_{ac}^{\mathrm{DS}}}(\cdot)$ into (3.40), I_4 can be evaluated. Thus, on using the expressions for I_3 and I_4 into (3.39), $P_{\mathrm{out}}^{\mathrm{DF}}(R_p)$ can be evaluated. Finally, considering $\lambda_{rab} = \lambda_{rac} = \lambda$ (without loss of generality) and applying the conditions on threshold γ_p, $P_{\mathrm{out}}^{\mathrm{DF}}(R_p)$ can be expressed, using (3.24) and (3.41), for the following cases:

- When $\gamma_p < \frac{\mu}{\rho_p}$,

$$\begin{aligned} P_{\mathrm{out}}^{\mathrm{DF}}(R_p) &\triangleq P_4(R_p) \\ &= \Bigg[F_{\Lambda_{ab}^{\mathrm{DS}}}(\gamma_p')F_{\Lambda_{ep}}(\gamma_p - \gamma_p') + \sum_{i=0}^{L-1}\left\{F_{\Lambda_{ab}^{\mathrm{DS}}}\left(\frac{i+1}{L}\gamma_p\right) - F_{\Lambda_{ab}^{\mathrm{DS}}}\left(\frac{i}{L}\gamma_p\right)\right\} \\ &\qquad \times F_{\Lambda_{ep}}\left(\frac{L-i}{L}\gamma_p\right)\Bigg]\bar{F}_{\Lambda_{ac}^{\mathrm{DS}}}(\gamma_p) \\ &+ F_{\Lambda_{ab}^{\mathrm{DS}}}(\gamma_p')F_{\Lambda_{ac}^{\mathrm{DS}}}(\gamma_p). \end{aligned} \tag{3.42}$$

- When $\frac{\mu}{\rho_p} \leq \gamma_p < \frac{\mu}{\rho_p} + \gamma_p'$,

$$\begin{aligned} P_{\mathrm{out}}^{\mathrm{DF}}(R_p) &\triangleq P_5(R_p) \\ &= \Bigg[F_{\Lambda_{ab}^{\mathrm{DS}}}(\gamma_p')F_{\Lambda_{ep}}(\gamma_p - \gamma_p') + \sum_{i=0}^{L-1}\left\{F_{\Lambda_{ab}^{\mathrm{DS}}}\left(\frac{i+1}{L}\gamma_p\right) - F_{\Lambda_{ab}^{\mathrm{DS}}}\left(\frac{i}{L}\gamma_p\right)\right\}\Bigg]\bar{F}_{\Lambda_{ac}^{\mathrm{DS}}}(\gamma_p) \\ &+ F_{\Lambda_{ab}^{\mathrm{DS}}}(\gamma_p')F_{\Lambda_{ac}^{\mathrm{DS}}}(\gamma_p). \end{aligned} \tag{3.43}$$

- When $\frac{\mu}{\rho_p} + \gamma_p' \leq \gamma_p < \frac{1}{\lambda^2}$,

$$\begin{aligned} P_{\mathrm{out}}^{\mathrm{DF}}(R_p) &\triangleq P_6(R_p) \\ &= \left[F_{\Lambda_{ab}^{\mathrm{DS}}}(\gamma_p') + \sum_{i=0}^{L-1}\left\{F_{\Lambda_{ab}^{\mathrm{DS}}}\left(\frac{i+1}{L}\gamma_p\right) - F_{\Lambda_{ab}^{\mathrm{DS}}}\left(\frac{i}{L}\gamma_p\right)\right\}\right)\Bigg]\bar{F}_{\Lambda_{ac}^{\mathrm{DS}}}(\gamma_p) \\ &+ F_{\Lambda_{ab}^{\mathrm{DS}}}(\gamma_p')F_{\Lambda_{ac}^{\mathrm{DS}}}(\gamma_p). \end{aligned} \tag{3.44}$$

- When $\gamma_p \geq \frac{1}{\lambda^2}$,

$$P_{\text{out}}^{\text{DF}}(R_p) = 1. \tag{3.45}$$

Hence, based on the above cases, the OP of the primary network for ADF relaying can be expressed as

$$P_{\text{out}}^{\text{DF}}(R_p) = \begin{cases} P_4(R_p), & \text{if } \gamma_p < \frac{\mu}{\rho_p}, \\ P_5(R_p), & \text{if } \frac{\mu}{\rho_p} \leq \gamma_p < \frac{\mu}{\rho_p} + \gamma_p', \\ P_6(R_p), & \text{if } \frac{\mu}{\rho_p} + \gamma_p' \leq \gamma_p < \frac{1}{\lambda^2}, \\ 1, & \text{otherwise }. \end{cases} \tag{3.46}$$

3.2.4 Ceiling Effects

In this subsection, we specifically discuss the two types of ceiling effects, viz., RCC and DLC which are induced by the HIs. The RCC effect is said to occur in the system when the relay ceases to cooperate with the primary communication due to undesired constraints on the threshold data rate γ_p. RCC can be observed from (3.37) and (3.46), wherein, the first and second terms account for both relay cooperation and DST, and the third term arises from the DST. Thus, when γ_p approaches the thresholds $\frac{\mu}{\tau_p} + \gamma_p'$ and $\frac{\mu}{\rho_p} + \gamma_p'$ for AAF and ADF relaying, respectively, relay cooperation ceases and the performance of the primary network thereafter, solely depends on the DST scheme. Further, as γ_p exceeds the thresholds $\frac{1}{\lambda_{rab}^2}$ and $\frac{1}{\lambda^2}$ for AAF and ADF relaying, respectively, the overall primary system goes into outage and this phenomenon is referred to as DLC. Hereby, based on these observations, one can define the tolerable limit of HIs level for the given rate requirement while designing a practical OCHSTN. For instance, from (3.37) and (3.46), it would be desirable to have impairment level such that $\lambda_{rab}^2 < \frac{1}{\gamma_p}$ and $\lambda^2 < \frac{1}{\gamma_p}$.

3.2.5 A Guideline to Decide Power Allocation Factor μ

To fulfill the QoS criteria for the primary network, it becomes important to select a power allocation strategy for ST. For this, we have to acquire a suitable value of μ which in turn controls the power at ST to guarantee the QoS for the primary network. Specifically, from (3.28) and (3.41), analyzing the conditions $x < \frac{\mu}{\tau_p}$ and $x < \frac{\mu}{\rho_p}$, the allowable range of μ for a certain threshold γ_p can be calculated as

$\frac{\gamma_p(1+\lambda_{rac}^2)}{1+\gamma_p-(\lambda_{rcb}^2+\lambda_{tc}^2)(1+\lambda_{rac}^2)\gamma_p} < \mu < 1$ and $\frac{\gamma_p}{1+\gamma_p-\gamma_p(\lambda_{tc}^2+\lambda_{rcb}^2)} < \mu < 1$ for AAF and ADF relaying, respectively. Note that a smaller value of μ can provide more power allocation for the secondary network and hence ascertain more spectrum sharing opportunities.

3.3 Outage Performance of Secondary Network

In this section, we derive the expressions of the OP for the secondary network under both AAF and ADF relaying schemes.

3.3.1 AAF Relaying

For a given target rate R_s, the OP of the secondary network for AAF relaying can be written as

$$P_{\text{out}}^{\text{AF}}(R_s) = \Pr\big[\Lambda_{ab}^{\text{DS}} \geq \gamma_p',\ \Lambda_{cd}^{\text{noc}} < \gamma_s\big] + \Pr\big[\Lambda_{ab}^{\text{DS}} < \gamma_p',\ \Lambda_{acd} < \gamma_s\big], \tag{3.47}$$

where $\gamma_s = 2^{2R_s} - 1$. Further, $P_{\text{out}}^{\text{AF}}(R_s)$ in (3.47) can be expressed as

$$P_{\text{out}}^{\text{AF}}(R_s) = \bar{F}_{\Lambda_{ab}^{\text{DS}}}(\gamma_p')\, F_{\Lambda_{cd}}^{\text{noc}}(\gamma_s) + F_{\Lambda_{ab}^{\text{DS}}}(\gamma_p')\, F_{\Lambda_{acd}}(\gamma_s). \tag{3.48}$$

Hereby, we first evaluate $F_{\Lambda_{acd}}(\cdot)$ as given in the following theorem.

Theorem 2. *The CDF $F_{\Lambda_{acd}}(x)$ under hybrid satellite-terrestrial channels of OCHSTN can be given by*

$$F_{\Lambda_{acd}}(x) = \begin{cases} \psi_2(x), & \text{if } x < \frac{\varepsilon(1-\mu)}{\tau_s}, \\ 1, & \text{if } x \geq \frac{\varepsilon(1-\mu)}{\tau_s}, \end{cases} \tag{3.49}$$

where $\psi_2(x)$ is given as

$$\begin{aligned}\psi_2(x) = 1 - 2\alpha_c \sum_{\kappa=0}^{m_{ac}-1}\sum_{l=0}^{\kappa}\sum_{m=0}^{l}\sum_{g=0}^{m+m_{cd}-1} \frac{\zeta(\kappa)}{(\eta_a)^{\kappa+1}}\frac{\kappa!}{l!}\frac{x^{l-m}(\phi_{1x})^m(\varepsilon x)^{m+m_{cd}-1-g}}{(\phi_{2x})^{m+m_{cd}}} \\ \times \binom{l}{m}\binom{m+m_{cd}-1}{g}\mathbb{N}^{m_{cd}} e^{-\left(\frac{M\phi_{1x}+\mathbb{N}\varepsilon x}{\phi_{2x}}\right)}\left(\frac{M\phi_{1x}\varepsilon x + Mx\phi_{2x}}{\mathbb{N}}\right)^{\frac{g-l+1}{2}} \\ \times \frac{1}{\Gamma(m_{cd})}M^{-(\kappa+1-l)}\mathcal{K}_{g-l+1}\left(\frac{2}{\phi_{2x}}\sqrt{(M\phi_{1x}\varepsilon x + Mx\phi_{2x})\mathbb{N}}\right),\end{aligned} \tag{3.50}$$

with $\phi_{1x} = \omega_s x - (1-\mu)$ (for $\phi_{1x} \geq 0, x \geq \frac{1-\mu}{\omega_s}$), $\phi_{2x} = \varepsilon(1-\mu) - \tau_s x$ (for $\phi_{2x} > 0, x < \frac{\varepsilon(1-\mu)}{\tau_s}$), and $\mathbb{N} = \frac{m_{cd}}{\Omega_{cd}\eta_c}$.

Proof. By following the similar steps as used to derive (3.29) in Appendix A, one can obtain the required results. ■

Note that, to show a significant effect of HIs, (3.50) is especially derived for high data rate requirements $\left(\gamma_s \geq \frac{1-\mu}{\omega_s}\right)$.

Next, $F^{\text{noc}}_{\Lambda_{cd}}(x)$ can be evaluated using (3.15) as

$$F^{\text{noc}}_{\Lambda_{cd}}(x) = \begin{cases} F_{\Lambda_{cd}}\left(\frac{x}{1-\lambda^2_{\text{eq}}\,x}\right), & \text{if } x < \frac{1}{\lambda^2_{\text{eq}}}, \\ 1, & \text{if } x \geq \frac{1}{\lambda^2_{\text{eq}}}. \end{cases} \tag{3.51}$$

Thus, on inserting the associated CDF expressions in (3.48), the required OP can be evaluated.

3.3.2 ADF Relaying

For a given target rate γ_s, the OP of the secondary network for ADF relaying can be written as

$$\begin{aligned} P^{\text{DF}}_{\text{out}}(R_s) &= \Pr\left[\Lambda^{\text{DS}}_{ab} \geq \gamma'_p,\ \Lambda^{\text{noc}}_{cd} < \gamma_s\right] + \Pr\left[\Lambda^{\text{DS}}_{ab} < \gamma'_p,\ \Lambda^{\text{DS}}_{ac} < \gamma_s,\ \Lambda^{\text{noc}}_{cd} < \gamma_s\right] \\ &\quad + \Pr\left[\Lambda^{\text{DS}}_{ab} < \gamma'_p,\ \Lambda^{\text{DS}}_{ac} \geq \gamma_s,\ \Lambda_{e_s} < \gamma_s\right]. \end{aligned} \tag{3.52}$$

We can express $P^{\text{DF}}_{\text{out}}(R_s)$ in (3.52) as

$$\begin{aligned} P^{\text{DF}}_{\text{out}}(R_s) &= \bar{F}_{\Lambda^{\text{DS}}_{ab}}(\gamma'_p) F^{\text{noc}}_{\Lambda_{cd}}(\gamma_s) + F_{\Lambda^{\text{DS}}_{ab}}(\gamma'_p) F_{\Lambda^{\text{DS}}_{ac}}(\gamma_s) F^{\text{noc}}_{\Lambda_{cd}}(\gamma_s) \\ &\quad + F_{\Lambda^{\text{DS}}_{ab}}(\gamma'_p) \bar{F}_{\Lambda^{\text{DS}}_{ac}}(\gamma_s) F_{\Lambda_{e_s}}(\gamma_s). \end{aligned} \tag{3.53}$$

As such, evaluating (3.53) requires the CDF $F_{\Lambda_{e_s}}(\gamma_s)$ which can be written, using (3.11), as

$$F_{\Lambda_{e_s}}(x) = \begin{cases} F_{\Lambda_{cd}}\left(\frac{x}{1-\mu-\rho_s x}\right), & \text{if } x < \frac{1-\mu}{\rho_s}, \\ 1, & \text{if } x \geq \frac{1-\mu}{\rho_s}, \end{cases} \tag{3.54}$$

which can be further simplified, on substituting the value of ρ_s, as

$$F_{\Lambda_{e_s}}(x) = \begin{cases} F_{\Lambda_{cd}}\left(\frac{x}{1-\mu-\rho_s x}\right), & \text{if } x < \frac{1}{\lambda^2_{\text{eq}}}, \\ 1, & \text{if } x \geq \frac{1}{\lambda^2_{\text{eq}}}. \end{cases} \tag{3.55}$$

Finally, inserting the associated CDF expressions along with (3.55) into (3.53), the required OP can be evaluated.

3.3.3 Ceiling Effect

For the secondary network, the ceiling effect comes into existence when ST can not transmit the data towards its destination node D due to undesired constraints on the threshold rate γ_s. This can be observed from (3.51) and (3.55) for AAF and ADF relaying, respectively. For instance, when $\gamma_s \geq \frac{1}{\lambda^2_{\text{eq}}}$, the secondary communication goes into outage and this corresponds to the ceiling effect for the secondary network. Based on this observation, one can design a practical OCHSTN by calculating mathematically the HIs level for a given data rate as $\lambda^2_{\text{eq}} < \frac{1}{\gamma_s}$.

3.4 AAF Relaying versus ADF Relaying Against HIs

We now investigate the robustness of AAF relaying and ADF relaying against the HIs. As elaborated in the previous sections, HIs can potentially limit the fundamental capacity of a system beyond a certain target rate. For AAF, [from (3.37)], one can notice that RCC occurs when $\gamma_p \geq \frac{\mu}{\tau_p} + \gamma_p'$, while DLC arises when $\gamma_p \geq \frac{1}{\lambda^2_{rab}}$. Whereas, for ADF, [from (3.46)], it can be seen that RCC occurs when $\gamma_p \geq \frac{\mu}{\rho_p} + \gamma_p'$, while DLC occurs when $\gamma_p \geq \frac{1}{\lambda^2}$. After carefully observing these limits, one can infer that the ADF can support slightly higher data rate than the AAF till occurrence of the first ceiling effect. To exemplify this, let us consider the case of equal HIs level i.e., $\lambda_{rac} = \lambda_{rab} = \lambda_{rcb} = \lambda_{rcd} = \lambda_{tc} = \lambda = 0.2$ and $\mu = 0.87$. For this set of values, RCC occurs for AAF relaying when $\gamma_p > (3.58 + \gamma_p') \approx (5.53 + \gamma_p')$ dB, whereas for ADF, it occurs when $\gamma_p > (4.35 + \gamma_p') \approx (6.38 + \gamma_p')$ dB. Hence, ADF relaying is more robust and resilient against the HIs as it can support higher data rate than its AAF counterpart. As such, for a given threshold data rate γ_p, the ADF relaying may provide a better outage performance than the AAF under the same level of impairments. In addition, the performance of the secondary network would also be improved for the case of ADF relaying as demonstrated via numerical results in the next section.

3.5 Numerical and Simulation Results

In this section, we perform numerical illustrations for the considered OCHSTN and validate our derived analytical results through Monte-Carlo simulations. We obtain the curves corresponding to the mathematical analysis for OCHSTN while consider-

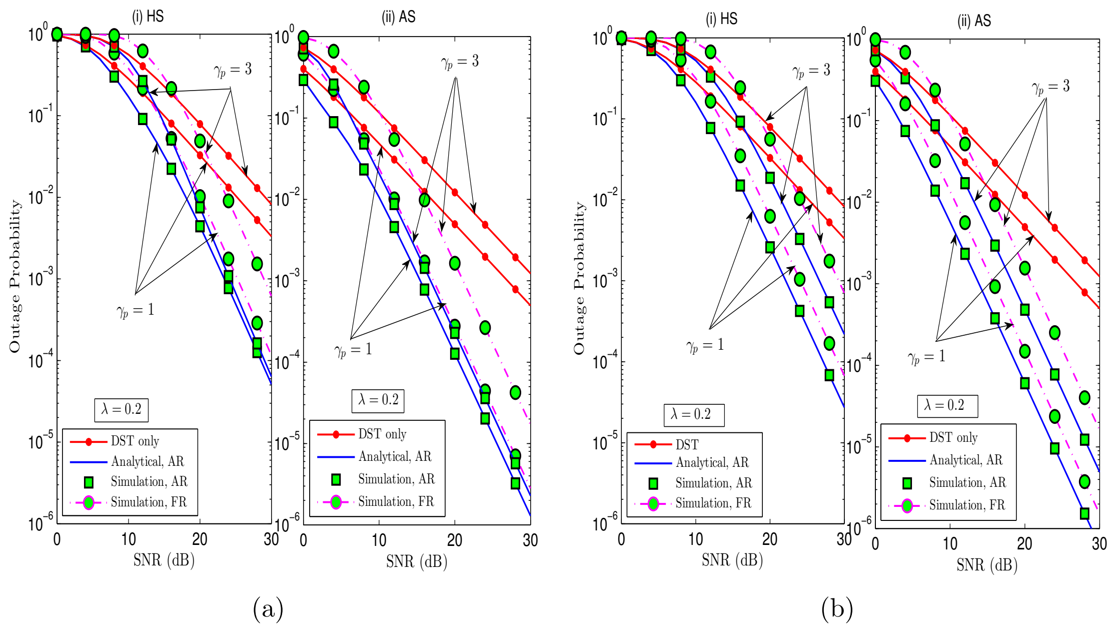

Figure 3.3: OP versus SNR curves with different γ_p for primary network (a) AF; (b) DF.

ing the two cases of AR protocol based relaying i.e., AAF and ADF. Herein, we set $m_{cb} = m_{cd} = 2$, $\Omega_{cb} = \Omega_{cd} = 1$, $\lambda_{rac} = \lambda_{rab} = \lambda_{rcb} = \lambda_{rcd} = \lambda_{tc} = \lambda$ as the level of HIs, and $\eta_a = \eta_c = \eta$ as the SNR. The shadowed-Rician fading parameters for the satellite links are considered under HS and AS [45] as $(m_{ai}, \flat_{ai}, \Omega_{ai} = 2, 0.063, 0.0005)$ and $(m_{ai}, \flat_{ai}, \Omega_{ai} = 5, 0.251, 0.279)$, $i \in \{b, c, d\}$, respectively. We set $L = 50$ in Section 3.2.3 to significantly reduce the approximation error [43]. For comparison purposes, we also obtain the curves for the competitive FR scheme using Monte-Carlo simulations. Further, Fig. 3.3 includes the curves for both HS and AS scenarios, whereas, the rest of the figures are specifically drawn for the AS scenario.

Fig. 3.3 exhibits the OP curves against SNR for primary network. Herein, we plot the analytical curves for two distinct values of threshold i.e., $\gamma_p = 1$ and $\gamma_p = 3$. For this, we set $\lambda = 0.2$ and depending upon the values of γ_p and λ, we have appropriately chosen the values of μ for the AAF and ADF relaying schemes based on spectrum sharing conditions given in Section 3.2.5. From the graph, one can see that the analytical curves are well aligned with the exact simulation results in the entire SNR regime. We observe that, for the higher values of threshold, HIs degrade the performance of the primary network significantly. However, its impact is relatively less while adopting AR protocol. We can clearly see that the proposed AR protocol provides better outage performance than the FR scheme. For further comparison, the OP curves for the benchmark DST scheme (without spectrum sharing) are also

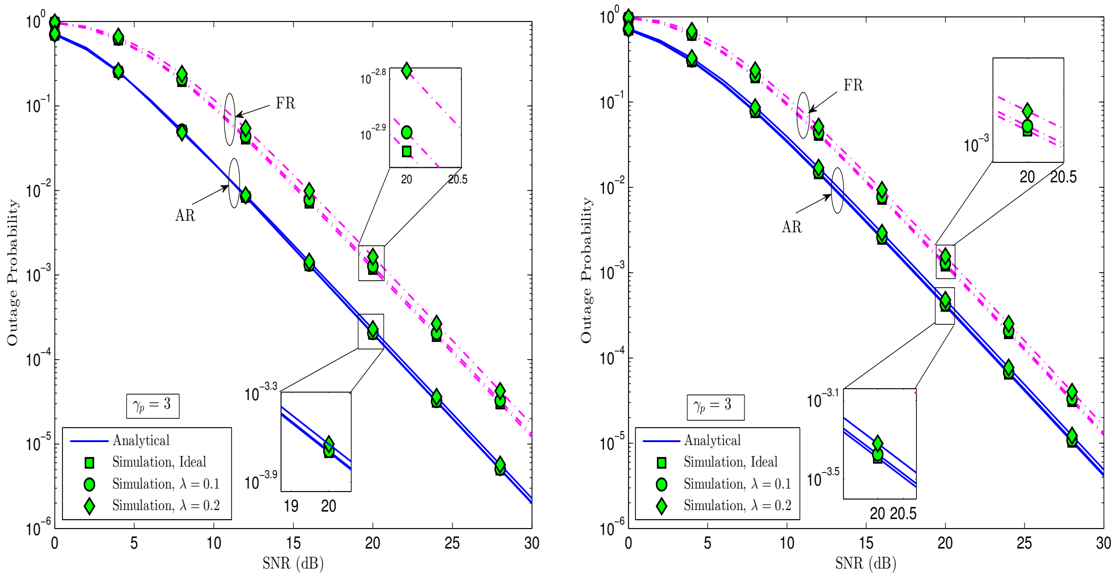

(a) (b)

Figure 3.4: OP versus SNR curves with different level of HIs for primary network (a) AF; (b) DF.

plotted. Hereby, one can observe the improvements in outage performance for the considered OCHSTN as compared to DST only scheme, especially in mid-to-high regime of SNR. Moreover, one can also visualize the relatively better performance when satellite links are subject to AS than their HS counterpart.

Fig. 3.4 illustrates the OP curves against SNR for the primary network for $\gamma_p = 3$. Herein, we plot the analytical curves for two distinct level of impairments i.e., $\lambda = 0.1$ and $\lambda = 0.2$. For comparison purposes, we also plot the curves for OCHSTN having ideal hardware set-up i.e., $\lambda = 0$. From the pertinent curves, it can be observed that as the level of impairments increases, performance of the FR protocol deviates more from the ideal system as compared with AR protocol. However, this deviation is relatively less for the FR-based DF scheme than the FR-based AF scheme.

Fig. 3.5 demonstrates the performance of the primary network against the threshold γ_p. Herein, to plot the various curves, we set SNR to 30 dB and the values of λ to 0 and 0.2. Further, we choose the value of μ as 0.87 while satisfying the conditions on μ, as mentioned in Section 3.2.5 for some values of the threshold (including both ideal and hardware impaired curves). Hereby, it can be clearly seen from the graph that the curves with HIs deviate from the ideal one as γ_p increases. When the threshold approaches $\gamma_p = \frac{\mu}{\tau_p} + \gamma_p'$ [refer to (3.37)] and $\gamma_p = \frac{\mu}{\rho_p} + \gamma_p'$ [refer to (3.46)] for AAF and ADF relaying, respectively, the RCC effect (denoted as RCC (HIs)) occurs which could cause the relay cooperation ineffectual, and thereby, the

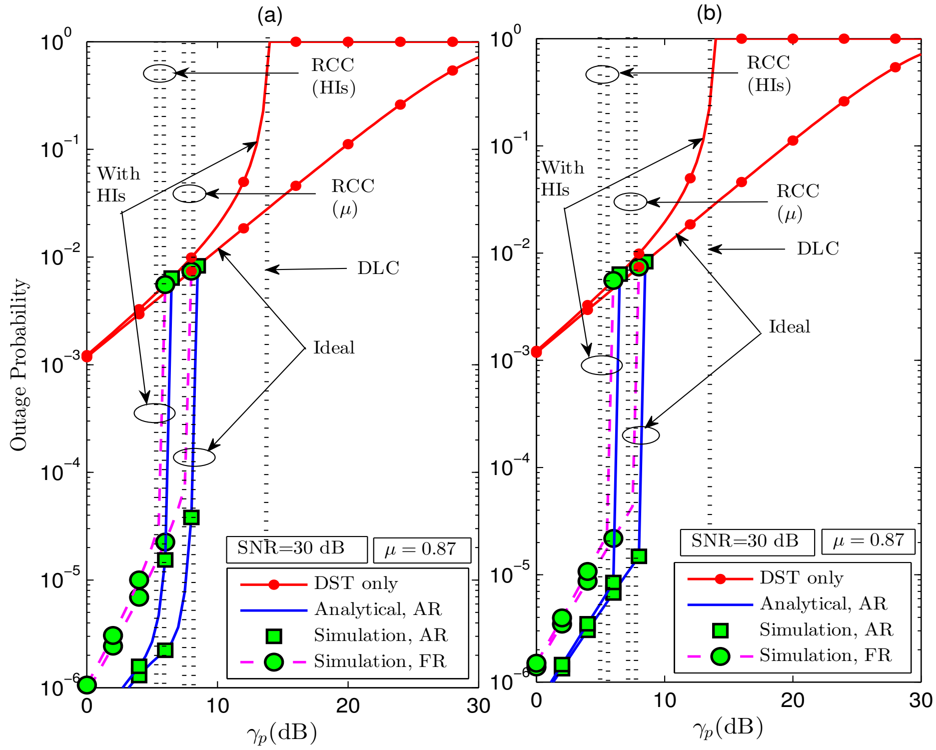

Figure 3.5: OP versus γ_p curves for primary network (a) AF; (b) DF.

performance of the primary network solely depends on the DST scheme. Interestingly, the RCC effect can also be seen for the ideal curves, however, at relatively higher values of threshold due to violation of the condition $\mu < 1$, this is denoted as RCC (μ). Moreover, one can note the relative increment of γ_p' in RCC threshold for the curves following AR protocol. Thus, the proposed protocol can satisfy the QoS requirements at higher data rates than its FR counterpart.

Fig. 3.6 exhibits the performance of secondary network against SNR based on the derived OP expression in Section 3.3. To show the significant impact of HIs, we specifically plot the curves for the high rate requirements, $\gamma_s \geq \frac{1-\mu}{\omega_s}$ (please refer to Theorem 2), and set the values as $\gamma_s = 1$ and $\gamma_s = 3$. Further, we set $\lambda = 0.2$ and based on the values of threshold $\gamma_s = \gamma_p$ and λ, we appropriately choose the respective values of μ for AAF and ADF relaying schemes. From the graph, one can note that the outage performance due to HIs degrades as value of γ_s increases. However, this degradation is dominant in the FR-based scheme than its AR counterpart. Moreover, the performance of the secondary network is improved significantly for the case of ADF relaying.

Fig. 3.7 depicts the OP curves against SNR for the secondary network for $\gamma_s = 3$. Herein, we consider two distinct level of impairments i.e., $\lambda = 0.1$, $\lambda = 0.2$ and,

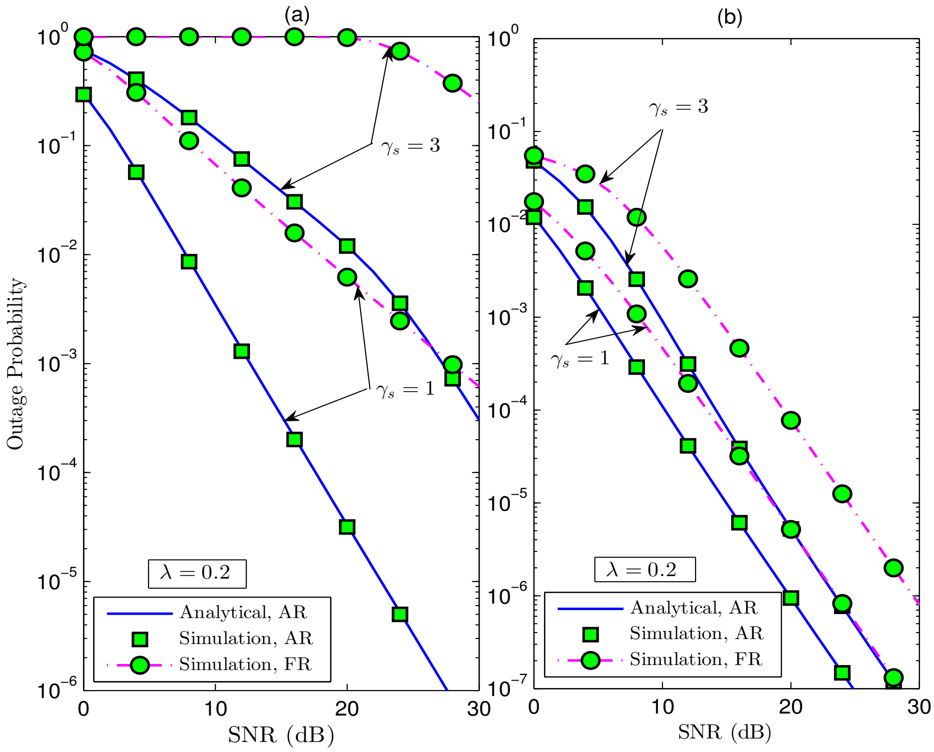

Figure 3.6: OP versus SNR curves with different γ_s for secondary network (a) AF; (b) DF.

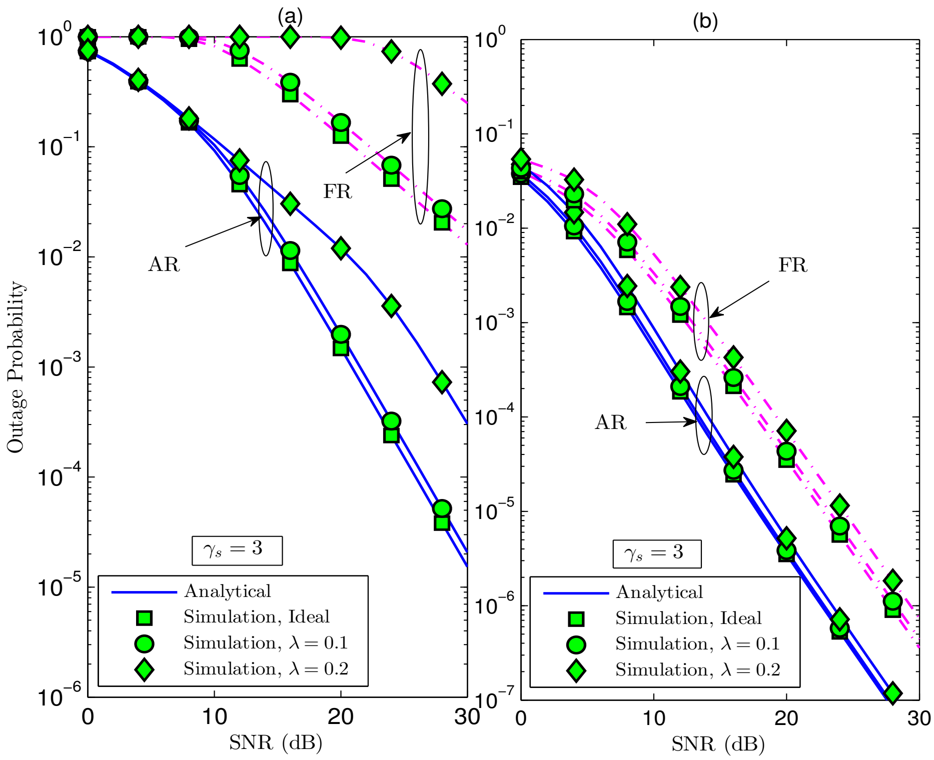

Figure 3.7: OP versus SNR curves with different level of HIs for secondary network (a) AF; (b) DF.

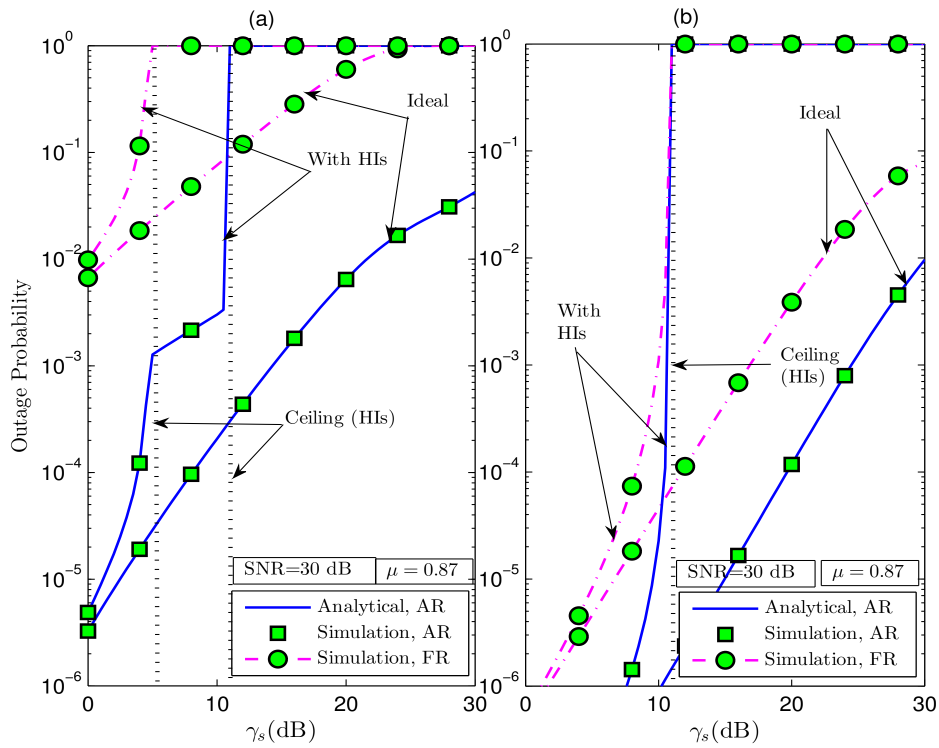

Figure 3.8: OP versus γ_s curves for secondary network (a) AF; (b) DF.

for comparison purposes, we also plot the curves for ideal hardware set-up ($\lambda = 0$). From the graph, one can visualize that the curves following the FR protocol deviate more from the ideal curve than the AR protocol as the level of impairments increases. However, this deviation is very less for both ADF relaying and FR-based DF schemes.

Fig. 3.8 illustrates the outage performance of the secondary network against the threshold γ_s. Herein, to plot the various curves, we set SNR to 30 dB and the values of λ to 0 and 0.2. Further, we choose the value of μ as 0.87, similar to that in Fig. 3.5. It can be clearly seen that curves with HIs deviate from the ideal one as γ_s increases. Referring to the case of AF relaying, when $\gamma_s \geq \frac{\varepsilon(1-\mu)}{\tau_s}$ [from (3.49)], the ceiling effect occurs for the curves following the FR protocol. However, for the curves following the AR protocol, the ceiling effect occurs at higher value of thresholds i.e., $\gamma_s \geq \frac{1}{\lambda_{\mathrm{eq}}^2}$ [from (3.51)]. Whereas, for DF relaying, the ceiling effect takes place for both FR-based and AR-based schemes when $\gamma_s \geq \frac{1}{\lambda_{\mathrm{eq}}^2}$. .

3.6 Summary

In this chapter, we investigated the performance of an OCHSTN while taking into account the practical HIs at the terrestrial user nodes. Considering the detrimental impact of HIs on the system performance, we proposed an AR protocol for both AF and DF operations, referred to as AAF and ADF respectively. For comparison purposes, we also considered the conventional FR-based AF and DF schemes. Further, for the AR-based analytical framework, OP expressions for the primary and secondary networks are derived over hybrid satellite-terrestrial channels. Hereby, we identified two ceiling effects for the primary network, namely RCC and DLC, invoked due to HIs. These effects were shown to be existent at higher values of target rate. It is found that once the RCC effect occurs, the performance of the primary network solely relies on the DST scheme. However, as the target data rate further increases, the DLC effect occurs which finally causes the system outage.

Above all, a comparison between AR and FR protocols reveals that AR can support relatively higher data rates and can compensate the impact of HIs significantly. It is also revealed that the ADF relaying is more resilient and robust as compared with all other schemes (i.e, FR-based AF and DF, and AAF). In addition, the performance of the secondary network is greatly improved for ADF relaying strategy.

CHAPTER 4

NOMA-ASSISTED OVERLAY MULTIUSER COGNITIVE HYBRID SATELLITE-TERRESTRIAL NETWORKS

Next-generation communication systems have to satisfy the demands of high data rates and a massive number of users efficiently. In this respect, the majority of works on CHSTNs, as discussed in previous chapters, consider the OMA scheme to serve multiple users, and thereby, only one user can be served at a time, and thus, the available spectrum resource in CHSTNs is still underutilized. Therefore, a NOMA scheme [59] has been exploited, which has the ability to serve multiple users in the same time/frequency resources. For this, it superimposes multiple signals in the power domain in transmitter side and uses the concept of SIC at receiver to de-multiplex the superimposed signals [60].

Recently, the NOMA scheme gained great interest in conjunction with satellite communication systems [61], [24], [25]. A general overview of the applications of NOMA scheme for the various satellite architectures was presented in [61]. In particular, the authors in [24] investigated the outage performance for the NOMA-based CHSTNs by considering the underlay spectrum sharing approach. Noting that, in an underlay scenario, the performance of the secondary user is limited, especially when it lies in the proximity of the PU. Motivated by this, the authors in [25] considered an overlay approach in their work. However, they have considered only a single PU with no direct DS communication.

Different from [25], in this chapter, we consider an overlay scenario that integrates the secondary terrestrial relay cooperation to primary DS communication in order to achieve a diversity gain for the primary network. Moreover, we consider the case of NOMA-assisted multiple PRs, while explicitly illustrating the spectrum sharing condition, which is the basis for any overlay spectrum sharing based system. It is worth pointing that such analysis postures new mathematical intricacies because of the involved joint effects of the overlay paradigm's sophisticated signal processing and multiple PRs. In a nutshell, our main contributions in this letter can be summarized as follows:

- We quantify the performance of a NOMA-assisted overlay multiuser cognitive satellite-terrestrial network (OMCSTN) in terms of OP of the primary and secondary networks by considering the pertinent heterogeneous fading models, and thereafter, compare its performance with the benchmark time-division multiple access (TDMA) and DS based schemes.
- We further explore the asymptotic outage performance for primary and secondary networks at a high SNR, and then derive their corresponding achievable diversity orders.
- Moreover, we investigate the impact of NOMA-based power allocation factor, for superimposing the PRs' signals, on the performance of the OMCSTN system. Based on this, we further provide a guideline to estimate the effective value of the spectrum sharing parameter.

The remainder of the chapter is structured as follows. In Section 4.1, we elaborate the proposed system model and derive the E-E signal-to-interference-plus-noise ratios (SINRs) over heterogeneous fading channels. In Section 4.2, we analyze the performance of the primary network by deriving the expressions of the OP for NOMA users. Section 4.3 investigates the outage performance of the secondary network. Numerical and simulations results are provided in Section 4.4, and finally, summary of the chapter is presented in Section 4.5.

4.1 System Descriptions

As depicted in Fig. 4.1, we consider an OMCSTN where a primary satellite source A (termed as primary transmitter (PT)) wants to communicate with its K PRs $\{B_k\}_{k=1}^{K}$ simultaneously by exploiting the NOMA scheme. Herein, ST node C can enjoy the access of licensed band of PU to communicate with a SR node D if ST assists the primary transmission between satellite A and terrestrial users B_k[1]. For

[1]A typical scenario for OMCSTN may comprise of source A representing a GEO satellite and nodes B_k could be handheld devices as incorporated in DVB-SH service (in S-band) [62], whereas the secondary nodes C and D can represent femtocell users who do not have a dedicated spectrum for their communication [53].

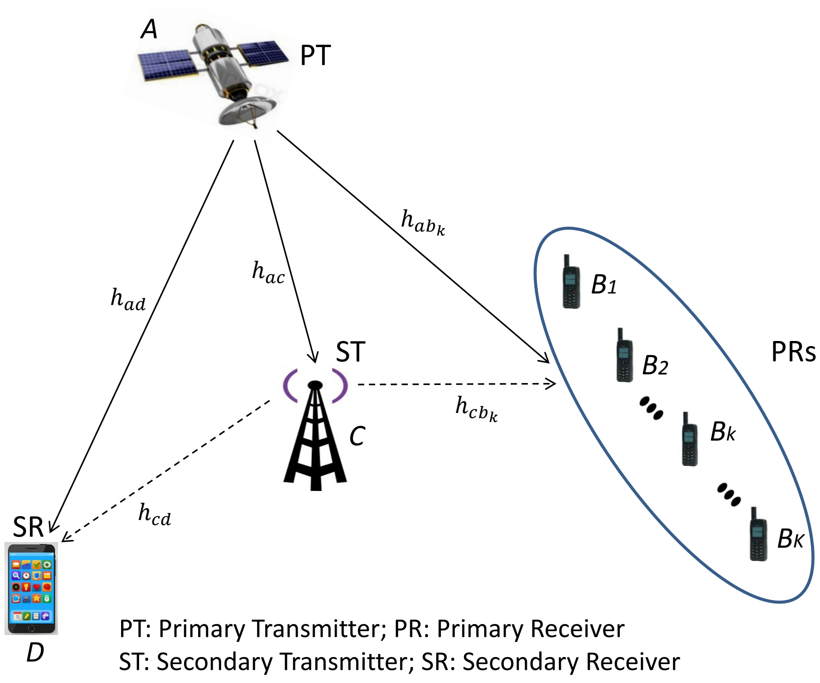

Figure 4.1: OMCSTN system model.

the subsequent analysis, we consider that the users B_1 and B_2 form a NOMA group, as the two-user NOMA case is reasonably followed in literature [25], [63] and is also adopted in 3GPP. Nevertheless, our analysis can be extended for any two users' pair in the cluster [64]. Moreover, we assume that DS links exist between nodes A and $\{B_k\}_{k=1}^{2}$. Further, the secondary node C applies an AF protocol to forward the primary's data. The various channel coefficients pertaining to the satellite links $A \to B_k$, $A \to C$, and $A \to D$ follow shadowed-Rician fading and are represented by h_{ab_k}, h_{ac}, and h_{ad}, respectively. Whereas, channel coefficients for terrestrial links $C \to B_k$ and $C{\to}D$ are denoted as h_{cb_k} and h_{ad}, respectively, and are subject to Nakagami-m fading. AWGN with mean zero and variance σ^2, is assumed to inflict all the receiving nodes.

Without loss of generality, PRs are ordered in terms of strong/weak users by their effective channel gains of the DS ($A \to B_k$) links, i.e., $|h_{ab_1}|^2 \leq |h_{ab_2}|^2$ [24], [59].

The overall communication follows the two-phase transmission scheme. In the first phase, satellite A broadcasts a superposing signal $x_a = \sqrt{\rho P_a} x_{b_1} + \sqrt{(1-\rho)P_a} x_{b_2}$ to B_k which is also being overheard by the secondary nodes C and D, where $\rho \in (0.5, 1)$ denotes the power allocation factor corresponding to user B_1, x_{b_k} represents the unit-energy information signal for user B_k, and P_a be the transmit power at A. Accordingly, the received signals at B_k, C, and D, denoted by y_{ab_k}, y_{ac}, and

y_{ad}, respectively, can be given as

$$y_{ai} = h_{ai}(\sqrt{\rho P_a} x_{b_1} + \sqrt{(1-\rho)P_a} x_{b_2}) + v_{ai}, \tag{4.1}$$

where $i \in \{b_k, c, d\}$ and v_{ai} be the AWGN variable. In the second phase, node C employs the AF-based relaying operation and superimposes the signals x_c and y_{ac} to generate a combined signal. For this simultaneous transmission, ST node splits its power P_c such that the fraction μP_c is used to forward the primary signal y_{ac} to node B_k, while the remaining portion $(1-\mu)P_c$ of the power is used to transmit its own information signal x_c to node D, where the factor $\mu \in (0,1)$ represents the spectrum sharing parameter. Thus, the signal transmitted by the ST node is given by

$$z_c = \sqrt{\mu P_c} \frac{y_{ac}}{\sqrt{|y_{ac}|^2}} + \sqrt{(1-\mu)P_c} x_c. \tag{4.2}$$

Hereby, the respective received signals at nodes B_k and D from C can be given as y_{cb_k} and y_{cd}, represented by

$$y_{cj} = h_{cj} z_c + v_{cj}, \tag{4.3}$$

where $j \in \{b_k, d\}$ and v_{cj} is the AWGN term. According to NOMA principle, the user with worse channel condition can decode its signal directly. Hence, the equivalent SINR at user B_1 through DS link is given by

$$\Lambda_{ab_1}^{\mathrm{DS}} = \frac{\rho \Lambda_{ab_1}}{(1-\rho)\Lambda_{ab_1} + 1}, \tag{4.4}$$

where $\Lambda_{ab_1} = \eta_a |h_{ab_1}|^2$ with $\eta_a = \frac{P_a}{\sigma^2}$. Now, user B_2 decodes the information of user B_1 based on the principle of SIC, and hence, the decoding SINR at user B_2 can be expressed as

$$\Lambda_{ab_2 \to b_1}^{\mathrm{DS}} = \frac{\rho \Lambda_{ab_2}}{(1-\rho)\Lambda_{ab_2} + 1}, \tag{4.5}$$

where $\Lambda_{ab_2} = \eta_a |h_{ab_2}|^2$. Based on above decoding SINR, user B_2 subtracts the information of user B_1 to decode its own information. Consequently, SINR at user

B_2 can be given as

$$\Lambda_{ab_2}^{\mathrm{DS}} = (1-\rho)\Lambda_{ab_2}. \tag{4.6}$$

Similar to (4.4), (4.5), and (4.6), we can express the SINRs via relay link at respective nodes[2] as

$$\Lambda_{acb_1} = \frac{\varepsilon_1 \mu \Lambda_{ac}\Lambda_{cb_1}}{\tau_1 \Lambda_{ac}\Lambda_{cb_1} + \Lambda_{ac} + \Lambda_{cb_1} + 1}, \tag{4.7}$$

$$\Lambda_{acb_2\to b_1} = \frac{\varepsilon_1 \mu \Lambda_{ac}\Lambda_{cb_2}}{\tau_1 \Lambda_{ac}\Lambda_{cb_2} + \Lambda_{ac} + \Lambda_{cb_2} + 1}, \tag{4.8}$$

$$\Lambda_{acb_2} = \frac{\varepsilon_2 \mu \Lambda_{ac}\Lambda_{cb_2}}{\tau_2 \Lambda_{ac}\Lambda_{cb_2} + \Lambda_{ac} + \Lambda_{cb_2} + 1}, \tag{4.9}$$

where $\tau_1 = (1-\mu)+(1-\rho)\mu$, $\tau_2 = 1-\mu$, $\varepsilon_1 = \rho$, $\varepsilon_2 = 1-\rho$, $\Lambda_{ac} = \eta_a|h_{ac}|^2$, and Λ_{cb_k} $= \eta_c|h_{cb_k}|^2$ with $\eta_c = \frac{P_c}{\sigma^2}$. From (4.1), it is observed that D overhears the primary signal in the first time slot. As such, it may utilize this overheard signal to cancel the interference term created at node D during the signal reception in the second time slot [35]. Consequently, the E-E SNR at D is obtained as

$$\Lambda_{acd} = \frac{(1-\mu)\Lambda_{cd}(\Lambda_{ac}+1)}{\mu\Lambda_{cd} + \Lambda_{ac} + 1}, \tag{4.10}$$

where $\Lambda_{cd} = \eta_c|h_{cd}|^2$.

4.2 Outage Performance of Primary Network

In this section, we analyze the performance of the primary network by explicitly deriving the OP expressions for user B_1 and user B_2 with the involvement of both DS and relay links. To proceed, we first present the statistical characterizations of the underlying hybrid fading channels.

4.2.1 Statistical Characterizations for Fading Channels

Considering the satellite links under the shadowed-Rician fading model, the PDF and CDF of $\Lambda_{ai} = \eta_a|h_{ai}|^2$, $i \in \{b_k, c, d\}$, can be expressed respectively as [18], [25]

$$f_{\Lambda_{ai}(x)} = \alpha_i \sum_{\kappa=0}^{m_{ai}-1} \frac{\zeta(\kappa)}{(\eta_a)^{\kappa+1}} x^{\kappa} \mathrm{e}^{-\left(\frac{\beta_i-\delta_i}{\eta_a}\right)x} \tag{4.11}$$

[2]Note that, for the primary system, the satellite has access to the ordering of the two pre-paired NOMA users (PRs) based on DS channel conditions only and not on the secondary relaying links. However, assuming that user B_2 is located nearer to ST than B_1, the same ordering can be maintained. It has also been followed for a basic cooperative relaying system in [65].

and

$$F_{\Lambda_{ai}}(x) = 1 - \alpha_i \sum_{\kappa=0}^{m_{ai}-1} \frac{\zeta(\kappa)}{(\eta_a)^{\kappa+1}} \sum_{p=0}^{\kappa} \frac{\kappa!}{p!} \left(\frac{\beta_i - \delta_i}{\eta_a}\right)^{-(\kappa+1-p)} x^p \mathrm{e}^{-\left(\frac{\beta_i-\delta_i}{\eta_a}\right)x}, \tag{4.12}$$

with $\alpha_i = (2\flat_{ai} m_{ai}/(2\flat_{ai} m_{ai} + \Omega_{ai}))^{m_{ai}}/2\flat_{ai}$, $\beta_i = 1/2\flat_{ai}$, $\delta_i = \Omega_{ai}/(2\flat_{ai})(2\flat_{ai} m_{ai} + \Omega_{ai})$, where $2\flat_{ai}$ is the average power of multipath component, Ω_{ai} be the average power of LoS component, m_{ai} is the integer-valued fading severity parameter, and $\zeta(\kappa) = (-1)^\kappa (1 - m_{ai})_\kappa \delta_i^\kappa / (\kappa!)^2$.

Since we consider Nakagami-m fading for the terrestrial links, the corresponding PDF and CDF of $\Lambda_{cj} = \eta_c |h_{cj}|^2$, $j \in \{b_k, d\}$, can be given by

$$f_{\Lambda_{cj}}(x) = \left(\frac{m_{cj}}{\Omega_{cj}\eta_c}\right)^{m_{cj}} \frac{x^{m_{cj}-1}}{\Gamma(m_{cj})} \mathrm{e}^{-\frac{m_{cj}}{\Omega_{cj}\eta_c}x} \tag{4.13}$$

and

$$F_{\Lambda_{cj}}(x) = \frac{1}{\Gamma(m_{cj})} \Upsilon\left(m_{cj}, \frac{m_{cj}}{\Omega_{cj}\eta_c} x\right), \tag{4.14}$$

where Ω_{cj} is the average power, m_{cj} be the fading severity.

4.2.2 Exact Outage Probability Analysis

User B_1

For a target rate R_p, the OP of user B_1 for the OMCSTN can be expressed with the utilization of MRC by making use of (4.4) and (4.7) as

$$\begin{aligned} P_{\mathrm{out}\to B_1}(R_p) &= \Pr\left[\frac{1}{2}\log_2\left(1 + \Lambda_{ab_1}^{\mathrm{DS}} + \Lambda_{acb_1}\right) < R_p\right] \\ &= \Pr\left[\left(\Lambda_{ab_1}^{\mathrm{DS}} + \Lambda_{acb_1}\right) < \gamma_p\right], \end{aligned} \tag{4.15}$$

where $\gamma_p = 2^{2R_p} - 1$. Hereby, (4.15) can be re-expressed as

$$P_{\mathrm{out}\to B_1}(R_p) = \int_0^{\gamma_p} F_{\Lambda_{acb_1}}(\gamma_p - y) f_{\Lambda_{ab_1}^{\mathrm{DS}}}(y) dy. \tag{4.16}$$

Now, to evaluate (4.16), we require the CDF $F_{\Lambda_{acb_1}}(\cdot)$, which is derived as follows in Lemma 1.

Lemma 1. *The CDF $F_{\Lambda_{acb_k}}(x)$ under hybrid satellite-terrestrial channels can be* *given by*

$$F_{\Lambda_{acb_k}}(x) = \begin{cases} 1, & \text{if } x \geq \frac{\varepsilon_k}{\tau_k}\mu, \\ \psi_k(x), & \text{if } x < \frac{\varepsilon_k}{\tau_k}\mu, \end{cases} \tag{4.17}$$

where $\psi_k(x)$ is given as

$$\begin{aligned} \psi_k(x) = 1 - 2\alpha_c \sum_{\kappa=0}^{m_{ac}-1} \sum_{l=0}^{\kappa} \sum_{m=0}^{l} \sum_{g=0}^{m+m_{cb_k}-1} & \frac{\zeta(\kappa)}{(\eta_a)^{\kappa+1}} \frac{\kappa!}{l!} M^{-(\kappa+1-l)} \frac{N^{m_{cb_k}}}{\Gamma(m_{cb_k})} \\ \times \binom{m+m_{cb_k}-1}{g} e^{-\left(\frac{(M+N)x}{\theta_{kx}}\right)} & \frac{(x)^{m+m_{cb_k}+l-1-g}}{\theta_{kx}^{m+m_{cb_k}}} \binom{l}{m} \\ \times \left(\frac{Mx^2 + Mx\theta_{kx}}{N}\right)^{\frac{g-l+1}{2}} & \mathcal{K}_{g-l+1}\left(\frac{2}{\theta_{kx}}\sqrt{(Mx^2 + Mx\theta_{kx})N}\right), \end{aligned} \tag{4.18}$$

with $\theta_{kx} = \varepsilon_k\mu - \tau_k x$ (for $\theta_{kx} > 0, x < \frac{\varepsilon_k}{\tau_k}\mu$), $M = \frac{\beta_c - \delta_c}{\eta_a}$, $N = \frac{m_{cb_k}}{\Omega_{cb_k}\eta_c}$.

Proof. See Appendix B. ∎

Now, on inserting (4.18) with $k = 1$ into (4.17), $F_{\Lambda_{acb_1}}(\cdot)$ can be evaluated at $x = \gamma_p$. It should be pointed out that the condition $x < \frac{\varepsilon_k}{\tau_k}\mu$ in (4.17) makes the ST's cooperation helpful, otherwise CDF takes on unity value. Hence, we bring off the performance analysis for the condition $x < \frac{\varepsilon_k}{\tau_k}\mu$. On using the expression for $F_{\Lambda_{acb_1}}(\gamma_p - y)$ in (4.16), it is yet observed to be extremely hard to get a closed-form solution. Hence, using an I-step staircase approximation approach [43] for the included triangular integral region in (4.16), the OP can be written as

$$P_{\text{out}\to B_1}(R_p) \approx \sum_{i=0}^{I-1} \left\{ F_{\Lambda_{ab_1}^{\text{DS}}}\left(\frac{i+1}{I}\gamma_p\right) - F_{\Lambda_{ab_1}^{\text{DS}}}\left(\frac{i}{I}\gamma_p\right) \right\} F_{\Lambda_{acb_1}}\left(\frac{I-i}{I}\gamma_p\right). \tag{4.19}$$

To evaluate (4.19), we first derive the CDF of $\Lambda_{ab_1}^{\text{DS}}$ using (4.4) as

$$F_{\Lambda_{ab_1}^{\text{DS}}}(x) = F_{\Lambda_{ab_1}}\left(\frac{x}{\rho - (1-\rho)x}\right). \tag{4.20}$$

Then, on using (4.12) into (4.20) and the resulting CDF expression along with (4.17) into (4.19), one can compute the OP for user B_1.

User B_2

For a target rate R_p, OP for user B_2 while employing the MRC scheme can be expressed as

$$P_{\text{out}\to B_2}(R_p) = 1 - \Pr\left[(\Lambda^{\text{DS}}_{ab_2\to b_1} + \Lambda_{acb_2\to b_1}) \geq \gamma_p,\ (\Lambda^{\text{DS}}_{ab_2} + \Lambda_{acb_2}) \geq \gamma_p\right]. \tag{4.21}$$

Following the similar steps in evaluating the OP for user B_1, we can calculate OP for user B_2 as

$$\begin{aligned} P_{\text{out}\to B_2}(R_p) \approx 1 - &\left[1 - \sum_{i=0}^{I-1}\left\{F_{\Lambda^{\text{DS}}_{ab_2\to b_1}}\left(\frac{i+1}{I}\gamma_p\right) - F_{\Lambda^{\text{DS}}_{ab_2\to b_1}}\left(\frac{i}{I}\gamma_p\right)\right\}\right. \\ &\qquad\qquad \left.\times F_{\Lambda_{acb_2\to b_1}}\left(\frac{I-i}{I}\gamma_p\right)\right] \\ &\times\left[1 - \sum_{i=0}^{I-1}\left\{F_{\Lambda^{\text{DS}}_{ab_2}}\left(\frac{i+1}{I}\gamma_p\right) - F_{\Lambda^{\text{DS}}_{ab_2}}\left(\frac{i}{I}\gamma_p\right)\right\}F_{\Lambda_{acb_2}}\left(\frac{I-i}{I}\gamma_p\right)\right]. \end{aligned} \tag{4.22}$$

To proceed, we need the expressions of CDFs $F_{\Lambda_{acb_2}}(\cdot)$, $F_{\Lambda_{acb_2\to b_1}}(\cdot)$, $F_{\Lambda^{\text{DS}}_{ab_2\to b_1}}(\cdot)$, and $F_{\Lambda^{\text{DS}}_{ab_2}}(\cdot)$. First, on inserting (4.18) with $k=2$ into (4.17), $F_{\Lambda_{acb_2}}(\cdot)$ can be deduced. However, $F_{\Lambda_{acb_2\to b_1}}(\cdot)$ follows the similar expression as $F_{\Lambda_{acb_1}}(\cdot)$ while replacing the terms m_{cb_1} and Ω_{cb_1} with m_{cb_2} and Ω_{cb_2}, respectively. Further, $F_{\Lambda^{\text{DS}}_{ab_2\to b_1}}(\cdot)$ follows the similar expression as given in (4.20) while inserting the channel parameters corresponding to user B_2. Furthermore, $F_{\Lambda^{\text{DS}}_{ab_2}}(\cdot)$ can be expressed using (4.6) as

$$F_{\Lambda^{\text{DS}}_{ab_2}}(x) = F_{\Lambda_{ab_2}}\left(\frac{x}{1-\rho}\right), \tag{4.23}$$

which can be readily evaluated using (4.12). Then, on inserting above CDF expressions into (4.22), one can calculate the required OP for user B_2.

4.2.3 Asymptotic Outage Probability Analysis

To get further insights, we provide the asymptotic OP expressions corresponding to users B_1 and B_2 at a high SNR ($\eta_a, \eta_c \to \infty$, with $\frac{\eta_a}{\eta_c}$ be a constant ratio), which are given below in Theorem 3.

Theorem 3. *The OP expressions in (4.19) and (4.22) can be approximated at high*

SNR, respectively, as

$$P^{asy}_{out\rightarrow B_1}(R_p) \approx \sum_{i=0}^{I-1} \frac{\alpha_{b_1}\gamma_p}{I\eta_a(\rho-(1-\rho)\gamma_p)} \left[\frac{\alpha_c(I-i)\gamma_p}{I\eta_a\theta_{1\frac{I-i}{I}\gamma_p}} + \frac{1}{\Gamma(m_{cb_1}+1)} \left(\frac{m_{cb_1}(I-i)\gamma_p}{\Omega_{cb_1}\eta_c I\theta_{1\frac{I-i}{I}\gamma_p}} \right)^{m_{cb_1}} \right] \tag{4.24}$$

and

$$P^{asy}_{out\rightarrow B_2}(R_p) \approx 1 - \left[1 - \sum_{i=0}^{I-1} \frac{\alpha_{b_2}\gamma_p}{I\eta_a(\rho-(1-\rho)\gamma_p)} \left(\frac{\alpha_c(I-i)\gamma_p}{I\eta_a\theta_{1\frac{I-i}{I}\gamma_p}} + \frac{1}{\Gamma(m_{cb_2}+1)} \left(\frac{m_{cb_2}(I-i)\gamma_p}{\Omega_{cb_2}\eta_c I\theta_{1\frac{I-i}{I}\gamma_p}} \right)^{m_{cb_2}} \right)\right] \times \left[1 - \sum_{i=0}^{I-1} \frac{\alpha_{b_2}\gamma_p}{I\eta_a(1-\rho)} \left(\frac{\alpha_c(I-i)\gamma_p}{I\eta_a\theta_{2\frac{I-i}{I}\gamma_p}} + \frac{1}{\Gamma(m_{cb_2}+1)} \left(\frac{m_{cb_2}(I-i)\gamma_p}{\Omega_{cb_2}\eta_c I\theta_{2\frac{I-i}{I}\gamma_p}} \right)^{m_{cb_2}} \right)\right]. \tag{4.25}$$

Proof. See Appendix C. ■

Remark 4.1: From (4.24) and (4.25), it can be found that the primary satellite network can achieve a diversity order of $1+\min(1, m_{cb_k})$ for each user, which is independent of the fading parameter m_{ai} of the satellite link. Note that this diversity order is higher than that obtained as $\min(1, m_{cb})$ in [25].

4.2.4 A Guideline to Decide Spectrum Sharing Parameter

With respect to the power allocation strategy for ST, we have to acquire a suitable value of μ while fulfilling the QoS criteria for the primary network. From (4.17), exploring the condition $x < \frac{\varepsilon_k}{\tau_k}\mu$, the allowable range of μ for a certain threshold γ_p can be calculated as $\frac{\gamma_p}{\rho-(1-\rho)\gamma_p+\gamma_p} < \mu < 1$ and $\frac{\gamma_p}{(1-\rho)+\gamma_p} < \mu < 1$ for users B_1 and B_2, respectively. Thus, the effective range of μ for the relay cooperation, satisfying the QoS criterion for both users, is $\max\left(\frac{\gamma_p}{\rho-(1-\rho)\gamma_p+\gamma_p}, \frac{\gamma_p}{(1-\rho)+\gamma_p}\right) < \mu < 1$. Consequently, ST can decide the critical value of μ for the spectrum sharing such that the OP of the primary network in OMCSTN lies below or equal to that of the DST scheme [35] (without spectrum sharing), as illustrated numerically in Section 4.4.

4.3 Outage Performance of Secondary Network

For a given target rate R_s, the OP of the secondary network can be written as

$$P_{\text{out}}(R_s) = \Pr\left[\frac{1}{2}\log_2(1+\Lambda_{acd}) < R_s\right] = \Pr\left[\Lambda_{acd} < \gamma_s\right], \tag{4.26}$$

where $\gamma_s = 2^{2R_s} - 1$. Hereby, $P_{\text{out}}(R_s)$ can be evaluated through the CDF $F_{\Lambda_{acd}}(x)$ at $x = gamma_s$ as given in Lemma 2.

Lemma 2. *The CDF $F_{\Lambda_{acd}}(x)$ under hybrid satellite-terrestrial channels can be given by*

$$\begin{aligned} F_{\Lambda acd}(x) = 1 - 2\alpha_c \sum_{\kappa=0}^{m_{ac}-1}\sum_{l=0}^{\kappa}\sum_{m=0}^{l}\sum_{g=0}^{m+m_{cd}-1} \frac{\zeta(\kappa)}{(\eta_a)^{\kappa+1}}\frac{\kappa!}{l!}\frac{1}{\Gamma(m_{cd})}\mathbb{M}^{-(\kappa+1-l)}\mathbb{N}^{m_{cd}}\binom{l}{m} \\ \times \frac{x^{l-m}(\phi_x)^m(x)^{m+m_{cd}-1-g}}{(1-\mu)^{m+m_{cd}}} e^{-\left(\frac{\mathbb{M}\phi_x+\mathbb{N}x}{1-\mu}\right)}\left(\frac{\mathbb{M}\phi_x x+\mathbb{M}x(1-\mu)}{\mathbb{N}}\right)^{\frac{g-l+1}{2}} \\ \times \binom{m+m_{cd}-1}{g}\mathcal{K}_{g-l+1}\left(\frac{2}{(1-\mu)}\sqrt{(\mathbb{M}\phi_x x+\mathbb{M}x(1-\mu))\mathbb{N}}\right), \end{aligned} \tag{4.27}$$

with $\phi_x = \mu x - (1-\mu)$, $\mathbb{M} = \frac{\beta_c-\delta_c}{\eta_a}$, and $\mathbb{N} = \frac{m_{cd}}{\Omega_{cd}\eta_c}$.

Proof. The proof of (4.27) follows the similar steps as for (4.18) in Appendix B and hence it is skipped here for brevity. ■

Remark 4.2: Note that (4.27) is specifically derived for the high rate requirements (i.e., for $\phi_x \geq 0, x \geq \frac{1-\mu}{\mu}$) at $x = \gamma_s$. Moreover, by following the similar steps as in Appendix C, one can derive the diversity order of $\min(1, m_{cd})$ for the secondary network.

4.4 Numerical and Simulation Results

In this section, we present numerical results for the considered OMCSTN. For this, we set $m_{cb_k} = 2$, $\Omega_{cb_k} = \Omega_{cd} = 1$, $\eta_a = \eta_c = \eta$ as the transmit SNR, and $R_p = R_s = 0.5$ so that $\gamma_p' = 0.414, \gamma_p = 1, \gamma_s = 1$. The shadowed-Rician fading parameters for the satellite links are considered under HS and AS as $(m_{ai}, \flat_{ai}, \Omega_{ai} = 2, 0.063, 0.0005)$ and $(m_{ai}, \flat_{ai}, \Omega_{ai} = 5, 0.251, 0.279)$, $i \in \{b_k, c, d\}$, respectively [45]. We set $I = 50$ in (4.19), (4.22), (4.24), and (4.25) to significantly reduce the approximation error [43].

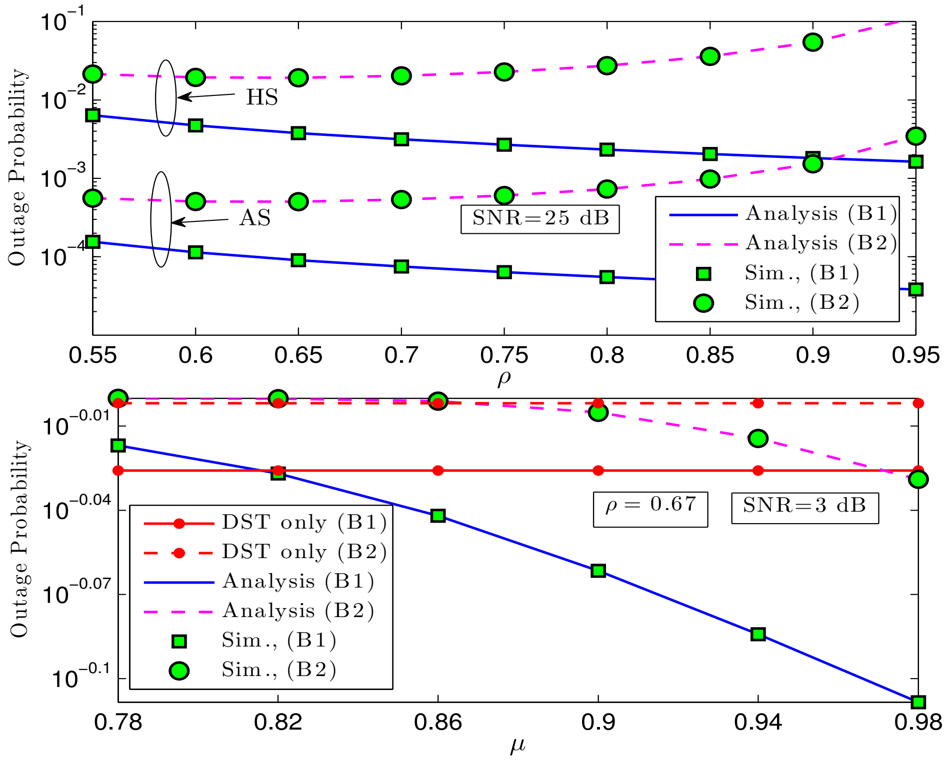

Figure 4.2: OP versus ρ and μ curves for primary network.

Fig. 4.2 depicts the outage performance of the primary network against two crucial parameters i.e., power allocation factor ρ and the spectrum sharing parameter μ. From the OP versus ρ curves, we can see that the OP decreases for user B_1 and increases for user B_2 as the value of ρ increases. However, outage performance improves for both users when satellite links are subject to AS. One can readily choose the appropriate value of ρ as 0.67. Consequently, the effective range of μ for the relay cooperation can be deduced as $\max(0.746, 0.751) < \mu < 1$, as mentioned in Section 4.2.4. Under this range of μ, we draw the curves for the OP versus μ for calculating the critical value of μ for spectrum sharing. For this, we assume DS links to undergo HS whereas the $A \rightarrow C$ link to AS. From the graph, one can note the critical value of μ for spectrum sharing as $\max(0.82, 0.86)$, while satisfying the QoS for both PUs.

Fig. 4.3 exhibits the OP curves against SNR for the primary network under the setting $\rho = 0.67$ and $\mu = 0.86$. First, we can verify that analytical and asymptotic curves are well aligned with the exact simulation results. For the comparison purposes, we have also shown the simulation curves for the TDMA scheme, and thereby, we illuminate the significant performance improvement of the primary network through proposed NOMA scheme. One can also visualize the relatively better

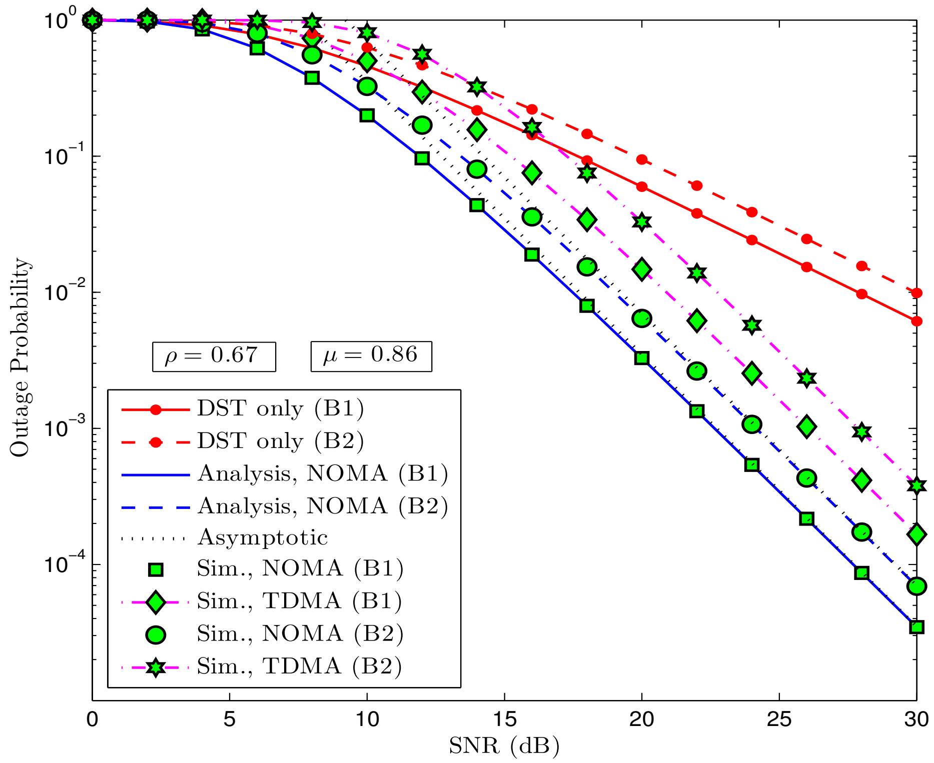

Figure 4.3: OP versus SNR curves for primary network.

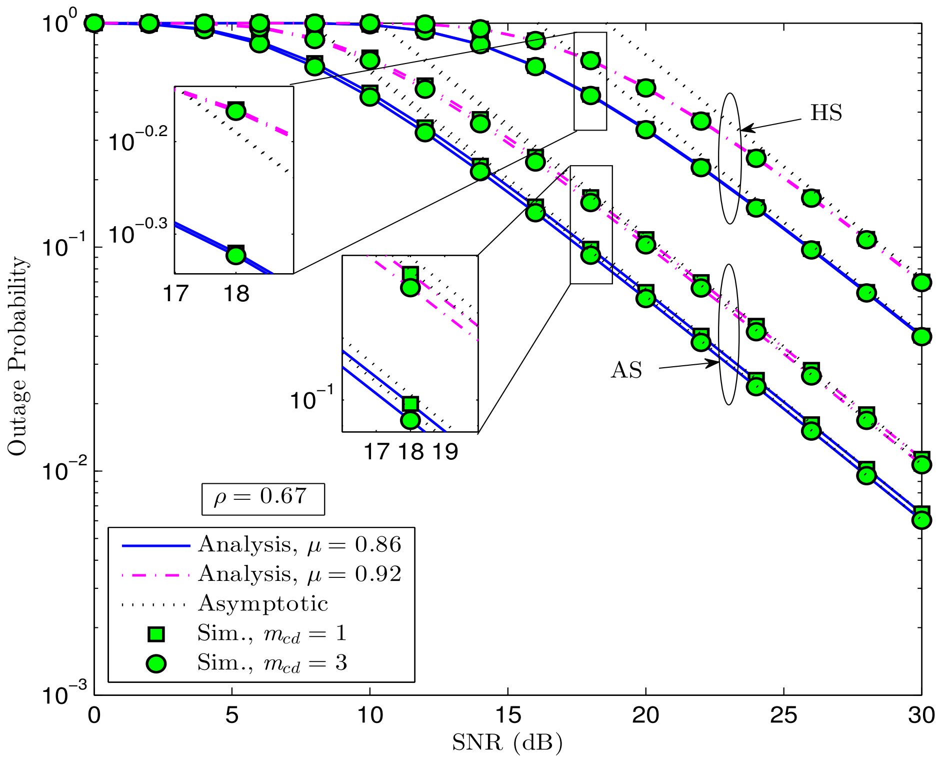

Figure 4.4: OP versus SNR curves for secondary network.

performance for the user B_1, as more power is allocated towards B_1 through a larger value of ρ. Further, for comparison, the simulation curves for the DST scheme (without spectrum sharing) are also plotted. One can readily verify the diversity order of $1 + \min(1, m_{cb_k})$ from the pertinent curves.

Fig. 4.4 depicts the OP curves against SNR for the secondary network for various values of μ and m_{cd}, under both HS and AS scenarios. We can see that the analytical and asymptotic curves are well aligned to the exact simulation results. One can also realize the relative improvements in outage performance for $\mu = 0.86$, as it provides more power allocation for the secondary network. Further, diversity order of $\min(1, m_{cd})$ can be verified from the various curves. Moreover, outage performance improves when satellite link is subject to AS as compared to HS scenario.

4.5 Summary

We investigated the performance of an OMCSTN wherein a secondary terrestrial network enjoys the access to spectrum with a primary satellite network in exchange for relay cooperation. Different from the existing works, we have considered the multiple PRs assisted through NOMA scheme for the performance evaluation. Above all, a comparison with benchmark schemes revealed that proposed NOMA-assisted OMCSTN provides remarkable performance improvement while utilizing the spectrum resource efficiently.

CHAPTER 5

FULL-DUPLEX/HALF-DUPLEX COOPERATIVE-NOMA IN UNDERLAY COGNITIVE HYBRID SATELLITE-TERRESTRIAL NETWORKS

In the previous chapters, we considered the overlay spectrum sharing approach for the analytical frameworks. Since the overlay approach employs sophisticated signal processing and coding techniques, the underlay approach is favoured and broadly utilized owing to its simplicity in implementation. Nevertheless, in underlay, the coverage and capacity of the secondary network remain limited due to the SU's transmit power constraints.

Future wireless networks have to meet the demands of high data rate and a huge number of users effectively. In this regard, the NOMA [64] has been regarded as one of the most promising techniques for the next-generation wireless networks, where the multiple users are served simultaneously based on the power domain in same time/frequency resources, providing higher spectral efficiency. Recently, the NOMA scheme has gained a great interest in conjunction with CHSTNs using underlay [24] and overlay [25]-[27] paradigms. In particular, authors in [24] derived the expression of ergodic capacity for the NOMA-based CHSTN. In [25] and [26], the authors evaluated the OP expressions for both primary and secondary networks using AF and DF based relaying protocols, respectively. Besides, authors in [27] analyzed a Vickrey auction-based secondary relay selection in NOMA-assisted overlay CHSTNs.

Meanwhile, the cooperative relaying technique has been introduced into the original NOMA scheme to obtain a spatial diversity gain for the far-away NOMA user with worse link quality, referred to as C-NOMA [13]. Therefore, the amalgamation of C-NOMA scheme into CHSTNs can remarkably ameliorate the performance against the stipulated transmit power constraints on the SUs. As such, it becomes favourable and reasonable to integrate the relaying technique into CR [34], [66] without deploying the extra relay nodes. But this improvement in the performance of CHSTNs requires additional bandwidth costs for the system owing to HD relaying, which may offset the performance gain guaranteed by cooperative communication.

To further improve the performance of CHSTNs, in this chapter, we focus on the C-NOMA scheme with FD relaying mode. Since in FD mode, the signal reception and transmission occur concurrently in the same frequency band, it suffers from a LI [67], [68] owing to its co-channel transmission. However, the effect of LI can be suppressed due to the advancement of antenna and signal processing technologies [69], which provides a solid chance for the realization of advantages brought by the FD mode, making CHSTNs more spectrally efficient. To this end, most of the existing works in CHSTNs are based on the conventional NOMA scheme and are conjectured the subsistence of pSIC [24]-[27]. However, in practice, the NOMA technique causes many implementation issues, such as complexity scaling and error propagation [28], [70], [71]. Consequently, these critical factors will lead to an error in decoding, causing residual IS, which may pose limitations on the capacity of the CHSTNs. Thus, it becomes essential to investigate the deleterious impacts of ipSIC on CHSTNs with FD C-NOMA scheme. Albeit few works have examined the system performance while integrating the C-NOMA scheme with HD relaying mode into their system model, they are particularly deliberated for the case of basic HSTNs [72], [73]. To the best of authors' knowledge, no work has yet looked into the comprehensive performance analysis of CHSTNs or even terrestrial underlay CRs (e.g., [74]) with FD/HD C-NOMA schemes under the impacts of both ipSIC and pSIC situations. It is worth pointing that analyzing the performance by considering various topics at the same time postures new mathematical intricacies because of the involved complicated hybrid channel modelling and multiple random variables (multiple integrals). Also, there is a lack of thorough performance analysis in terms of OP, ESR, and throughput. Note that such analyses are important for perceiving the repercussion of ipSIC/pSIC on CHSTNs with FD/HD C-NOMA schemes and to realize the implementation of such networks in the 5G and beyond wireless environments.

Impelled by the above discussion, in this chapter, we analyze the performance of an underlay CHSTN (UCHSTN) comprising a primary satellite source with its multiple terrestrial PRs and a ST with its two pre-paired users that are deployed on the ground based on the C-NOMA scheme. Herein, the nearby NOMA-strong user works in FD mode while employing the DF relaying strategy for improving the performance of the far-away NOMA-weak user. It is important to note that in CR scenario, both primary and secondary networks are allowed to transmit over the same frequency band, thus, we consider their mutual interference over each other [75]. Also, we perform a more comprehensive analysis of UCHSTN while taking into account the situations of ipSIC and pSIC for both the FD C-NOMA scheme and the benchmark HD C-NOMA scheme for comparison purposes, represented as FD-ipSIC, FD-pSIC, HD-ipSIC, and HD-pSIC, respectively. The major contributions of the chapter are emphasized as follows:

- For the proposed UCHSTN, we first derive the OP expressions of the primary satellite network for a predefined outage constraint at one of the opportunistically selected PR among L PRs under the FD/HD C-NOMA schemes. This facilitates the transmit power allocation for the SUs based on satisfying the QoS constraint at the PRs in terms of OP. Hereby, we illustrate that multiple PRs manifest the advantages of improved primary OP, which allows allocation of more transmit powers for the SUs.

- Based on the SUs' transmit powers, we investigate the performance of the secondary terrestrial network while deriving the analytical expressions of OP and ESR for the FD C-NOMA scheme, under the appropriately modelled shadowed-Rician fading for the satellite links and Nakagami-m fading for the terrestrial links. For this, the situations of both ipSIC and pSIC are taken into account. Further, for comparison purposes, the performance of benchmark HD C-NOMA scheme is analyzed under both situations. Also, a performance comparison is carried out through simulations in anticipation to the conventional OMA scheme.

- Further, to provide more insights, the asymptotic OP expressions are derived at a high SNR, and the corresponding diversity orders are obtained for the various cases. We demonstrate that zero diversity order results for the cases of FD-ipSIC, FD-pSIC, and HD-ipSIC, due to LI and/or residual IS. However, the performance in case of HD-pSIC is notably improved at high SNR due to a non-zero diversity order.

- Relying on the derived OP and ESR expressions, we also investigate the throughput performance for the two specific transmission scenarios i.e., delay-limited and delay-tolerant, respectively. Hereby, we illustrate that for the case of ipSIC, the FD C-NOMA scheme offers higher throughput than the HD C-NOMA scheme in the entire regime of SNRs. However, for the case of pSIC, the HD C-NOMA can provide higher throughput than its FD C-NOMA counterpart at high SNR region. Also, FD/HD C-NOMA schemes present higher throughput than the OMA scheme under ipSIC/pSIC situations in the low SNR regime. On the contrary, in the high SNR regime, the OMA scheme can outperform the FD C-NOMA under ipSIC/pSIC and HD C-NOMA under ipSIC. Moreover, the delay-tolerant transmission scenario has a remarkably higher throughput than the delay-limited scenario.

The rest of the chapter is ordered as follows. In Section 5.1, the system model of UCHSTN is framed while deriving the expressions for SINRs over heterogeneous fading channels. In Section 5.2, the transmit powers at SUs are calculated for both FD C-NOMA and HD C-NOMA schemes numerically to satisfy the QoS criterion at the best selected PR among L PRs. In Section 5.3, we investigate the performance of the secondary terrestrial network by analyzing the OP, ESR, and throughput. Numerical and simulation results are presented in Section 5.4. Finally, Section 5.5 summarizes the chapter.

5.1 System Descriptions

This section first provides a detailed description of the considered system model and thereafter characterizes the pertinent hybrid channel model, followed by the derivation of SINR expressions for NOMA users.

5.1.1 System Model

As illustrated in Fig. 5.1, we consider an UCHSTN where a secondary terrestrial network shares the spectrum with the primary satellite network. The primary network comprises a satellite source (PT) A with its intended L multiple destinations (PRs) $\{B_l\}_{l=1}^{L}$, whereas the secondary network consists of a ST node C with its

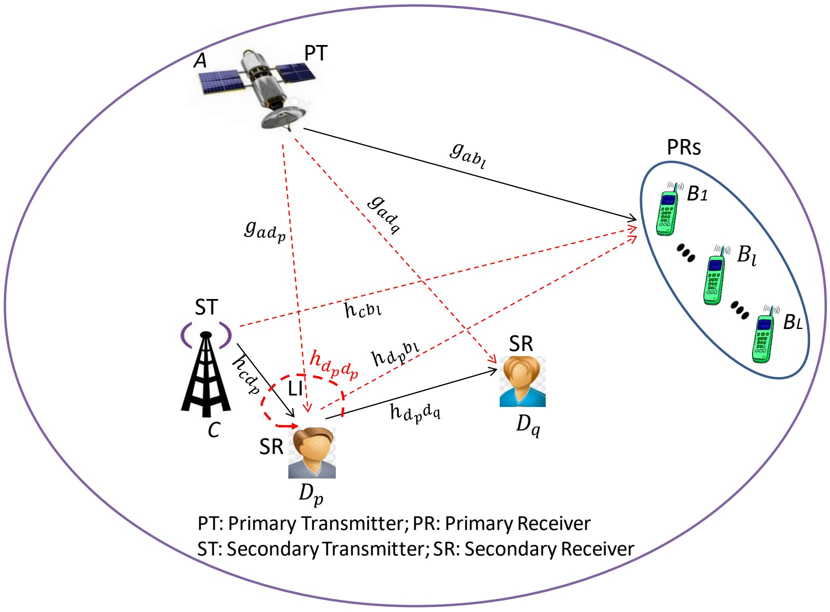

Figure 5.1: UCHSTN system model with transmission links ($\rightarrow$) and interference links ($\dashrightarrow$).

corresponding SRs D_p and D_q which are deployed based on the C-NOMA scheme[1]. We assume that the direct link between secondary source C and its receiver D_q is masked due to severe shadowing, blocking, etc. [76], [77]. It could be possible in highly shadowed regions like shopping malls, tunnels, etc., where the user D_q does not have a reliable direct communication link with the source C. Therefore, the user D_p acts as a DF relay to decode and forward the information of user D_q. As mentioned earlier, D_p works in FD mode, thus, to perform its operation, node D_p is equipped with two antennas[2] i.e., one for the signal reception and other for the signal transmission. However, rest of the network nodes are assumed to be the single antenna nodes[3]. All the channels are assumed to follow block fading so that they remain unchanged for a block duration but may change independently in the next block transmission. The various channel coefficients for the satellite links $A \rightarrow B_l$, $A \rightarrow D_p$, and $A \rightarrow D_q$ are denoted as g_{ab_l}, g_{ad_p}, and g_{ad_q}, respectively, and are subject to shadowed-Rician fading. Whereas, the terrestrial links $C \rightarrow D_p$, $C \rightarrow B_l$,

[1]In a practical situation, primary source A represents a GEO satellite and nodes $\{B_l\}_{l=1}^{L}$ may constitute the handheld devices as integrated in the DVB-SH service (in S-band) [7]. Whereas, the secondary source C could be a femtocell BS underlying in a macrocell with its nearby user D_p and far-away user D_q [53].

[2]The relay equipped with two separate antennas is always helpful not only for FD mode due to LI suppression but also for the HD mode which gets benefitted from it owing to the adjustment of antenna configuration separately in two directions [78].

[3]For applications that combine Internet-of-Things (IoT) with cellular networks, sensors and/or devices in the future massive machine-type communication networks are generally equipped with a single antenna [79].

$D_p \to D_p$, $D_p \to D_q$, and $D_p \to B_l$ undergo independent Nakagami-m fading distributions, and channel coefficients corresponding to them are represented by h_{cd_p}, h_{cb_l}, $h_{d_pd_p}$, $h_{d_pd_q}$, and $h_{d_pb_l}$, respectively. All the receiving nodes are assumed to be inflicted by the AWGN i.e., modelled as $\mathcal{CN}(0, \sigma^2)$.

For the subsequent system description, we first mark the statistics of the underlying hybrid fading channels.

5.1.2 Channel Model

For the satellite links, a widely adopted shadowed-Rician fading model is considered. Accordingly, the PDF of the channel gains $|g_{aj}|^2$, $j \in \{b_l, d_p, d_q\}$, can be given as [24]-[27]

$$f_{|g_{aj}|^2}(x) = \alpha_j \, \mathrm{e}^{-\beta_j x} \, {}_1F_1\left(m_{aj}; 1; \delta_j x\right), \; x \geq 0, \tag{5.1}$$

with $\alpha_j = (2\flat_{aj} m_{aj}/(2\flat_{aj} m_{aj} + \Omega_{aj}))^{m_{aj}}/2\flat_{aj}$, $\beta_j = 1/2\flat_{aj}$, $\delta_j = \Omega_{aj}/(2\flat_{aj})(2\flat_{aj} m_{aj} + \Omega_{aj})$, where $2\flat_{aj}$ is the average power of multipath component, Ω_{aj} be the average power of LoS component, and m_{aj} is the fading severity parameter.

Considering the numerous practical effects, such as free-space loss, antenna pattern, etc., the scaling parameter[4] of the satellite links $\sqrt{Q_j}$, $j \in \{b_l, d_p, d_q\}$, can be given as [80]

$$\sqrt{Q_j} = \frac{c\sqrt{G_j(\varphi_j)G_j}}{4\pi f d_{aj}\sqrt{K_B T B}}, \tag{5.2}$$

with c being the speed of light, f is the carrier frequency, $d_{aj} \approx 35786$ km is the distance between the satellite A and the user j, $K_B = 1.38 \times 10^{-23}$ J/°K be the Boltzman constant, T being the receiver noise temperature, and B is the carrier bandwidth. Besides, G_j is the antenna gain at user j, whereas $G_j(\varphi_j)$ is the satellite beam gain based on both satellite beam pattern and position of the user j, and approximately given as [81]

$$G_j(\varphi_j) = G_{\max}\left(\frac{J_1(u_j)}{2u_j} + 36\frac{J_3(u_j)}{u_j^3}\right)^2, \tag{5.3}$$

with $u_j = 2.07123\frac{\sin\varphi_j}{\sin\varphi_{j3\mathrm{dB}}}$, while $G_{\max}$ represents the maximal beam gain. φ_j is the

[4]It is noteworthy that the GEO satellite is positioned at a very large distance from the ground, i.e., 35786 km, and the beamwidth of satellite antenna pattern is of the order of less than 1°. Thus, it is reasonable to consider the equal scaling parameters for all the terrestrial users.

angle between user j and beam centre with respect to the satellite, and $\varphi_{j3\mathrm{dB}}$ be the 3-dB angle.

Hereby, simplifying the term ${}_1F_1\left(m_{aj};1;\delta_j x\right)$ in (5.1) and considering $\widetilde{\eta_a}=\eta_a Q_j$, where $\eta_a=\frac{P_a}{\sigma^2}$ with P_a being the transmit power through satellite A, one can express the PDF of $\Lambda_{aj}=\widetilde{\eta_a}|g_{aj}|^2$, for the arbitrary integer values of the fading severity parameters, as [4], [5]

$$f_{\Lambda_{aj}(x)}=\alpha_j\sum_{\kappa=0}^{m_{aj}-1}\frac{\xi_j(\kappa)}{(\widetilde{\eta_a})^{\kappa+1}}x^{\kappa}\mathrm{e}^{-\left(\frac{\beta_j-\delta_j}{\widetilde{\eta_a}}\right)x}, \tag{5.4}$$

where $\xi_j(\kappa)=(-1)^{\kappa}(1-m_{aj})_{\kappa}\delta_j^{\kappa}/(\kappa!)^2$. Now, carrying out the integration of the PDF in (5.4) using [41, eq. 3.351.2], the CDF $F_{\Lambda_{aj}}(x)$ can be obtained as

$$F_{\Lambda_{aj}}(x)=1-\alpha_j\sum_{\kappa=0}^{m_{aj}-1}\sum_{p=0}^{\kappa}\frac{\xi_j(\kappa)}{(\widetilde{\eta_a})^{\kappa+1}}\frac{\kappa!}{p!}\left(\frac{\beta_j-\delta_j}{\widetilde{\eta_a}}\right)^{-(\kappa+1-p)}x^{p}\mathrm{e}^{-\left(\frac{\beta_j-\delta_j}{\widetilde{\eta_a}}\right)x}. \tag{5.5}$$

Since the terrestrial links are subject to Nakagami-m fading, the respective PDF and CDF of $\Lambda_{ij}=\eta_i|h_{ij}|^2$, for $i\in\{c\}$ with $j\in\{b_l,d_p\}$ and $i\in\{d_p\}$ with $j\in\{b_l,d_p,d_q\}$, can be given as

$$f_{\Lambda_{ij}}(x)=\left(\frac{m_{ij}}{\Omega_{ij}\eta_i}\right)^{m_{ij}}\frac{x^{m_{ij}-1}}{\Gamma(m_{ij})}\mathrm{e}^{-\frac{m_{ij}}{\Omega_{ij}\eta_i}x} \tag{5.6}$$

and

$$F_{\Lambda_{ij}}(x)=\frac{1}{\Gamma(m_{ij})}\Upsilon\left(m_{ij},\frac{m_{ij}}{\Omega_{ij}\eta_i}x\right), \tag{5.7}$$

where Ω_{ij} is the average power and m_{ij} be the fading severity parameter.

5.1.3 Signal Model

During the k-th time slot, SU source node C broadcasts a superposing signal $x_c[k]=\sqrt{\rho P_c}x_{d_p}[k]+\sqrt{(1-\rho)P_c}x_{d_q}[k]$ towards its receiving nodes D_p and D_q with $x_{d_p}[k]$ and $x_{d_q}[k]$ represent the unit-energy information signals for user D_p and D_q, respectively, P_c being the transmit power through node C, and $\rho\in(0,1)$ denotes the power allocation factor corresponding to user D_p. However, for performing the adequate NOMA operation, relatively more power is allocated towards the weak user, and thus, ρ becomes limited to $(0,0.5)$ [76].

When D_p operates in FD mode, an imperfect self-interference cancellation scheme is assumed to be executed [82], leading to a residual LI at D_p, whose channel $h_{d_p d_p}$ is subject to Nakagami-m fading[5], as mentioned earlier. Hereby, D_p simultaneously receives the superposed signal from secondary source C, LI signal due to FD relaying, and interference signal from primary satellite source. Accordingly, the resultant signal at D_p can be expressed as

$$y_{d_p}[k] = h_{cd_p} x_c[k] + h_{d_p d_p} \sqrt{\omega P_{d_p}} x_{\mathrm{LI}}[k-\tau] + \sqrt{P_a Q_{d_p}} g_{ad_p} x_a[k] + v_{d_p}[k], \tag{5.8}$$

where P_{d_p} is the transmit power through node D_p, $v_{d_p}[k]$ is the AWGN variable, $x_{\mathrm{LI}}[k-\tau]$ is the unit energy LI signal, where τ being the processing delay at node D_p, with an integer $\tau \geq 1$ and $k \geq \tau$. Further, $\omega = 1$ and $\omega = 0$ denote the respective cases of FD and HD relaying modes. Note that in HD mode, the overall transmission occurs in two phases [72], [73]. It is worthwhile to mention that the transmit power allocation[6] for the SUs (i.e., P_c and P_{d_p}) will be executed based on satisfying the QoS constraint at the PRs in terms of OP, as explained later in Section 5.2.

Now, based on the NOMA principle, SIC is performed by the strong user D_p for decoding the signal of weak user D_q. Thus, the received SINR at D_p to decode the information x_{d_q} can be given as

$$\Lambda_{d_p \to d_q} = \frac{(1-\rho)\Lambda_{cd_p}}{\rho \Lambda_{cd_p} + \omega \Lambda_{d_p d_p} + \Lambda_{ad_p} + 1}, \tag{5.9}$$

where $\Lambda_{cd_p} = \eta_c |h_{cd_p}|^2$ with $\eta_c = \frac{P_c}{\sigma^2}$, $\Lambda_{d_p d_p} = \eta_{d_p} |h_{d_p d_p}|^2$ with $\eta_{d_p} = \frac{P_{d_p}}{\sigma^2}$, and $\Lambda_{ad_p} = \widetilde{\eta}_a |g_{ad_p}|^2$.

Afterwards, user D_p decodes its own signal x_{d_p} by removing x_{d_q} from x_c. However, owing to the decoding error and hardware imperfections, the SIC could be imperfect in realistic conditions [86]. Thereby, we consider that a residual interfer-

[5]In general, the PDF of magnitude of the LI channel coefficient depends on the type of cancellation/isolation techniques used to mitigate the self-interference [83]. Based on the experiment-driven results reported in many papers, when strong passive suppression is employed, the LoS component is efficiently suppressed, and the LI channel can be regarded as Rayleigh-fading channel. As a generalization, we consider here a Nakagami-m fading distribution corresponding to LI channel [84].

[6]The transmit power calculations for SUs in various previous works, e.g., [18], [20], [66], [84] are relied upon satisfying the instantaneous interference threshold criterion at the PRs, which finally requires the knowledge of instantaneous channel gains of the links between SUs and PUs. However, in a practical situations, channels may subject to fast fading due to high mobility, thus it becomes hard to get the instantaneous channel gains [75], [85].

ence exists, leading to an ipSIC term. Thus, after the ipSIC, the SINR at node D_p can be obtained as

$$\Lambda_{d_p} = \frac{\rho \Lambda_{cd_p}}{\varsigma(1-\rho)\Lambda_{D_p} + \omega \Lambda_{d_p d_p} + \Lambda_{ad_p} + 1}, \tag{5.10}$$

where $\varsigma = 0$ and $\varsigma = 1$ refer to the respective situations of pSIC and ipSIC, $\Lambda_{D_p} = \eta_c |h_{D_p}|^2$ with h_{D_p} is the residual IS channel coefficient at node D_p, and is subject to Nakagami-m fading [87] with its respective fading severity parameter and average channel power gain as m_{D_p} and Ω_{D_p}.

Hereafter, user D_p invokes DF relaying protocol, and decodes and forwards the signal x_{d_q} to user D_q, thus, a processing delay τ is introduced. Accordingly, during the k-th time slot, the received signal at D_q can be represented as

$$y_{d_q}[k] = \sqrt{P_{d_p}} h_{d_p d_q} x_{d_q}[k-\tau] + \sqrt{P_a Q_{d_q}} g_{ad_q} x_a[k] + v_{d_q}[k], \tag{5.11}$$

where $v_{d_q}[k]$ is the AWGN variable. Hereby, the received SINR at D_q through node D_p (relay) can be expressed as

$$\Lambda_{d_q} = \frac{\Lambda_{d_p d_q}}{\Lambda_{ad_q} + 1}, \tag{5.12}$$

where $\Lambda_{d_p d_q} = \eta_{d_p} |h_{d_p d_q}|^2$ and $\Lambda_{ad_q} = \widetilde{\eta}_a |g_{ad_q}|^2$.

5.2 Primary Outage Constraint Based SUs' Transmit Power Calculation

In this section, we derive the OP expressions of the primary satellite network for a predefined outage constraint at the best selected PR among L PRs under the FD/HD C-NOMA schemes. Importantly, these analyses help in solving the transmit power allocation problem for the SUs based on the average channel gains of the link from itself to PRs.

5.2.1 FD C-NOMA Scheme

During the k-th time slot, the primary satellite source A broadcasts a unit energy signal $x_a[k]$ (with $\mathbb{E}[|x_a[k]|^2] = 1$) towards its L PRs. Accordingly, the received signal at node B_l can be given as

$$y_{b_l}[k] = \sqrt{P_a Q_{b_l}} g_{ab_l} x_a[k] + \sqrt{P_c} h_{cb_l} x_c[k] + \sqrt{P_{d_p}} h_{d_p b_l} x_{d_q}[k-\tau] + v_{b_l}[k], \quad (5.13)$$

where $v_{b_l}[k]$ is the AWGN variable. As such, using (5.13), the SINR at node B_l can be expressed as

$$\Lambda_{b_l}^{\text{Pri}} = \frac{\Lambda_{ab_l}}{\Lambda_{cb_l} + \Lambda_{d_p b_l} + 1}, \quad (5.14)$$

where $\Lambda_{ab_l} = \widetilde{\eta}_a |g_{ab_l}|^2$, $\Lambda_{cb_l} = \eta_c |h_{cb_l}|^2$, and $\Lambda_{d_p b_l} = \eta_{d_p} |h_{d_p b_l}|^2$.

As stated earlier, in UCHSTN, the secondary nodes C and D_p have to satisfy the QoS criterion at node B_l while tuning their transmit powers. To quantify this QoS criterion, the OP of primary transmission should be kept below a predefined outage constraint ζ_{th}. Therefore, for a given target rate R_p, the OP of the primary link $A \to B_l$ can be expressed using (5.14) as

$$P_{\text{out},l}^{\text{Pri}}(R_p) = \Pr\left[\log_2\left(1 + \Lambda_{b_l}^{\text{Pri}}\right) < R_p\right] \leq \zeta_{\text{th}}, \quad (5.15)$$

which can be re-written as

$$P_{\text{out},l}^{\text{Pri}}(R_p) = \Pr\left[\Lambda_{b_l}^{\text{Pri}} < \gamma_p\right] \leq \zeta_{\text{th}}, \quad (5.16)$$

where $\gamma_p = 2^{R_p} - 1$. Hereby, we calculate the overall primary OP by using the selection[7] criteria for the best satellite user based on maximizing $\Lambda_{b_l}^{\text{Pri}}$ as

$$P_{\text{out}}^{\text{Pri}}(R_p) = \Pr\Big[\max_{l \in \{1,\ldots,L\}} \Lambda_{b_l}^{\text{Pri}} < \gamma_p\Big] \leq \zeta_{\text{th}}, \quad (5.17)$$

which can be re-expressed while applying order statistics for L independent PRs as

[7] The source satellite A needs to be informed about the index of the selected user through a reverse feeder link [88]. However, it would be intricate to acquire the perfect feedback at satellite A due to long distance, propagation delay, atmospheric attenuation, etc. [89]. Similar to our work, majority of the earlier works on HSTNs have relied on assumptions of perfect CSI and/or perfect feedback for a benchmark performance analysis, e.g., [20], [80]. Although work in [90] has dealt with the issue of CSI acquisition in HSTNs, the analysis of feedback delay and outdated CSI over the satellite links still remains a challenging research problem.

[80]

$$P_{\text{out}}^{\text{Pri}}(R_p) = \prod_{l=1}^{L} F_{\Lambda_{b_l}^{\text{Pri}}}(\gamma_p) \leq \zeta_{\text{th}}. \tag{5.18}$$

Now, (5.18) can be further solved while assuming equal power $P_{d_p} = P_c$ (and thereby $\eta_{d_p} = \eta_c$) [91], as follows in Theorem 4.

Theorem 4. *The OP of primary satellite network under the FD C-NOMA scheme can be expressed using (5.18) as*

$$\begin{aligned} P_{out}^{Pri}(R_p) = \prod_{l=1}^{L} \Bigg(1 - & \sum_{\kappa=0}^{m_{ab_l}-1} \sum_{m=0}^{\kappa} \sum_{v=0}^{m} \sum_{g=0}^{m-v} \alpha_{b_l} \frac{\xi_{b_l}(\kappa)}{(\widetilde{\eta}_a)^{\kappa+1}} \frac{\kappa!}{m!} \frac{\Gamma(v+m_{cb_l})}{\Gamma(m_{cb_l})} \binom{m}{v} \binom{m-v}{g} \\ & \times e^{-\left(\gamma_p \frac{\beta_{b_l}-\delta_{b_l}}{\widetilde{\eta}_a}\right)} \left(\gamma_p \frac{\beta_{b_l}-\delta_{b_l}}{\widetilde{\eta}_a} + \frac{m_{cb_l}}{\Omega_{cb_l}\eta_c} \right)^{-\left(v+m_{cb_l}\right)} \frac{\Gamma(g+m_{d_pb_l})}{\Gamma(m_{d_pb_l})} \\ & \times \left(\gamma_p \frac{\beta_{b_l}-\delta_{b_l}}{\widetilde{\eta}_a} + \frac{m_{d_pb_l}}{\Omega_{d_pb_l}\eta_c} \right)^{-\left(g+m_{d_pb_l}\right)} \left(\frac{\beta_{b_l}-\delta_{b_l}}{\widetilde{\eta}_a} \right)^{-(\kappa+1-m)} \\ & \times \gamma_p^m \left(\frac{m_{cb_l}}{\Omega_{cb_l}\eta_c} \right)^{m_{cb_l}} \left(\frac{m_{d_pb_l}}{\Omega_{d_pb_l}\eta_c} \right)^{m_{d_pb_l}} \Bigg) \leq \zeta_{th}. \end{aligned} \tag{5.19}$$

Proof. See Appendix D. ■

Now, for a given ζ_{th}, the transmit SNR η_c (involving transmit power P_c) can be calculated numerically by evaluating the expression in (5.19) using any computing software like MATHEMATICA or MAPLE.

5.2.2 HD C-NOMA Scheme

Similar to (5.13), the received signal at node B_l under the HD C-NOMA scheme can be given during the k-th time slot as

$$y_{b_l}[k] = \sqrt{P_a Q_{b_l}} g_{ab_l} x_a[k] + \sqrt{P_c} h_{cb_l} x_c[k] + v_{b_l}[k]. \tag{5.20}$$

As such, using (5.20), the SINR at node B_l can be expressed as

$$\Lambda_{b_l}^{\text{Pri}} = \frac{\Lambda_{ab_l}}{\Lambda_{cb_l} + 1}. \tag{5.21}$$

Hereby, using similar steps as in FD C-NOMA scheme, the overall primary OP for a given target rate R_p can be evaluated using (5.21) into (5.18), as given in Lemma 3.

Lemma 3. *The OP of primary satellite network under the HD C-NOMA scheme can be expressed using (5.18) and (5.21) as*

$$P_{out}^{Pri}(R_p) = \prod_{l=1}^{L} \left(1 - \sum_{\kappa=0}^{m_{ab_l}-1} \sum_{v=0}^{\kappa} \sum_{g=0}^{v} \alpha_{b_l} \frac{\xi_{b_l}(\kappa)}{(\widetilde{\eta}_a)^{\kappa+1}} \frac{\kappa!}{v!} \frac{\Gamma(v-g+m_{cb_l})}{\Gamma(m_{cb_l})} \binom{v}{g} \right.$$
$$\times \left(\gamma_p \frac{\beta_{b_l} - \delta_{b_l}}{\widetilde{\eta}_a} + \frac{m_{cb_l}}{\Omega_{cb_l}\eta_c} \right)^{-(v-g+m_{cb_l})} \left(\frac{\beta_{b_l} - \delta_{b_l}}{\widetilde{\eta}_a} \right)^{-(\kappa+1-v)}$$
$$\left. \times \gamma_p^v e^{-\left(\gamma_p \frac{\beta_{b_l}-\delta_{b_l}}{\widetilde{\eta}_a}\right)} \left(\frac{m_{cb_l}}{\Omega_{cb_l}\eta_c} \right)^{m_{cb_l}} \right) \leq \zeta_{th}. \tag{5.22}$$

Proof. Proof of Lemma 3 can be followed using the similar steps as for Theorem 4 in Appendix D. ■

Now, for a given ζ_{th}, by evaluating the expression in (5.22) with respect to η_c similar to (5.19), the transmit SNR η_c can be calculated numerically at node C. Likewise, one can assess the transmit SNR η_{d_p} at node D_p, while following the expression in (5.22) by replacing the terms m_{cb_l}, Ω_{cb_l}, and η_c with $m_{d_pb_l}$, $\Omega_{d_pb_l}$, and η_{d_p}, respectively.

Remark 5.1: The above-stated transmit power calculations require only the average channel gains of the link from itself to PRs, i.e., $C \to B_l$ and $D_p \to B_l$. Average channel gains are relatively more stable and can save the feedback channel resources [34], [75], [85] as compared with instantaneous channel gains. Moreover, the average channel gains have more realistic significance, as their knowledge can be acquired by using the frequency of the radio waves, transmission distance, etc.

Remark 5.2: Impact of multiple PRs can be realized in the form of improved primary OP from (5.19) and (5.22), which allows the SUs' transmit powers to be increased numerically under the fixed values of ζ_{th}. Moreover, the transmit powers calculated for SUs under the HD C-NOMA scheme are relatively more as compared to the FD C-NOMA scheme, as the FD mode allows simultaneous transmissions from both nodes C and D_p. Its implications will be further elaborated in the Numerical Results and Discussion section.

5.3 Performance Evaluation

In this section, we analyze the performance of the secondary terrestrial network while deriving the analytical expressions of OP, ESR, and throughput for the various cases viz., FD-ipSIC, FD-pSIC, HD-ipSIC, and HD-pSIC. In addition, we investigate the outage performance at a high SNR, and thereby calculate the achievable diversity orders for the respective cases.

5.3.1 Outage Probability Analysis

To characterize the outage behaviour of the secondary network, we derive the exact and asymptotic OP expressions as follows:

Exact Outage Probability Analysis

To start with, we define that secondary network goes into outage when either user D_p or user D_q are unable to decode their respective signals. To successfully detect x_{d_p}, user D_p should decode both x_{d_q} and x_{d_p} signals. On the other hand, to successfully detect x_{d_q} at user D_q, x_{d_q} should be decoded at both D_p and D_q nodes. Accordingly, the OP of the secondary network for the given SINR thresholds γ_{d_p} and γ_{d_q} can be appraised as

$$P_{\text{out}}^{\text{Sec}} = 1 - \Pr\big[\Lambda_{d_p \to d_q} \geq \gamma_{d_q}, \Lambda_{d_p} \geq \gamma_{d_p}, \Lambda_{d_q} \geq \gamma_{d_q}\big]. \tag{5.23}$$

Since Λ_{d_q} is independent from both $\Lambda_{d_p \to d_q}$ and Λ_{d_p}, (5.23) can be re-expressed as

$$P_{\text{out}}^{\text{Sec}} = 1 - \underbrace{\Pr\big[\Lambda_{d_p \to d_q} \geq \gamma_{d_q}, \Lambda_{d_p} \geq \gamma_{d_p}\big]}_{\chi_1} \underbrace{\Pr\big[\Lambda_{d_q} \geq \gamma_{d_q}\big]}_{\chi_2}, \tag{5.24}$$

wherein for FD mode, $\gamma_{d_q} = \gamma_{d_q}^{\text{FD}} = 2^{R_{d_q}-1}$ and $\gamma_{d_p} = \gamma_{d_p}^{\text{FD}} = 2^{R_{d_p}-1}$, with R_{d_q} and R_{d_p} are the target rates to detect the signals x_{d_q} and x_{d_p}, respectively. Similarly, for HD mode, $\gamma_{d_q} = \gamma_{d_q}^{\text{HD}} = 2^{2R_{d_q}-1}$, $\gamma_{d_p} = \gamma_{d_p}^{\text{HD}} = 2^{2R_{d_p}-1}$. Hereby, following (5.24), the final expression of $P_{\text{out}}^{\text{Sec}}$ can be provided with the help of Theorem 5 as given below.

Theorem 5. *Depending on the various cases, the OP of the secondary network under the hybrid satellite-terrestrial channels can be given as*

$$P_{out}^{Sec} = \begin{cases} P_{out}^{FD\text{-}ipSIC} = 1 - \chi_1^{FD\text{-}ipSIC}\chi_2^{FD}, & \textit{for FD-ipSIC}, \\ P_{out}^{FD\text{-}pSIC} = 1 - \chi_1^{FD\text{-}pSIC}\chi_2^{FD}, & \textit{for FD-pSIC}, \\ P_{out}^{HD\text{-}ipSIC} = 1 - \chi_1^{HD\text{-}ipSIC}\chi_2^{HD}, & \textit{for HD-ipSIC}, \\ P_{out}^{HD\text{-}pSIC} = 1 - \chi_1^{HD\text{-}pSIC}\chi_2^{HD}, & \textit{for HD-pSIC}, \end{cases} \tag{5.25}$$

where $\chi_1^{FD\text{-}pSIC} = \sum_{m=0}^{\mathrm{m}_{cd_p}-1} \sum_{g=0}^{m} \sum_{\kappa=0}^{\mathrm{m}_{ad_p}-1} \sum_{u=0}^{m-g} Q_{m,g,\kappa,u}^{FD}$, $\chi_1^{HD\text{-}pSIC} = \sum_{m=0}^{\mathrm{m}_{cd_p}-1} \sum_{g=0}^{m} \sum_{\kappa=0}^{\mathrm{m}_{ad_p}-1} Q_{m,g,\kappa}^{HD}$, *with the respective expressions for the other involved terms can be given as in (5.26) and (5.27). And, the corresponding expressions for χ_2^{FD} and χ_2^{HD} can be readily obtained from (5.28) on substituting $\chi_2 = \chi_2^{FD}$ with $\gamma_{d_q} = \gamma_{d_q}^{FD}$ and $\chi_2 = \chi_2^{HD}$ with $\gamma_{d_q} = \gamma_{d_q}^{HD}$.*

Proof. See Appendix E. ∎

$$\begin{aligned}
\chi_1^{\text{FD-ipSIC}} &= \sum_{m=0}^{m_{cd_p}-1}\sum_{g=0}^{m}\sum_{\kappa=0}^{m_{ad_p}-1}\sum_{u=0}^{m-g}\sum_{v=0}^{m-g-u}\left(\frac{m_{cd_p}\gamma_{d_p}^{\text{FD}}}{\Omega_{cd_p}\eta_c\rho}+\frac{m_{D_p}}{\Omega_{D_p}\eta_c(1-\rho)}\right)^{-(v+m_{D_p})}\\
&\times Q_{m,g,\kappa,u}^{\text{FD}}\binom{m-g-u}{v}\frac{\Gamma\left(v+m_{D_p}\right)}{\Gamma(m_{D_p})}\left(\frac{m_{D_p}}{\Omega_{D_p}\eta_c(1-\rho)}\right)^{m_{D_p}},\\
\text{with } Q_{m,g,\kappa,u}^{\text{FD}} &= \left(\frac{m_{cd_p}\gamma_{d_p}^{\text{FD}}}{\Omega_{cd_p}\eta_c\rho}\right)^{m}\frac{(\kappa+u)!}{m!}\binom{m}{g}\left(\frac{m_{d_pd_p}}{\Omega_{d_pd_p}\eta_{d_p}}\right)^{m_{d_pd_p}}\alpha_{d_p}\\
&\times\frac{\xi_{d_p}(\kappa)}{(\widetilde{\eta}_a)^{\kappa+1}}\mathrm{e}^{-\left(\frac{m_{cd_p}\gamma_{d_p}^{\text{FD}}}{\Omega_{cd_p}\eta_c\rho}\right)}\left(\frac{m_{cd_p}\gamma_{d_p}^{\text{FD}}}{\Omega_{cd_p}\eta_c\rho}+\frac{m_{d_pd_p}}{\Omega_{d_pd_p}\eta_{d_p}}\right)^{-(g+m_{d_pd_p})}\\
&\times\binom{m-g}{u}\frac{\Gamma(g+m_{d_pd_p})}{\Gamma(m_{d_pd_p})}\left(\frac{m_{cd_p}\gamma_{d_p}^{\text{FD}}}{\Omega_{cd_p}\eta_c\rho}+\frac{\beta_{d_p}-\delta_{d_p}}{\widetilde{\eta}_a}\right)^{-(\kappa+u+1)}. \qquad (5.26)
\end{aligned}$$

$$\begin{aligned}
\chi_1^{\text{HD-ipSIC}} &= \sum_{m=0}^{m_{cd_p}-1}\sum_{g=0}^{m}\sum_{\kappa=0}^{m_{ad_p}-1}\sum_{v=0}^{m-g}Q_{m,g,\kappa}^{\text{HD}}\left(\frac{m_{D_p}}{\Omega_{D_p}\eta_c(1-\rho)}\right)^{m_{D_p}}\binom{m-g}{v}\\
&\times\frac{\Gamma(v+m_{D_p})}{\Gamma(m_{D_p})}\left(\frac{m_{cd_p}\gamma_{d_p}^{\text{HD}}}{\Omega_{cd_p}\eta_c\rho}+\frac{m_{D_p}}{\Omega_{D_p}\eta_c(1-\rho)}\right)^{-(v+m_{D_p})},\\
\text{with } Q_{m,g,\kappa}^{\text{HD}} &= \left(\frac{m_{cd_p}\gamma_{d_p}^{\text{HD}}}{\Omega_{cd_p}\eta_c\rho}\right)^{m}\frac{(g+\kappa)!}{m!}\binom{m}{g}\alpha_{d_p}\frac{\xi_{d_p}(\kappa)}{(\widetilde{\eta}_a)^{\kappa+1}}\\
&\times\left(\frac{m_{cd_p}\gamma_{d_p}^{\text{HD}}}{\Omega_{cd_p}\eta_c\rho}+\frac{\beta_{d_p}-\delta_{d_p}}{\widetilde{\eta}_a}\right)^{-(g+\kappa+1)}\mathrm{e}^{-\left(\frac{m_{cd_p}\gamma_{d_p}^{\text{HD}}}{\Omega_{cd_p}\eta_c\rho}\right)}. \qquad (5.27)
\end{aligned}$$

$$\begin{aligned}
\chi_2 = 1-\sum_{\kappa=0}^{m_{ad_q}-1}\alpha_{d_q}\frac{\xi_{d_q}(\kappa)\kappa!}{(\beta_{d_q}-\delta_{d_q})^{\kappa+1}} &+ \sum_{m=0}^{m_{d_pd_q}-1}\sum_{g=0}^{m}\sum_{\kappa=0}^{m_{ad_q}-1}\left(\frac{m_{d_pd_q}\gamma_{d_q}}{\Omega_{d_pd_q}\eta_c}\right)^{m}\frac{(g+k)!}{m!}\\
&\times\left(\frac{m_{d_pd_q}\gamma_{d_q}}{\Omega_{d_pd_q}\eta_c}+\frac{\beta_{d_q}-\delta_{d_q}}{\widetilde{\eta}_a}\right)^{-(g+\kappa+1)}\\
&\times\binom{m}{g}\alpha_{d_q}\frac{\xi_{d_q}(\kappa)}{(\widetilde{\eta}_a)^{\kappa+1}}\mathrm{e}^{-\left(\frac{m_{d_pd_q}\gamma_{d_q}}{\Omega_{d_pd_q}\eta_c}\right)}. \qquad (5.28)
\end{aligned}$$

Asymptotic Outage Probability Analysis

For attaining more insights, we approximate the derived OP expression in (5.25) at a high SNR region ($\eta_c, \eta_{d_p} \to \infty$, with $\frac{\eta_c}{\eta_{d_p}}$ be a constant ratio) to calculate the achievable diversity orders for the various cases with the help of Lemma 4 as given below.

Lemma 4. *Referring to (5.25), the asymptotic OP expressions of secondary network (say it $P^{Sec}_{out,asy}$) for various cases under the hybrid satellite-terrestrial channels can be given in (5.29)-(5.32).*

Proof. See Appendix F. ∎

$$\begin{aligned}
P^{\text{FD-ipSIC}}_{\text{out,asy}} &= \Bigg[\sum_{m=0}^{m_{cd_p}} \sum_{g=0}^{m_{cd_p}-m} \sum_{\kappa=0}^{m_{ad_p}-1} \sum_{t=0}^{m_{cd_p}-m-g} \varphi^{\text{FD}}_{m,g,\kappa} \binom{m_{cd_p}-m-g}{t} \frac{\Gamma(t+m_{D_p})}{\Gamma(m_{D_p})} \\
&\quad \times \left\{ \widetilde{\eta_a}^{\,g} \left(\frac{m_{cd_p}\gamma^{\text{FD}}_{d_p}}{\Omega_{cd_p}\eta_c\rho}\right)^{m_{cd_p}} \left(\frac{\Omega_{d_pd_p}\eta_{d_p}}{m_{d_pd_p}}\right)^{m} \left(\frac{\Omega_{D_p}\eta_c(1-\rho)}{m_{D_p}}\right)^{t} \right\}\Bigg] \\
&\quad + \Bigg[\sum_{m=0}^{m_{d_pd_q}} \sum_{\kappa=0}^{m_{ad_q}-1} \psi_{m,\kappa} \left\{ \widetilde{\eta_a}^{\,m} \left(\frac{m_{d_pd_q}\gamma^{\text{FD}}_{d_q}}{\Omega_{d_pd_q}\eta_c}\right)^{m_{d_pd_q}} \right\}\Bigg], \\
\text{with } \varphi^{\text{FD}}_{m,g,\kappa} &= \frac{(g+\kappa)!}{m_{cd_p}!} \binom{m_{cd_p}}{m} \frac{\Gamma(m+m_{d_pd_p})}{\Gamma(m_{d_pd_p})} \alpha_{d_p} \frac{\xi_{d_p}(\kappa)}{(\beta_{d_p}-\delta_{d_p})^{g+\kappa+1}} \binom{m_{cd_p}-m}{g}, \\
\psi_{m,\kappa} &= \frac{(m+\kappa)!}{m_{d_pd_q}!} \binom{m_{d_pd_q}}{m} \alpha_{d_q} \frac{\xi_{d_q}(\kappa)}{(\beta_{d_q}-\delta_{d_q})^{m+\kappa+1}}.
\end{aligned} \tag{5.29}$$

$$\begin{aligned}
P^{\text{FD-pSIC}}_{\text{out,asy}} &= \Bigg[\sum_{m=0}^{m_{cd_p}} \sum_{g=0}^{m_{cd_p}-m} \sum_{\kappa=0}^{m_{ad_p}-1} \varphi^{\text{FD}}_{m,g,\kappa} \left\{ \widetilde{\eta_a}^{\,g} \left(\frac{m_{cd_p}\gamma^{\text{FD}}_{d_p}}{\Omega_{cd_p}\eta_c\rho}\right)^{m_{cd_p}} \left(\frac{\Omega_{d_pd_p}\eta_{d_p}}{m_{d_pd_p}}\right)^{m} \right\}\Bigg] \\
&\quad + \Bigg[\sum_{m=0}^{m_{d_pd_q}} \sum_{\kappa=0}^{m_{ad_q}-1} \psi_{m,\kappa} \left\{ \widetilde{\eta_a}^{\,m} \left(\frac{m_{d_pd_q}\gamma^{\text{FD}}_{d_q}}{\Omega_{d_pd_q}\eta_c}\right)^{m_{d_pd_q}} \right\}\Bigg].
\end{aligned} \tag{5.30}$$

$$
\begin{aligned}
P_{\text{out,asy}}^{\text{HD-ipSIC}} =& \left[\sum_{m=0}^{m_{cd_p}} \sum_{g=0}^{m_{cd_p}-m} \sum_{\kappa=0}^{m_{ad_p}-1} \varphi_{m,\kappa}^{\text{HD}} \frac{\Gamma(g+m_{D_p})}{\Gamma(m_{D_p})} \binom{m_{cd_p}-m}{g} \right. \\
& \left. \times \left\{ \widetilde{\eta_a}^{m} \left(\frac{m_{cd_p}\gamma_{d_p}^{\text{HD}}}{\Omega_{cd_p}\eta_c\rho} \right)^{m_{cd_p}} \left(\frac{\Omega_{D_p}\eta_c(1-\rho)}{m_{D_p}} \right)^{g} \right\} \right] \\
& + \left[\sum_{m=0}^{m_{d_pd_q}} \sum_{\kappa=0}^{m_{ad_q}-1} \psi_{m,\kappa} \left\{ \widetilde{\eta_a}^{m} \left(\frac{m_{d_pd_q}\gamma_{d_q}^{\text{HD}}}{\Omega_{d_pd_q}\eta_c} \right)^{m_{d_pd_q}} \right\} \right], \\
\text{with } \varphi_{m,\kappa}^{\text{HD}} =& \frac{(m+\kappa)!}{m_{cd_p}!} \binom{m_{cd_p}}{m} \alpha_{d_p} \frac{\xi_{d_p}(\kappa)}{(\beta_{d_p}-\delta_{d_p})^{m+\kappa+1}}.
\end{aligned} \tag{5.31}
$$

$$
\begin{aligned}
P_{\text{out,asy}}^{\text{HD-pSIC}} =& \left[\sum_{m=0}^{m_{cd_p}} \sum_{\kappa=0}^{m_{ad_p}-1} \varphi_{m,\kappa}^{\text{HD}} \left\{ \widetilde{\eta_a}^{m} \left(\frac{m_{cd_p}\gamma_{d_p}^{\text{HD}}}{\Omega_{cd_p}\eta_c\rho} \right)^{m_{cd_p}} \right\} \right] \\
& + \left[\sum_{m=0}^{m_{d_pd_q}} \sum_{\kappa=0}^{m_{ad_q}-1} \psi_{m,\kappa} \left\{ \widetilde{\eta_a}^{m} \left(\frac{m_{d_pd_q}\gamma_{d_q}^{\text{HD}}}{\Omega_{d_pd_q}\eta_c} \right)^{m_{d_pd_q}} \right\} \right].
\end{aligned} \tag{5.32}
$$

Remark 5.3: In (5.29) and (5.30), substituting $m = m_{cd_p}$ into the first terms, one can assess the diversity orders for FD-ipSIC and FD-pSIC as $\min(0, m_{d_pd_q})$, i.e., zero. Similarly, in (5.31), substituting $m = 0$ into the first term, diversity order of zero can be achieved. We are doing such kind of substitutions to observe the dominant terms at high SNR region, which is reflected by the minimum power raised to $\frac{1}{\eta_c}$ and finally tells the diversity order. On the contrary, for the case of HD-pSIC in (5.32), the achievable diversity order is $\min(m_{cd_p}, m_{d_pd_q})$.

5.3.2 Ergodic Sum Rate Analysis

When the achievable rates of the users are decided by their channel conditions, ESR is an important measure for investigating the performance. ESR is defined as the expected value of E-E mutual information [42]. For the considered secondary network, it can be represented as

$$
C_{\text{esr}} = C_{d_p} + C_{d_q}, \tag{5.33}
$$

where C_{d_p} and C_{d_q} are the respective ergodic rates for user D_p and D_q.

Evaluation of C_{d_p}

Relying on the condition that D_p can detect x_{d_q}, the realizable ergodic rate of user D_p can be expressed [77], [92] as $C_{d_p} = \mathbb{E}\left[\log_2\left(1+\Lambda_{d_p}\right)\right]$. Accordingly, the ergodic rate for user D_p can be evaluated with the help of Theorem 6 as follows:

Theorem 6. *Depending on the various cases, the ergodic rate for user D_p under the hybrid satellite-terrestrial channels can be given as*

$$C_{d_p} = \begin{cases} C_{d_p}^{\text{FD-ipSIC}}, & \text{for FD-ipSIC},\\ C_{d_p}^{\text{FD-pSIC}}, & \text{for FD-pSIC},\\ C_{d_p}^{\text{HD-ipSIC}}, & \text{for HD-ipSIC},\\ C_{d_p}^{\text{HD-pSIC}}, & \text{for HD-pSIC}, \end{cases} \tag{5.34}$$

with the respective expressions for the involved cases can be given in (5.35)-(5.38), wherein, for FD mode, we substitute $\lambda = 1$ owing to the single phase of transmission, and for HD mode, we consider $\lambda = 2$ due to the requirements of two phases of transmission.

Proof. See Appendix G. ∎

$$C_{d_p}^{\text{FD-ipSIC}} = \sum_{m=0}^{m_{cd_p}-1}\sum_{g=0}^{m}\sum_{\kappa=0}^{m_{ad_p}-1}\sum_{u=0}^{m-g}\sum_{v=0}^{m-g-u}\mathcal{M}_{m,g,\kappa,u}^{\text{FD}}\left(\frac{\Omega_{D_p}\eta_c(1-\rho)}{m_{D_p}}\right)^{v}\frac{1}{\Gamma(m_{D_p})}\binom{m-g-u}{v}$$
$$\times\left(\int_0^{\infty}\theta^{m}\mathrm{e}^{-\left(\frac{m_{cd_p}\theta}{\Omega_{cd_p}\eta_c\rho}\right)}G_{1,1}^{1,1}\left[\theta\,\middle|\,\begin{matrix}0\\0\end{matrix}\right]G_{1,1}^{1,1}\left[\frac{m_{cd_p}\Omega_{d_pd_p}\eta_{d_p}}{m_{d_pd_p}\Omega_{cd_p}\eta_c\rho}\theta\,\middle|\,\begin{matrix}1-g-m_{d_pd_p}\\0\end{matrix}\right]\right.$$
$$\left.\times G_{1,1}^{1,1}\left[\frac{m_{cd_p}\widetilde{\eta}_a}{\Omega_{cd_p}\eta_c\rho(\beta_{d_p}-\delta_{d_p})}\theta\,\middle|\,\begin{matrix}-\kappa-u\\0\end{matrix}\right]G_{1,1}^{1,1}\left[\frac{m_{cd_p}\Omega_{D_p}\eta_c(1-\rho)}{m_{D_p}\Omega_{cd_p}\eta_c\rho}\theta\,\middle|\,\begin{matrix}1-v-m_{D_p}\\0\end{matrix}\right]d\theta\right),$$
$$\text{with } \mathcal{M}_{m,g,\kappa,u}^{\text{FD}} = \frac{1}{\lambda\ln 2}\left(\frac{m_{cd_p}}{\Omega_{cd_p}\eta_c\rho}\right)^{m}\frac{1}{m!}\binom{m}{g}\frac{1}{\Gamma(m_{d_pd_p})}\alpha_{d_p}\frac{\xi_{d_p}(\kappa)}{(\widetilde{\eta}_a)^{\kappa+1}}$$
$$\times\left(\frac{\Omega_{d_pd_p}\eta_{d_p}}{m_{d_pd_p}}\right)^{g}\left(\frac{\beta_{d_p}-\delta_{d_p}}{\widetilde{\eta}_a}\right)^{-(\kappa+u+1)}\binom{m-g}{u}. \tag{5.35}$$

$$C_{d_p}^{\text{FD-pSIC}} = \sum_{m=0}^{m_{cd_p}-1}\sum_{g=0}^{m}\sum_{\kappa=0}^{m_{ad_p}-1}\sum_{u=0}^{m-g}\mathcal{M}_{m,g,\kappa,u}^{\text{FD}}\left(\int_0^{\infty}\theta^{m}\mathrm{e}^{-\left(\frac{m_{cd_p}\theta}{\Omega_{cd_p}\eta_c\rho}\right)}G_{1,1}^{1,1}\left[\theta\,\middle|\,\begin{matrix}0\\0\end{matrix}\right]\right.$$
$$\left.\times G_{1,1}^{1,1}\left[\frac{m_{cd_p}\widetilde{\eta}_a}{\Omega_{cd_p}\eta_c\rho(\beta_{d_p}-\delta_{d_p})}\theta\,\middle|\,\begin{matrix}-\kappa-u\\0\end{matrix}\right]G_{1,1}^{1,1}\left[\frac{m_{cd_p}\Omega_{d_pd_p}\eta_{d_p}}{m_{d_pd_p}\Omega_{cd_p}\eta_c\rho}\theta\,\middle|\,\begin{matrix}1-g-m_{d_pd_p}\\0\end{matrix}\right]d\theta\right). \tag{5.36}$$

$$C_{d_p}^{\text{HD-ipSIC}} = \sum_{m=0}^{m_{cd_p}-1} \sum_{g=0}^{m} \sum_{\kappa=0}^{m_{ad_p}-1} \sum_{v=0}^{m-g} \mathcal{M}_{m,g,\kappa}^{\text{HD}} \frac{1}{\Gamma(m_{D_p})} \left(\frac{\Omega_{D_p}\eta_c(1-\rho)}{m_{D_p}}\right)^{v} \binom{m-g}{v}$$
$$\times \left(\int_0^{\infty} \theta^m \mathrm{e}^{-\left(\frac{m_{cd_p}\theta}{\Omega_{cd_p}\eta_c\rho}\right)} G_{1,1}^{1,1}\left[\theta \,\middle|\, \begin{matrix} 0 \\ 0 \end{matrix}\right] G_{1,1}^{1,1}\left[\frac{m_{cd_p}\Omega_{D_p}\eta_c(1-\rho)}{m_{D_p}\Omega_{cd_p}\eta_c\rho}\theta \,\middle|\, \begin{matrix} 1-v-m_{d_p} \\ 0 \end{matrix}\right]\right.$$
$$\left.\times\, G_{1,1}^{1,1}\left[\frac{m_{cd_p}\widetilde{\eta}_a}{\Omega_{cd_p}\eta_c\rho(\beta_{d_p}-\delta_{d_p})}\theta \,\middle|\, \begin{matrix} -\kappa-g \\ 0 \end{matrix}\right] d\theta\right),$$
$$\text{with } \mathcal{M}_{m,g,\kappa}^{\text{HD}} = \frac{1}{\lambda \ln 2}\left(\frac{m_{cd_p}}{\Omega_{cd_p}\eta_c\rho}\right)^{m} \frac{1}{m!}\binom{m}{g} \alpha_{d_p} \frac{\xi_{d_p}(\kappa)}{(\widetilde{\eta}_a)^{\kappa+1}} \left(\frac{\beta_{d_p}-\delta_{d_p}}{\widetilde{\eta}_a}\right)^{-(\kappa+g+1)}. \quad (5.37)$$

$$C_{d_p}^{\text{HD-pSIC}} = \sum_{m=0}^{m_{cd_p}-1} \sum_{g=0}^{m} \sum_{\kappa=0}^{m_{ad_p}-1} \mathcal{M}_{m,g,\kappa}^{\text{HD}} \left(\frac{\Omega_{cd_p}\eta_c\rho}{m_{cd_p}}\right)^{m+1} G_{1,[1:1],0,[1:1]}^{1,1,1,1,1}\left[\begin{matrix} \frac{\widetilde{\eta}_a}{\beta_{d_p}-\delta_{d_p}} \\ \frac{\Omega_{cd_p}\eta_c\rho}{m_{cd_p}} \end{matrix} \,\middle|\, \begin{matrix} (1+m),1 \\ (-g-k);0 \\ -- \\ 0;0 \end{matrix}\right], \quad (5.38)$$

where $G_{1,[A:C],0,[B:D]}^{1,N,N_1,M,M_1}[\cdot|\cdot]$ be the Meijer-G function with two variables [94]. Although the ergodic rate expressions in (5.35), (5.36), and (5.37) are presented in one-integral form, it can be efficiently computed using symbolic software like Mathematica or Maple and consumes much less time than the computer simulation approach. Moreover, the derived ergodic rate expression in (5.38) carries Meijer's G-function of two variables which can be quantified using the approach as given in [95, Table II].

Evaluation of C_{d_q}

Using the SINR expressions in (5.9) and (5.12), the ergodic rate for user D_q [72] can be evaluated as

$$C_{d_q} = \min\Big[\underbrace{\mathbb{E}\left[\log_2\left(1+\Lambda_{d_p\to d_q}\right)\right]}_{\Psi_1},\ \underbrace{\mathbb{E}\left[\log_2\left(1+\Lambda_{d_q}\right)\right]}_{\Psi_2}\Big]. \quad (5.39)$$

Starting with the evaluation of Ψ_1, it can be written as

$$\Psi_1 = \frac{1}{\lambda \ln 2}\mathbb{E}\left[\ln\left(1+\frac{(1-\rho)\eta_c|h_{cd_p}|^2}{\rho\eta_c|h_{cd_p}|^2+\omega\eta_{d_p}|h_{d_pd_p}|^2+\widetilde{\eta}_a|g_{ad_p}|^2+1}\right)\right], \quad (5.40)$$

which can be further simplified as

$$\Psi_1 = \frac{1}{\lambda \ln 2}\Big[\underbrace{\mathbb{E}\left[\ln\left(1+\widetilde{\eta_a}|g_{ad_p}|^2+\eta_c|h_{cd_p}|^2+\omega\eta_{d_p}|h_{d_pd_p}|^2\right)\right]}_{\phi_1} - \underbrace{\mathbb{E}\left[\ln\left(1+\widetilde{\eta_a}|g_{ad_p}|^2+\rho\eta_c|h_{cd_p}|^2+\omega\eta_{d_p}|h_{d_pd_p}|^2\right)\right]}_{\phi_2}\Big]. \tag{5.41}$$

Hereby, we first evaluate the term ϕ_2. Since ϕ_2 includes two different fading distributions, the closed-form solution for ϕ_2 seems to be mathematically intractable. Thus, we approximate ϕ_2 based on the results provided in [42], [96] as

$$\mathbb{E}\left[\ln(1+x)\right] \approx \ln\left(1+\mathbb{E}[x]\right) - \frac{\mathbb{E}[x^2]-(\mathbb{E}[x])^2}{2(1+\mathbb{E}[x])^2}. \tag{5.42}$$

Accordingly, ϕ_2 can be given as in (5.43).

$$\begin{aligned}\phi_2 \approx\; & \ln\Big(1+\widetilde{\eta_a}\mathbb{E}\left[|g_{ad_p}|^2\right]+\rho\eta_c\mathbb{E}\left[|h_{cd_p}|^2\right]+\omega\eta_{d_p}\mathbb{E}\left[|h_{d_pd_p}|^2\right]\Big) \\ & + \frac{\Big(\widetilde{\eta_a}\mathbb{E}\left[|g_{ad_p}|^2\right]+\rho\eta_c\mathbb{E}\left[|h_{cd_p}|^2\right]+\omega\eta_{d_p}\mathbb{E}\left[|h_{d_pd_p}|^2\right]\Big)^2}{2\Big(1+\widetilde{\eta_a}\mathbb{E}\left[|g_{ad_p}|^2\right]+\rho\eta_c\mathbb{E}\left[|h_{cd_p}|^2\right]+\omega\eta_{d_p}\mathbb{E}\left[|h_{d_pd_p}|^2\right]\Big)^2} \\ & - \frac{\begin{array}{c}\widetilde{\eta_a}^2\mathbb{E}\left[\left(|g_{ad_p}|^2\right)^2\right]+\rho^2\eta_c^2\mathbb{E}\left[\left(|h_{cd_p}|^2\right)^2\right]+\omega^2\eta_{d_p}^2\mathbb{E}\left[\left(|h_{d_pd_p}|^2\right)^2\right] \\ +2\widetilde{\eta_a}\mathbb{E}\left[|g_{ad_p}|^2\right]\rho\eta_c\mathbb{E}\left[|h_{cd_p}|^2\right] \\ +2\rho\eta_c\mathbb{E}\left[|h_{cd_p}|^2\right]\omega\eta_{d_p}\mathbb{E}\left[|h_{d_pd_p}|^2\right]+2\widetilde{\eta_a}\mathbb{E}\left[|g_{ad_p}|^2\right]\omega\eta_{d_p}\mathbb{E}\left[|h_{d_pd_p}|^2\right]\end{array}}{2\Big(1+\widetilde{\eta_a}\mathbb{E}\left[|g_{ad_p}|^2\right]+\rho\eta_c\mathbb{E}\left[|h_{cd_p}|^2\right]+\omega\eta_{d_p}\mathbb{E}\left[|h_{d_pd_p}|^2\right]\Big)^2}.\end{aligned} \tag{5.43}$$

However, to compute (5.43), it further requires the n-th order moments of $|g_{ad_p}|^2$, $|h_{cd_p}|^2$, and $|h_{d_pd_p}|^2$. As such, n-th order moments of w, $w \in \{|g_{ad_p}|^2, |h_{cd_p}|^2, |h_{d_pd_p}|^2\}$, can be expressed as

$$\mathbb{E}\left[w^n\right] = \int_0^\infty y^n f_w(y)dy. \tag{5.44}$$

Thus, for $w = |g_{ad_p}|^2$, substituting (5.1) into (5.44) and expanding ${}_1F_1\left(m_{ad_p};1;\delta_{d_p}x\right)$ in terms of Meijer-G functions via [41, eq. 9.34.8] as

$${}_1F_1\left(m_{ad_p};1;\delta_{d_p}x\right) = \frac{1}{\Gamma(m_{ad_p})}G_{1,2}^{1,1}\left[-\delta_{d_p}y \,\middle|\, \begin{array}{c}1-m_{ad_p}\\ 0,0\end{array}\right], \tag{5.45}$$

and then simplifying the resultant expression in (5.44) with the help of [41, eq.

9.813.1], we get

$$\mathbb{E}\left[|g_{ad_p}|^{2n}\right] = \frac{\alpha_{d_p}}{\Gamma(m_{ad_p})\beta_{d_p}^{n+1}} G_{2,2}^{1,2}\left[-\frac{\delta_{d_p}}{\beta_{d_p}} \middle| \begin{matrix} -n, 1-m_{ad_p} \\ 0, 0 \end{matrix}\right]. \tag{5.46}$$

Similar to (5.46), one can evaluate the n-th order moments for $w = |h_{cd_p}|^2$ and $w = |h_{d_pd_p}|^2$ by substituting (5.6) into (5.44), and simplifying the resultant expression using [41, eq. 3.351.3] as

$$\mathbb{E}\left[|h_{cd_p}|^{2n}\right] = \left(\frac{\Omega_{cd_p}}{m_{cd_p}}\right)^n \frac{\Gamma(n+m_{cd_p})}{\Gamma(m_{cd_p})} \tag{5.47}$$

and

$$\mathbb{E}\left[|h_{d_pd_p}|^{2n}\right] = \left(\frac{\Omega_{d_pd_p}}{m_{d_pd_p}}\right)^n \frac{\Gamma(n+m_{d_pd_p})}{\Gamma(m_{d_pd_p})}. \tag{5.48}$$

Now, substituting (5.46), (5.47), and (5.48) with $n = 1, 2$ into (5.43), one can obtain the expression for ϕ_2. Further, with $\rho = 1$, (5.43) leads to the expression for ϕ_1. Hereby, substituting ϕ_1 and ϕ_2 into (5.41), we obtain the expression of Ψ_1. Next, Ψ_2 can be expressed using (5.12) as

$$\Psi_2 = \frac{1}{\lambda \ln 2}\mathbb{E}\left[\ln\left(1 + \frac{\eta_{d_p}|h_{d_pd_q}|^2}{\widetilde{\eta}_a|g_{ad_q}|^2+1}\right)\right], \tag{5.49}$$

which can be re-expressed as

$$\Psi_2 = \frac{1}{\lambda \ln 2}\Big[\underbrace{\mathbb{E}\big[\ln\left(1+\widetilde{\eta}_a|g_{ad_q}|^2 + \eta_{d_p}|h_{d_pd_q}|^2\right)\big]}_{\phi_3} - \underbrace{\mathbb{E}\left[\ln\left(1+\widetilde{\eta}_a|g_{ad_q}|^2\right)\right]}_{\phi_4}\Big]. \tag{5.50}$$

Hereby, we first evaluate the term ϕ_3. Interestingly, ϕ_3 can be deduced from (5.43) while substituting $\rho = 1$, $\omega = 0$, and replacing the indices c with d_p and d_p with d_q. Now, the remaining task is to assess ϕ_4 which can be expressed as

$$\phi_4 = \mathbb{E}\left[\ln\left(1+\widetilde{\eta}_a|g_{ad_q}|^2\right)\right] = \int_0^\infty \ln(1+\widetilde{\eta}_a y) f_{|g_{ad_q}|^2}(y)dy. \tag{5.51}$$

Now, expanding $\ln(1+\widetilde{\eta_a}y)$ in terms of Meijer-G function via [93, eq. 11] as

$$\ln(1+\widetilde{\eta_a}y) = G_{2,2}^{1,2}\left[\widetilde{\eta_a}y \,\middle|\, \begin{matrix} 1,1 \\ 1,0 \end{matrix}\right], \tag{5.52}$$

and then expanding (5.1) in the form of Meijer-G function via [41, eq. 9.34.8] and substituting with (5.52) into (5.51), we get the expression of ϕ_4, which can be simplified with the aid of [94, eq. 2.6.2] as

$$\phi_4 = \frac{\alpha_{d_q}}{\Gamma(m_{ad_q})\beta_{d_q}} G_{1,[2:1],0,[2:2]}^{1,2,1,1,1}\left[\begin{matrix} \frac{\widetilde{\eta_a}}{\beta_{d_q}} \\ -\frac{\delta_{d_q}}{\beta_{d_q}} \end{matrix} \,\middle|\, \begin{matrix} 1,1 \\ 1,1;1-m_{ad_q} \\ -- \\ 1,0;0,0 \end{matrix}\right]. \tag{5.53}$$

After, substituting ϕ_3 and ϕ_4 into (5.50), Ψ_2 can be evaluated. Further, inserting the expressions of Ψ_1 and Ψ_2 into (5.39), expression for C_{d_q} can be obtained.

Corollary 5.1: The ergodic rate for user D_q working under the FD and HD modes can be evaluated while following the above steps by substituting $\omega = 1$ and $\omega = 0$, respectively. Also, we substitute $\lambda = 1$ and $\lambda = 2$ for the FD mode and HD mode, respectively, as per the preceding discussion. Moreover, the ergodic rates remain the same for user D_q under both ipSIC and pSIC situations.

Remark 5.4: Since Meijer-G function with two variables is not available in standard mathematical packages, we refer the algorithm in [95, Table II] an efficient Mathematica implementation of this function in order to give numerical results based on eqs. (5.38) and (5.53). With this implementation, ESR can be evaluated fast and accurately. This computability, therefore, can be helpful to discuss the insightful results in comparison to respective Monte Carlo simulation outcomes in the Numerical Results section. However, it will require the increased implementation cost for executing the algorithm.

5.3.3 Throughput Analysis

The throughput is a key performance measure to characterize the spectrum utilization. It can be defined as the target rate that can be accomplished successfully by the secondary network over hybrid fading channels. Relying on the results derived in Sub-sections 5.3.1 and 5.3.2, we obtain here the expressions of throughput for the delay-limited and delay-tolerant transmission scenarios, respectively, as follows:

Delay-Limited Transmission Scenario

In this scenario, the throughput can be obtained by evaluating the OP for a fixed transmission rate R_s [97], by setting $R_{d_p} = R_{d_q} = R_s$, as

$$\Re^{\ell} = \left(1 - P_{\text{out}}^{\text{Sec}}\left(R_s\right)\right) R_s. \tag{5.54}$$

Delay-Tolerant Transmission Scenario

In this scenario, the throughput can be obtained by evaluating the ESR at any rate less than or equal to the evaluated ESR [98] as

$$\Re^{t} = C_{\text{esr}}. \tag{5.55}$$

From (5.54), one can observe that the maximum achievable throughput of the secondary network for the delay-limited scenario is R_s, which could be attained for the HD-pSIC case at high SNR region, as the OP approaches to zero. Whereas from (5.55), the maximum achievable throughput for the delay-tolerant scenario depends on the evaluated ESR, and thus, possess higher value than the delay-limited scenario, as illustrated through numerical results in the next section.

5.4 Numerical and Simulation Results

In this section, we carry out numerical analysis for the considered UCHSTN under the C-NOMA scheme and endorse our derived theoretical results through Monte-Carlo simulations. We plot the curves using analytical expressions for the earlier discussed cases i.e., FD-ipSIC, FD-pSIC, HD-ipSIC, and HD-pSIC. Also, for drawing the various analytical curves, we adopt i.i.d. channels towards the multiple PRs, while considering that they are clustered relatively close together [45], [42]. Thus, for convenience, we drop the index l from all the notations of the pertaining channel parameters in this section. Further, for comparison purposes, simulation curves for the conventional OMA scheme are also drawn, which requires three time slots to execute its operation. During the first and second time slots, node C transmits the information x_{d_p} and x_{d_q}, respectively, towards the node D_p, whereas during the third time slot, D_p forwards the information x_{d_q} towards the node D_q using

Table 5.1: Satellite Link Parameters [with $j \in \{b, d_p, d_q\}$]

Parameters	**Value**
Orbit	GEO
Carrier frequency	$f = 2$ GHz
Carrier bandwidth	$B = 15$ MHz
3-dB angle	$\varphi_{j3\text{dB}} = 0.8°$
Angle between user j and satellite beam centre	$\varphi_j = 0.2°$
Antenna gain of user j	$G_j = 4$ dB
Maximal beam gain	$G_{\max} = 48$ dB
Receiver noise temperature	$T = 300°$ K

the DF relaying strategy. Table 5.1 enlists some parameters related to the satellite links [80]. To get the numerical results, we adopt a two-dimensional (2-D) network layout [21], where the network nodes C, D_p, D_q, and B are located at the coordinates $(0, 0)$, $(0.5, -0.5)$, $(1, 0)$, and $(2, 1)$, respectively. Acquiring the path-loss model, the parameter Ω_{ij} of the channel gain is calculated by $\Omega_{ij} = d_{ij}^{-\vartheta}$ for $i \in \{c\}$ with $j \in \{b, d_p\}$ and $i \in \{d_p\}$ with $j \in \{b, d_p, d_q\}$, d_{ij} is the normalized distance between nodes i and j, and $\vartheta = 4$ [99] be the path-loss exponent. We set the various system parameters, unless otherwise specified, as $R_p = 0.5$ bps/Hz, $R_{d_p} = R_{d_q} = 1$ bps/Hz as the target rates, $m_{cd_p} = \{1, 3\}$, $m_{D_p} = \{1, 3\}$, $m_{d_pd_p} = 2$, $m_{d_pd_q} = 2$, $m_{cb} = 1$, $m_{d_pb} = 1$, with $m_e \triangleq \{m_{cd_p}, m_{D_p}, m_{d_pd_q}\}$, as the fading severity parameters, $\Omega_{D_p} = 0.01$ [70] and $\Omega_{d_pd_p} = 0.1$ [92] as the respective mean values of the IS and LI channel power gains, $\rho = 0.3$ [25] as the NOMA-based power allocation factor, and $\sigma^2 = 1$ as the noise variance. The various satellite links are considered under HS and AS with their corresponding shadowed-Rician fading parameters [45] as $(m_{aj}, \flat_{aj}, \Omega_{aj} = 2, 0.063, 0.0005)$ and $(m_{aj}, \flat_{aj}, \Omega_{aj} = 5, 0.251, 0.279)$, $j \in \{b, d_p, d_q\}$.

Fig. 5.2 illuminates the OP curves for primary network against the primary SNR η_a. This figure analyzes the transmit power allocation for the SUs. For this, we set $\eta_c = \eta_{d_p} = 15$ dB. From the figure, one can visualize the performance improvements in outage curves for HD C-NOMA scheme over FD C-NOMA scheme as the FD mode allows simultaneous transmissions from both the SUs i.e., C and D_p. The outage performance improves further while considering the case of multiple PRs [refer to (5.19) and (5.22)] and AS scenario. Such improvements in the outage performance allow more SUs' powers for transmissions for a predefined primary outage constraint ζ_{th}. As an illustration, let us consider the case of AS scenario under the setting $\zeta_{\text{th}} = 10^{-2}$ and $\eta_a = 30$ dB. For this set of values, the corresponding

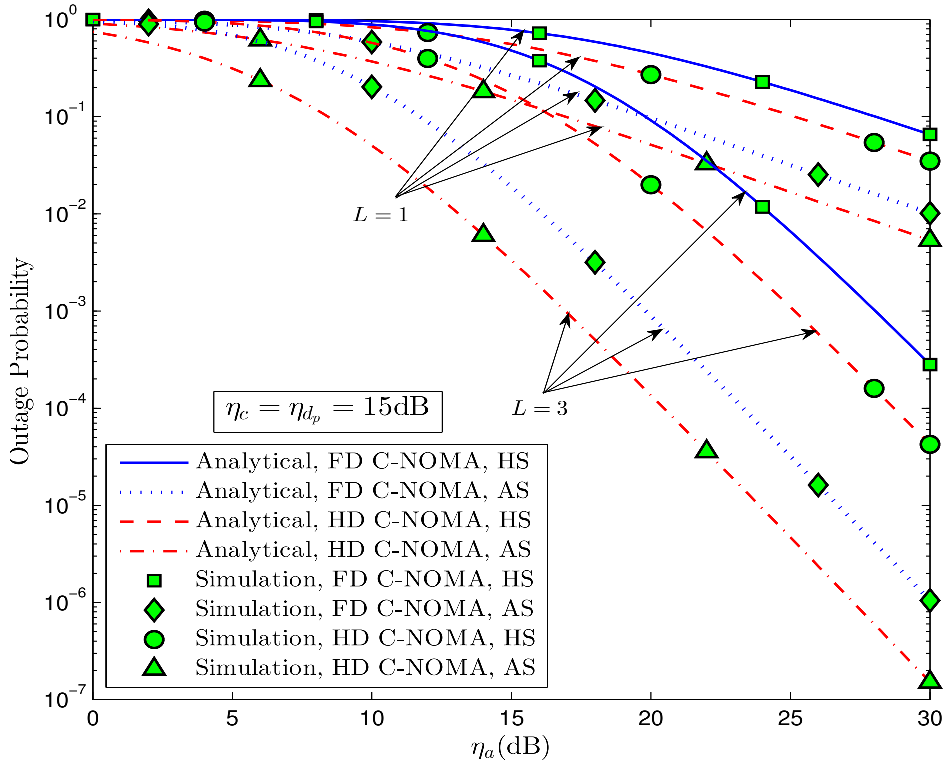

Figure 5.2: OP of the primary network against the primary SNR η_a.

numerical values of calculated transmit powers ($\eta_c = \eta_{d_p}$) for SUs for $L = 1$ under the FD C-NOMA scheme and HD C-NOMA scheme are 10.9 dB and 12.94 dB. Now, considering $L = 3$ for the same set of values, the respective numerical values of calculated transmit powers for SUs under the FD C-NOMA scheme and HD C-NOMA scheme increase to 24.2 dB and 27.38 dB.

Fig. 5.3 exhibits the OP curves for secondary network against the primary outage constraint ζ_{th} under the setting $\eta_a = 30$ dB. The analytical and asymptotic curves for the OP of the secondary network for various cases are drawn according to (5.25) and (5.29)-(5.32), respectively. We can observe that the asymptotic curves are well aligned with analytical and simulated curves in the high regime of ζ_{th}. FD C-NOMA scheme outperforms HD C-NOMA scheme for the case of ipSIC in the entire SNR regime. Although the transmit powers calculated for SUs under the HD C-NOMA are relatively more as compared to the FD C-NOMA, as the FD mode allows simultaneous transmissions from both nodes C and D_p, the impacts of IS and/or LI channel power gain become dominant at high SNR regime for both FD C-NOMA and HD C-NOMA schemes, and thus, making the corresponding diversity orders as zero. Hence, their performance comparisons are primarily done on the requirement of transmission bandwidth, which is two times more for HD C-NOMA scheme as

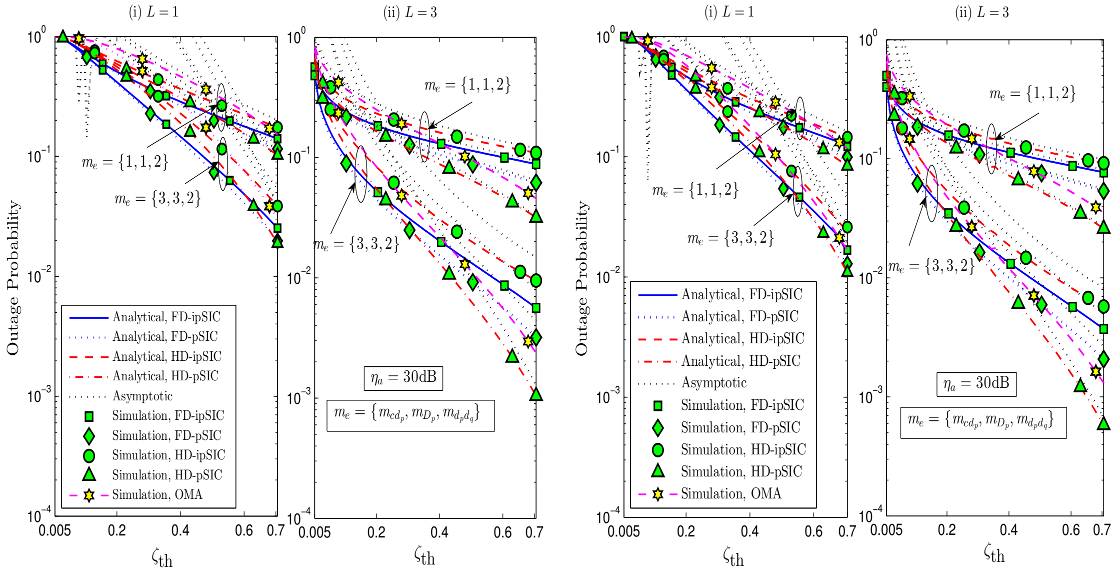

(a) (b)

Figure 5.3: OP of the secondary network against the primary outage constraint $\zeta_{\rm th}$ (a) HS; (b) AS.

required in FD C-NOMA scheme. Consequently, the target SINR threshold (for a fixed value of target rate) relatively increases for the HD C-NOMA scheme, which degrades its performance in the entire SNR regime. On the contrary, for the case of pSIC, FD C-NOMA outperforms HD C-NOMA in the low SNR regime only. As such, in the high SNR regime, the impact of LI becomes dominant for the case of FD C-NOMA, which finally degrades its outage performance while causing the corresponding diversity order as zero. Nevertheless, for the case of HD C-NOMA, one can verify the achievable diversity order of $\min(m_{cd_p}, m_{d_pd_q})$ from the pertinent curves. Hence, the superiority of FD C-NOMA is not apparent with the impact of LI increasing at high SNR regime. With the above reasoning, one can also visualize that under ipSIC/pSIC situations, the FD/HD C-NOMA schemes illuminate the better outage performance than the OMA scheme in the low SNR regime. On the contrary, in the high SNR regime, the OMA scheme can outperform the FD C-NOMA under ipSIC/pSIC and HD C-NOMA under ipSIC. Further, there are significant improvements in the OP curves pertaining to all the possible cases while considering multiple PRs as it allows more SUs' powers for transmissions. Also, the performance relatively improves for the same set of parameters when satellite links are subject to AS (as in Fig. 5.3(b)) than its HS counterpart (as in Fig. 5.3(a)).

Fig. 5.4 depicts the OP versus primary interference power η_a curves while considering the HS and AS sets of scenarios. For this, we set $\zeta_{\rm th} = 0.3$. From the figure,

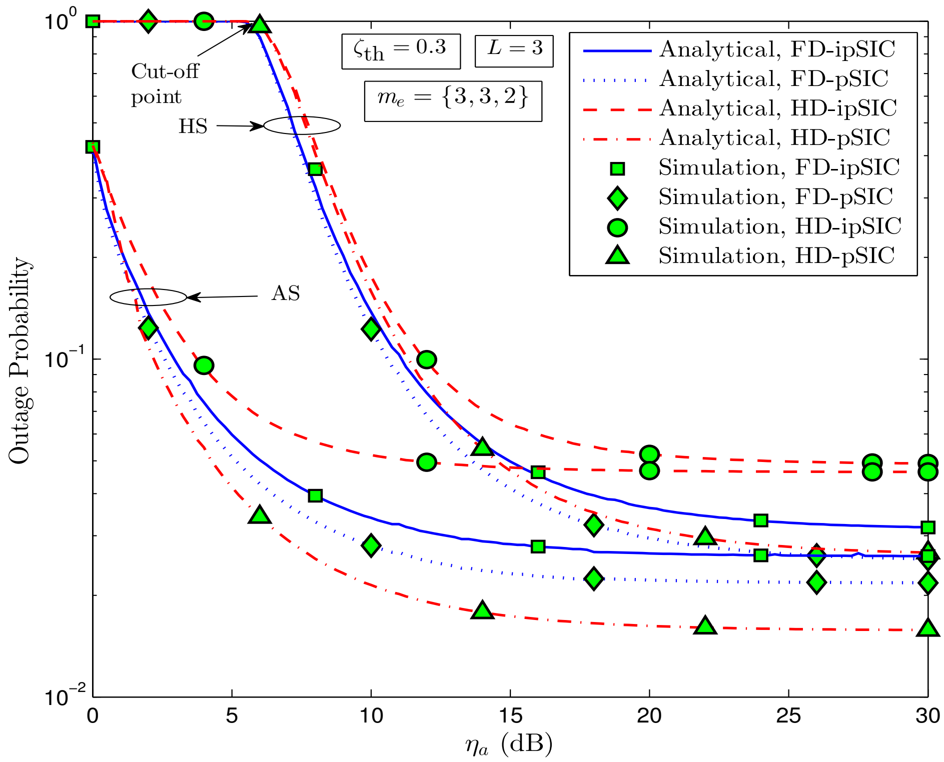

Figure 5.4: OP of the secondary network against the primary interference power η_a.

under HS scenario, one can note that at the lower values of η_a, a cut-off point exists below which the secondary network remains in the outage. This is primarily due to the more stringent QoS requirements from the PRs. Nevertheless, this cut-off point relatively vanishes at the early stage of η_a when satellite links are subject to AS. Further, at the higher values of η_a, an outage floor appears in the performance, owing to the dominance of the interference from the primary satellite.

Fig. 5.5 illustrates the ESR curves against the primary outage constraint ζ_{th} under the setting $\eta_a = 30$ dB. The exact analytical curves for the ESR are plotted according to (5.33) for the various cases. From the figure, one can envisage the notable ESR performance improvements for the HD-pSIC case as compared to all other cases at higher values of ζ_{th} (high SNR region). This is primarily due to the impacts of LI and/or IS channel power gains which become dominant at high regime of SNR for all the cases, except HD-pSIC. Similar to the reasoning in Fig. 5.3, one can also visualize that under ipSIC/pSIC situations, the FD/HD C-NOMA schemes depict relatively higher values of ESR than the OMA scheme in the low SNR regime. On the contrary, in the high SNR regime, the OMA scheme can provide a higher value of ESR than the FD C-NOMA under ipSIC/pSIC and HD C-NOMA under ipSIC. Further, the ESR value increases while considering the case of multiple PRs.

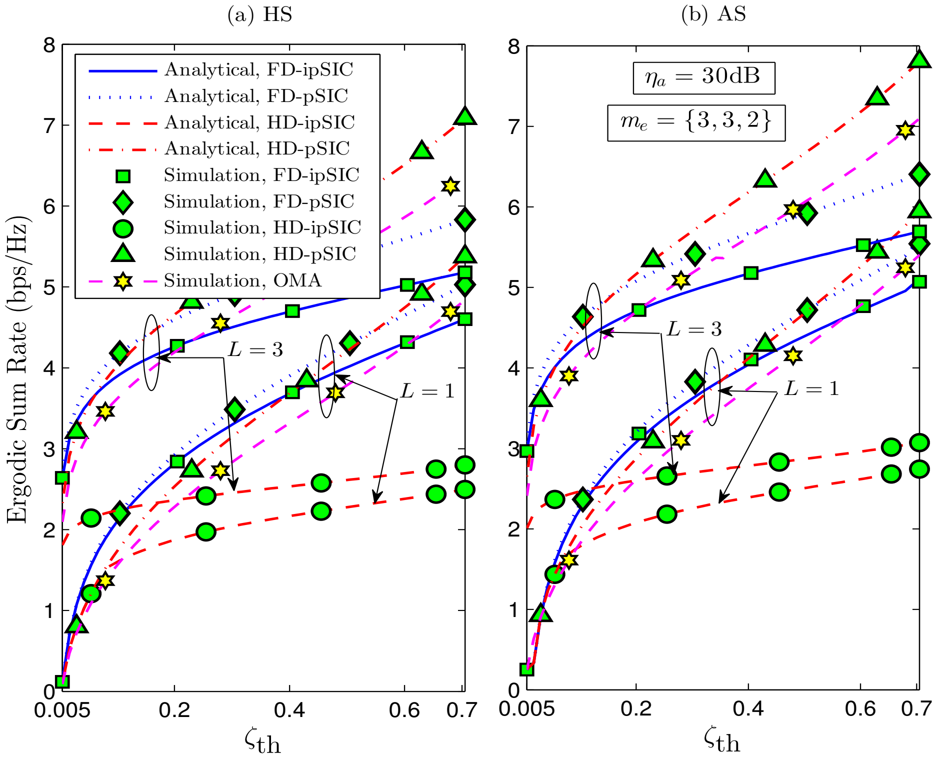

Figure 5.5: ESR of the secondary network against the primary outage constraint ζ_{th}.

Moreover, one can note the higher value of ESR when satellite links are subject to AS (as in Fig. 5.5(b)) than its HS counterpart (as in Fig. 5.5(a)) for the same set of parameters.

Fig. 5.6 demonstrates the ESR curves against the primary interference power η_a under both HS and AS scenarios. For this, we set $\zeta_{\text{th}} = 0.3$. From the figure, under HS scenario, one can note that there exists a cut-off point below which the ESR remains zero, owing to more stringent QoS requirements from the PRs at the lower values of η_a. More importantly, this point disappears when satellite links undergo AS. Further, there comes an ESR ceiling in the curves at higher values of η_a. This is primarily due to the dominance of interference from the primary satellite.

Fig. 5.7 depicts the throughput curves against the primary outage constraint ζ_{th} under the setting η_a as 30 dB. Herein, the analytical curves are drawn for the two specific transmission scenarios i.e., delay-limited and delay-tolerant, according to (5.54) and (5.55), respectively. From the figure, it can be seen that the throughput for the delay-tolerant scenario is higher than the delay-limited scenario. As such, in delay-limited scenario, the OP approaches to some lower constant value or zero value at higher values of ζ_{th}, and hence, the throughput is only determined by the

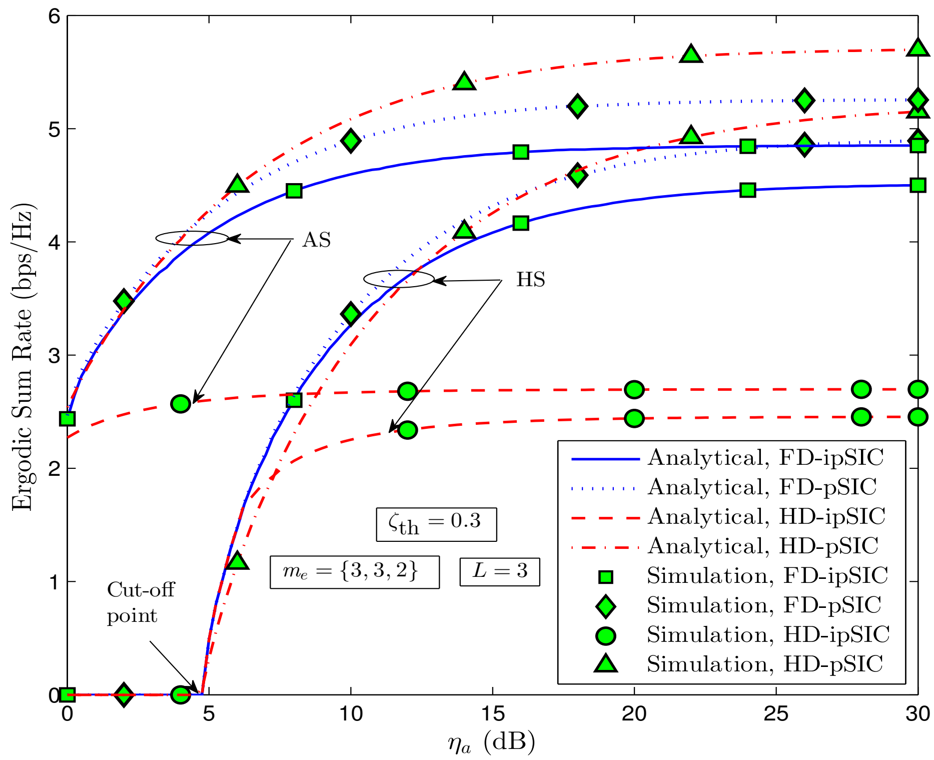

Figure 5.6: ESR of the secondary network against the primary interference power η_a.

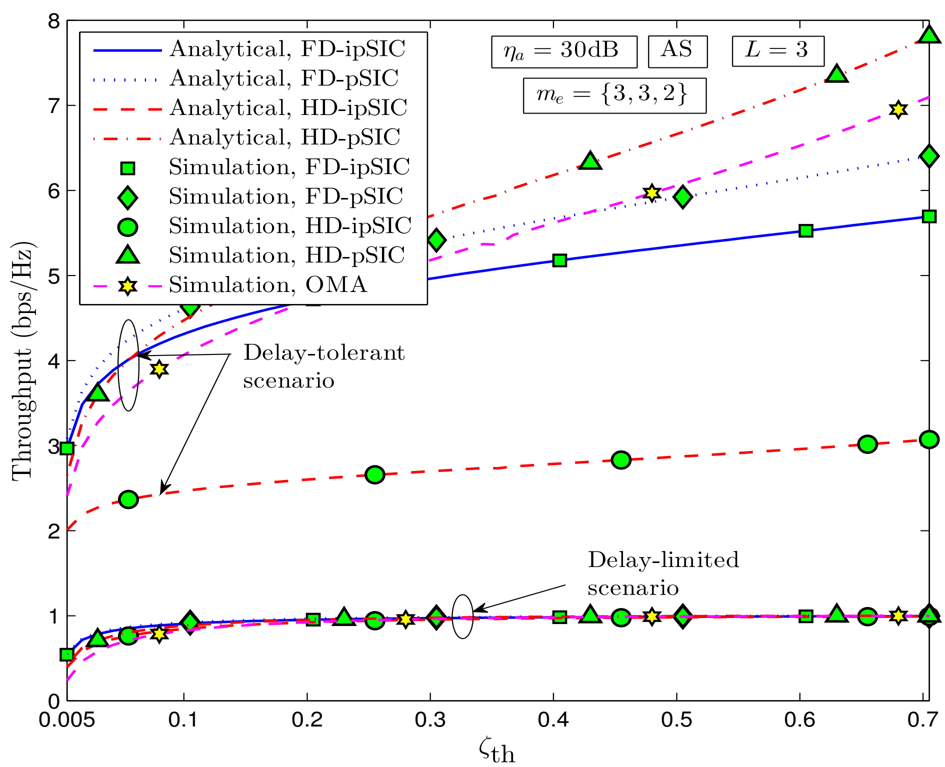

Figure 5.7: Throughput of the secondary network against the primary outage constraint ζ_{th}.

fixed transmission rate of the secondary network. On the contrary, the throughput in delay-tolerant scenario depends on the evaluated ESR.

5.5 Summary

We investigated the performance of an UCHSTN wherein a secondary terrestrial network shares the spectrum with primary satellite network to communicate with intended receivers that are deployed based on the C-NOMA scheme. Considering the mutual interference between the primary and secondary networks, the transmit powers at SUs were calculated for a predefined primary outage constraint at the best selected PR among L PRs under the FD/HD C-NOMA schemes. Based on these calculated powers, we further quantified the performance of the secondary network by analyzing the OP, ESR, and throughput. Also, for the comprehensive evaluation, both pSIC and ipSIC situations were taken into account for the FD mode and the benchmark HD mode for comparison purposes. Our studies reveal that multiple PRs manifest the advantage of improved performance towards the secondary network. Further, it is illustrated that the outage performance corresponding to HD-pSIC case is notably improved at high SNR region over all the discussed cases, caused by a non-zero diversity order. Above all, the conclusions can be drawn that for the case of ipSIC, the FD C-NOMA scheme outperforms the HD C-NOMA scheme in the entire regime of SNRs. However, for the case of pSIC, the performance of HD C-NOMA scheme is remarkably ameliorated at high SNR in contrast to the FD C-NOMA scheme.

CHAPTER 6

CACHE-FREE/CACHE-AIDED TWR-NOMA IN UNDERLAY COGNITIVE HYBRID SATELLITE-TERRESTRIAL NETWORKS

So far, we have analyzed the performance of CHSTNs by considering the various spectral-efficient schemes in the past chapters, for instance, multiuser scenario, AR protocol, NOMA, FD C-NOMA, however, by employing the OWR technique in their analytical frameworks. As such, TWR technique is deemed more spectral-efficient when compared with its OWR counterpart [11]. Whereas, NOMA has been viewed as one of the most promising technologies for future wireless networks to satisfy the needs of high spectral efficiency and massive connectivity. Thus, exploiting the TWR technique into NOMA-based CHSTNs can further enlarge the coverage and capacity of the secondary network [29]. On another front, wireless caching is being explored for addressing the demands of growing capacity for rich multimedia traffic in the 5G and beyond cellular networks [14]. This results in reduced latency and subsequently increased spectral efficiency [16]. Hence, integrating the caching technique further in TWR-NOMA-based CHSTN will not only mitigate the IUI significantly but also reduce the OP and average E-E transmission times.

To this end, most of the existing works on NOMA-based CHSTNs [24]-[27], [100] are relied on the OWR networks and have not considered the potential attributes of wireless caching. Also, they have conjectured the subsistence of pSIC with no residual interference incurred. However, in practice, there is SIC error prorogation in the NOMA technique due to imperfect decoding and many implementations issues, such as complexity scaling [28], which may pose limitations on the capacity of the CHSTNs. Thus, it would be significant to investigate the deleterious impacts of ipSIC on CHSTNs with both cache-free (CF) and cache-aided (CA) TWR-NOMA schemes. Albeit few works have examined the system performance while incorporating the wireless caching into their system model, they are particularly intended for the case of basic HSTNs [101], [102]. To the best of our knowledge, no work has yet been reported on the performance analysis of CHSTNs with CF/CA TWR-NOMA schemes under the impact of ipSIC. It is worth pointing that analyzing the performance by considering various topics at the same time postures new mathematical intricacies because of the involved complicated hybrid channel modelling and multiple random variables (multiple integrals). Note that such analysis is important for perceiving the repercussion of ipSIC on CHSTNs with CF/CA TWR-NOMA schemes and to realize the implementation of such networks in the 5G and beyond wireless environments.

In light of the above discussion, in this chapter, we analyze the performance of an underlay CHSTN comprising a primary satellite source with its multiple terrestrial PRs and two NOMA secondary terrestrial users exchanging their information with the help of a half-duplex DF-based secondary relay. It is important to note that in CR scenario, both primary and secondary networks are allowed to transmit over the same frequency band, thus, we consider their mutual interference over each other [18], [75]. Further, we demonstrate that there exists an IUI which may cause a detrimental impact on the performance of the secondary network. Consequently, to achieve the improved performance and subsequently the low latency requirements, the wireless content caching is employed, whereby the relay can store the most popular contents of both the NOMA users. In summary, the major contributions of the chapter are emphasized as follows:

- For the considered CHSTN, we first derive the OP expression of the primary satellite network for a predefined outage constraint at one of the opportunistically selected PR among K PRs. This facilitates the transmit power allocation for the SUs based on satisfying the QoS constraint at the PRs in terms of OP. Hereby, we illustrate that multiple PRs manifest the advantages of improved primary OP, which allows allocation of more transmit powers for the SUs.

- Based on the SUs' transmit powers and considering the realistic assumption of ipSIC, we investigate the performance of the secondary terrestrial network under the CF/CA TWR-NOMA schemes while deriving the analytical expressions of OP, throughput, and average E-E transmission times, under the appropriately modelled shadowed-Rician fading for the satellite links and Nakagami-m fading for the terrestrial links.

- Further, to provide more insights, the asymptotic OP expressions are derived at a high SNR, and the corresponding diversity orders are obtained for the CF TWR-NOMA and CA TWR-NOMA schemes. We demonstrate that zero diversity order results for both the schemes due to inevitable IUI. Nevertheless, the performance under CA TWR-NOMA scheme is notably improved as compared to CF TWR-NOMA scheme, owing to the reduced IUI and the efficient utilization of available spectrum resources.

The rest of the chapter is ordered as follows. In Section 6.1, the system model of CHSTN is framed while deriving the expressions for SINRs over heterogeneous fading channels. The caching scheme against the CA TWR-NOMA scheme is also elaborated here. In Section 6.2, the transmit powers at SUs are calculated to satisfy the QoS criterion at the best selected PR among K PRs. In Section 6.3 and Section 6.4, we investigate the performance of the secondary terrestrial network by analyzing the OP, throughput, and average E-E transmission times under the CF TWR-NOMA and CA TWR-NOMA schemes, respectively. Numerical and simulation results are presented in Section 6.5, and finally, Section 6.6 summarizes the chapter.

6.1 System Descriptions

This section first provides a detailed description of the proposed CHSTN system model, pertinent hybrid channel model, and thereafter derives the SINR expressions at the various nodes for the communication purpose, followed by elaborating the caching scheme.

6.1.1 System Model

Herein, we first discuss the system model for CHSTN under the proposed CF TWR-NOMA scheme. Although the Fig. 6.1 is drawn with respect to the CA TWR-NOMA scheme, the same figure can be applicable for its CF counterpart while excluding some of the link/parts such as caching phase, cache content, and content storages and replacing adaptive transmission (Tx) link with Tx link. As illustrated in the figure[1], a secondary terrestrial network shares the spectrum with the primary satellite network. The primary network comprises a satellite source A with its intended K multiple destinations (PRs) $\{B_k\}_{k=1}^{K}$, whereas the secondary network consists of two SU nodes D_p and D_q exchanging their information with the aid of a half-duplex DF-based secondary relay node C. We assume that D_p lies closer to the relay with better channel conditions and the direct link between nodes D_p and D_q is masked due to severe shadowing, blocking, etc. [103]. It is further assumed that all the network nodes are equipped with a single antenna device[2]. All the channels are assumed to follow block fading so that they remain unchanged for a block duration but may change independently in the next block transmission. The various channel coefficients for the satellite links $A \to B_k$, $A \to D_p$, $A \to C$, and $A \to D_q$ are denoted as g_{ab_k}, g_{ad_p}, g_{ac}, and g_{ad_q}, respectively, and are subject to shadowed-Rician fading. Whereas, the terrestrial links $D_p \to C$, $C \to D_p$, $D_q \to C$, $C \to D_q$, $D_p \to B_k$, $C \to B_k$, and $D_q \to B_k$ undergo independent Nakagami-m fading distributions, and channel coefficients corresponding to them are represented by h_{d_pc}, h_{cd_p}, h_{d_qc}, h_{cd_q}, $h_{d_pb_k}$, h_{cb_k}, and $h_{d_qb_k}$, respectively. All the receiving nodes are assumed to be inflicted by the AWGN i.e., modelled as $\mathcal{CN}(0, \sigma^2)$.

For the subsequent system description, we first mark the statistics of the underlying hybrid fading channels.

6.1.2 Channel Model

For the satellite links, a widely adopted shadowed-Rician fading model is considered. Accordingly, the PDF of the channel gains $|g_{aj}|^2$, $j \in \{b_k, d_p, c, d_q\}$, can be given as [24]-[27]

$$f_{|g_{aj}|^2}(x) = \alpha_j \, \mathrm{e}^{-\beta_j x} \, {}_1F_1 \left(m_{aj}; 1; \delta_j x\right), \ x \geq 0, \tag{6.1}$$

with $\alpha_j = (2\flat_{aj} m_{aj}/(2\flat_{aj} m_{aj} + \Omega_{aj}))^{m_{aj}}/2\flat_{aj}$, $\beta_j = 1/2\flat_{aj}$, $\delta_j = \Omega_{aj}/(2\flat_{aj})(2\flat_{aj} m_{aj} + \Omega_{aj})$, where $2\flat_{aj}$ is the average power of multipath component, Ω_{aj} be the average power of LoS component, and m_{aj} is the fading severity parameter.

Considering the numerous practical effects, such as free-space loss, antenna pat-

[1]In a practical situation, primary source A represents a GEO satellite and nodes $\{B_k\}_{k=1}^{K}$ may constitute the handheld devices as integrated in the DVB-SH service (in S-band) [7]. Whereas, the SU nodes could be the femtocell users underlying in a macrocell [53]. In another scenario, SUs can represent a general device-to-device (D2D) communication system.

[2]For applications that combine IoT with cellular networks, sensors and/or devices in the future massive machine-type communication networks are generally equipped with a single antenna [79].

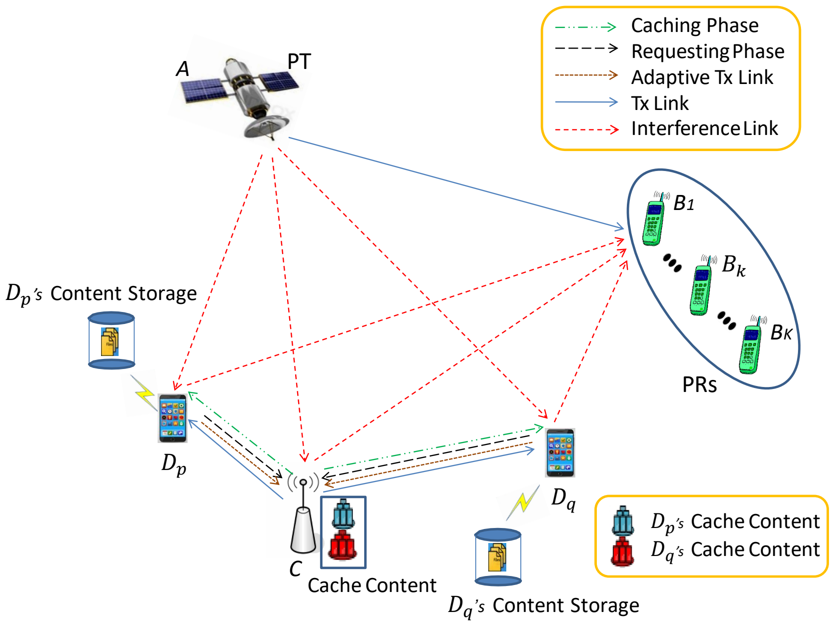

Figure 6.1: CHSTN system model.

tern, etc., the scaling parameter[3] of the satellite links $\sqrt{Q_j}$, $j \in \{b_k, d_p, c, d_q\}$, can be given as [80]

$$\sqrt{Q_j} = \frac{c\sqrt{G_j(\varphi_j)G_j}}{4\pi f d_{aj}\sqrt{K_B T \mathbb{B}_c}}, \tag{6.2}$$

with c being the speed of light, f is the carrier frequency, $d_{aj} \approx 35786$ km is the distance between satellite A and the user j, $K_B = 1.38 \times 10^{-23}$ J/°K be the Boltzman constant, T being the receiver noise temperature, and $\mathbb{B}_c$ is the carrier bandwidth. Besides, G_j is the antenna gain at user j, whereas $G_j(\varphi_j)$ is the satellite beam gain based on both the satellite beam pattern and position of the user j, and approximately given by [81]

$$G_j(\varphi_j) = G_{\max}\left(\frac{J_1(u_j)}{2u_j} + 36\frac{J_3(u_j)}{u_j^3}\right)^2, \tag{6.3}$$

with $u_j = 2.07123\frac{\sin\varphi_j}{\sin\varphi_{j3\text{dB}}}$. $G_{\max}$ represents the maximal beam gain, φ_j is the angle between user j and beam centre with respect to the satellite, and $\varphi_{j3\text{dB}}$ be the 3-dB angle.

Hereby, simplifying the term ${}_1F_1\left(m_{aj}; 1; \delta_j x\right)$ in (6.1) and considering $\widetilde{\eta_a} = \eta_a Q_j$, where $\eta_a = \frac{P_a}{\sigma^2}$, with P_a being the transmit power through satellite A, one can

[3]It is noteworthy that the GEO satellite is positioned at a very large distance from the ground, i.e., 35786 km, and the beamwidth of satellite antenna pattern is of the order of less than 1°. Thus, it is reasonable to consider the equal scaling parameters for all the terrestrial users.

express the PDF of $\Lambda_{aj} = \widetilde{\eta}_a|g_{aj}|^2$, for the arbitrary integer values of the fading severity parameters, as [4], [5]

$$f_{\Lambda_{aj}(x)} = \alpha_j \sum_{\kappa=0}^{m_{aj}-1} \frac{\xi_j(\kappa)}{(\widetilde{\eta}_a)^{\kappa+1}} x^{\kappa} \mathrm{e}^{-\left(\frac{\beta_j-\delta_j}{\widetilde{\eta}_a}\right)x}, \tag{6.4}$$

where $\xi_j(\kappa) = (-1)^{\kappa}(1-m_{aj})_{\kappa}\delta_j^{\kappa}/(\kappa!)^2$. Now, carrying out the integration of the PDF in (6.4) using [41, eq. 3.351.2], the CDF $F_{\Lambda_{aj}}(x)$ can be obtained as

$$F_{\Lambda_{aj}}(x) = 1 - \alpha_j \sum_{\kappa=0}^{m_{aj}-1} \sum_{p=0}^{\kappa} \frac{\xi_j(\kappa)}{(\widetilde{\eta}_a)^{\kappa+1}} \frac{\kappa!}{p!} \left(\frac{\beta_j-\delta_j}{\widetilde{\eta}_a}\right)^{-(\kappa+1-p)} x^p \mathrm{e}^{-\left(\frac{\beta_j-\delta_j}{\widetilde{\eta}_a}\right)x}. \tag{6.5}$$

Since the terrestrial links are subject to Nakagami-m fading, the respective PDF and CDF of $\Lambda_{ij} = \eta_i|h_{ij}|^2$, for $i,\ j \in \{b_k, d_p, c, d_q\}$ (with $i \neq j,\ i \notin \{b_k\}$) and for $i \in \{d_p\}$, $j \notin \{d_q\}$, and vice-versa, can be given as

$$f_{\Lambda_{ij}}(x) = \left(\frac{m_{ij}}{\Omega_{ij}\eta_i}\right)^{m_{ij}} \frac{x^{m_{ij}-1}}{\Gamma(m_{ij})} \mathrm{e}^{-\frac{m_{ij}}{\Omega_{ij}\eta_i}x} \tag{6.6}$$

and

$$F_{\Lambda_{ij}}(x) = \frac{1}{\Gamma(m_{ij})} \Upsilon\left(m_{ij}, \frac{m_{ij}}{\Omega_{ij}\eta_i}x\right), \tag{6.7}$$

where Ω_{ij} is the average power and m_{ij} be the fading severity parameter.

6.1.3 Signal Model

The overall communication in the considered CHSTN occurs in two transmission phases based on the CF TWR-NOMA scheme. During the first phase, nodes D_p and D_q transmit their respective signals x_{d_p} and x_{d_q}, complying with unit-energy $\left(\mathbb{E}[|x_{d_p}|^2] = 1, \mathbb{E}[|x_{d_q}|^2] = 1\right)$, towards the relay node C. Accordingly, the received signal at node C can be represented as

$$y_c = \omega_1\sqrt{P_{d_p}}h_{d_pc}x_{d_p} + \omega_2\sqrt{P_{d_q}}h_{d_qc}x_{d_q} + \sqrt{P_aQ_c}g_{ac}x_a + v_c, \tag{6.8}$$

where P_{d_p} and P_{d_q} are the transmit powers through node D_p and D_q, respectively, v_c be the AWGN variable, and ω_1 and ω_2 are the multiplying coefficients whose values are one under the CF TWR-NOMA scheme. Hereby, based on the NOMA protocol, relay employs the SIC technique [103] to first decode the transmitted signal x_{d_p} by the nearby NOMA user which has better channel conditions. Thus, the SINR at relay can be given as

$$\Lambda_{D_p\to C}=\frac{\omega_1\Lambda_{d_pc}}{\omega_2\underbrace{\Lambda_{d_qc}}_{\text{IUI}}+\Lambda_{ac}+1},\tag{6.9}$$

where $\Lambda_{d_pc}=\eta_{d_p}|h_{d_pc}|^2$ with $\eta_{d_p}=\frac{P_{d_p}}{\sigma^2}$, $\Lambda_{d_qc}=\eta_{d_q}|h_{d_qc}|^2$ with $\eta_{d_q}=\frac{P_{d_q}}{\sigma^2}$, and $\Lambda_{ac}=\widetilde{\eta_a}|g_{ac}|^2$. Afterwards, relay decodes the signal x_{d_q} by removing x_{d_p} from the received signal. However, owing to the decoding error and hardware imperfections, the SIC could be imperfect in realistic conditions. Thereby, we consider that a residual interference exists, leading to an ipSIC term. Thus, after the ipSIC, the SINR at relay can be obtained as

$$\Lambda_{D_q\to C}=\frac{\omega_2\Lambda_{d_qc}}{\omega_1\Lambda_C+\Lambda_{ac}+1},\tag{6.10}$$

where $\Lambda_C=\eta_{d_p}|h_C|^2$ with h_C is the residual IS channel coefficient at node C, and is subject to Nakagami-m fading [87] with its respective fading severity parameter and average channel power gain as m_C and Ω_C.

During the second transmission phase, SU relay node C broadcasts the superposing signal $x_c=\sqrt{(1-\rho)P_c}x_{d_p}+\sqrt{\rho P_c}x_{d_q}$ towards the receiving nodes D_p and D_q with P_c being the transmit power through node C and $\rho\in(0,1)$ denotes the NOMA-based power allocation factor corresponding to signal x_{d_q} or the desired signal of nearby NOMA user D_p. Further, for performing the adequate NOMA operation, relatively more power is allocated towards the signal x_{d_p} or the desired signal of distant user D_q who has worse channel conditions, and thus, ρ becomes limited to $(0,0.5)$ [103]. Hereby, the received signal at node D_i, $i\in\{p,q\}$, can be expressed as

$$y_{d_i}=h_{cd_i}x_c+\sqrt{P_aQ_{d_i}}g_{ad_i}x_a+v_{d_i},\tag{6.11}$$

with v_{d_i} be the AWGN variable. Then user D_q will directly decode its desired signal x_{d_p} with an SINR as

$$\Lambda_{D_q,x_{d_p}}=\frac{(1-\rho)\Lambda_{cd_q}}{\rho\Lambda_{cd_q}+\Lambda_{ad_q}+1},\tag{6.12}$$

where $\Lambda_{cd_q} = \eta_c|h_{cd_q}|^2$ with $\eta_c = \frac{P_c}{\sigma^2}$ and $\Lambda_{ad_q} = \widetilde{\eta}_a|g_{ad_q}|^2$. It is worthwhile to mention that the transmit power allocation[4] for the SUs (i.e., P_{d_p}, P_c and P_{d_q}) will be executed based on satisfying the QoS constraint at the PRs in terms of OP, as explained later in Section 6.2.

Now, based on the NOMA principle, SIC is performed at D_p. Thus, the received SINR at D_p to decode the signal x_{d_p} can be given as

$$\Lambda_{D_p,x_{d_p}} = \frac{(1-\rho)\Lambda_{cd_p}}{\rho\Lambda_{cd_p} + \Lambda_{ad_p} + 1}, \tag{6.13}$$

with $\Lambda_{cd_p} = \eta_c|h_{cd_p}|^2$ and $\Lambda_{ad_p} = \widetilde{\eta}_a|g_{ad_p}|^2$. Afterwards, user D_p decodes its desired signal x_{d_q} by removing x_{d_p} from the received signal. Similar to (6.9), it will be subject to residual interference, leading to the ipSIC term. Thus, after the ipSIC, the SINR at node D_p to decode the signal x_{d_q} can be obtained as

$$\Lambda_{D_p,x_{d_q}} = \frac{\rho\Lambda_{cd_p}}{(1-\rho)\Lambda_{D_p} + \Lambda_{ad_p} + 1}, \tag{6.14}$$

where $\Lambda_{D_p} = \eta_c|h_{D_p}|^2$ with h_{D_p} is the residual IS channel coefficient at node D_p, and is subject to Nakagami-m fading with its respective fading severity parameter and average channel power gain as m_{D_p} and Ω_{D_p}.

6.1.4 Caching Scheme

Herein, we discuss the caching strategy under the proposed CA TWR-NOMA scheme. As depicted in Fig. 6.1, we denote the library of content files corresponding to NOMA users D_p and D_q as $F_{d_p} \triangleq \{1, 2, ..., N_{d_p}\}$ and $F_{d_q} \triangleq \{1, 2, ..., N_{d_q}\}$, respectively. Following the Zipf distribution for the content popularity model [105], the i-th $\left(i \in F_{d_p}\right)$ and j-th $\left(j \in F_{d_q}\right)$ files with popularity profiles f_i and f_j satisfy $\sum_{i=1}^{N_{d_p}} f_i = 1$ and $\sum_{j=1}^{N_{d_q}} f_j = 1$, respectively. Further, relying on the statistical property of Zipf distribution, the probability of requesting the i-th and j-th most popular files can

[4]The transmit power calculations for SUs in various previous works, e.g., [18], [20], [24], [104] are relied upon satisfying the instantaneous interference threshold criterion at the PRs, which finally requires the knowledge of instantaneous channel gains of the links between SUs and PUs. However, in a practical situations, channels may subject to fast fading due to high mobility, thus it becomes hard to get the instantaneous channel gains [75], [85].

be given, respectively, as [106]

$$f_i = \frac{i^{-\theta_{d_p}}}{\sum_{m=1}^{N_{d_p}} m^{-\theta_{d_p}}} \text{ and } f_j = \frac{j^{-\theta_{d_q}}}{\sum_{m=1}^{N_{d_q}} m^{-\theta_{d_q}}}, \tag{6.15}$$

where θ_{d_p} and θ_{d_q} (with $\theta_{d_p}, \theta_{d_q} > 0$) are the Zipf distribution parameters correspond to the content files of user D_p and user D_q, respectively. The larger values of θ_{d_p} and θ_{d_q} express to request on the most popular content file(s), whereas the smaller values intend to the more uniform content requests.

Assume that relay has local storage (cache) capacity that can cache up to $\mathbb{C}$ ($\mathbb{C} < N_{d_p} + N_{d_q}$) files with $\mathbb{C} = \mathbb{C}_{d_p} + \mathbb{C}_{d_q}$, $\mathbb{C}_{d_p}$ and $\mathbb{C}_{d_q}$ are the cache sizes corresponding to store the contents of NOMA users D_p and D_q, respectively. Further, without loss of generality, most popular content (MPC) based caching scheme is considered, whereby during the caching phase, the relay can store the most popular content files of users D_p and D_q. It is further assumed that the caching phase has already been taken place to consider the next stage i.e., requesting phase. Hereby, NOMA users send the request to relay for exchange their information with each other. Accordingly, based on the available contents, the relay decides whether to fetch the desired contents from the NOMA users or to transmit directly from the relay itself. Corresponding to this, adaptive Tx links are shown from NOMA users to relay node C, as in Fig. 6.1. Further, depending on the content files of NOMA users cached by the relay, one of the following four scenarios can occur associated with values of ω_1 and ω_2 as follows:

Scenario (a): The relay has cached desired files of both the NOMA users, no transmission is required from any of the users to relay; $\omega_1 = 0$, $\omega_2 = 0$.

Scenario (b): The relay has cached the desired file of user D_q but has had a cache miss for user D_p, no transmission is required from user D_p to relay; $\omega_1 = 0$, $\omega_2 = 1$.

Scenario (c): The relay has had a cache miss for user D_q but has cached the desired file of user D_p, no transmission is required from user D_q to relay; $\omega_1 = 1$, $\omega_2 = 0$.

Scenario (d): The relay has had cache misses for both users, transmissions are required from both the users to relay; $\omega_1 = 1$, $\omega_2 = 1$.

Hereby, referring to the eqs. (6.8)-(6.14), one can write the SINR expressions for the above-mentioned scenarios on substituting with associated values of ω_1 and ω_2

under the CA TWR-NOMA scheme. Also, from these modified equations, one can observe that the IUI can be significantly reduced based on the contents cached at the relay. Nevertheless, the impact of this will better be illustrated in Section 6.5.

6.2 Primary Outage Constraint Based SUs' Transmit Power Calculation

In this section, we derive the OP expressions of the primary satellite network for a predefined outage constraint at the best selected PR among K PRs under the CF/CA TWR-NOMA schemes. Importantly, these analyses help in solving the transmit power allocation problem for the SUs based on the average channel gains of the link from itself to PRs.

6.2.1 CF TWR-NOMA Scheme

Since the overall communication under CF TWR-NOMA scheme takes place in two consecutive time phases, we calculate the transmit powers for SUs during both the phases separately, denoted as "Case I" and "Case II" as follows:

Case I

During the first transmission phase of CF TWR-NOMA scheme, the primary satellite source A broadcasts a unit energy signal x_a (with $\mathbb{E}[|x_a|^2] = 1$) towards its K PRs. Accordingly, the received signal at node B_k can be given as

$$y_{b_k} = \sqrt{P_a Q_{b_k}} g_{ab_k} x_a + \sqrt{P_{d_p}} h_{d_p b_k} x_{d_p} + \sqrt{P_{d_q}} h_{d_q b_k} x_{d_q} + v_{b_k}, \tag{6.16}$$

where v_{b_k} is the AWGN variable. As such, using (6.16), the SINR at node B_k can be expressed as

$$\Lambda_{b_k}^{\text{Pri}} = \frac{\Lambda_{ab_k}}{\Lambda_{d_p b_k} + \Lambda_{d_q b_k} + 1}, \tag{6.17}$$

where $\Lambda_{ab_k} = \widetilde{\eta_a} |g_{ab_k}|^2$, $\Lambda_{d_p b_k} = \eta_{d_p} |h_{d_p b_k}|^2$, and $\Lambda_{d_q b_k} = \eta_{d_q} |h_{d_q b_k}|^2$.

As stated earlier, in CHSTN, the secondary nodes D_p and D_q have to satisfy the QoS criterion at node B_k while tuning their transmit powers. To quantify this QoS criterion, the OP of primary transmission should be kept below a predefined outage constraint ζ_{th}. Therefore, for a given target rate R_p, the OP of the primary link

$A \rightarrow B_k$ can be written using (6.17) as

$$P_{\text{out},k}^{\text{Pri}}(R_p) = \Pr\left[\log_2(1 + \Lambda_{b_k}^{\text{Pri}}) < R_p\right] \leq \zeta_{\text{th}}, \tag{6.18}$$

which can be re-written as

$$P_{\text{out},k}^{\text{Pri}}(R_p) = \Pr\left[\Lambda_{b_k}^{\text{Pri}} < \gamma_p\right] \leq \zeta_{\text{th}}, \tag{6.19}$$

where $\gamma_p = 2^{R_p} - 1$. Hereby, we calculate the overall primary OP by using the selection criteria for the best satellite user based on maximizing $\Lambda_{b_k}^{\text{Pri}}$ as

$$P_{\text{out}}^{\text{Pri}}(R_p) = \Pr\left[\max_{k \in \{1,\ldots,K\}} \Lambda_{b_k}^{\text{Pri}} < \gamma_p\right] \leq \zeta_{\text{th}}, \tag{6.20}$$

which can be represented while applying order statistics for K independent PRs [80] as

$$P_{\text{out}}^{\text{Pri}}(R_p) = \prod_{k=1}^{K} F_{\Lambda_{b_k}^{\text{Pri}}}(\gamma_p) \leq \zeta_{\text{th}}. \tag{6.21}$$

Now, (6.21) can be further solved while assuming equal power $P_{d_q} = P_{d_p}$ (and thereby $\eta_{d_q} = \eta_{d_p}$) [91], as follows in Theorem 7.

Theorem 7. *The OP of primary satellite network after the first transmission phase of CF TWR-NOMA scheme can be expressed using (6.21) as*

$$\begin{aligned} P_{out}^{Pri}(R_p) = \prod_{k=1}^{K} \Bigg(1 - & \sum_{\kappa=0}^{m_{ab_k}-1} \sum_{m=0}^{\kappa} \sum_{v=0}^{m} \sum_{g=0}^{m-v} \alpha_{b_k} \frac{\xi_{b_k}(\kappa)}{(\widetilde{\eta}_a)^{\kappa+1}} \frac{\kappa!}{m!} \frac{\Gamma(v + m_{d_p b_k})}{\Gamma(m_{d_p b_k})} \binom{m-v}{g} \\ & \times e^{-\left(\gamma_p \frac{\beta_{b_k} - \delta_{b_k}}{\widetilde{\eta}_a}\right)} \left(\gamma_p \frac{\beta_{b_k} - \delta_{b_k}}{\widetilde{\eta}_a} + \frac{m_{d_p b_k}}{\Omega_{d_p b_k} \eta_{d_p}}\right)^{-\left(v + m_{d_p b_k}\right)} \frac{\Gamma(g + m_{d_q b_k})}{\Gamma(m_{d_q b_k})} \\ & \times \left(\gamma_p \frac{\beta_{b_k} - \delta_{b_k}}{\widetilde{\eta}_a} + \frac{m_{d_q b_k}}{\Omega_{d_q b_k} \eta_{d_p}}\right)^{-\left(g + m_{d_q b_k}\right)} \left(\frac{m_{d_p b_k}}{\Omega_{d_p b_k} \eta_{d_p}}\right)^{m_{d_p b_k}} \binom{m}{v} \\ & \times \gamma_p^{m} \left(\frac{\beta_{b_k} - \delta_{b_k}}{\widetilde{\eta}_a}\right)^{-(\kappa+1-m)} \left(\frac{m_{d_q b_k}}{\Omega_{d_q b_k} \eta_{d_p}}\right)^{m_{d_q b_k}} \Bigg) \leq \zeta_{th}. \end{aligned} \tag{6.22}$$

Proof. See Appendix H. ■

Now, for a given ζ_{th}, the transmit SNR η_{d_p} (involving transmit power P_{d_p}) can be calculated numerically by evaluating the expression in (6.22) with respect to η_{d_p} using any computing software like MATHEMATICA or MAPLE.

Case II

Similar to (6.16), the received signal at node B_k during the second transmission phase of CF TWR-NOMA scheme can be given as

$$y_{b_k} = \sqrt{P_a Q_{b_k}} g_{ab_k} x_a + \sqrt{P_c} h_{cb_k} x_c + v_{b_k}. \tag{6.23}$$

As such, using (6.23), the SINR at node B_k can be expressed as

$$\Lambda_{b_k}^{\mathrm{Pri}} = \frac{\Lambda_{ab_k}}{\Lambda_{cb_k} + 1}. \tag{6.24}$$

Hereby, using similar steps as in Case I, the overall primary OP for a given target rate R_p can be evaluated using (6.24) into (6.21) as given in Lemma 5.

Lemma 5. *The OP of primary satellite network after the second transmission phase of CF TWR-NOMA scheme can be expressed using (6.21) and (6.24)as*

$$\begin{aligned} P_{out}^{Pri}(R_p) = \prod_{k=1}^{K} \Bigg(1 - & \sum_{\kappa=0}^{m_{ab_k}-1} \sum_{v=0}^{\kappa} \sum_{g=0}^{v} \alpha_{b_k} \frac{\xi_{b_k}(\kappa)}{(\widetilde{\eta}_a)^{\kappa+1}} \frac{\kappa!}{v!} \frac{\Gamma(v-g+m_{cb_k})}{\Gamma(m_{cb_k})} \\ & \times \binom{v}{g} \gamma_p^v e^{-\left(\gamma_p \frac{\beta_{b_k}-\delta_{b_k}}{\widetilde{\eta}_a}\right)} \left(\gamma_p \frac{\beta_{b_k}-\delta_{b_k}}{\widetilde{\eta}_a} + \frac{m_{cb_k}}{\Omega_{cb_k}\eta_c} \right)^{-\left(v-g+m_{cb_k}\right)} \\ & \times \left(\frac{\beta_{b_k}-\delta_{b_k}}{\widetilde{\eta}_a} \right)^{-(\kappa+1-v)} \left(\frac{m_{cb_k}}{\Omega_{cb_k}\eta_c} \right)^{m_{cb_k}} \Bigg) \leq \zeta_{th}. \end{aligned} \tag{6.25}$$

Proof. Proof of Lemma 5 can be followed using the similar steps as for Theorem 7 in Appendix H. ■

Now, for a given ζ_{th}, by evaluating the expression in (6.25) with respect to η_c similar to (6.22), the transmit SNR η_c can be calculated numerically at node C.

6.2.2 CA TWR-NOMA Scheme

As discussed in CA TWR-NOMA scheme, four scenarios can occur depending on the content files of NOMA users cached by the relay. Thereby, the transmit power through relay node C in all the scenarios can be calculated similar to the Case II. Similarly, the respective transmit powers through NOMA users D_q and D_p in Scenario (b) and Scenario (c) can be calculated as in Case II, by replacing the terms m_{cb_k}, Ω_{cb_k}, and η_c with $m_{d_qb_k}$, $\Omega_{d_qb_k}$, and η_{d_q} and with $m_{d_pb_k}$, $\Omega_{d_pb_k}$, and η_{d_p}, respectively. However, the transmit powers through NOMA users in Scenario (d) can be calculated similar to the Case I.

Remark 6.1: The above-stated transmit power calculations require only the average channel gains of the link from itself to PRs, i.e., $D_p \to B_k$, $C \to B_k$, and $D_q \to B_k$. Average channel gains are relatively more stable and can save the feedback channel resources [75], [85] as compared with instantaneous channel gains. Moreover, the average channel gains have more realistic significance, as their knowledge can be acquired by using the frequency of the radio waves, transmission distance, etc.

Remark 6.2: Impact of multiple PRs can be realized in the form of improved primary OP from (6.22) and (6.25), which allows the SUs' transmit powers to be increased numerically under the fixed values of ζ_{th}. Moreover, the transmit powers calculated for SUs under the Case I are relatively less as compared to the Case II, as the Case I allows simultaneous transmissions from both the nodes D_p and D_q. Its implications will be further elaborated in Section 6.5.

6.3 Performance Evaluation Under the CF TWR-NOMA Scheme

In this section, we analyze the performance of the secondary terrestrial network under the CF TWR-NOMA scheme while deriving the analytical expressions of OP, throughput, and average E-E transmission times for the $D_p \to C \to D_q$ link and $D_q \to C \to D_p$ link, denoted as "Link #1" and "Link #2," respectively. Also, we investigate the outage performance at a high SNR, and thereby assess the achievable diversity orders for both the links.

6.3.1 Outage Probability Analysis

When the achievable rates of the users are decided by their QoS, the OP is an essential measure for analyzing the performance. Thus, to characterize the outage behaviour of the secondary network, we derive the exact and asymptotic OP expressions for the Link #1 and Link #2 as follows:

Exact Outage Probability Analysis of the Link #1

To start with, we define that the Link #1 goes into the outage when either relay node C or user D_q is unable to decode the signal x_{d_p}. It is noteworthy that decoding of the signal x_{d_q} at the relay has nothing to do with the OP of the Link #1, as user D_q directly detects the signal x_{d_p}. Accordingly, the OP of the Link #1 for a given SINR threshold γ_{d_q} can be appraised as

$$\begin{aligned} P_{\text{out}}^{\text{Link \#1, CF}} &= 1 - \Pr\left[\Lambda_{D_p \to C} \geq \gamma_{d_q},\ \Lambda_{D_q, x_{d_p}} \geq \gamma_{d_q}\right] \\ &= 1 - \underbrace{\Pr\left[\Lambda_{D_p \to C} \geq \gamma_{d_q}\right]}_{\chi_1} \underbrace{\Pr\left[\Lambda_{D_q, x_{d_p}} \geq \gamma_{d_q}\right]}_{\chi_2}, \end{aligned} \tag{6.26}$$

where $\gamma_{d_q} = 2^{2R_{d_q}-1}$, with R_{d_q} being the target rate of the Link #1. Hereby, the final expression of $P_{\text{out}}^{\text{Link \#1, CF}}$ can be provided with the help of Theorem 8 as given below.

Theorem 8. *The expression $P_{out}^{Link\ \#1,\ CF}$ in (6.26) requires the evaluations of the probability terms χ_1 and χ_2 under the hybrid satellite-terrestrial channels, which can be provided as in (6.27) and (6.28), respectively, with $T_1 = \frac{\gamma_{d_q}}{(1-\rho)-\rho\gamma_{d_q}}$.*

$$\begin{aligned} \chi_1 = & \sum_{m=0}^{m_{d_pc}-1} \sum_{g=0}^{m} \sum_{\kappa=0}^{m_{ac}-1} \sum_{v=0}^{m-g} \left(\frac{m_{d_pc}\gamma_{d_q}}{\Omega_{d_pc}\eta_{d_p}}\right)^m \frac{(g+\kappa)!}{m!} \alpha_c \frac{\xi_c(\kappa)}{(\widetilde{\eta}_a)^{\kappa+1}} \\ & \times \binom{m}{g} e^{-\left(\frac{m_{d_pc}\gamma_{d_q}}{\Omega_{d_pc}\eta_{d_p}}\right)} \left(\frac{m_{d_qc}}{\Omega_{d_qc}\eta_{d_q}}\right)^{m_{d_qc}} \frac{\Gamma(v+m_{d_qc})}{\Gamma(m_{d_qc})} \binom{m-g}{v} \\ & \times \left(\frac{m_{d_pc}\gamma_{d_q}}{\Omega_{d_pc}\eta_{d_p}} + \frac{\beta_c-\delta_c}{\widetilde{\eta}_a}\right)^{-(g+\kappa+1)} \left(\frac{m_{d_pc}\gamma_{d_q}}{\Omega_{d_pc}\eta_{d_p}} + \frac{m_{d_qc}}{\Omega_{d_qc}\eta_{d_q}}\right)^{-(v+m_{d_qc})}. \end{aligned} \tag{6.27}$$

$$\begin{aligned} \chi_2 = & \sum_{m=0}^{m_{cd_q}-1} \sum_{g=0}^{m} \sum_{\kappa=0}^{m_{ad_q}-1} \left(\frac{m_{cd_q}T_1}{\Omega_{cd_q}\eta_c}\right)^m \frac{(g+\kappa)!}{m!} \binom{m}{g} \alpha_{d_q} \\ & \times \frac{\xi_{d_q}(\kappa)}{(\widetilde{\eta}_a)^{\kappa+1}} \left(\frac{m_{cd_q}T_1}{\Omega_{cd_q}\eta_c} + \frac{\beta_{d_q}-\delta_{d_q}}{\widetilde{\eta}_a}\right)^{-(g+\kappa+1)} e^{-\left(\frac{m_{cd_q}T_1}{\Omega_{cd_q}\eta_c}\right)}. \end{aligned} \tag{6.28}$$

Proof. See Appendix I. ■

Exact Outage Probability Analysis of the Link #2

Herein, we define the complementary event of the outage for the Link #2. For this, the relay node C should decode the signal x_{d_p} as well as the signal x_{d_q}, and then user D_p should also be able to decode both the signals x_{d_p} and x_{d_q}. Thus, the probability of the complementary event can be expressed as $\Pr\left[\Lambda_{D_p \to C} \geq \gamma_{d_q},\ \Lambda_{D_q \to C} \geq \gamma_{d_p},\ \Lambda_{D_p, x_{d_p}} \geq \gamma_{d_q},\ \Lambda_{D_p, x_{d_q}} \geq \gamma_{d_p}\right]$, where $\gamma_{d_p} = 2^{2R_{d_p}-1}$ is the SINR threshold with

R_{d_p} being the target rate of the Link #2. Thus, the OP of the Link #2 can be formulated as

$$\begin{aligned} P_{\text{out}}^{\text{Link \#2, CF}} &= 1 - \Pr\left[\Lambda_{D_p\to C} \geq \gamma_{d_q},\ \Lambda_{D_q\to C} \geq \gamma_{d_p}, \Lambda_{D_p,x_{d_p}} \geq \gamma_{d_q},\ \Lambda_{D_p,x_{d_q}} \geq \gamma_{d_p}\right] \\ &= 1 - \underbrace{\Pr\left[\Lambda_{D_p\to C} \geq \gamma_{d_q},\ \Lambda_{D_q\to C} \geq \gamma_{d_p}\right]}_{J_1} \underbrace{\Pr\left[\Lambda_{D_p,x_{d_p}} \geq \gamma_{d_q},\ \Lambda_{D_p,x_{d_q}} \geq \gamma_{d_p}\right]}_{J_2}. \end{aligned} \tag{6.29}$$

Hereby, the final expression of $P_{\text{out}}^{\text{Link \#2, CF}}$ can be provided with the help of Theorem 9 as given below.

Theorem 9. *The expression $P_{out}^{\text{Link \#2, CF}}$ in (6.29) needs the computations of the probability terms J_1 (with $J_1 = \varphi_1 - \varphi_2$) and J_2 under the hybrid satellite-terrestrial channels, which can be presented in (6.30)-(6.32). Therein, $T_2 = \gamma_{d_q}(1+\gamma_{d_p})$, $T_3 = \gamma_{d_p}\gamma_{d_q}$, and $\mathcal{M} = \frac{m_{d_pc}}{\Omega_{d_pc}\eta_{d_p}} + \frac{m_{d_qc}}{\Omega_{d_qc}\eta_{d_q}\gamma_{d_q}}$.*

$$\begin{aligned} \varphi_1 = &\sum_{m=0}^{m_{d_qc}-1}\sum_{g=0}^{m_{d_pc}-1}\sum_{u=0}^{g}\sum_{v=0}^{m}\sum_{\kappa=0}^{m_{ac}-1}\sum_{s=0}^{m-v}\sum_{q=0}^{g-u}\left(\frac{m_{d_qc}\gamma_{d_p}}{\Omega_{d_qc}\eta_{d_q}}\right)^m\left(\frac{m_{d_pc}}{\Omega_{d_pc}\eta_{d_p}}\right)^g\left(\frac{m_C}{\Omega_C\eta_{d_p}}\right)^{m_C} \\ &\times \frac{(u+v+\kappa)!}{m!\,g!}\binom{g}{u}\binom{g-u}{q}\left(\frac{m_{d_qc}\gamma_{d_p}}{\Omega_{d_qc}\eta_{d_q}} + \frac{m_{d_pc}T_3}{\Omega_{d_pc}\eta_{d_p}} + \frac{m_C}{\Omega_C\eta_{d_p}}\right)^{-(s+q+m_C)} \\ &\times \binom{m-v}{s}\binom{m}{v}\binom{m-g}{v}\alpha_c\frac{\xi_c(\kappa)}{(\widetilde{\eta}_a)^{\kappa+1}}e^{-\left(\frac{m_{d_qc}\gamma_{d_p}}{\Omega_{d_qc}\eta_{d_q}}\right)}e^{-\left(\frac{m_{d_pc}T_2}{\Omega_{d_pc}\eta_{d_p}}\right)}\frac{\Gamma(s+q+m_C)}{\Gamma(m_C)} \\ &\times T_2^g\left(\frac{T_3}{T_2}\right)^q\left(\frac{\beta_c-\delta_c}{\widetilde{\eta}_a} + \frac{m_{d_qc}\gamma_{d_p}}{\Omega_{d_qc}\eta_{d_q}} + \frac{m_{d_pc}T_2}{\Omega_{d_pc}\eta_{d_p}}\right)^{-(u+v+\kappa+1)}. \end{aligned} \tag{6.30}$$

$$\begin{aligned} \varphi_2 = &\sum_{m=0}^{m_{d_qc}-1}\sum_{g=0}^{m}\sum_{v=0}^{m-g}\sum_{u=0}^{g+m_{d_pc}-1}\sum_{\kappa=0}^{m_{ac}-1}\sum_{s=0}^{u}\sum_{q=0}^{u-s}\left(\frac{m_{d_qc}}{\Omega_{d_qc}\eta_{d_q}}\right)^m\left(\frac{m_{d_pc}}{\Omega_{d_pc}\eta_{d_p}}\right)^{m_{d_pc}}(-1)^{m-g} \\ &\times \left(\frac{m_C}{\Omega_C\eta_{d_p}}\right)^{m_C}\frac{(v+\kappa+s)!}{m!\,u!}\binom{u-s}{q}\left(\frac{1}{\gamma_{d_q}}\right)^g\left(\mathcal{M}T_3 + \frac{m_C}{\Omega_C\eta_{d_p}}\right)^{-(q+m_C)} \\ &\times \binom{m}{g}\binom{m-g}{v}\binom{u}{s}\alpha_c\frac{\xi_c(\kappa)}{(\widetilde{\eta}_a)^{\kappa+1}}\frac{\Gamma(q+m_C)\Gamma(g+m_{d_qc})}{\Gamma(m_C)\Gamma(m_{d_qc})}T_2^u\left(\frac{T_3}{T_2}\right)^q \\ &\times e^{\left(\frac{m_{d_qc}}{\Omega_{d_qc}\eta_{d_q}}\right)}e^{-(\mathcal{M}T_2)}\left(\frac{\beta_c-\delta_c}{\widetilde{\eta}_a} - \frac{m_{d_qc}}{\Omega_{d_qc}\eta_{d_q}} + \mathcal{M}T_2\right)^{-(v+\kappa+s+1)}. \end{aligned} \tag{6.31}$$

$$
\begin{aligned}
J_2 = & \sum_{m=0}^{m_{cd_p}-1} \sum_{g=0}^{m} \sum_{\kappa=0}^{m_{ad_p}-1} \sum_{u=0}^{m-g} \left(\frac{m_{cd_p}\gamma_{d_p}}{\Omega_{cd_p}\eta_c\rho} \right)^{m} \left(\frac{m_{D_p}}{\Omega_{D_p}\eta_c} \right)^{m_{D_p}} \frac{(g+\kappa)!}{m!} \binom{m}{g} \\
& \times \left(\frac{m_{D_p}}{\Omega_{D_p}\eta_c} + \frac{m_{cd_p}\gamma_{d_p}(1-\rho)}{\Omega_{cd_p}\eta_c\rho} \right)^{-(u+m_{D_p})} \left(\frac{\beta_{d_p}-\delta_{d_p}}{\widetilde{\eta}_a} + \frac{m_{cd_p}\gamma_{d_p}}{\Omega_{cd_p}\eta_c\rho} \right)^{-(g+\kappa+1)} \\
& \times \binom{m-g}{u} (1-\rho)^u \alpha_{d_p} \frac{\xi_{d_p}(\kappa)}{(\widetilde{\eta}_a)^{\kappa+1}} \frac{\Gamma(u+m_{D_p})}{\Gamma(m_{D_p})} e^{-\left(\frac{m_{cd_p}\gamma_{d_p}}{\Omega_{cd_p}\eta_c\rho}\right)}. \qquad (6.32)
\end{aligned}
$$

Proof. See Appendix J. ∎

Asymptotic Outage Probability Analysis

For attaining more insights, we approximate the derived OP expressions in (6.26) and (6.29) at a high SNR region ($\eta_{d_p}, \eta_c, \eta_{d_q} \to \infty$, with $\frac{\eta_{d_p}}{\eta_c}$, $\frac{\eta_c}{\eta_{d_q}}$, and $\frac{\eta_{d_q}}{\eta_{d_p}}$ are the constant ratios) to calculate the achievable diversity orders for the Link #1 and Link #2, respectively with the help of Lemma 6 as given below. Although we have tried our best to present the asymptotic results for both the links, the result corresponding to the Link #2 is not leading to a straightforward diversity order result, so we omitted it from the chapter. Nevertheless, we have included the asymptotic curves for the Link #2 as well later in the Numerical Results section.

Lemma 6. *Referring to (6.26), the asymptotic OP expression for the Link #1 (say it $P_{out,\ asy}^{Link\ \#1,\ CF}$) under the hybrid satellite-terrestrial channels can be given as $P_{out,\ asy}^{Link\ \#1,\ CF} = \bar{\chi_1} + \bar{\chi_2}$, with $\bar{\chi_1}$ and $\bar{\chi_2}$ are the respective approximated expressions at the high SNR against the complementary events of χ_1 and χ_2, as given in (6.33) and (6.34), respectively.*

$$
\begin{aligned}
\bar{\chi_1} = & \sum_{m=0}^{m_{d_pc}} \sum_{g=0}^{m_{d_pc}-m} \sum_{\kappa=0}^{m_{ac}-1} \binom{m_{d_pc}}{m} \binom{m_{d_pc}-m}{g} \left(\frac{m_{d_pc}\gamma_{d_q}}{\Omega_{d_pc}\eta_{d_p}} \right)^{m_{d_pc}} \\
& \times \frac{\Gamma(g+\kappa+1)}{\Gamma(m_{d_pc}+1)} \frac{\Gamma(m+m_{d_qc})}{\Gamma(m_{d_qc})} \frac{\alpha_c\xi_c(\kappa)\widetilde{\eta}_a{}^{g}}{(\beta_c-\delta_c)^{g+\kappa+1}} \left(\frac{\Omega_{d_qc}\eta_{d_q}}{m_{d_qc}} \right)^{m}. \qquad (6.33)
\end{aligned}
$$

$$
\bar{\chi_2} = \sum_{m=0}^{m_{cd_q}} \sum_{\kappa=0}^{m_{ad_q}-1} \binom{m_{cd_q}}{m} \left(\frac{m_{cd_q}T_1}{\Omega_{cd_q}} \right)^{m_{cd_q}} \frac{\Gamma(m+\kappa+1)}{\Gamma(m_{cd_q}+1)} \alpha_{d_q} \frac{\xi_{d_q}(\kappa)\widetilde{\eta}_a{}^{m}}{(\beta_{d_q}-\delta_{d_q})^{m+\kappa+1}} \left(\frac{1}{\eta_c} \right)^{m_{cd_q}}. \qquad (6.34)
$$

Proof. See Appendix K. ■

Remark 6.3: In (6.33), substituting $m = m_{d_pc}$, one can assess the diversity order for the Link #1 as $\min(0, m_{cd_q})$, i.e., zero, owing to the IUI. We are doing such kind of substitutions to observe the dominant terms at high SNR region, which is reflected by the minimum power raised to $\frac{1}{\eta_c}$ and finally tells the diversity order. Similarly, for (6.29), on can attain a zero diversity order theoretically for the Link #2 due to the presence of IUI.

6.3.2 Throughput Analysis

The throughput is key performance measure to characterize the spectrum utilization. It can be defined as the target rate that can be accomplished successfully by the secondary network over hybrid fading channels. Relying on the results derived in Section 6.3.1, we obtain here the expression of throughput for the secondary terrestrial network as follows:

The throughput can be obtained by evaluating the OP for the Link #1 and Link #2 at the fixed transmission rates of R_{d_q} and R_{d_p} [97], respectively, as

$$\Re^{\mathrm{CF}} = (1 - P_{\mathrm{out}}^{\mathrm{Link\ \#1,\ CF}})\, R_{d_q} + (1 - P_{\mathrm{out}}^{\mathrm{Link\ \#2,\ CF}})\, R_{d_p}. \tag{6.35}$$

From (6.35), one can observe that the maximum achievable throughput of the secondary network is $R_{d_q} + R_{d_p}$, which could be attained when $P_{\mathrm{out}}^{\mathrm{Link\ \#1,\ CF}}$ and $P_{\mathrm{out}}^{\mathrm{Link\ \#2,\ CF}}$ approach zero.

6.3.3 Average End-to-End Transmission Time

In the next-generation wireless networks, minimizing the network latency is considered to be the prime design objectives while deploying the networks in practice. Thus, we focus here to estimate the average E-E transmission times for sending the packets through Link #1 and Link #2. According to the third Shannon theorem, the transmission time varies inversely proportional to the transmission rate of the channel [107]. Hence, the time taken in transferring a packet from the source node S_i to destination node S_j is given by

$$\mathcal{T}_{ij} = \frac{L}{\mathcal{B}_s \log_2 (1 + \Lambda_{ij})} = \frac{\widetilde{\mathcal{B}_s}}{\log_e (1 + \Lambda_{ij})}, \tag{6.36}$$

where L is the length of the packet, $\mathcal{B}_s$ be the channel bandwidth, and $\widetilde{\mathcal{B}_s} = \frac{L \log_e(2)}{\mathcal{B}_s}$. Further, it is assumed that the transmitted packet reaches the destination successfully before time-out. Also, the feedback/acknowledgement time is assumed to be negligible as compared to the packet transmission time [57].

Relying on the condition that both relay and user D_p can successfully detect signal x_{d_p}, the average E-E transmission times for sending the packets through Link #1 and Link #2 can be provided as

$$\mathcal{T}^{\text{Link \#1, CF}} = \tau_1 + \tau_2 \tag{6.37}$$

and

$$\mathcal{T}^{\text{Link \#2, CF}} = \tau_3 + \tau_4, \tag{6.38}$$

where $\tau_1 = \mathbb{E}[\mathcal{T}_{d_pc}] = \frac{\widetilde{B_s}}{\mathbb{E}\left[\log_e\left(1+\Lambda_{D_p \to C}\right)\right]}$, $\tau_2 = \mathbb{E}[\mathcal{T}_{cd_q}] = \frac{\widetilde{B_s}}{\mathbb{E}\left[\log_e\left(1+\Lambda_{D_q, x_{d_p}}\right)\right]}$, $\tau_3 = \mathbb{E}[\mathcal{T}_{d_qc}] = \frac{\widetilde{B_s}}{\mathbb{E}\left[\log_e\left(1+\Lambda_{D_q \to C}\right)\right]}$, and $\tau_4 = \mathbb{E}[\mathcal{T}_{cd_p}] = \frac{\widetilde{B_s}}{\mathbb{E}\left[\log_e\left(1+\Lambda_{D_p, x_{d_q}}\right)\right]}$. Computation of these terms is quite cumbersome to derive the closed-form expressions for (6.37) and (6.38). Consequently, we evaluate them through Monte-Carlo simulations.

6.4 Performance Evaluation Under the CA TWR-NOMA Scheme

In this section, we analyze the performance of the secondary terrestrial network under the CA TWR-NOMA scheme in terms of performance measures as discussed in Section 6.3. Since Section 6.3 has already made the solid foundation corresponding to the various performance measures, we present here the discussion against CA TWR-NOMA scheme more in abstract form.

6.4.1 Outage Probability Analysis

Exact Outage Probability Analysis of the Link #1

As discussed in Section 6.1, based on the contents cached at the relay, four scenarios are possible. Consequently, the OP associated with content file in each scenario relies on the popularity profile. Thus, the overall OP will be the sum of OP weighted by their popularity profiles in each scenario as follows:

$$P_{\text{out}}^{\text{Link \#1, CA}} = P_{\text{out}}^{\text{Link \#1, (a)}} \sum_{i=1}^{\mathbb{C}_{d_p}} f_i \sum_{j=1}^{\mathbb{C}_{d_q}} f_j + P_{\text{out}}^{\text{Link \#1, (b)}} \sum_{i=1}^{\mathbb{C}_{d_p}} f_i \sum_{j=\mathbb{C}_{d_q}+1}^{N_{d_q}} f_j + P_{\text{out}}^{\text{Link \#1, (c)}} \sum_{i=\mathbb{C}_{d_p}+1}^{N_{d_p}} f_i \sum_{j=1}^{\mathbb{C}_{d_q}} f_j + P_{\text{out}}^{\text{Link \#1, (d)}} \sum_{i=\mathbb{C}_{d_p}+1}^{N_{d_p}} f_i \sum_{j=\mathbb{C}_{d_q}+1}^{N_{d_q}} f_j, \quad (6.39)$$

where $P_{\text{out}}^{\text{Link \#1, (a)}} = 1 - \underbrace{\Pr\left[\Lambda_{D_q,x_{d_p}} \geq \gamma'_{d_q}\right]}_{\chi_3}$ with $\gamma'_{d_q} = 2^{R_{d_q}} - 1$, $P_{\text{out}}^{\text{Link \#1, (b)}} = 1 - \chi_2$, $P_{\text{out}}^{\text{Link \#1, (c)}} = 1 - \underbrace{\Pr\left[\Lambda_{D_p\to C} \geq \gamma_{d_q}\right]}_{\chi_1^{\text{no-IUI}}} \chi_2$, and $P_{\text{out}}^{\text{Link \#1, (d)}} = P_{\text{out}}^{\text{Link \#1, CF}}$. As such, χ_3 can be referred from (6.28) while substituting $T_1 = \frac{\gamma'_{d_q}}{(1-\rho)-\rho\gamma'_{d_q}}$. Next, $\chi_1^{\text{no-IUI}}$ can be acquired as

$$\chi_1^{\text{no-IUI}} = \sum_{m=0}^{m_{d_pc}-1} \sum_{g=0}^{m} \sum_{\kappa=0}^{m_{ac}-1} \left(\frac{m_{d_pc}\gamma_{d_q}}{\Omega_{d_pc}\eta_{d_p}}\right)^m \frac{(g+\kappa)!}{m!} \alpha_c \frac{\xi_c(\kappa)}{(\widetilde{\eta}_a)^{\kappa+1}} \times \left(\frac{m_{d_pc}\gamma_{d_q}}{\Omega_{d_pc}\eta_{d_p}} + \frac{\beta_c - \delta_c}{\widetilde{\eta}_a}\right)^{-(g+\kappa+1)} \binom{m}{g} \mathrm{e}^{-\left(\frac{m_{d_pc}\gamma_{d_q}}{\Omega_{d_pc}\eta_{d_p}}\right)}. \quad (6.40)$$

Exact Outage Probability Analysis of the Link #2

$$P_{\text{out}}^{\text{Link \#2, CA}} = P_{\text{out}}^{\text{Link \#2, (a)}} \sum_{i=1}^{\mathbb{C}_{d_p}} f_i \sum_{j=1}^{\mathbb{C}_{d_q}} f_j + P_{\text{out}}^{\text{Link \#2, (b)}} \sum_{i=1}^{\mathbb{C}_{d_p}} f_i \sum_{j=\mathbb{C}_{d_q}+1}^{N_{d_q}} f_j + P_{\text{out}}^{\text{Link \#2, (c)}} \sum_{i=\mathbb{C}_{d_p}+1}^{N_{d_p}} f_i \sum_{j=1}^{\mathbb{C}_{d_q}} f_j + P_{\text{out}}^{\text{Link \#2, (d)}} \sum_{i=\mathbb{C}_{d_p}+1}^{N_{d_p}} f_i \sum_{j=\mathbb{C}_{d_q}+1}^{N_{d_q}} f_j, \quad (6.41)$$

where $P_{\text{out}}^{\text{Link \#2, (a)}} = 1 - \underbrace{\Pr\left[\Lambda_{D_p,x_{d_p}} \geq \gamma'_{d_q}, \Lambda_{D_p,x_{d_q}} \geq \gamma'_{d_p}\right]}_{J_3}$ with $\gamma'_{d_p} = 2^{R_{d_p}} - 1$, $P_{\text{out}}^{\text{Link \#2, (b)}} = 1 - \underbrace{\Pr\left[\Lambda_{D_q\to C} \geq \gamma_{d_p}\right]}_{J_4^{\text{no-IUI}}} J_2$, $P_{\text{out}}^{\text{Link \#2, (c)}} = 1 - \underbrace{\Pr\left[\Lambda_{D_p\to C} \geq \gamma_{d_q}\right]}_{\chi_1^{\text{no-IUI}}} J_2$, and $P_{\text{out}}^{\text{Link \#2, (d)}} = P_{\text{out}}^{\text{Link \#2, CF}}$. As such, J_3 can be referred from (6.32) while replacing γ_{d_p} with γ'_{d_p}. Next, $J_4^{\text{no-IUI}}$ can be obtained as

$$J_4^{\text{no-IUI}} = \sum_{m=0}^{m_{d_qc}-1} \sum_{g=0}^{m} \sum_{\kappa=0}^{m_{ac}-1} \left(\frac{m_{d_qc}\gamma_{d_p}}{\Omega_{d_qc}\eta_{d_q}}\right)^m \frac{(g+\kappa)!}{m!} \alpha_c \frac{\xi_c(\kappa)}{(\widetilde{\eta}_a)^{\kappa+1}} \times \left(\frac{m_{d_qc}\gamma_{d_p}}{\Omega_{d_qc}\eta_{d_q}} + \frac{\beta_c - \delta_c}{\widetilde{\eta}_a}\right)^{-(g+\kappa+1)} \binom{m}{g} \mathrm{e}^{-\left(\frac{m_{d_qc}\gamma_{d_p}}{\Omega_{d_qc}\eta_{d_q}}\right)}. \quad (6.42)$$

Asymptotic Outage Probability Analysis

Herein, we approximate (6.39) at a high SNR region to get the asymptotic OP expression for the Link #1 under the CA TWR-NOMA scheme. Accordingly, all the involved OP terms have to be approximated at the high SNR. As such, $P_{\text{out, asy}}^{\text{Link \#1, (a)}}$ can be referred from (6.34) while substituting $T_1 = \frac{\gamma'_{d_q}}{(1-\rho)-\rho\gamma'_{d_q}}$. Next, $P_{\text{out, asy}}^{\text{Link \#1, (b)}} = \bar{\chi}_2$, $P_{\text{out, asy}}^{\text{Link \#1, (c)}} = \overline{\chi_1^{\text{no-IUI}}} + \bar{\chi}_2$ with $\overline{\chi_1^{\text{no-IUI}}}$ is given below, whereas $P_{\text{out, asy}}^{\text{Link \#1, (d)}} = P_{\text{out, asy}}^{\text{Link \#1, CF}}$,

$$\overline{\chi_1^{\text{no-IUI}}} = \sum_{m=0}^{m_{d_pc}} \sum_{\kappa=0}^{m_{ac}-1} \binom{m_{d_pc}}{m} \left(\frac{m_{d_pc}\gamma_{d_q}}{\Omega_{d_pc}\eta_{d_p}}\right)^{m_{d_pc}} \frac{\Gamma(m+\kappa+1)}{\Gamma(m_{d_pc}+1)} \frac{\alpha_c \xi_c(\kappa)\widetilde{\eta}_a{}^m}{(\beta_c-\delta_c)^{m+\kappa+1}}. \tag{6.43}$$

Hereby, substituting all the involved approximated OP terms into (6.39), one can assess the diversity order for the Link #1 as zero. Similarly, for (6.41), on can attain a zero diversity order theoretically for the Link #2.

6.4.2 Throughput Analysis

Relying on the results derived in Section 6.4.1, we obtain here the expression of throughput for the secondary terrestrial network as

$$\Re^{\text{CA}} = (1 - P_{\text{out}}^{\text{Link \#1, CA}})\, R_{d_q} + (1 - P_{\text{out}}^{\text{Link \#2, CA}})\, R_{d_p}. \tag{6.44}$$

6.4.3 Average End-to-End Transmission Time

The average E-E transmission times for Link #1 and Link #2 can be expressed as sum of the transmission times weighted by their popularity profiles in each scenario, respectively, as

$$\begin{aligned}\mathcal{T}^{\text{Link \#1, CA}} &= \tau_2 \sum_{i=1}^{\mathbb{C}_{d_p}} f_i \sum_{j=1}^{\mathbb{C}_{d_q}} f_j + (\tau_2+\tau_3) \sum_{i=1}^{\mathbb{C}_{d_p}} f_i \sum_{j=\mathbb{C}_{d_q}+1}^{N_{d_q}} f_j \\ &+ (\tau_1+\tau_2) \sum_{i=\mathbb{C}_{d_p}+1}^{N_{d_p}} f_i \sum_{j=1}^{\mathbb{C}_{d_q}} f_j + (\tau_1+\tau_2) \sum_{i=\mathbb{C}_{d_p}+1}^{N_{d_p}} f_i \sum_{j=\mathbb{C}_{d_q}+1}^{N_{d_q}} f_j\end{aligned} \tag{6.45}$$

and

$$\begin{aligned}\mathcal{T}^{\text{Link \#2, CA}} &= \tau_4 \sum_{i=1}^{\mathbb{C}_{d_p}} f_i \sum_{j=1}^{\mathbb{C}_{d_q}} f_j + (\tau_3+\tau_4) \sum_{i=1}^{\mathbb{C}_{d_p}} f_i \sum_{j=\mathbb{C}_{d_q}+1}^{N_{d_q}} f_j \\ &+ (\tau_1+\tau_4) \sum_{i=\mathbb{C}_{d_p}+1}^{N_{d_p}} f_i \sum_{j=1}^{\mathbb{C}_{d_q}} f_j + (\tau_3+\tau_4) \sum_{i=\mathbb{C}_{d_p}+1}^{N_{d_p}} f_i \sum_{j=\mathbb{C}_{d_q}+1}^{N_{d_q}} f_j.\end{aligned} \tag{6.46}$$

As discussed in previous section, we calculate the above average E-E transmission times through Monte-Carlo simulations.

6.5 Numerical and Simulation Results

In this section, we carry out numerical analysis for the considered CHSTN under the CF/CA TWR-NOMA schemes and endorse our derived theoretical results through Monte-Carlo simulations. For drawing the various analytical curves, we follow i.i.d. channels towards the multiple PRs, while considering that they are clustered relatively close together [42], [45]. Thus, for convenience, we drop the index k from all the notations of the pertaining channel parameters in this section. Table 6.1 enlists some parameters related to the satellite links [80]. To get the numerical results, we adopt a 2-D network layout, where the network nodes B, D_p, C, and D_q are located at the coordinates $(2, 1)$, $(-0.3, 0.5)$, $(0, 0)$, and $(0.7, 0.5)$, respectively. Acquiring the path-loss model [99], the parameter Ω_{ij} of the channel gain is calculated by $\Omega_{ij} = d_{ij}^{-\vartheta}$ for $i,\ j \in \{b, d_p, c, d_q\}$ (with $i \neq j$, $i \notin \{b\}$) and for $i \in \{d_p\}$, $j \notin \{d_q\}$, and vice-versa, d_{ij} is the normalized distance between nodes i and j, and $\vartheta = 4$ be the path-loss exponent. We set the various system parameters, unless otherwise specified, as $R_p = 0.5$ bps/Hz and $R_{d_p} = R_{d_q} = 0.5$ bps/Hz as the target rates, $m_{d_pc} = m_{cd_p} = 2$, $m_{d_qc} = m_{cd_q} = 1$, $m_{D_p} = m_C = 2$, and $m_{d_pb} = m_{cb} = m_{d_qb} = 2$ as the fading severity parameters, $\Omega_{D_p} = \Omega_C = 0.01$ [92] as the mean values of the IS channel power gain, $\rho = 0.3$ [25] as the NOMA-based power allocation factor, and $\sigma^2 = 1$ as the noise variance. The various satellite links are considered under HS and AS with their corresponding shadowed-Rician fading parameters [45] as $(m_{aj}, \flat_{aj}, \Omega_{aj} = 2, 0.063, 0.0005)$ and $(m_{aj}, \flat_{aj}, \Omega_{aj} = 5, 0.251, 0.279)$, $j \in \{b, d_p, c, d_q\}$. Next, the parameters related to considered caching scheme are set as $N_{d_p} = N_{d_q} = 200$ as the sizes of content catalogs, $\theta_{d_p} = \theta_{d_q} = \theta = 2$ as the Zipf distribution parameters, and $\mathbb{C}_{d_p} = \mathbb{C}_{d_q} = 20$ as the cache sizes.

Fig. 6.2 illuminates the transmit power allocation for the SUs against the various values of primary outage constraint ζ_{th} and primary interference power η_a. For this, we consider two cases viz., Case I and Case II, as discussed in Section 6.2. From the figure, one can visualize that the transmit power increases as the values of ζ_{th} and η_a increase against their predefined values. Moreover, the transmit powers allocated for SUs under the Case I are relatively less as compared to the Case II, as the Case

Table 6.1: Satellite Link Parameters [with $j \in \{b, c, d_p, d_q\}$]

Parameters	Value
Orbit	GEO
Carrier frequency	$f = 2$ GHz
Carrier bandwidth	$\mathbb{B}_c = 15$ MHz
3-dB angle	$\varphi_{j3\text{dB}} = 0.8°$
Angle between user j and satellite beam centre	$\varphi_j = 0.2°$
Antenna gain of user j	$G_j = 4$ dB
Maximal beam gain	$G_{\max} = 48$ dB
Receiver noise temperature	$T = 300°$ K

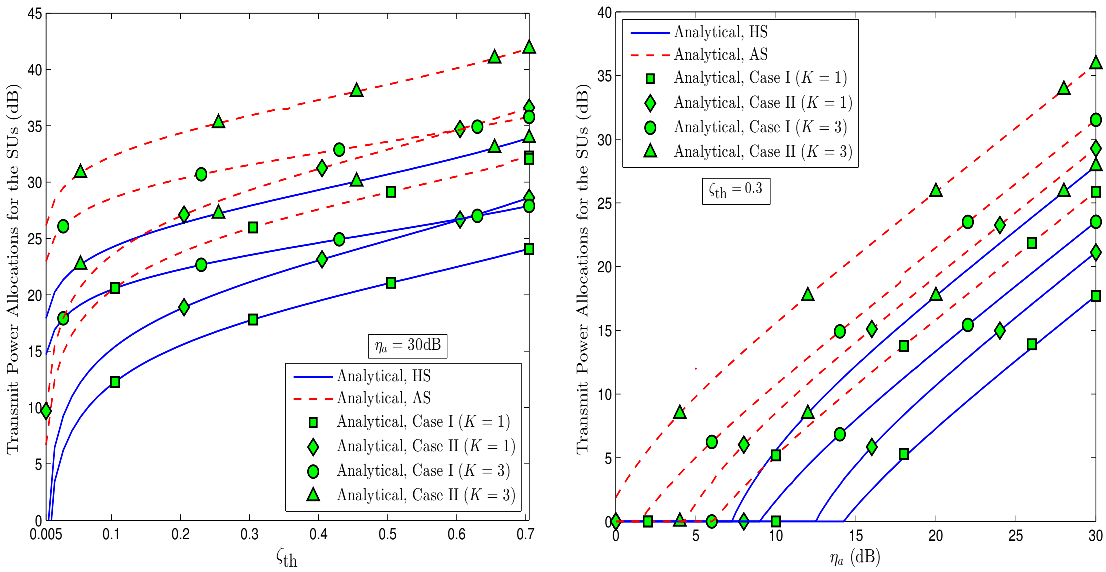

(a) (b)

Figure 6.2: Transmit power allocation for the SUs against the primary (a) outage constraint ζ_{th}; (b) interference power η_a.

I allows simultaneous transmissions from both the nodes D_p and D_q. The transmit power increases further while considering the case of multiple PRs [refer to (6.22) and (6.25)] and AS scenario. Such increments in transmit power happen owing to the improved primary outage performance. As an illustration, let us consider the AS scenario under the setting $\zeta_{\text{th}} = 10^{-2}$ and $\eta_a = 30$ dB. For this set of values, the corresponding numerical values of calculated transmit powers for SUs for $K = 1$ under the Case I and Case II are 10.9 dB and 12.94 dB. Now, considering $K = 3$ for the same set of values, the respective numerical values of calculated transmit powers for SUs under the Case I and Case II increase to 24.2 dB and 27.38 dB.

Fig. 6.3 exhibits the analytical and asymptotic OP curves for the secondary network under the CF/CA TWR-NOMA schemes against the primary outage constraint ζ_{th} with setting η_a as 30 dB. We can observe that the asymptotic curves are

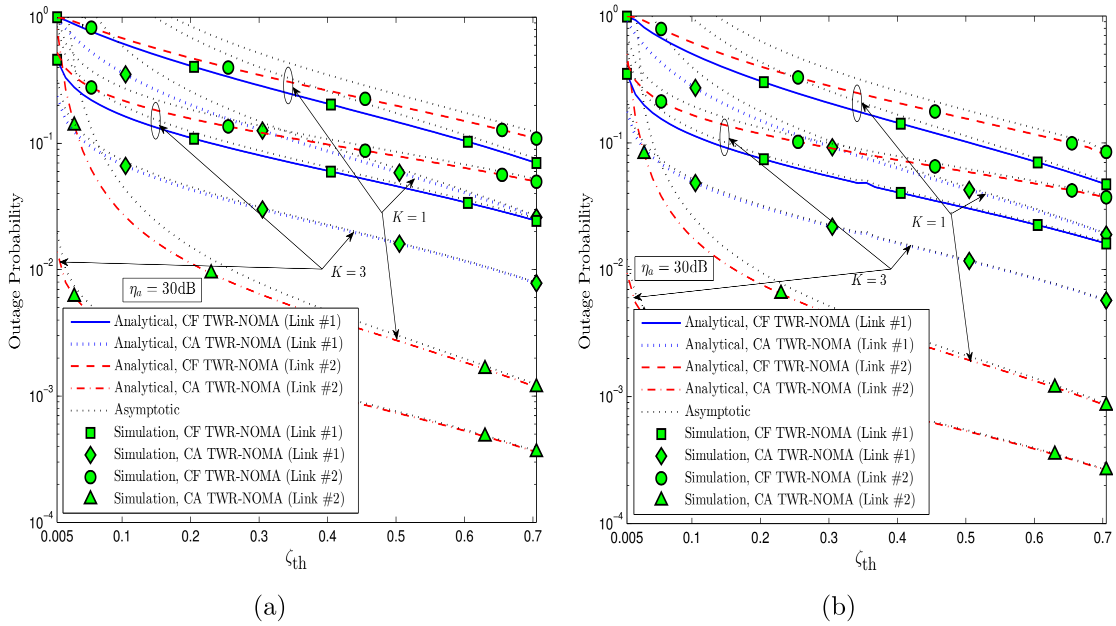

Figure 6.3: OP of the secondary network against the primary outage constraint ζ_{th} (a) HS; (b) AS.

well aligned with analytical and simulated curves in the high regime of ζ_{th}. One can further visualize the relatively better outage performance for the Link #1 as compared to the Link #2 under the CF TWR-NOMA scheme. It is primarily due to the more power allocation towards the signal x_{d_p} or the desired signal of distant user D_q and the absence of any ipSIC effect. However, the results are contradictory under the CA TWR-NOMA scheme, owing to the involvement of the various other parameters/factors while deriving the OP expression. Also, one can notice a remarkable performance enhancement under the CA TWR-NOMA scheme over the CF TWR-NOMA scheme, as the prior one efficiently utilizes the available spectrum resources based on the contents cached at the relay, and thus, the impact of IUI is significantly reduced. Further, there are notable improvements in the OP curves pertaining to both the schemes while considering multiple PRs as it allows more SUs' powers for transmissions. Furthermore, the performance relatively improves for the same set of parameters when satellite links are subject to AS (as in Fig. 6.3(b)) than its HS counterpart (as in Fig. 6.3(a)).

Fig. 6.4 depicts the OP versus primary interference power η_a curves while considering the HS and the AS sets of scenarios. For this, we set $\zeta_{\text{th}} = 0.3$. From the figure, under HS scenario, one can note that at the lower values of η_a, a cut-off point exists below which the secondary network remains in the outage. This is primarily due to the more stringent QoS requirements from the PRs. Nevertheless, this cut-off

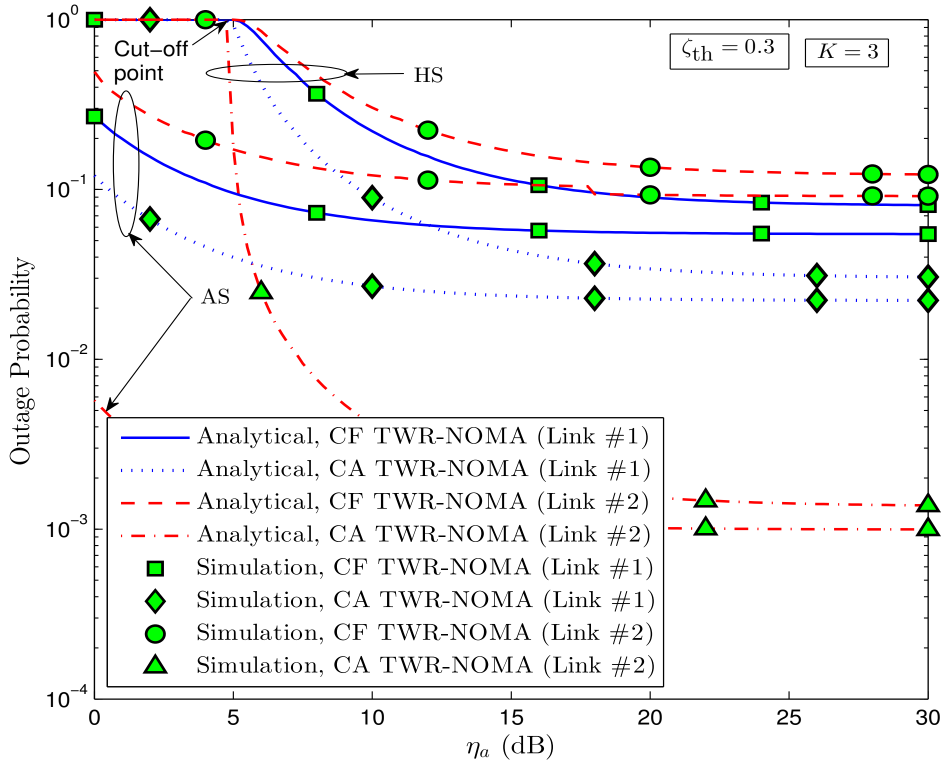

Figure 6.4: OP of the secondary network against the primary interference power η_a.

point relatively vanishes at the early stage of η_a when satellite links are subject to AS. Further, at the higher values of η_a, an outage floor appears in the performance, owing to the dominance of the interference from the primary satellite.

Fig. 6.5 illustrates the throughput curves against the primary outage constraint ζ_{th} under the setting η_a as 30 dB. From the figure, it can be seen that the throughput for the CF/CA TWR-NOMA schemes initially increase as the value of ζ_{th} increases, but saturates at the higher values of ζ_{th}. As such, at the higher values of ζ_{th}, the OP saturates at some lower constant value, and hence, the throughput is only determined by the fixed transmission rates of both the links in the secondary network. Based on the reasoning presented in the description of Fig. 6.3, the throughput of the secondary network under the CA TWR-NOMA scheme is notably high than its CF counterpart. Also, the impact of multiple PRs can be seen in the form of increased throughput.

Fig. 6.6 demonstrates and compares the average E-E transmission times for sending the packets through Link #1 and Link #2 under the proposed CF/CA TWR-NOMA schemes. For this, we assume the channel bandwidth and packet length as $\mathcal{B}_s = 1$ MHz and $L = 10240$ bits, respectively. From the figure, it can be visualized

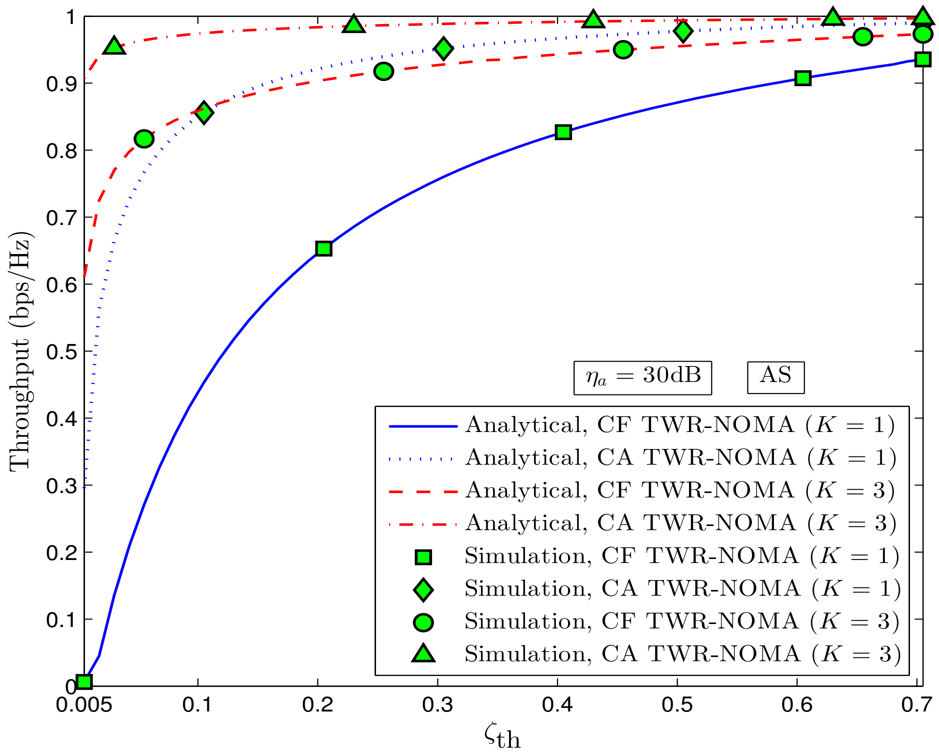

Figure 6.5: Throughput of the secondary network against the primary outage constraint ζ_{th}.

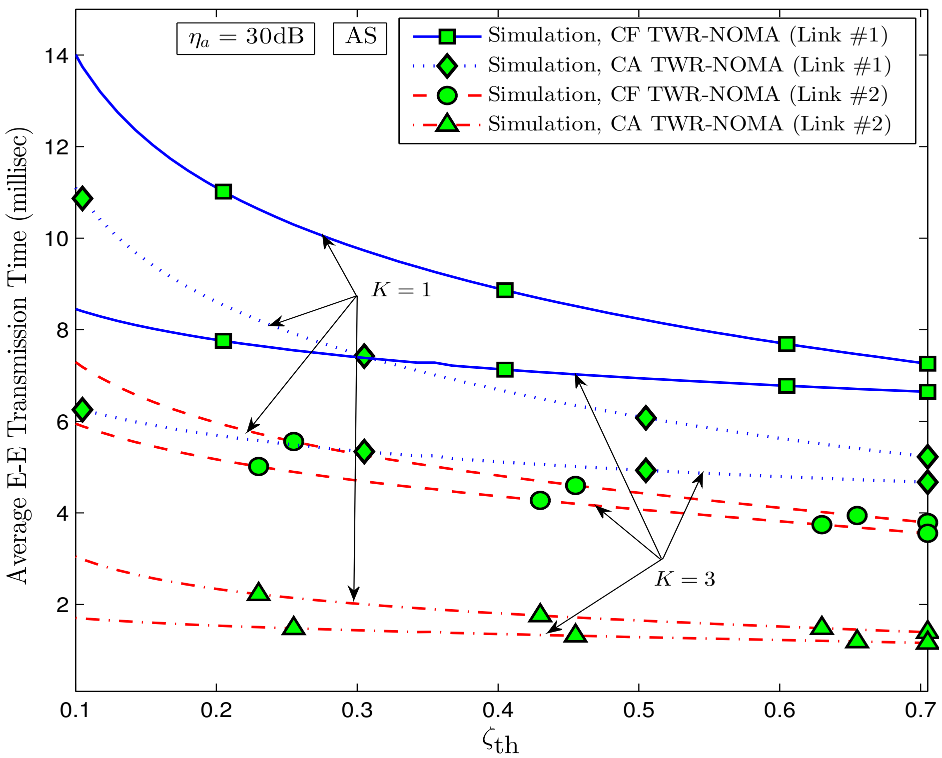

Figure 6.6: Average E-E transmission time against the primary outage constraint ζ_{th}.

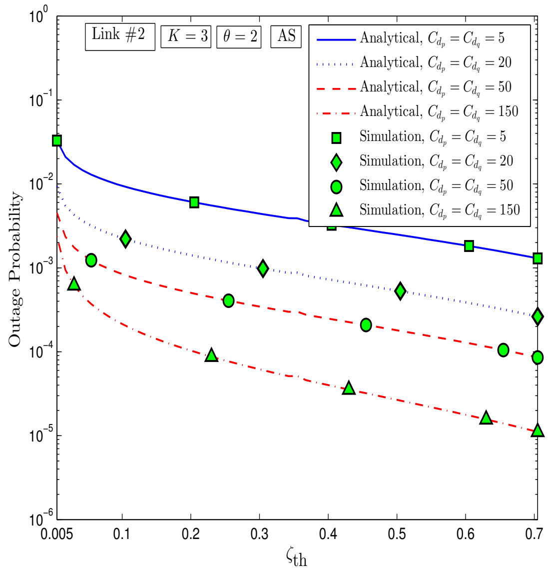

(a)

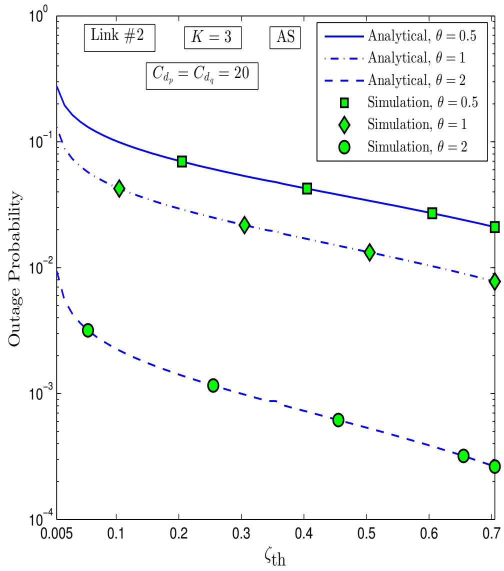

(b)

Figure 6.7: Impacts of caching parameters on the outage performance (a) Cache size; (b) Zipf distribution parameter.

that the transmission time under the CA TWR-NOMA scheme is relatively less than the transmission time under the CF TWR-NOMA scheme, as the prior one efficiently utilizes the available spectrum resources based on the contents cached at the relay. For instance, under the Scenario (a), only one time slot is required to exchange the information between NOMA users, which reduces the overall transmission time significantly. The transmission time gradually decreases as the value of ζ_{th} increases. It further decreases while considering the case of multiple PRs.

Fig. 6.7 illuminates the impacts of Zipf distribution parameter θ and cache size on the outage performance of the Link #2. Subsequently, in Fig. 6.7 (a), the impact of various cache sizes on the outage performance for a fixed value of θ is illustrated. Hereby, one can observe that the outage performance improves while increasing the value of cache size, as most of the time, both NOMA users can retrieve their contents from the relay itself. Consequently, the available spectrum resources will be utilized more efficiently, and the outage performance will be ameliorated accordingly. In Fig. 6.7 (b), the outage performance improves as the value of θ increases. The higher value of θ implies that both NOMA users will request the lower-index files with high popularity, which can be easily stored in the relay with limited cache capacity during the off-peak traffic period.

6.6 Summary

We investigated the performance of an underlay CHSTN wherein a secondary terrestrial network shares the spectrum with the primary satellite network for exchanging the information between two NOMA users with the aid of a half-duplex DF-based secondary relay. It is demonstrated further there exists an inevitable IUI causing detrimental impacts on the performance of the secondary network. Consequently, to improve the performance and subsequently the low latency requirements, we exploited the wireless content caching, whereby the relay can store the most popular contents of both the NOMA users. Considering the mutual interference between the primary and secondary networks, the transmit powers at SUs were calculated for a predefined primary outage constraint at the best selected PR among K PRs. Based on these calculated powers and considering the realistic assumption of ipSIC, we further quantified the performance of the secondary network by analyzing the OP, throughput, and average E-E transmissions times under the CF/CA TWR-NOMA schemes. Our studies revealed that multiple PRs manifest the advantage of improved performance towards the secondary network. It is also illustrated from the asymptotic OP analysis that a zero diversity order results for both the proposed schemes due to unavoidable IUI. Nevertheless, the performance corresponding to CA TWR-NOMA scheme is notably improved over its CF TWR-NOMA counterpart, owing to the reduced IUI and the efficient utilization of available spectrum resources.

CHAPTER 7

CONCLUSIONS AND FUTURE WORKS

In this chapter, we present the conclusions derived from the work in this thesis and provide the possible directions for the future works.

7.1 Conclusions

This thesis presented a comprehensive performance analysis of CHSTNs with various spectral-efficient schemes. The primary objective of the thesis was to provide various system designs for future networks which can efficiently utilize the precious spectrum resources. Firstly, we analyzed the performance of CHSTNs in which a secondary terrestrial network competes for spectrum access with the primary satellite network. Therein, a multiuser downlink scenario for the CHSTNs was explored where opportunistic selection criterion for the best satellite user is designed by exploiting both direct and relay links in an optimal manner. In addition, we provided useful insights on the power splitting factor to explore additional spectrum sharing opportunities towards the secondary network. Then, we investigated the performance of CHSTNs while taking into account the practical HIs at the terrestrial user nodes. Considering the detrimental impact of HIs on the system performance, we proposed an AR protocol for both AF and DF operations. The proposed AR protocol invokes secondary relay cooperation adaptively, relying upon the limited feedback mechanism from the PU. Thereby, it efficiently utilizes the available degrees-of-freedom to improve the performance of CHSTN even in the presence of HIs. Next, different from the above discussed works, we considered the multiple PRs assisted through NOMA scheme for the performance evaluation. Thereby, a comparison with the benchmark OMA scheme reveals that the proposed NOMA-assisted CHSTN provides remarkable performance improvement while utilizing the spectrum resource efficiently. Further, we investigated the performance of an underlay CHSTN wherein a secondary terrestrial network shares the spectrum with the primary satellite network to communicate with intended receivers that are deployed based on the C-NOMA scheme. Our studies reveal that multiple PRs manifest the advantage of improved performance towards the secondary network. Additionally, it is illustrated that the outage performance corresponding to HD-pSIC case is notably improved at high SNR region over all the discussed cases, caused by a non-zero diversity order. Moreover, the conclusions can be drawn that for the case of ipSIC, the FD C-NOMA scheme outperforms the HD C-NOMA scheme in the entire regime of SNRs, however, for the case of pSIC, the performance of HD C-NOMA scheme is remarkably ameliorated at a high SNR in contrast to the FD C-NOMA scheme. Lastly, we explored the performance of an underlay CHSTN wherein a secondary terrestrial network shares the spectrum with the primary satellite network for exchanging the information between two NOMA users with the aid of a HD DF-based secondary relay. To mitigate the impact of inevitable IUI in such TWR-NOMA based CHSTN, the wireless content caching was exploited, which provides a remarkable performance improvement for CHSTN, owing to the efficient utilization of available spectrum resources.

In essence, we have comprehensively investigated the performance of CHSTNs to offer useful insights into the practical design. We have proposed various schemes and strategies which can improve the spectral efficiency and reliability of the CHSTNs and eventually facilitate their deployment for the next-generation wireless systems.

7.2 Future Works

With emerging 5G communication, there are many open problems related to the topics of this thesis that could be treated in future research. Some future prospects for the research work are given in the sequel.

Since spectrum efficiency is key objective for future networks, their analysis has gained significant research attention. To further increase the spectral efficiency and throughput of the CHSTNs, exploiting multiple-input-multiple-output (MIMO) technology while deploying a multi-antenna satellite with multi-user configuration can be viewed as an important direction. In MIMO systems, multiple antennas are employed at the transceiver nodes to provide a high data rate.

In addition, due to the coexistence of PUs and SUs together, the CHSTNs are susceptible to security threats. Consequently, it would be important and interesting to develop the strategies for the physical layer security of the CHSTNs. Dealing with security breaches is of paramount importance and one of the main challenges in designing the 5G networks.

On another front, reconfigurable intelligent surface (RIS) is a promising technology to enhance the coverage and performance of wireless networks. The rate and energy efficiency of wireless channels can be improved by deploying software-controlled metasurfaces to reflect signals from the source to the destination, especially when the direct path is weak. As such, the disruptive RIS concept of controlling the propagation channels via software provides attractive performance gains to the communication networks, including higher data rates, improved user fairness, etc. With these potential attributes, of course, analyzing the performance of CHSTNs using RIS is welcome as a new future research direction.

Further, with the recent advances in deep learning architectures/algorithms and open-source artificial intelligence (AI)/machine learning (ML) tools, the application of AI/ML in wireless networks including HSTNs is increasingly getting attention. Therefore, the focus of future research can be to develop novel ML-assisted resource management algorithms to address the challenges of multi-dimensional and large search spaces, and evolving objectives and constraints.

Besides, in this thesis work, one can also study the resource allocation in CHSTNs based on the optimization of the performance metrics. For instance, it would be interesting and challenging to find the optimal values of overlay-based spectrum sharing parameter and NOMA-based power allocation factor.

With the above mentioned prospects, the existing body of knowledge in the design of CHSTNs can be further expanded.

APPENDIX A

DERIVATION OF (3.29)

The CDF $F_{\Lambda_{acb}}(x) = \Pr\left[\Lambda_{acb} < x\right]$ is expressed, using (3.6), as

$$F_{\Lambda_{acb}}(x) = \Pr\left[\frac{\mu\Lambda_{ac}\Lambda_{cb}}{\tau_p\Lambda_{ac}\Lambda_{cb} + \varepsilon\Lambda_{ac} + \omega_p\Lambda_{cb} + 1} < x\right] = \Pr\left[\Lambda_{ac} < \frac{x(1+\omega_p\Lambda_{cb})}{\theta_x\Lambda_{cb} - \varepsilon x}\right], \tag{A.1}$$

which can be further evaluated as

$$F_{\Lambda_{acb}}(x) = 1 - \int_{\frac{\varepsilon x}{\theta_x}}^{\infty} \bar{F}_{\Lambda_{ac}}\left(\frac{x(1+\omega_p y)}{\theta_x y - \varepsilon x}\right) f_{\Lambda_{cb}}(y) dy. \tag{A.2}$$

With $\theta_x > 0$, we exploit (3.18) and (3.19) into (A.2), and then simplify using binomial expansion [41, eq. 1.111] to obtain $F_{\Lambda_{acb}}(x)$ as given in (3.28) with

$$\psi_1(x) = 1 - \alpha_c \sum_{\kappa=0}^{m_{ac}-1} \sum_{l=0}^{\kappa} \sum_{m=0}^{l} \sum_{g=0}^{m+m_{cb}-1} \frac{\zeta(\kappa)}{(\eta_a)^{\kappa+1}} \frac{\kappa!}{l!} M^{-(\kappa+1-l)} \frac{N^{m_{cb}}}{\Gamma(m_{cb})} \frac{x^l \omega_p^m (\varepsilon x)^{m+m_{cb}-1-g}}{\theta_x^{m+m_{cb}}}$$
$$\times \binom{l}{m}\binom{m+m_{cb}-1}{g} \mathrm{e}^{-\left(\frac{(\omega_p M + N\varepsilon)x}{\theta_x}\right)} \int_0^{\infty} t^{(g-l+1)-1} \mathrm{e}^{-\left(\frac{\frac{M\varepsilon x^2}{\theta_x} + Mx}{t} - \frac{N}{\theta_x} t\right)} dt. \tag{A.3}$$

Now, on simplifying the integration in (A.3) using [41, eq. 3.471.9], one can arrive at (3.29) which completes the proof.

APPENDIX B

DERIVATION OF (4.18)

The CDF $F_{\Lambda_{acb_k}}(x) = \Pr\big[\Lambda_{acb_k} < x\big]$ can be expressed using (4.7) or (4.9) in a generalized form as

$$F_{\Lambda_{acb_k}}(x) = \Pr\left[\Lambda_{ac} < \frac{x(1+\Lambda_{cb_k})}{\theta_{kx}\Lambda_{cb_k} - x}\right], \tag{B.1}$$

which can be further evaluated as

$$F_{\Lambda_{acb_k}}(x) = 1 - \int_{\frac{x}{\theta_{kx}}}^{\infty} \bar{F}_{\Lambda_{ac}}\left(\frac{x(1+y)}{\theta_{kx}y - x}\right) f_{\Lambda_{cb_k}}(y)dy. \tag{B.2}$$

Now, exploiting (4.12) and (4.13) into (B.2), and simplifying using binomial expansion [41, eq. 1.111], we obtain

$$\begin{aligned}\psi_k(x) = 1 - \alpha_c &\sum_{\kappa=0}^{m_{ac}-1} \sum_{l=0}^{\kappa} \sum_{m=0}^{l} \sum_{g=0}^{m+m_{cb_k}-1} \frac{\zeta(\kappa)}{(\eta_a)^{\kappa+1}} \frac{\kappa!}{l!} M^{-(\kappa+1-l)} N^{m_{cb_k}} \\ &\times \frac{(x)^{m+l+m_{cb_k}-1-g}}{\theta_{kx}^{m+m_{cb_k}}} \binom{l}{m} \binom{m+m_{cb_k}-1}{g} \frac{1}{\Gamma(m_{cb_k})} \\ &\times \mathrm{e}^{-\left(\frac{(M+N)x}{\theta_{kx}}\right)} \int_0^{\infty} t^{(g-l+1)-1} \mathrm{e}^{-\left(\frac{\frac{Mx^2}{\theta_{kx}}+Mx}{t} - \frac{N}{\theta_{kx}}t\right)} dt. \end{aligned} \tag{B.3}$$

Now, solving the integral in (B.3) using [41, eq. 3.471.9], one can arrive at (4.18).

APPENDIX C

DERIVATIONS OF (4.24) AND (4.25)

To derive the asymptotic OP expression for primary network, we first approximate the SINR expressions in (4.7) and (4.9) by neglecting the unity term from denominator and using the fact $\frac{XY}{X+Y} < \min(X, Y)$ [45] to represent

$$\Lambda_{acb_k} < \frac{\mu}{\tau_k + \frac{1}{\min(\Lambda_{cb_k}, \Lambda_{ac})}}. \tag{C.1}$$

Hence, the corresponding CDF can be expressed as

$$F_{\Lambda_{acb_k}}(x) \simeq F_{\Lambda_{ac}}\left(\frac{x}{\theta_{kx}}\right) + F_{\Lambda_{cb_k}}\left(\frac{x}{\theta_{kx}}\right). \tag{C.2}$$

At high SNR the respective CDFs used in (4.12) and (4.14) can be approximated as

$$F_{\Lambda_{ai}}(x) \approx \frac{\alpha_i}{\eta_a} x \text{ and } F_{\Lambda_{cj}}(x) \approx \frac{1}{\Gamma(m_{cj}+1)}\left(\frac{m_{cj}x}{\Omega_{cj}\eta_c}\right)^{m_{cj}}. \tag{C.3}$$

Consequently, (C.2) can be represented as

$$F_{\Lambda_{acb_k}}(x) \simeq \frac{\alpha_c x}{\eta_a \theta_{kx}} + \frac{1}{\Gamma(m_{cb_k}+1)}\left(\frac{m_{cb_k}x}{\Omega_{cb_k}\eta_c\theta_{kx}}\right)^{m_{cb_k}}. \tag{C.4}$$

Now, on using (C.4) into (4.19) and (4.22), one can arrive at (4.24) and (4.25), respectively.

APPENDIX D

DERIVATION OF (5.19)

On using (5.14) into (5.16), $\Pr\left[\Lambda_{b_l}^{\text{pri}} < \gamma_p\right]$ can be expressed as

$$\Pr\left[\Lambda_{b_l}^{\text{Pri}} < \gamma_p\right] = \Pr\left[\frac{\Lambda_{ab_l}}{\Lambda_{cb_l} + \Lambda_{d_p b_l} + 1} < \gamma_p\right], \tag{D.1}$$

which can be re-expressed as

$$\Pr\left[\Lambda_{b_l}^{\text{Pri}} < \gamma_p\right] = 1 - \int_0^\infty \left(\int_0^\infty \left(\int_{\gamma_p(y+z+1)}^\infty f_{\Lambda_{ab_l}}(x)dx \right) f_{\Lambda_{cb_l}}(y)dy \right) f_{\Lambda_{d_p b_l}}(z)dz. \tag{D.2}$$

Now, on substituting the PDFs $f_{\Lambda_{ab_l}}(x)$ and $f_{\Lambda_{cb_l}}(y)$ corresponding to the satellite and terrestrial links, respectively from (5.4) and (5.6), and further solving the associated integral w.r.t. x in (D.2) using [41, eq. 3.351.2] and binomial expansion [41, eq. 1.111], we obtain

$$\begin{aligned}\Pr\left[\Lambda_{b_l}^{\text{Pri}} < \gamma_p\right] = 1 - &\sum_{\kappa=0}^{m_{ab_l}-1} \sum_{m=0}^{\kappa} \sum_{v=0}^{m} \alpha_{b_l} \frac{\xi_{b_l}(\kappa)}{(\widetilde{\eta_a})^{\kappa+1}} \frac{\kappa!}{m!} \frac{1}{\Gamma(m_{cb_l})} \left(\frac{m_{cb_l}}{\Omega_{cb_l}\eta_c} \right)^{m_{cb_l}} \\ &\times \left(\frac{\beta_{b_l} - \delta_{b_l}}{\widetilde{\eta_a}} \right)^{-(\kappa+1-m)} \gamma_p^m \mathrm{e}^{-\left(\gamma_p \frac{\beta_{b_l}-\delta_{b_l}}{\widetilde{\eta_a}}\right)} \binom{m}{v} \\ &\times \left(\int_0^\infty y^{v+m_{cb_l}-1} \mathrm{e}^{-\left(\gamma_p \frac{\beta_{b_l}-\delta_{b_l}}{\widetilde{\eta_a}} + \frac{m_{cb_l}}{\Omega_{cb_l}\eta_c}\right) y} dy \right) \\ &\times \left(\int_0^\infty (z+1)^{m-v} \mathrm{e}^{-\left(\gamma_p z \frac{\beta_{b_l}-\delta_{b_l}}{\widetilde{\eta_a}}\right)} f_{\Lambda_{d_p b_l}}(z)dz \right).\end{aligned} \tag{D.3}$$

Hereby, substituting the PDF expression of $f_{\Lambda_{d_p b_l}}(z)$ into (D.3), then computing the associated integrals using [41, eq. 3.351.3], and finally applying the order statistics using (5.18), one can get the desired OP expression of the primary satellite network for a given primary outage constraint ζ_{th} under the FD C-NOMA scheme, as given in (5.19).

APPENDIX E

DERIVATION OF (5.25)

Referring to (5.24), χ_1 can be written for the case of FD-ipSIC using (5.9) and (5.10) as

$$\begin{aligned}\chi_1^{\text{FD-ipSIC}} = \Pr\Big[&\Lambda_{cd_p} \geq T_1(\Lambda_{d_pd_p} + \Lambda_{ad_p} + 1),\\ &\Lambda_{cd_p} \geq T_2(\Lambda_{d_pd_p} + \Lambda_{ad_p} + \Lambda_{D_p} + 1)\Big],\end{aligned} \tag{E.1}$$

where $T_1 = \frac{\gamma_{d_q}^{\text{FD}}}{(1-\rho)-\rho\gamma_{d_q}^{\text{FD}}}$ and $T_2 = \frac{\gamma_{d_p}^{\text{FD}}}{\rho}$. Subsequently, (E.1) can be evaluated as

$$\begin{aligned}\chi_1^{\text{FD-ipSIC}} &= U(T_1 - T_2)\int_{\frac{1}{T_3}}^{\infty}\left(\int_0^{T_3w-1}\left(\int_{T_3w-z-1}^{\infty}\left(\int_{T_1(y+z+1)}^{\infty} f_{\Lambda_{cd_p}}(x)dx\right)\right.\right.\\ &\qquad\qquad \left.\left. f_{\Lambda_{d_pd_p}}(y)dy\right) f_{\Lambda_{ad_p}}(z)dz\right) f_{\Lambda_{D_p}}(w)dw\\ &+ U(T_1 - T_2)\int_{\frac{1}{T_3}}^{\infty}\left(\int_0^{T_3w-1}\left(\int_0^{T_3w-z-1}\left(\int_{T_2(y+z+w+1)}^{\infty} f_{\Lambda_{cd_p}}(x)dx\right)\right.\right.\\ &\qquad\qquad \left.\left. f_{\Lambda_{d_pd_p}}(y)dy\right) f_{\Lambda_{ad_p}}(z)dz\right) f_{\Lambda_{D_p}}(w)dw\\ &+ U(T_2 - T_1)\int_0^{\infty}\left(\int_0^{\infty}\left(\int_0^{\infty}\left(\int_{T_2(y+z+w+1)}^{\infty} f_{\Lambda_{cd_p}}(x)dx\right)\right.\right.\\ &\qquad\qquad \left.\left. f_{\Lambda_{d_pd_p}}(y)dy\right) f_{\Lambda_{ad_p}}(z)dz\right) f_{\Lambda_{D_p}}(w)dw,\end{aligned} \tag{E.2}$$

where $T_3 = \frac{T_2}{T_1-T_2}$ and $U(x)$ is unit-step function whose value is 1, when $x > 0$, and 0 otherwise. Nevertheless, for the feasible range of ρ, $T_2 > T_1$, thus, (E.2) can be simplified as

$$\chi_1^{\text{FD-ipSIC}} = \int_0^\infty \Bigg(\int_0^\infty \Bigg(\int_0^\infty \Bigg(\int_{T_2(y+z+w+1)}^\infty f_{\Lambda_{cd_p}}(x)dx \Bigg) f_{\Lambda_{d_pd_p}}(y)dy \Bigg) f_{\Lambda_{ad_p}}(z)dz \Bigg) f_{\Lambda_{D_p}}(w)dw. \tag{E.3}$$

Hereby, the final expression of $\chi_1^{\text{FD-ipSIC}}$ can be derived as in (5.26), using [41, eqs. (3.351.2) and (3.351.3)] and binomial expansion [41, eq. 1.111]. Similarly, the expression of $\chi_1^{\text{HD-ipSIC}}$ can be evaluated as in (5.27). Now, we proceed to obtain the expression of χ_2 as follows:

Referring to (5.24), χ_2 can be expressed using (5.12) as

$$\chi_2 = 1 - \Pr\left[\frac{\Lambda_{d_pd_q}}{\Lambda_{ad_q} + 1} < \gamma_{d_q} \right], \tag{E.4}$$

which can be re-expressed as

$$\chi_2 = 1 - \int_0^\infty \Bigg(\int_0^{\gamma_{d_q}(z+1)} f_{\Lambda_{d_pd_q}}(x)dx \Bigg) f_{\Lambda_{ad_q}}(z)dz. \tag{E.5}$$

Now, computing the associated integrals using [41, eqs. (3.351.1) and (3.351.3)] and binomial expansion [41, eq. 1.111], one can acquire the desired expression of χ_2 as in (5.28).

APPENDIX F

DERIVATIONS OF (5.29)-(5.32)

Referring to (5.24), χ_1 can be re-expressed for the case of FD-ipSIC using (E.3) as

$$\chi_1^{\text{FD-ipSIC}} = 1 - \int_0^\infty \left(\int_0^\infty \left(\int_0^\infty \left(\int_0^{T_2(y+z+w+1)} f_{\Lambda_{cd_p}}(x)dx \right) f_{\Lambda_{d_pd_p}}(y)dy \right) f_{\Lambda_{ad_p}}(z)dz \right) f_{\Lambda_{D_p}}(w)dw. \tag{F.1}$$

Now, substituting (E.5) (with $\gamma_{d_q} = \gamma_{d_q}^{\text{FD}}$) and (F.1) into (5.24), the asymptotic OP expression of secondary network for the FD-ipSIC can be represented as

$$P_{\text{out,asy}}^{\text{FD-ipSIC}} = \int_0^\infty \left(\int_0^\infty \left(\int_0^\infty \left(\int_0^{T_2(y+z+w+1)} f_{\Lambda_{cd_p}}(x)dx \right) f_{\Lambda_{d_pd_p}}(y)dy \right) f_{\Lambda_{ad_p}}(z)dz \right) f_{\Lambda_{D_p}}(w)dw + \int_0^\infty \left(\int_0^{\gamma_{d_q}^{\text{FD}}(z+1)} f_{\Lambda_{d_pd_q}}(x)dx \right) f_{\Lambda_{ad_q}}(z)dz, \tag{F.2}$$

where the product term leading to a higher order is neglected. Hereby, inserting the involved PDF expressions in (F.2), and then simplifying the integral expression in [41, eq. (3.351.1)] while making use of the series expansion of $\Upsilon(\alpha, x)$ [41, eq. 8.354.1] as

$$\Upsilon(\alpha, x) = x^\alpha \sum_{\varepsilon=0}^{\infty} \frac{(-1)^\varepsilon x^\varepsilon}{\varepsilon!(\alpha+\varepsilon)} \underset{x\to 0}{\simeq} \frac{x^\alpha}{\alpha}, \tag{F.3}$$

one can earn the expression of $P_{\text{out,asy}}^{\text{FD-ipSIC}}$ as in (5.29) using the similar steps as for Theorem 5. Similarly, the asymptotic OP expressions of the secondary network for other discussed cases can be evaluated as in (5.30)-(5.32).

APPENDIX G

DERIVATION OF (5.34)

The ergodic rate for user D_p can be expressed using (5.10) as

$$C_{d_p} = \frac{1}{\lambda}\mathbb{E}\left[\log_2\left(1+\underbrace{\left(\frac{\rho\Lambda_{cd_p}}{\varsigma(1-\rho)\Lambda_{D_p}+\omega\Lambda_{d_pd_p}+\Lambda_{ad_p}+1}\right)}_{\Theta}\right)\right]$$
$$= \frac{1}{\lambda\ln 2}\int_0^\infty \frac{1-F_\Theta(\theta)}{1+\theta}d\theta. \tag{G.1}$$

In particular, we consider the case of HD-pSIC and derive the corresponding ergodic rate expression as in (5.38). For this, we substitute $\omega = 0$ and $\varsigma = 0$ in (G.1). Thus, the involved CDF term $F_\Theta(\theta)$ can be calculated as

$$F_\Theta(\theta) = \Pr\left[\frac{\rho\Lambda_{cd_p}}{\Lambda_{ad_p}+1} < \theta\right] = 1 - \int_0^\infty\left(\int_{\frac{\theta}{\rho}(z+1)}^\infty f_{\Lambda_{cd_p}}(x)dx\right)f_{\Lambda_{ad_p}}(z)dz. \tag{G.2}$$

Now, substituting the involved PDF expressions and simplifying using [41, eqs. (3.351.2) and (3.351.3)] and binomial expansion [41, eq. 1.111], the CDF $F_\Theta(\theta)$ can be computed. Consequently, inserting this CDF expression into (G.1), ergodic rate for user D_p under HD-pSIC case can be expressed as

$$C_{d_p}^{\text{HD-pSIC}} = \sum_{m=0}^{m_{cd_p}-1}\sum_{g=0}^{m}\sum_{\kappa=0}^{m_{ad_p}-1}\frac{1}{\lambda\ln 2}\left(\frac{m_{cd_p}}{\Omega_{cd_p}\eta_c\rho}\right)^m\frac{(g+\kappa)!}{m!}\binom{m}{g}\alpha_{d_p}$$
$$\times\frac{\xi_{d_p}(\kappa)}{(\widetilde{\eta}_a)^{\kappa+1}}\left(\frac{\beta_{d_p}-\delta_{d_p}}{\widetilde{\eta}_a}\right)^{-(g+\kappa+1)}\int_0^\infty\theta^m\mathrm{e}^{-\left(\frac{m_{cd_p}\theta}{\Omega_{cd_p}\eta_c\rho}\right)}$$
$$\times\left(1+\frac{m_{cd_p}\widetilde{\eta}_a}{\Omega_{cd_p}\eta_c\rho(\beta_{d_p}-\delta_{d_p})}\theta\right)^{-(g+\kappa+1)}(1+\theta)^{-1}d\theta. \tag{G.3}$$

Now, expanding the last two terms inside the integral in terms of Meijer-G function via [93, eq. 10] as

$$(1+x)^{\alpha} = \frac{1}{\Gamma(-\alpha)} G_{1,1}^{1,1}\left[x \,\middle|\, \begin{matrix} \alpha+1 \\ 0 \end{matrix}\right], \tag{G.4}$$

and then solving the integral using [94, eq. (2.6.2)], one can get the expression for $C_{d_p}^{\text{HD-pSIC}}$ as in (5.38). Likewise, one can derive the ergodic rate expressions of user D_p for the other involved cases in (5.34).

APPENDIX H

DERIVATION OF (6.22)

On using (6.17) into (6.19), $\Pr\left[\Lambda_{b_k}^{\text{pri}} < \gamma_p\right]$ can be expressed as

$$\Pr\left[\Lambda_{b_k}^{\text{Pri}} < \gamma_p\right] = \Pr\left[\frac{\Lambda_{ab_k}}{\Lambda_{d_p b_k} + \Lambda_{d_q b_k} + 1} < \gamma_p\right], \tag{H.1}$$

which can be further evaluated as

$$\Pr\left[\Lambda_{b_k}^{\text{Pri}} < \gamma_p\right] = 1 - \int_0^{\infty}\left(\int_0^{\infty}\left(\int_{\gamma_p(y+z+1)}^{\infty} f_{\Lambda_{ab_k}}(x)dx\right) f_{\Lambda_{d_p b_k}}(y)dy\right) f_{\Lambda_{d_q b_k}}(z)dz. \tag{H.2}$$

Now, on inserting the PDFs $f_{\Lambda_{ab_k}}(x)$ and $f_{\Lambda_{d_p b_k}}(y)$ corresponding to the satellite and terrestrial links, respectively from (6.4) and (6.6), and further solving the associated integral w.r.t. x in (H.2) using [41, eq. 3.351.2] and binomial expansion [41, eq. 1.111], we obtain

$$\begin{aligned}
\Pr\left[\Lambda_{b_k}^{\text{Pri}} < \gamma_p\right] = 1 - &\sum_{\kappa=0}^{m_{ab_k}-1}\sum_{m=0}^{\kappa}\sum_{v=0}^{m} \alpha_{b_k}\frac{\xi_{b_k}(\kappa)}{(\widetilde{\eta}_a)^{\kappa+1}}\left(\frac{\beta_{b_k}-\delta_{b_k}}{\widetilde{\eta}_a}\right)^{-(\kappa+1-m)} \\
&\times \frac{\kappa!}{m!}\frac{1}{\Gamma(m_{d_p b_k})}\gamma_p^m \mathrm{e}^{-\left(\gamma_p\frac{\beta_{b_k}-\delta_{b_k}}{\widetilde{\eta}_a}\right)}\left(\frac{m_{d_p b_k}}{\Omega_{d_p b_k}\eta_{d_p}}\right)^{m_{d_p b_k}} \\
&\times \binom{m}{v}\left(\int_0^{\infty} y^{v+m_{d_p b_k}-1}\mathrm{e}^{-\left(\gamma_p\frac{\beta_{b_k}-\delta_{b_k}}{\widetilde{\eta}_a}+\frac{m_{d_p b_k}}{\Omega_{d_p b_k}\eta_{d_p}}\right)y}dy\right) \\
&\times \left(\int_0^{\infty}(z+1)^{m-v}\mathrm{e}^{-\left(\gamma_p z\frac{\beta_{b_k}-\delta_{b_k}}{\widetilde{\eta}_a}\right)} f_{\Lambda_{d_q b_k}}(z)dz\right).
\end{aligned} \tag{H.3}$$

Hereby, substituting the PDF $f_{\Lambda_{d_q b_k}}(z)$ using (6.6), then computing the involved integrals using [41, eq. 3.351.3], and finally applying the order statistics using (6.21), one can get the desired OP expression of the primary satellite network for a given primary outage constraint ζ_{th} under the Case I, as given in (6.22).

APPENDIX I

DERIVATIONS OF (6.27) AND (6.28)

Referring to (6.26), it requires the evaluations of the terms χ_1 and χ_2. As such, χ_1 can be written using (6.9) as

$$\chi_1 = \Pr\left[\frac{\Lambda_{d_p c}}{\Lambda_{d_q c} + \Lambda_{ac} + 1} \geq \gamma_{d_q}\right]. \tag{I.1}$$

Subsequently, (I.1) can be solved as

$$\chi_1 = \int_0^\infty \left(\int_0^\infty \left(\int_{\gamma_{d_q}(y+z+1)}^\infty f_{\Lambda_{d_p c}}(x)dx\right) f_{\Lambda_{ac}}(y)dy\right) f_{\Lambda_{d_q c}}(z)dz. \tag{I.2}$$

Now, on inserting the involved PDF expressions and using [41, eqs. (3.351.2) and (3.351.3)], and binomial expansion [41, eq. 1.111], the final expression of χ_1 can be derived as in (6.27). Next, using the above similar steps, one can acquire the desired expression of χ_2 as in (6.28).

APPENDIX J

DERIVATIONS OF (6.30)-(6.32)

Referring to (6.29), $P_{\text{out}}^{\text{Link \#2, CF}}$ requires the calculations of J_1 and J_2. As such, J_1 can be represented using (6.9) and (6.10) as

$$J_1 = \Pr\left[\frac{\Lambda_{d_p c}}{\Lambda_{d_q c} + \Lambda_{ac} + 1} \geq \gamma_{d_q},\ \frac{\Lambda_{d_q c}}{\Lambda_C + \Lambda_{ac} + 1} \geq \gamma_{d_p}\right], \tag{J.1}$$

which can be re-expressed as

$$J_1 = \Pr\left[\Lambda_{d_q c} \geq \gamma_{d_p}\left(\Lambda_C + \Lambda_{ac} + 1\right), \Lambda_{d_q c} < \frac{\Lambda_{d_p c}}{\gamma_{d_q}} - \Lambda_{ac} - 1\right]. \tag{J.2}$$

Hereby, (J.2) can be evaluated as

$$J_1 = \int_0^\infty \left(\int_0^\infty \left(\int_{T_3 w + T_2 z + T_2}^\infty \left(\int_{\gamma_{d_p}(w+z+1)}^{\frac{y}{\gamma_{d_q}} - z - 1} f_{\Lambda_{d_q c}}(x) dx\right) f_{\Lambda_{d_p c}}(y) dy\right) f_{\Lambda_{ac}}(z) dz\right) f_{\Lambda_C}(w) dw. \tag{J.3}$$

Now, (J.3) can be simplified using (6.7) as $J_1 = \varphi_1 - \varphi_2$, with φ_1 and φ_2 can be written as

$$\varphi_1 = \int_0^\infty \left(\int_0^\infty \left(\int_{T_3 w + T_2 z + T_2}^\infty \Upsilon\left(m_{d_q c}, \frac{m_{d_q c}}{\Omega_{d_q c}\eta_{d_q}}\left(\frac{y}{\gamma_{d_q}} - z - 1\right)\right) f_{\Lambda_{d_p c}}(y) dy\right) f_{\Lambda_{ac}}(z) dz\right) f_{\Lambda_C}(w) dw \tag{J.4}$$

and

$$\varphi_2 = \int_0^\infty \left(\int_0^\infty \left(\int_{T_3 w + T_2 z + T_2}^\infty \Upsilon\left(m_{d_q c}, \frac{m_{d_q c}}{\Omega_{d_q c}\eta_{d_q}} \left(\gamma_{d_p}(w+z+1) \right) \right) f_{\Lambda_{d_p c}}(y) dy \right) f_{\Lambda_{ac}}(z) dz \right) f_{\Lambda_C}(w) dw. \tag{J.5}$$

Hereby, exploiting the series expansion for the lower incomplete Gamma function using [41, eq. 8.352.6], then inserting the involved PDF expressions, and using similar steps as in Appendix H, one can obtain the expressions for φ_1 and φ_2 as provided in (6.30) and (6.31), respectively.

Next, J_2 can be written using (6.13) and (6.14) as

$$J_2 = \Pr\Big[\Lambda_{cd_p} \geq T_1(\Lambda_{ad_p} + 1), \Lambda_{cd_p} \geq T_4((1-\rho)\Lambda_{D_p} + \Lambda_{ad_p} + 1)\Big], \tag{J.6}$$

where $T_4 = \frac{\gamma_{d_p}}{\rho}$. Subsequently, (J.6) can be computed as

$$\begin{aligned} J_2 = {} & U(T_1 - T_4) \int_{\frac{1}{T_5}}^\infty \left(\int_{T_5 w - 1}^\infty \left(\int_{T_1(z+1)}^\infty f_{\Lambda_{cd_p}}(x) dx \right) f_{\Lambda_{ad_p}}(z) dz \right) f_{\Lambda_{D_p}}(w) dw \\ & + U(T_1 - T_4) \int_{\frac{1}{T_5}}^\infty \left(\int_0^{T_5 w - 1} \left(\int_{T_4((1-\rho)w+z+1)}^\infty f_{\Lambda_{cd_p}}(x) dx \right) f_{\Lambda_{ad_p}}(z) dz \right) f_{\Lambda_{D_p}}(w) dw \\ & + U(T_4 - T_1) \int_0^\infty \left(\int_0^\infty \left(\int_{T_4((1-\rho)w+z+1)}^\infty f_{\Lambda_{cd_p}}(x) dx \right) f_{\Lambda_{ad_p}}(z) dz \right) f_{\Lambda_{D_p}}(w) dw, \end{aligned} \tag{J.7}$$

where $T_5 = \frac{T_4(1-\rho)}{T_1 - T_4}$ and $U(x)$ is unit-step function whose value is 1, when $x > 0$, and 0 otherwise. Nevertheless, for the feasible range of ρ, $T_4 > T_1$, thus, (J.7) can be simplified as

$$J_2 = \int_0^\infty \left(\int_0^\infty \left(\int_{T_4((1-\rho)w+z+1)}^\infty f_{\Lambda_{cd_p}}(x) dx \right) f_{\Lambda_{ad_p}}(z) dz \right) f_{\Lambda_{D_p}}(w) dw. \tag{J.8}$$

Hereby, substituting the associated PDF expressions and using [41, eqs. (3.351.2) and (3.351.3)], and binomial expansion [41, eq. 1.111], the final expression of J_2 can be derived as in (6.32).

APPENDIX K

DERIVATIONS OF (6.33) AND (6.34)

Referring to (6.26), it can be re-expressed as

$$P_{\text{out}}^{\text{Link \#1, CF}} = 1 - \left(1 - \Pr\left[\Lambda_{D_p \to C} < \gamma_{d_q}\right]\right)\left(1 - \Pr\left[\Lambda_{D_q, x_{d_p}} < \gamma_{d_q}\right]\right), \tag{K.1}$$

which can be approximated as

$$P_{\text{out, asy}}^{\text{Link \#1, CF}} = \underbrace{\Pr\left[\Lambda_{D_p \to C} < \gamma_{d_q}\right]}_{\bar{\chi_1}} + \underbrace{\Pr\left[\Lambda_{D_q, x_{d_p}} < \gamma_{d_q}\right]}_{\bar{\chi_2}}, \tag{K.2}$$

where the product terms leading to a higher order are neglected. Hereby, $\bar{\chi_1}$ and $\bar{\chi_2}$ can be evaluated using (6.9) and (6.12), respectively, as

$$\bar{\chi_1} = \int_0^\infty \left(\int_0^\infty \left(\int_0^{\gamma_{d_q}(y+z+1)} f_{\Lambda_{d_pc}}(x)dx\right) f_{\Lambda_{ac}}(y)dy\right) f_{\Lambda_{d_qc}}(z)dz \tag{K.3}$$

$$\text{and } \bar{\chi_2} = \int_0^\infty \left(\int_0^{T_1(y+1)} f_{\Lambda_{cd_q}}(x)dx\right) f_{\Lambda_{ad_q}}(y)dy. \tag{K.4}$$

Now, inserting the involved PDF expressions in (K.3) and (K.4), and then simplifying the integral expression in [41, eq. (3.351.1)] while making use of the series expansion of $\Upsilon(\alpha, x)$ [41, eq. 8.354.1] as

$$\Upsilon(\alpha, x) = x^\alpha \sum_{\varepsilon=0}^{\infty} \frac{(-1)^\varepsilon x^\varepsilon}{\varepsilon!(\alpha+\varepsilon)} \underset{x \to 0}{\simeq} \frac{x^\alpha}{\alpha}, \tag{K.5}$$

one can earn the expressions of $\bar{\chi_1}$ and $\bar{\chi_2}$, and subsequently the expression for $P_{\text{out, asy}}^{\text{Link \#1}}$.

REFERENCES

[1] B. Evans *et al.*, "Integration of satellite and terrestrial systems in future multimedia communications," *IEEE Trans. Wireless Commun.*, vol. 12, no. 5, pp. 72-80, Oct. 2005.

[2] G. G. Kota and S. Kim, "Satellite component of NGN: Integrated and hybrid networks," *Int. J. Satell. Commun.*, vol. 29, no. 3, pp. 191-208, May 2010.

[3] V. Sakarellos, C. Kourogiorgas, and A. Panagopoulos, "Cooperative hybrid land mobile satellite-terrestrial broadcasting systems: Outage probability evaluation and accurate simulation," *Wireless Pers. Commun.*, vol. 79, no. 2, pp. 1471-1481, Nov. 2014.

[4] M. R. Bhatnagar and M. K. Arti, "Performance analysis of AF based hybrid satellite-terrestrial cooperative network over generalized fading channels," *IEEE Commun. Lett.*, vol. 17, no. 10, pp. 1912-1915, Oct. 2013.

[5] P. K. Upadhyay and P. K. Sharma, "Max-max user-relay selection scheme in multiuser and multirelay hybrid satellite-terrestrial relay systems," *IEEE Commun. Lett.*, vol. 20, no. 2, pp. 268-271, Feb. 2016.

[6] S. Sreng, B. Escrig, and M. Boucheret, "Exact symbol error probability of hybrid/integrated satellite-terrestrial cooperative network," *IEEE Trans. Wireless Commun.*, vol. 12, no. 3, pp. 1310-1319, Mar. 2013.

[7] "ETSI TS 102 585 V1. 1. 2 Digital Video Broadcasting (DVB); System specifications for satellite services to handheld devices (SH) below 3 GHz," Apr. 2008.

[8] S. Haykin, "Cognitive radio: Brain-empowered wireless communications," *IEEE J. Sel. Areas Commun.*, vol. 23, no. 2, pp. 201-220, Feb. 2005.

[9] A. Goldsmith, S. A. Jafar, I. Maric, and S. Srinivasa, "Breaking spectrum gridlock with cognitive radios: An information theoretic perspective," *Proc. IEEE*, vol. 97, no. 5, pp. 894-914, May 2009.

[10] S. Vassaki, M. I. Poulakis, A. D. Panagopoulos, and P. Constantinou, "Power allocation in cognitive satellite terrestrial networks with QoS constraints," *IEEE Commun. Lett.*, vol. 17, no. 7, pp. 1344-1347, May 2013.

[11] C. E. Shannon, "Two-way communication channels," in *Proc. 4th Berkeley Symp. Math., Statist., Probab.*, vol. 1, 1961, pp. 611-644.

[12] Z. Ding *et al.*, "A survey on non-orthogonal multiple access for 5G networks: Research challenges and future trends," *IEEE J. Sel. Areas Commun.*, vol. 35, no. 10, pp. 2181-2195, Oct. 2017.

[13] Z. Ding, M. Peng, and H. V. Poor, "Cooperative non-orthogonal multiple access in 5G systems," *IEEE Commun. Lett.*, vol. 19, no. 8, pp. 1462-1465, Aug. 2015.

[14] Y. Fadlallah *et al.*, "Coding for caching in 5G networks," *IEEE Commun. Mag.*, vol. 55, no. 2, pp. 106-113, Feb. 2017.

[15] X. Wang, M. Chen, T. Taleb, A. Ksentini, and V. C. M. Leung, "Cache in the air: Exploiting content caching and delivery techniques for 5G systems," *IEEE Commun. Mag.*, vol. 52, no. 2, pp. 131-139, Feb. 2014.

[16] C. Yang, Y. Yao, Z. Chen, and B. Xia, "Analysis on cache-enabled wireless heterogeneous networks," *IEEE Trans. Wireless Commun.*, vol. 15, no. 1, pp. 131-145, Jan. 2016.

[17] J. G. Andrews *et al.*, "What will 5G be?," *IEEE J. Sel. Areas Commun.*, vol. 32, no. 6, pp. 1065-1082, Jun. 2014.

[18] K. An, M. Lin, W. Zhu, Y. Huang, and G. Zheng, "Outage performance of cognitive hybrid satellite-terrestrial networks with interference constraint," *IEEE Trans. Veh. Technol.*, vol. 65, no. 11, pp. 9397-9404, Nov. 2016.

[19] S. Shi, G. Li, K. An, Z. Li, and G. Zheng, "Optimal power control for real-time applications in cognitive satellite-terrestrial networks," *IEEE Commun. Lett.*, vol. 21, no. 8, pp. 1815-1818, Mar. 2017.

[20] O. Y. Kolawole, S. Vuppala, M. Sellathurai, and T. Ratnarajah, "On the performance of cognitive satellite-terrestrial networks," *IEEE Trans. Cogn. Commun. Net.*, vol. 3, no. 4, pp. 668-683, Dec. 2017.

[21] P. K. Sharma, P. K. Upadhyay, D. B. da Costa, P. S. Bithas, and A. G. Kanatas, "Performance analysis of overlay spectrum sharing in hybrid satellite-terrestrial systems with secondary network selection," *IEEE Trans. Wireless Commun.*, vol. 16, no. 10, pp. 6586-6601, Oct. 2017.

[22] L. Erwu, W. Dongyao, L. Jimin, S. Gang, and J. Shan, "Performance evaluation of bandwidth allocation in 802.16j mobile multi-hop relay networks," in *Proc. IEEE Veh. Technol. Conf. (VTC)-Spring*, Dublin, Ireland, Apr. 2007, pp. 939-943.

[23] T. Schenk, *RF Imperfections in High-Rate Wireless Systems: Impact and Digital Compensation.*, Springer 2008.

[24] X. Yan, H. Xiao, C. Wang, and K. An, "On the ergodic capacity of NOMA-based cognitive hybrid satellite terrestrial networks," in *Proc. IEEE Int. Conf. Commun. in China (ICCC)*, Qingdao, China, Oct. 2017, pp. 1-5.

[25] X. Zhang *et al.*, "Outage performance of NOMA-based cognitive hybrid satellite-terrestrial overlay networks by amplify-and-forward protocols," *IEEE Access*, vol. 7, pp. 85372-85381, Jun. 2019.

[26] V. Singh, P. K. Upadhyay, and M. Lin, "On the performance of NOMA-assisted overlay multiuser cognitive satellite-terrestrial networks," *IEEE Wireless Commun. Lett.*, vol. 9, no. 5, pp. 638-642, May 2020.

[27] X. Zhang *et al.*, "Vickrey auction-based secondary relay selection in cognitive hybrid satellite-terrestrial overlay networks with non-orthogonal multiple access," *IEEE Wireless Commun. Lett.*, vol. 9, no. 5, pp. 628-632, May 2020.

[28] G. Im and J. H. Lee, "Outage probability for cooperative NOMA systems with imperfect SIC in cognitive radio networks," *IEEE Commun. Lett.*, vol. 23, no. 4, pp. 692-695, Apr. 2019.

[29] Y. Yang, H. Hu, J. Xu, and G. Mao, "Relay technologies for WiMAX and LTE-advanced mobile systems," *IEEE Commun. Mag.*, vol. 47, no. 10, pp. 100-105, Oct. 2009.

[30] A. Abdi, W. C. Lau, M.-S. Alouini, and M. Kaveh, "A new simple model for land mobile satellite channels: First- and second-order statistics," *IEEE Trans. Wireless Commun.*, vol. 2, no. 3, pp. 519-528, May 2003.

[31] C. Loo, "A statistical model for a land mobile satellite link," *IEEE Trans. Veh. Technol.*, vol. 34, no. 3, pp. 122-127, Aug. 1985.

[32] P. Kumar and K. Dhaka, "Performance of wireless powered DF relay system under Nakagami-m fading: Relay assists energy-constrained source," *IEEE Syst. Journ.*, vol. 14, no. 2, pp. 2497-2507, Jun. 2020.

[33] S. K. Sharma, S. Chatzinotas, and B. Ottersten, "Cognitive radio techniques for satellite communication systems," in *Proc. IEEE Veh. Tech. Conf. (VTC) Fall*, Las Vegas, NV, Sep. 2013, pp. 1-5.

[34] Y. Zou, J. Zhu, B. Zheng, and Y.-D. Yao, "An adaptive cooperation diversity scheme with best-relay selection in cognitive radio networks," *IEEE Trans. Signal Process.*, vol. 58, no. 10, pp. 5438-5445, Oct. 2010.

[35] Y. Han, A. Pandharipande, and S. H. Ting, "Cooperative decode-and-forward relaying for secondary spectrum access," *IEEE Trans. Wireless Commun.*, vol. 8, no. 10, pp. 4945-4950, Oct. 2009.

[36] V. Singh, P. K. Upadhyay, K.-J. Lee, and D. B. da Costa, "Cooperative and cognitive hybrid satellite-terrestrial networks," *Cognitive Radio Mobile Communications and Wireless Networks*, M.H. Rehmani and R. Dhaou (Eds.), EAI/Springer Innovations in Communications and Computing Book Series, Cham, Switzerland, 2019.

[37] T. K. Kim, H. M. Kim, M. G. Song, and G. H. Im, "Improved spectrum-sharing protocol for cognitive radio networks with multiuser cooperation," *IEEE Trans. Commun.*, vol. 63, no. 4, pp. 1121-1135, Apr. 2015.

[38] T. Q. Duong, P. L. Yeoh, V. N. Q. Bao, M. Elkashlan, and N. Yang, "Cognitive relay networks with multiple primary transceivers under spectrum-sharing," *IEEE Signal Process. Lett.*, vol. 19, no. 11, pp. 741-744, Nov. 2012.

[39] F. R. V. Guimarães, D. B. da Costa, T. A. Tsiftsis, C. C. Cavalcante, and G. K. Karagiannidis, "Multiuser and multirelay cognitive radio networks under spectrum-sharing constraints," *IEEE Trans. Veh. Technol.*, vol. 63, no. 1, pp. 433-439, Jan. 2014.

[40] L. Fan, X. Lei, T. Q. Duong, R. Q. Hu, and M. Elkashlan, "Multiuser cognitive relay networks: Joint impact of direct and relay communications," *IEEE Trans. Wireless Commun.*, vol. 13, no. 9, pp. 5043-5055, Sep. 2014.

[41] I. S. Gradshteyn and I. M. Ryzhik, *Tables of Integrals, Series and Products*, 6th ed. New York: Academic Press, 2000.

[42] K. An, M. Lin, and T. Liang, "On the performance of multiuser hybrid satellite-terrestrial relay networks with opportunistic scheduling," *IEEE Commun. Lett.*, vol. 19, no. 10, pp. 1722-1725, Oct. 2015.

[43] C. Zhang, J. Ge, J. Li, Y. Rui, and M. Guizani, "A unified approach for

calculating outage performance of two-way AF relaying over fading channels," *IEEE Trans. Veh. Technol.*, vol. 64, no. 3, pp. 1218-1229, Mar. 2015.

[44] H. A. Suraweera, R. H. Y. Louie, Y. Li, G. K. Karagiannidis, and B. Vucetic, "Two hop amplify-and-forward transmission in mixed Rayleigh and Rician fading channels," *IEEE Commun. Lett.*, vol. 13, no. 4, pp. 227-229, Apr. 2009.

[45] N. I. Miridakis, D. D. Vergados, and A. Michalas, "Dual-hop communication over a satellite relay and shadowed Rician channels," *IEEE Trans. Veh. Technol.*, vol. 64, no. 9, pp. 4031-4040, Sep. 2015.

[46] M. Jia, X. Gu, Q. Guo, W. Xiang, and N. Zhang, "Broadband hybrid satellite-terrestrial communication systems based on cognitive radio toward 5G," *IEEE Wireless Commun.*, vol. 23, no. 6, pp. 96-106, Dec. 2016.

[47] Z. Lin, M. Lin, J.-B. Wang, Y. Huang, and W. Zhu, "Robust secure beamforming for 5G cellular networks coexisting with satellite networks," *IEEE J. Sel. Areas Commun.*, vol. 36, no. 4, pp. 932-945, Apr. 2018.

[48] M. Lin, Z. Lin, W.-P. Zhu, and J.-B. Wang, "Joint beamforming for secure communication in cognitive satellite terrestrial networks," *IEEE J. Sel. Areas Commun.*, vol. 36, no. 5, pp. 1017-1029, May 2018.

[49] E. Björnson, M. Matthaiou, and M. Debbah, "A new look at dual-hop relaying: Performance limits with hardware impairments," *IEEE Trans. Commun.*, vol. 61, no. 11, pp. 4512-4525, Nov. 2013.

[50] K. Guo, M. Lin, B. Zhang, W. P. Zhu, J. B. Wang, and T. A. Tsiftsis, "On the performance of LMS communication with hardware impairments and interference," *IEEE Trans. Commun.*, vol. 67, no. 2, pp. 1490-1505, Feb. 2019.

[51] K. Guo, K. An, B. Zhang, Y. Huang, and G. Zheng, "Outage analysis of cognitive hybrid satellite-terrestrial networks with hardware impairments and multi-primary users," *IEEE Wireless Commun. Lett.*, vol. 7, no. 5, pp. 816-819, Oct. 2018.

[52] K. Guo, K. An, B. Zhang, Y. Huang, D. Guo, G. Zheng, and S. Chatzinotas, "On the performance of the uplink satellite multiterrestrial relay networks with hardware impairments and interference," *IEEE Syst. Journ.*, vol. 13, no. 3, pp. 2297-2308, Sept. 2019.

[53] M. Xia and S. Aïssa, "Modeling and analysis of cooperative relaying in spectrum-sharing cellular systems," *IEEE Trans. Veh. Technol.*, vol. 65, no. 11, pp. 9112-9122, Nov. 2016.

[54] N. Chuberre, O. Courseille, P. Laine, L. Roullet, T. Quignon, and M. Tatard, "Hybrid satellite and terrestrial infrastructure for mobile broadcast services delivery: An outlook to the Unlimited Mobile TV system performance," *Int. J. Sat. Commun.*, vol. 26, no. 5, pp. 405-426, Aug. 2008.

[55] "8 Hints for making and interpreting EVM measurements," *Tech. Rep., Agilent Technologies*, 2005.

[56] K. Guo, B. Zhang, Y. Huang, and D. Guo, "Performance analysis of two-way satellite terrestrial relay networks with hardware impairments," *IEEE Wireless Commun. Lett.*, vol. 6, no. 4, pp. 430-433, May 2017.

[57] N. B. Mehta, V. Sharma, and G. Bansal, "Performance analysis of a cooperative system with rateless codes and buffered relays," *IEEE Trans. Wireless Commun.*, vol. 10, no. 4, pp. 1069-1081, Apr. 2011.

[58] I. Stanojev, O. Simeone, Y. B.-Ness, and C. You, "Performance of multirelay collaborative hybrid-ARQ protocols over fading channels," *IEEE Commun. Lett.*, vol. 10, no. 7, pp. 522-524, Jul. 2006.

[59] Z. Yang, Z. Ding, P. Fan, and N. Al-Dhahir, "A general power allocation scheme to guarantee quality of service in downlink and uplink NOMA systems," *IEEE Trans. Commun.*, vol. 15, no. 11, pp. 7244-7257, Nov. 2016.

[60] X. Yue *et al.*, "Outage behaviors of NOMA-based satellite network over Shadowed-Rician fading channels," *IEEE Trans. Veh. Technol.*, vol. 69, no. 6, pp. 6818-6821, Jun. 2020.

[61] X. Yan *et al.*, "The application of power-domain non-orthogonal multiple access in satellite communication networks," *IEEE Access*, vol. 7, pp. 63531-63539, May 2019.

[62] "EN 302 583 V1.1.1 DVB-SH standard; Framing structure, channel coding and modulation for satellite services to handheld devices (SH) below 3 GHz," Jul. 2007.

[63] Z. Xiao, L. Zhu, J. Choi, P. Xia, and X. Xia, "Joint power allocation and beamforming for non-orthogonal multiple access (NOMA) in 5G millimeter wave communications," *IEEE Trans. Wireless Commun.*, vol. 17, no. 5, pp. 2961-2974, May 2018.

[64] Z. Ding, F. Adachi, and H. V. Poor, "The application of MIMO to nonorthogonal multiple access," *IEEE Trans. Wireless Commun.*, vol. 15, no. 1, pp. 537-552, Jan. 2016.

[65] Y. Zhang, J. Ge, and E. Serpedin, "On the performance of a nonorthogonal multiple-access technique for downlink MIMO cooperative networks," *Trans Emerg. Telecomm. Technol.*, vol. 29, no. 1, Jan. 2018.

[66] P. Lai, H. Bai, Y. Huang, Z. Chen, and T. Liu, "Performance evaluation of underlay cognitive hybrid satellite-terrestrial relay networks with relay selection scheme," *IET Commun.*, vol. 13, no. 16, pp. 2550-2557, Jun. 2019.

[67] A. C. Cirik, M. C. Filippou, and T. Ratnarajah, "Transceiver design in full-duplex MIMO cognitive radios under channel uncertainties," *IEEE Trans. Cogn. Commun. Netw.*, vol. 2, no. 1, pp. 1-14, Mar. 2016.

[68] Z. Zhang, Z. Ma, M. Xiao, Z. Ding, and P. Fan, "Full-duplex device-to-device-aided cooperative non-orthogonal multiple access," *IEEE Trans. Veh. Technol.*, vol. 66, no. 5, pp. 4467-4471, May 2017.

[69] T. Riihonen, S. Werner, and R. Wichman, "Mitigation of loopback self-interference in full-duplex MIMO relays," *IEEE Trans. Signal Process.*, vol. 59, no. 12, pp. 5983-5993, Dec. 2011.

[70] X. Yue *et al.*, "Secure communications in a unified non-orthogonal multiple access framework," *IEEE Trans. Commun.*, vol. 19, no. 3, pp. 2163-2178, Mar. 2020.

[71] X. Li *et al.*, "Hardware impaired ambient backscatter NOMA systems: Reliability and security," *IEEE Trans. Commun.*, vol. 69, no. 4, pp. 2723-2736, Apr. 2021.

[72] X. Yan, H. Xiao, K. An, G. Zheng, and W. Tao, "Hybrid satellite terrestrial relay networks with cooperative non-orthogonal multiple access," *IEEE Commun. Lett.*, vol. 22, no. 5, pp. 978-981, May 2018.

[73] X. Li, Y. Chen, P. Xue, G. Lv, and M. Shu, "Outage performance for satellite-assisted cooperative NOMA systems with coordinated direct and relay transmission," *IEEE Commun. Lett.*, vol. 24, no. 10, pp. 2285-2289, Oct. 2020.

[74] X. Wang, M. Jia, Q. Guo, I. W. Ho, and F. C. Lau, "Full-duplex relaying cognitive radio network with cooperative nonorthogonal multiple access," *IEEE Syst. Journ.*, vol. 13, no. 4, pp. 3897-3908, Dec. 2019.

[75] S. Solanki, P. K. Upadhyay, D. B. da Costa, P. S. Bithas, and A. G. Kanatas, "Performance analysis of cognitive relay networks with RF hardware impairments and CEEs in the presence of primary users' interference," *IEEE Trans. Cogn. Commun. Netw.*, vol. 4, no. 2, pp. 406-421, Jun. 2018.

[76] C. Guo, L. Zhao, C. Feng, Z. Ding, and H. Chen, "Energy harvesting enabled NOMA systems with full-duplex relaying," *IEEE Trans. Veh. Technol.*, vol. 68, no. 7, pp. 7179-7183, Jul. 2019.

[77] L. Zhang *et al.*, "Performance analysis and optimization in downlink NOMA systems with cooperative full-duplex relaying," *IEEE J. Sel. Areas Commun.*, vol. 35, no. 10, pp. 2398-2412, Oct. 2017.

[78] T. Riihonen, S. Werner, and R. Wichman, "Hybrid full-duplex/half-duplex relaying with transmit power adaptation," *IEEE Trans. Wireless Commun.*, vol. 10, no. 9, pp. 3074-3085, Sep. 2011.

[79] S. Arzykulov, G. Nauryzbayev, T. A. Tsiftsis, B. Maham, and M. Abdallah, "On the outage of underlay CR-NOMA networks with detect-and-forward relaying," *IEEE Trans. Cogn. Commun. Netw.*, vol. 5, no. 3, pp. 795-804, Sep. 2019.

[80] K. Guo *et al.*, "Performance analysis of hybrid satellite-terrestrial cooperative networks with relay selection," *IEEE Trans. Veh. Technol.*, vol. 69, no. 8, pp. 9053-9067, Jun. 2020.

[81] G. Zheng, S. Chatzinotas, and B. Ottersten, "Generic optimization of linear precoding in multibeam satellite systems," *IEEE Trans. Wireless Commun.*, vol. 11, no. 6, pp. 2308-2320, Jun. 2012.

[82] I. Krikidis, H. A. Suraweera, P. J. Smith, and C. Yuen, "Full-duplex relay selection for amplify-and-forward cooperative networks," *IEEE Trans. Wireless Commun.*, vol. 11, no. 12, pp. 4381-4393, Dec. 2012.

[83] M. Duarte, C. Dick, and A. Sabharwal, "Experiment-driven characterization of full-duplex wireless systems," *IEEE Trans. Wireless Commun.*, vol. 11, no. 12, pp. 4296-4307, Dec. 2012.

[84] M. G. Khafagy, M.-S. Alouini, and S. Aïssa, "Full-duplex relay selection in cognitive underlay networks," *IEEE Trans. Commun.*, vol. 66, no. 10, pp. 4431-4443, Oct. 2018.

[85] S. Hatamnia, S. Vahidian, S. Aïssa, B. Champagne, and M. Ahmadian-Attari, "Network-coded two-way relaying in spectrum sharing systems with quality-of-service requirements," *IEEE Trans. Veh. Technol.*, vol. 66, no. 2, pp. 1299-1312, Feb. 2017.

[86] X. Li *et al.*, "Full-duplex cooperative NOMA relaying systems with I/Q imbalance and imperfect SIC," *IEEE Wireless Commun. Lett.*, vol. 9, no. 1, pp. 17-20, Jan. 2020.

[87] V. Aswathi and A. V. Babu, "Full/half duplex cooperative NOMA under

imperfect successive interference cancellation and channel state estimation errors," *IEEE Access*, vol. 7, pp. 179961-179984, Dec. 2019.

[88] M. A.Vazquez *et al.*, "Precoding, scheduling and link adaptation in mobile interactive multibeam satellite systems," *IEEE J. Sel. Area Commun.*, vol. 36, no. 5, pp. 971–980, May 2018.

[89] W. Lu, K. An, and T. Liang, "Robust beamforming design for sum secrecy rate maximization in multibeam satellite systems," *IEEE Trans. Aerosp. Electron. Syst.*, vol. 55, no. 3, pp. 1568-1572, Jun. 2019.

[90] M. K. Arti, "Channel estimation and detection in satellite communication systems," *IEEE Trans. Veh. Technol.*, vol. 65, no. 12, pp. 10173-10179, Dec. 2016.

[91] K. Hamdi, W. Zhang, and K. B. Letaief, "Joint beamforming and scheduling in cognitive radio networks," in *Proc. IEEE Global Commun. Conf. (GLOBECOM)*, Washington, DC, USA, Nov. 2007, pp. 2977-2981.

[92] X. Yue, Y. Liu, S. Kang, A. Nallanathan, and Z. Ding, "Exploiting full/half duplex user relaying in NOMA systems," *IEEE Trans. Commun.*, vol. 66, no. 2, pp. 560-575, Feb. 2018.

[93] V. S. Adamchik and O. I. Marichev, "The algorithm for calculating integrals of hypergeometric type functions and its realization in reduce systems," in *Proc. Int. Symp. Symbolic and Algebraic Comput. (ISSAC)*, Tokyo, Japan, Aug. 1990, pp. 212-224.

[94] A. M. Mathai and R. K. Saxena, *The H-function with applications in statistics and other disciplines*, New Delhi, India: Wiley Eastern, 1978.

[95] I. S. Ansari, S. Al-Ahmadi, F. Yilmaz, M.-S. Alouini, and H. Yanikomeroglu, "A new formula for the BER of binary modulations with dual-branch selection over generalized-K composite fading channels," *IEEE Trans. Commun.*, vol. 59, no. 10, pp. 2654-2658, Oct. 2011.

[96] Y. Huang *et al.*, "Performance analysis of multiuser multiple antenna relaying networks with co-channel interference and feedback delay," *IEEE Trans. Commun.*, vol. 62, no. 1, pp. 59-73, Jan. 2014.

[97] S. Solanki, V. Singh, and P. K. Upadhyay, "RF energy harvesting in hybrid two-way relaying systems with hardware impairments," *IEEE Trans. Veh. Technol.*, vol. 68, no. 12, pp. 11792-11805, Dec. 2019.

[98] A. A. Nasir, X. Zhou, S. Durrani, and R. A. Kennedy, "Relaying protocols for wireless energy harvesting and information processing," *IEEE Trans. Wireless Commun.*, vol. 12, no. 7, pp. 3622-3636, Jul. 2013.

[99] Y. Liu, L. Wang, M. Elkashlan, T. Q. Duong, and A. Nallanathan, "Two way relay networks with wireless power transfer: Design and performance analysis," *IET Commun.*, vol. 10, no. 14, pp. 1810-1819, Jun. 2016.

[100] V. Singh, V. Bankey, and P. K. Upadhyay, "Underlay cognitive hybrid satellite-terrestrial networks with cooperative-NOMA," in *Proc. IEEE Wireless Commun. Netw. Conf. (WCNC)*, Seoul, South Korea, May 2020, pp. 1-6.

[101] K. An, Y. Li, T. Liang, and X. Yan, "On the performance of cache-enabled hybrid satellite-terrestrial relay networks," *IEEE Wireless Commun. Lett.*, vol. 8, no. 5, pp. 1506-1509, Oct. 2019.

[102] X. Zhang *et al.*, "On the performance of hybrid satellite-terrestrial content delivery networks with non-orthogonal multiple access," *IEEE Wireless Commun. Lett.*, vol. 10, no. 3, pp. 454-458, Mar. 2021.

[103] X. Yue, Y. Liu, S. Kang, A. Nallanathan, and Y. Chen, "Modeling and analysis of two-way relay non-orthogonal multiple access systems," *IEEE Trans. Commun.*, vol. 66, no. 9, pp. 3784-3796, Sep. 2018.

[104] H.-N. Nguyen *et al.*, "Reliable and secure transmission in multiple antennas hybrid satellite-terrestrial cognitive networks relying on NOMA," *IEEE Access*, vol. 8, pp. 215044-215056, Dec. 2020.

[105] L. Breslau, P. Cao, L. Fan, G. Phillips, and S. Shenker, "Web caching and Zipf-like distributions: Evidence and implications," in *Proc. IEEE Int. Conf. Computer Commun. (INFOCOM)*, San Diego, CA, USA, Mar. 1999, pp. 1-8.

[106] A. Kalantari, M. Fittipaldi, S. Chatzinotas, T. X. Vu, and B. Ottersten, "Cache-assisted hybrid satellite-terrestrial backhauling for 5G cellular networks," in *Proc. IEEE Global Commun. Conf. (GLOBECOM)*, Singapore, Dec. 2017, pp. 1-6.

[107] F. Khan, K. Tourki, M.-S. Alouini, and K. Qaraqe, "Delay performance of a broadcast spectrum sharing network in Nakagami-m fading," *IEEE Trans. Veh. Technol.*, vol. 63, no. 3, pp. 1350-1364, Mar. 2014.

List of Publications

A. Publications from PhD Thesis Work

A1. In Refereed Journals

1. **V. Singh** and P. K. Upadhyay, "Exploiting cache-free/cache-aided TWR-NOMA in cognitive hybrid satellite-terrestrial networks," ***IEEE Transactions on Vehicular Technology***, under review.

2. **V. Singh** and P. K. Upadhyay, "Exploiting FD/HD cooperative-NOMA in underlay cognitive hybrid satellite-terrestrial networks," ***IEEE Transactions on Cognitive Communication and Networking***, Jun. 2021, doi:10.1109/TCCN.2021.3089164.

3. **V. Singh**, S. Solanki, P. K. Upadhyay, D. B. da Costa, and J. M. Moualeu, "Performance analysis of hardware-impaired overlay cognitive satellite-terrestrial networks with adaptive relaying protocol,"***IEEE Systems Journal***, vol. 1, no. 15, pp. 192-203, Mar. 2021.

4. **V. Singh**, P. K. Upadhyay, and M. Lin, "On the performance of NOMA-assisted overlay multiuser cognitive satellite-terrestrial networks,"***IEEE Wireless Communication Letters***, vol. 9, no. 5, pp. 638-642, May 2020.

5. **V. Singh**, S. Solanki, and P. K. Upadhyay, "Cognitive relaying cooperation in satellite-terrestrial systems with multiuser diversity,"***IEEE Access***, vol. 6, pp. 65539-65547, Oct. 2018.

A2. In Refereed Conference Proceedings

1. **V. Singh**, V. Bankey, and P. K. Upadhyay "Underlay cognitive hybrid satellite-terrestrial networks with cooperative-NOMA,"in ***Proc. IEEE Wireless Communications and Networking Conference (WCNC)***, Seoul, South Korea, May 2020, pp. 1-6.

2. **V. Singh**, S. Solanki, P. K. Upadhyay, D. B. da Costa, and J. M. Moualeu, "Impact of hardware impairments on cognitive satellite-terrestrial relaying with a direct link,"in ***Proc. IEEE 17th Annual Consumer Communications*** & ***Networking Conference (CCNC)***, Las Vegas, USA, Jan. 2020, pp. 1-6.

B. Other Publications During PhD

B1. Book Chapter

1. **V. Singh**, P. K. Upadhyay, K.-J. Lee, and D. B. da Costa, "Cooperative and cognitive hybrid satellite-terrestrial networks," *Cognitive Radio Mobile Communications and Wireless Networks*, M.H. Rehmani and R. Dhaou (Eds.), **EAI/Springer Innovations in Communications and Computing Book Series**, Cham, Switzerland, 2019.

B2. In Refereed Journals

1. A. K. Shukla, **V. Singh**, P. K. Upadhyay, A. Kumar, and J. M. Moualeu "Performance analysis of energy harvesting-assisted overlay cognitive NOMA systems with incremental relaying," ***IEEE Open Journal of the Communications Society***, vol. 2, pp. 1558-1576, Jun. 2021.

2. C. K. Singh, **V. Singh**, P. K. Upadhyay, and M. Lin, "Energy harvesting in overlay cognitive NOMA systems with hardware impairments," ***IEEE Systems Journal***, Jun. 2021, doi: 10.1109/JSYST.2021.3082552.

3. S. Solanki, **V. Singh**, and P. K. Upadhyay, "RF energy harvesting in hybrid two-way relaying systems with hardware impairments," ***IEEE Transactions on Vehicular Technology***, vol. 68, no. 12, pp. 11792-11805, Dec. 2019.

B3. In Refereed Conference Proceedings

1. V. Bankey, **V. Singh**, and P. K. Upadhyay "Physical layer secrecy of NOMA-based hybrid satellite-terrestrial relay networks," in ***Proc. IEEE Wireless Communications and Networking Conference (WCNC)***, Seoul, South Korea, May 2020, pp. 1-6.

2. **V. Singh** and P. K. Upadhyay, "Cognitive hybrid satellite-terrestrial relay networks with simultaneous energy and information transmission," in ***Proc. IEEE International Conference on Advanced Networks and Telecommunications Systems (ANTS)***, Indore, India, Dec. 2018, pp. 1-6.

3. **V. Singh**, P. K. Upadhyay, D. B. da Costa, and Ugo S. Dias, "Hybrid satellite-terrestrial spectrum sharing systems with RF energy harvesting," in ***Proc. IEEE 29th Annual International Symposium on Personal, Indoor and Mobile Radio Communications (PIMRC)***, Bologna, Italy, Sep. 2018, pp. 306-311.